UNIVERSITEIT VAN PRETORIA
UNIVERSITY OF PRETORIA
YUNIBESITHI YA PRETORIA

Cobalt organometallic compounds by electrochemistry

By

Winny Kgabo Maboya

Submitted in partial fulfilment of the requirements for the degree of Master of Science in the Faculty of Natural and Agricultural Sciences

University of Pretoria

Pretoria

December, 2006

DECLARATION

I declare that this dissertation is my own work. It is being submitted for the Degree of Master of Science in the University of Pretoria, Pretoria. It has not been submitted before for any degree or examination in any other University.

_____

W K Maboya

____ day of _____ _____

ABSTRACT

The electrochemical oxidation of $CoCl_2(PPh_3)_2$ was investigated in a mixture of acetonitrile and pentanol (1:1) at a platinum disk working electrode using Cyclic Voltammetry (CV) and Chronoamperometry.

Elemental Analysis and Infrared Spectroscopy were used to characterise the synthesized compounds i.e. $CoCl_2(PPh_3)_2$ and $CoCl(PPh_3)_3$.

Cyclic Voltammetry was utilised for the examination of different working electrode materials that could be used for the anodic voltammetric studies of $CoCl_2(PPh_3)_2$, to characterise the reactants and products of each electrode reaction, to investigate the chloride binding ability to a $CoCl(PPh_3)_3$ complex, and to evaluate the electrocatalytic substitution of chloride by PPh_3 from the complex $CoCl_2(PPh_3)_2$. Use of ferrocene as an internal standard during the anodic studies of $CoCl_2(PPh_3)_2$ was also evaluated.

The number of electron involved in the electrode process, Co^{II} to Co^{III} from $CoCl_2(PPh_3)_2$ and diffusion coefficient of ferrocene in a mixture of acetonitrile and pentanol (1:1) were determined using Chronoamperometry.

Ultraviolet-Visible (UV-Vis) and ^{31}P Nuclear Magnetic Resonance (^{31}P NMR) spectra were used to assist with the characterisation of the electrode reactions involved during oxidation of $CoCl_2(PPh_3)_2$.

DEDICATION

In memory of my father in law

Albert Kgabo Maboya

ACKNOWLEDGEMENTS

I would like to send my acknowledgements to the following parties:

- First and foremost I would like to thank God for giving me the strength and for keeping me healthy throughout the course of the project.
- Prof. Ignacy Cukrowski for all his guidance, supervision, and for the helpful discussions throughout the project.
- Sasol and NRF for the financial support.
- My husband, Hosea for being a mother and father to our little boy, without your support I would never have done this; I could not have asked for a better husband – Thank you. My little boy, Kagiso for understanding that mummy cannot be there the entire time and being patient, "you are a star" and to my daughter Reshoketswe.
- The entire Electrochemistry Research Group for being like my second family.
- Finally, University of Pretoria for allowing me to use their research facilities.

TABLE OF CONTENTS

LIST OF FIGURES

LIST OF TABLES

LIST OF SYMBOLS

μ	Micro
$J_i(x)$	Flux of species i (mol $s^{-1}cm^{-2}$) at distance x from the surface
D	Diffusion coefficient (cm^2 s^{-1})
$\delta C_i(x)/\delta x$	Concentration gradient at distance x
$\delta \phi(x)/\delta x$	Potential gradient
z	Charge (dimensionless)
C	Concentration ($mol.cm^{-3}$)
$v(x)$	Velocity (cm s^{-1})
A	Area of electrode (cm^2)
i_j	Current component at any value of x arising from a flow of species j (A)
$i_{m,j}$	Migration current of species j (A)
F	Faraday's constant (96485 A s)
R	Gas constant (8.316 J K^{-1} mol^{-1}) or solution resistance
T	Temperature (K)
E_λ	Switching potential (V)
$E_{1/2}$ or $E°$	Half-wave potential (V)

E_{pa}	Anodic peak potential (V)
E_{pc}	Cathodic peak potential (V)
I_{pa}	Anodic peak current (A)
I_{pc}	Cathodic peak current (A)
β	Beta
γ	Gamma
δ	Sigma
E_p	Peak potential (V)
M	Molar concentration (mol dm^{-3})
p	Para
m	Meta
o	Ortho
$j_{p,ox}$	Peak current density
d	Distance (mm)
t	Time (s)
k°	Standard heterogeneous rate constant (cm/s)
α	Cathodic transfer coefficient
1 – α	Anodic transfer coefficient

n	Number of electrons
v	Scan rate (V s^{-1})
π	Pi bonding
D^*	Dispersion coefficient
ID	Internal diameter
Ω	Ohm

LIST OF ABBREVIATIONS

AE	Auxiliary electrode
Ag | AgCl	Silver-silver chloride
Ag | $AgNO_3$	Silver-silver nitrate
A.R.	Analytical reagent
t-BuNC	Tert-butyl isocyanide
$CDCl_3$	Deuterated chloroform
$ClNCH_3TPP$	Chloro-N-methyl-α,β,γ,δ-tetraphenylporphirins
$ClMNCH_3TPP$	Chloro-N-methyl-α,β,γ,δ-tetraphenylporphinatometal (II) (M = Co, Zn)
CoTETPc	Cobalt-tetra-{2-(2-thienyl)ethoxy}phthalocyanine
CoTPP	Cobalt-tetraphenylporphirin
C.P.	Chemically pure
Cp	Cyclopentadienyl
CV	Cyclic Voltammetry
dbbip	2,6-(1'-butylbenzimidazol-2'-yl)pyridine
DMF	Dimethylformamide
DMSO	Dimethylsulfoxide

ESR	Electron Spin Resonance
EPR	Electron Paramagnetic Resonance
ETC	Electron transfer chain
$FeCp_2$	Ferrocene
FIA	Flow Injection Analysis
GC	Glassy carbon
IR	Infrared Spectroscopy
KF	Karl Fischer
NMR	Nuclear Magnetic Resonance Spectroscopy
OMC	Octamethyl corrole
(OMC)Co(PPh_3)	(octamethylcorrolato) cobalt (III) triphenylphosphine
OMTX-PC	tri-X-phenyl octamethylcorrole
OTE	Optically transparent working electrode
PEEK	Polyetheretherketones
PET	Poly(ethyleneterephthalate)
PhCN	Benzonitrile
^{31}P NMR	Phosphorus NMR
PPh_3	Triphenylphosphine

RE	Reference electrode
Redox	Electron transfer reaction involving either oxidation or reduction
RX	Aryl- or alkyl-halides (R = CH_3 etc X = Cl, Br etc.)
SCE	Saturated calomel electrode
TBAP	Tetrabutyl ammonium perchlorate
$TBAPF_6$	Tetrabutyl ammonium hexafluorophospate
TEAP	Tetraethyl ammonium perchlorate
THF	Tetrahydrofuran
TPP	Tetraphenylporphirin
UHP	Ultra High Purity
UV-Vis	Ultraviolet-Visible Spectroscopy
WE	Working electrode

CHAPTER 1 INTRODUCTION

In this chapter, a review of some electrochemical principles necessary to be considered when one is performing an electrochemical experiment (i.e. mass transport and its modes, and double layer structure) is presented. A review of the theory on electrochemical studies of cobalt inorganic and organometallic compounds, electrochemical flow cells, and a theory of electrocatalysis is also presented.

1.1 PRINCIPLES OF ELECTROCHEMISTRY

The electrochemical reaction is a heterogeneous electron transfer. It takes place at the interface between the electrode and the solution. Only redox active species present at the interface can undergo this electron transfer. The electrochemical reaction at the interface makes the composition in the nearby solution different from the bulk of the solution further away. Because the solution tends to become homogeneous, redox active species diffuse between the bulk and the perturbed zone, in which the reactant is depleted, widens. Convection due to heating or stirring makes the solution rapidly more homogeneous, thus reducing this zone from about 100 μm to less than 1 μm [1].

Unlike most spectroscopic methods, electrochemical measurements are actually made on only a minute fraction of the sample confined to a highly inhomogeneous environment, the electrode-solution interface. The coupling and interplay within this region of such phenomena as interfacial charge transfer, diffusional mass transfer, adsorption, chemisorptions, homogeneous phase chemical reaction, convection and dissolution can cloud the interpretation of electrochemical data and discourage the practically minded analyst. On the other hand, electrochemistry offers an invaluable tool for fundamental investigation of these processes, each of importance in its own right. In either case, the ultimate success of the experimenter will depend on a firm grasp of the underlying physical principles [2].

The interface between an electrolyte solution and an electrode has come to be known as the electrical double layer [2]. The double layer is much thinner than the diffusion layer because it is only a few molecular layers thick. Under the applied potential, the liquid and solid

layers are charged at their interface. Heterogeneity is a common thread binding all electroanalytical methods. The act of placing an electrode in contact with a solution creates a phase boundary that differentiates identical solute molecules into two types; those at a distance from the electrode and those close enough to participate in the fascinating mutual interactions known collectively as electrochemistry. This is not a trivial distinction, for often it is the bulk-phase properties alone which are of analytical concern [2].

Imagine, for example, a positively polarized mercury surface immersed in a solution of sodium chloride. In this case, the positive electrode surface attracts the negative chloride ions because of electrostatic action, van der Waals' forces, and specific chemical effects. As a result, a layer of essentially non-hydrated chloride ions will accumulate very close to the electrode surface, forming what is known as the *inner Helmholtz layer*. Because of the presence of this negatively charged chloride ions, a double layer is said to exist. Just beyond this layer is a second layer of tightly held hydrated chloride ions, a layer that marks the boundary of the *outer Helmholtz layer*. Beyond this a *diffuse layer* extends with a net charge whose ionic atmosphere contains ions of one sign in excess of their normal concentration and those of the other sign in defect [3]. This assemblage of charged layers is commonly referred to as simply the double layer (Fig. 1.1).

The simplest reactions involve only mass transfer of a reactant to the electrode, heterogeneous electron transfer involving non adsorbed species and mass transfer of the product to the bulk solution. Mass transfer, the movement of material from one location in solution to another arises either from differences in electrical or chemical potential at the two locations or from movement of a volume element of solution. The modes of mass transfer are [4]:

1. Migration: movement of a charged body under the influence of an electric field (a gradient of electrical potential).
2. Diffusion: movement of a species under the influence of a gradient of chemical potential (i.e. a concentration gradient).
3. Convection: stirring or hydrodynamic transport. Generally fluid flow occurs because of natural convection (convection caused by density gradients) and forced convection, and may be characterized by stagnant regions, laminar flow, and turbulent flow.

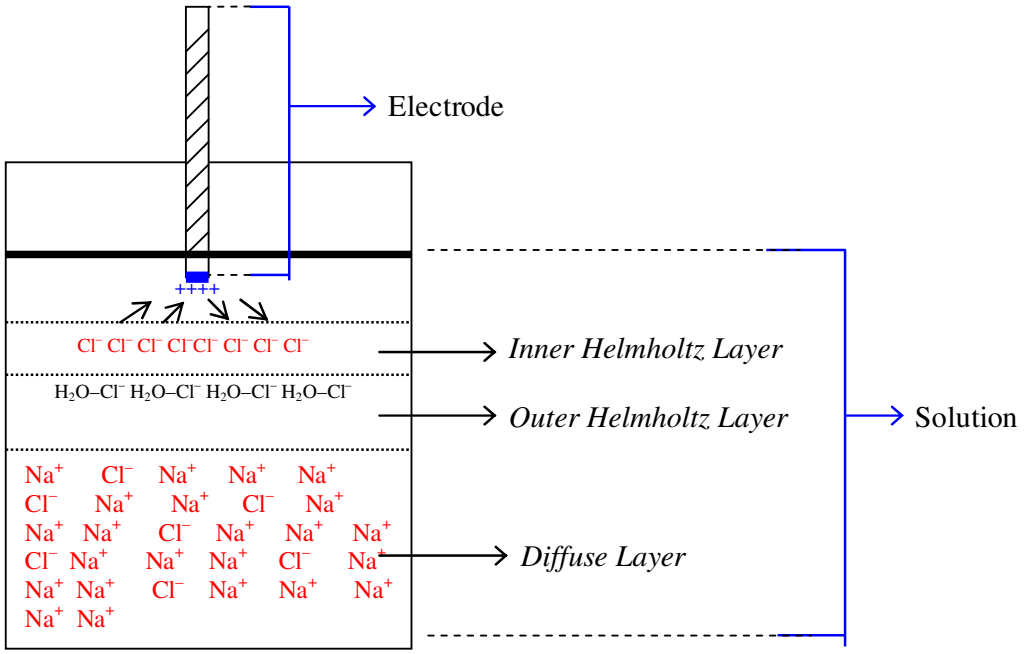

Figure 1.1 Structure of an electrical double-layer.

Mass transfer to an electrode is governed by the Nernst-Planck equation, written for one-dimensional mass transfer along the x-axis as [4]:

$$J_i(x) = -D_i \frac{\delta C_i(x)}{\delta x} - \frac{z_i F}{RT} D_i C_i \frac{\delta \phi(x)}{\delta x} + C_i v(x) \qquad (1.1)$$

where $J_i(x)$ is the flux of species i (mol $s^{-1}cm^{-2}$) at distance x from the surface, D_i is the diffusion coefficient (cm^2 s^{-1}), $\delta C_i(x)/\delta x$ is the concentration gradient at distance x, $\delta \phi(x)/\delta x$ is the potential gradient, z_i and C_i are the charge (dimensionless) and the concentration (mol.cm^{-3}) of species i, respectively, and $v(x)$ is the velocity (cm s^{-1}) with which a volume element in solution moves along the axis. The three terms on the right-hand side represent the contributions of diffusion, migration, and convection, respectively, to the flux [4].

A rigorous solution is generally not very easy when all three forms of mass transfer are in effect; hence electrochemical systems are frequently designed so that one or more of the contributions to mass transfer are negligible. For example, the migrational component can be reduced to negligible levels by addition of an inert electrolyte (a supporting electrolyte)

at a concentration much larger than that of the electroactive species. Convection can be avoided by preventing stirring and vibrations in the electrochemical cell [4].

In the bulk of solution (away from the electrode), concentration gradients are generally small, and the total current is carried mainly by migration [4] where all charged species contribute. For species *j* in the bulk region of a linear mass-transfer system having a cross-sectional area *A*, $i_j = i_{m,j}$

$$i_j = \frac{z^2{}_j F^2 A D_j C_j}{RT} \cdot \frac{\delta\phi}{\delta x} \tag{1.2}$$

where i_j is the current component at any value of *x* arising from a flow of species *j* and $i_{m,j}$ is the migration current of species *j*.

In migration, the driving force responsible for moving the species to (or away from) the electrode surface is the force exerted on a charged particle by a potential gradient existing in the body of the solution. Thus, for example, a potential gradient in an electrolytic solution will cause a current to flow within the body of the solution such that negative species will move one way, positive the other, and neutral species will remain unaffected. The rate of movement of a charged particle depends upon the magnitude of its charge, size, degree of hydration, etc. In conductometric measurements, migration is the sole factor that limits the current. In other cases, such as polarography, it is desirable to eliminate the contribution of migration, and this is accomplished by addition of an excess (about 100-fold) of an inert electrolyte that, in turn, decreases the potential gradient to a value sufficiently small so that diffusion and/ or convection processes becomes current-limiting [3]. In general, it simplifies the mathematical treatment of electrochemical systems by elimination of the $\delta\phi/\delta x$ term in the mass transport equation [4].

Although migration carries the current in the bulk solution during electrolysis, diffusional transport occurs in the vicinity of the electrodes, because concentration gradients of the electroactive species arise there. Indeed, under some circumstances, the flux of electroactive species to the electrode is due almost completely to diffusion [4].

In many respects, the simplest and best understood process influencing electrochemistry is diffusion. Diffusion is a factor virtually in every type of electroanalytical measurement, yet it is most often introduced as a set of elemental laws, devoid of physical significance [2]. This transport mode has its origin in a gradient of chemical potential or, more simply, in a concentration gradient. Thus, if the concentration of the species in the bulk of the solution is greater than its concentration at the electrode surface (because of the electrode reaction), the species will tend to diffuse from the bulk of the solution towards the electrode surface. Whereas the direction of diffusion is from the regions of larger to smaller concentrations, its rate is proportional to the magnitude of the concentration differences and to certain characteristic properties of the diffusing species and medium. Three types of diffusion transport exist, mainly linear, cylindrical and spherical diffusion. Diffusion that takes place in a single direction (diffusion to a plane surface) is termed linear diffusion and is mathematically and experimentally the simplest case [3].

Depending on the size of the electrode and the volume of electrolytic solution used, one can distinguish between three limiting cases of diffusion. The simplest case is an electrode in a thin-layer cell with a very low ratio of cell volume to electrode surface. Under these conditions mass transport within the cell is negligible and diffusion is the only mode of mass transport. By reducing the ratio between the electrode surface and the electrolyte volume, one approximates the normal situation of a voltammetric experiment with semi-infinite planar diffusion. With the transition to extremely small electrode surfaces, the conditions change yet again, and the diffusion process becomes dependent on the size and geometry of the electrode [5].

As one might expect, the voltammetric current-voltage curves of these three cases differ markedly. In the case of a thin electroactive layer, the cathodic and anodic waves appear as perfect mirror images. “Normal” electrodes produce the characteristic cyclic voltammograms, and extremely small electrodes (ultramicroelectrodes) yield steady-state current-voltage curves, which resemble the classic polarograms as well as the current-voltage curves of rotating electrodes (Figure 1.2) [5].

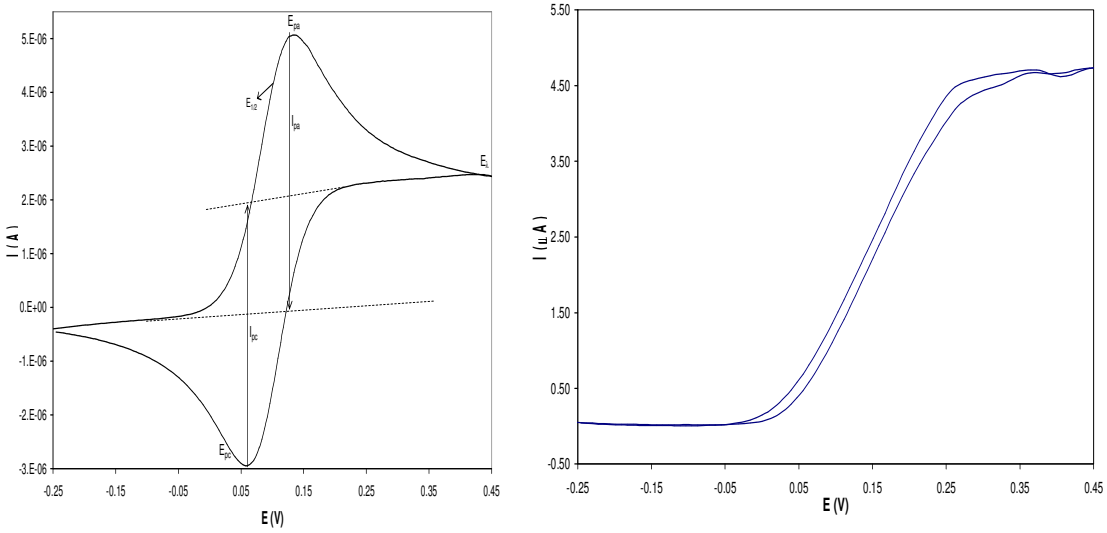

Figure 1.2 Typical voltammetric current-voltage curves. Left: for a semi-infinite diffusion obtained using a "normal" electrode; right: for semi-infinite hemispheric diffusion obtained using extremely small electrodes (ultramicroelectrodes). E_λ = switching potential, $E_{1/2}$ = half-wave potential, E_{pa} and E_{pc} = anodic and cathodic peak potential, I_{pa} and I_{pc} = anodic and cathodic peak current. A typical curve obtained in thin-layer solution can be obtained from Ref [5].

Convection is accomplished whenever the solution bearing the species is stirred into the path of the electrode. This is often called hydrodynamic transport. This stirring action increases the rate of transport of the species to the electrode and quantitative treatment of this mode of mass transport is exceedingly difficult. Convection is frequently employed in electroanalytical techniques (examples include the rotating electrode, mercury electrodes, vibrating electrodes, and even the stirring action employed at the working electrode in coulometric titrations, etc.), because of its increased sensitivity. Frequently one must resort to the use of empirical expressions in the interpretation of these techniques [3].

1.2 ELECTROCHEMISTRY OF COBALT INORGANIC AND ORGANOMETALLIC COMPOUNDS

Most electrochemical studies of cobalt were mainly for analytical purposes; simultaneous determinations of cobalt, nickel, copper and so on were shown to be possible by using complexing agents. The modern trend in the field of polarography of cobalt was to establish the relationship between the structures or bonding types of cobalt complexes and their electrode processes; this was because cobalt complexes, among transition metal complexes, are large in number and exhibit substantial variety in their bonding nature from compound

to compound. In these studies, non-aqueous polarography attracted special attention and promised to provide clues for the elucidation of electron transfer mechanisms of the electrode reactions and their correlation to the electronic configuration of a great variety of mixed ligand complexes [6].

The most striking feature of non-aqueous polarography is that, by adopting aprotic non-aqueous solvents, the Co(III) complexes, which would otherwise lead to a loss of ligands in the lower oxidation states of cobalt, are reduced in a stepwise fashion with a complete retention of the original configuration. For example, the pathway Co(III) → Co(II) → Co(I) → Co(0) takes place without a loss of ligands in aprotic solvents, although the appropriate valence orbital are, of course, delocalized over the entire complex molecule [6].

Voltammetric techniques such as current-controlled oscillopolarography, cyclic voltammetry, controlled-current or –potential electrolytic studies, and investigations of anodic oxidation have attracted much attention in the field of electrochemistry of cobalt as powerful tools, along with classical or conventional polarographic and chronopotentiometric studies, for probing the redox processes of the Co(III)/Co(II) and Co(II)/Co(I) couples in solution. This is partly because a number of electrode processes of an inert-inert type with π-electron systems, which were recently discovered for π-bonded cobalt complexes in organic solvents, made it possible to follow structurally the fate of the electrolyzed cobalt complexes in solution, not only in the reduction process but also in the counter process of oxidation with auxiliary instrumental methods of measurements such as ESR, NMR and magnetic susceptibility [6].

The electrode processes of the completely “inert-inert” or “inert-labile” types are the ones in which it is easiest and simplest to determine the assignments of the polarographic waves. The terms “inert” and “labile” are used with regard to the “lability” of ligands bound to the cobalt towards solvolysis, i.e., the ligand exchange reactions with solvent molecules, whilst the terms as defined by Taube [7] are independent of the nature of the medium. For either extreme case this consists of the complex remaining structurally intact or, alternatively, undergoing a rapid dissociative equilibrium upon reduction. Moreover, the complete retention of the structures in non-aqueous media makes it possible to relate the structures in both the oxidized and reduced forms to the redox reaction of the electrode processes. For this reason cyclic voltammetry or controlled-current oscillopolarography are powerful

methods not only for the examination of the reversibility of the electrode reaction, but also for the identification of the cobalt species responsible for the conventional polarographic waves. Here the interpretation is facilitated because the cathodic reductions can be observed and compared with the anodic oxidations in the same experiment [6].

The electrochemical studies of cobalt complexes with tetraphenylporphirins (TPP) are well documented in the literature [6, 8–13]. The electrochemical behaviour of cobalt (II) complexes with tetraphenylporphirins was studied by cyclic voltammetry. The [Co^{II}TPP] complex and its products, which were obtained by its controlled-potential electrochemical oxidation, were studied by electrochemical spin resonance (ESR) spectra. The first oxidation occurred at E_p = + 0.52 V, on the central Co(II) atom and all subsequent oxidations occurred at the TPP ligand. The potentials of the central cobalt (II) oxidation showed a linear dependence on the third ionization potential of the ion, whereas the ligand oxidation potentials were approximately independent of the cobalt (II) ion. This distinguishes between the cobalt oxidation change and ligand oxidation [6, 8]. Cyclic voltammogram distinctly showed three one-electron reversible steps [8]:

$$[Co^{II}(TPP)] \xleftrightarrow{+0.52\,V} [Co^{III}(TPP)]^{+} \quad (1.3)$$

$$[Co^{III}(TPP)]^{+} \xleftrightarrow{+1.19\,V} [Co^{III}(TPP)]^{2+} \quad (1.4)$$

$$[Co^{III}(TPP)]^{2+} \xleftrightarrow{+1.42\,V} [Co^{III}(TPP)]^{3+} \quad (1.5)$$

On the other hand, the free ligand H_2TPP gave two one-electron irreversible oxidation steps [8]:

$$[H_2TPP] \xleftrightarrow{+1.00\,V} [H_2TPP]^{+} \xleftrightarrow{+1.20\,V} [H_2TPP]^{2+} \quad (1.6)$$

The voltammetric behaviour of cobalt (II) with chloro-N-methyl-$\alpha,\beta,\gamma,\delta$-tetraphenylporphirins ($ClNCH_3TPP$) was studied by cyclic voltammetry [9]. The half-wave potentials for the reversible metal oxidation in acetonitrile occurred at 0.77 V for Co(II) – Co(III) (all $E_{1/2}$ values were reported vs. Ag | AgCl). Following the oxidation of the metal centre, the porphirin ligands were oxidized. The half-wave potentials for oxidation of the tetraphenylporphirin ligand in $ClNCH_3TPP$ occurred at 1.30 and 1.60 V. The ligand oxidations for the N-methyltetraphenylporphirin complexes in general were found at E_p

values of 1.2 – 1.3 and 1.4 – 1.6 V. The cyclic voltammogram of the corresponding zinc (II) complex was recorded to verify the assignment of metal centre and ligand oxidation. The oxidation of the ClZnN-CH_3TPP complex occurred at 1.05 and 1.5 V with no wave appearing in the region 0.0 – 0.9 V. Cyclic voltammetry of $\alpha,\beta,\gamma,\delta$-tetraphenylporphinatocobalt (II) in benzonitrile with 0.10 M tetraphenyl ammonium perchlorate gave the values $E_{1/2}$ = 0.50 V [Co(II) – Co(III)], 1.19 V (ligand oxidation), and 1.6 V (ligand oxidation) [9], agreeing reasonably with the literature values of 0.52 V, 1.19 V and 1.42 V [8].

The electrochemistry of five- and six-coordinate cobalt (III) δ-bonded porphyrins was reported in pyridine (py), tetrahydrofuran (THF), and methylene chloride (CH_2Cl_2) containing 0.1 M tetrabutyl ammonium perchlorate (TBAP) or 0.1 M tetrabutyl ammonium hexafluorophosphate ($TBAPF_6$) as supporting electrolyte [10]. Each complex undergoes up to two reductions and two oxidations, all of which occur at the porphyrin π ring system. Cyclic voltammogram of (TPP)Co(CH_3) and (TPP)Co(CH_2Cl_2) each revealed two reversible one-electron oxidations and a single one-electron or multi-electron reduction within the potential range of the solvent. The singly reduced (TPP)Co(CH_2Cl) and (TPP)Co(C_2H_5) complexes were stable in THF, but this was not the case for (TPP)Co(CH_3), which revealed two one-electron waves in this solvent. Electrooxidized, (TPP)Co(CH_3) and (TPP)Co(CH_2Cl) were relatively stable in CH_2Cl_2 on the conventional cyclic voltammetry time scale, and both neutral derivatives were characterized by two well-defined one-electron oxidations at potentials of 0.96 and 1.19 V. Cyclic voltammogram of (TPP)Co(C_2H_5)(py) in pyridine showed one irreversible oxidation at E_p = 0.81 V and one irreversible reduction at E_p = – 1.49 V leading to the formation of $[(TPP)Co(py)_2]^+$ and $[C_2H_5N(C_2H_5)]^+$ [10].

Cyclic voltammetry and controlled-potential electrolysis were used to investigate the electrochemical reduction of $CoBr_2$ in dimethylformamide (DMF) and DMF + pyridine mixtures [14]. Cyclic voltammogram of $CoBr_2$ at a platinum electrode displayed an irreversible reduction wave at – 1.17 V versus SCE. The reduction of Co(II) led to a Co(I) species at – 1.4 V. On the time scale of slow cyclic voltammetry or of an electrolysis, Co(I) led to solid Co(0) and Co(II) by disproportionation. The regeneration of Co(II) was effective until its total consumption, which required two electrons per molecule. After the scan rate was increased, a second reduction wave appeared at – 1.75 V, and it was assigned to the product generated at – 1.4 V. As the scan rate was increased, the disproportionation reaction

was progressively kinetically frozen and more Co(I) remained in the diffusion layer when its reduction potential was reached (E = – 1.75 V), the reduction of Co(I) also led to solid Co(0). The electrochemical reactions were as follows [14]:

E = – 1.4 V: E $Co^{II}X_2 + e^- \leftrightarrow Co^{I}X + X^-$ (1.7)

C $2Co^{I}X \rightarrow Co(s) + Co^{II}X_2$ (1.8)

E $Co^{II}X_2 + e^- \leftrightarrow Co^{I}X + X^-$ (1.9)

E = – 1.75 V: $Co^{I}X + e^- \rightarrow Co(s) + X^-$ (1.10)

The electrochemical behaviour of $CoBr_2$ was also studied in acetonitrile and pyridine mixtures in the presence of allyl acetate (1 molar equivalent vs. $CoBr_2$) and increasing amounts of ethyl 4-iodobenzoate [15]. In the absence of aromatic halide the voltammogram exhibited two successive reduction waves. The first wave occurred at -1.3 V ascribed to the reduction of Co(II) to Co(I) followed by fast complexation with allyl acetate which led to (η^2-allylOAc)cobalt(I), the latter complex being more stable than the original Co(I) and giving rise to a reoxidation wave Co(II). The resulting (η^2-allylOAc)cobalt(I) was reduced at the second reduction wave E_p = -1.5 V to (η^2-allylOAc)cobalt(0). In the presence of ethyl 4-iodobenzoate, the intensity of the wave at -1.3 V increased and reached a maximum (twice the initial intensity), and the oxidation wave for Co(II) decreased [15].

The first oxidative electrochemistry of cobalt (III) corroles was reported in THF, DMF, benzonitrile (PhCN), and CH_2Cl_2 containing 0.10 M TBAP as supporting electrolyte [16]. The investigated compound was represented as (OMC)Co(PPh_3) where OMC was the trianion of 2,3,7,8,12,13,17,18-octamethyl corrole. The CV of the complex revealed up to three oxidations and two reductions waves depending upon solvent. The (OMC)Co(PPh_3) complex revealed three one-electron reversible oxidations in PhCN at high scan rate, the number of abstracted electrons was calculated by controlled-potential coulometry as well as by analysis of the current-voltage curves obtained by cyclic voltammetry. The first oxidation occurred at 0.19 V in PhCN while the latter two processes occurred at 0.76 and 1.54 V. The first two one-electron waves were reversible at all scan rates, but the third oxidation became irreversible at lower scan rates (0.5 V/s). (OMC)Co(PPh_3) complex showed three one-electron oxidations in CH_2Cl_2, at 0.18 V, 0.80 V and 1.68 V. (OMC)Co(PPh_3) complex showed two one-electron oxidations in THF and DMF at 0.30 V,

0.80 V (THF) and 0.25 V, 0.83 V (DMF) respectively. The electrochemical reactions were as follows [16]:

$$(OMC)Co^{III}(PPh_3) \leftrightarrow [(OMC)Co^{III}(PPh_3)]^{+} + e^{-} \quad (1.11)$$

$$[(OMC)Co^{III}(PPh_3)]^{+} \leftrightarrow [(OMC)Co^{III}(PPh_3)]^{2+} + e^{-} \quad (1.12)$$

$$[(OMC)Co^{III}(PPh_3)]^{2+} \leftrightarrow [(OMC)Co^{III}(PPh_3)]^{3+} + e^{-} \quad (1.13)$$

Complexes of (5,10,15-tri-X-phenyl-2,3,7,8,12,13,17,18-octamethylcorrolato)cobalt(III) triphenylphosphine, (OMTX-PC)Co(PPh_3), where X = *p*-OCH_3, *p*-CH_3, *p*-Cl, *m*-Cl, *m*-F, *o*-Cl, *o*-F, or H, were synthesized and characterized in non-aqueous media using electrochemical, spectroelectrochemical, and EPR techniques [17]. Each cobalt (III) derivative showed two one-electron reductions, the first of which involved a Co(III)/Co(II) conversion and concomitant loss of the bound PPh_3 ligand. Four one-electron oxidations were also observed for the investigated compounds, and this contrasts with the oxidative properties of related cobalt (II) porphyrins which revealed a maximum of three one-electron oxidation waves under similar conditions. The first one-electron oxidation of each cobalt(III) corrole was metal-centred and resulted in formation of Co(IV) corrole as ascertained by EPR spectroscopic characterization of the electrogenerated species [17].

The fact that Co(III) corroles can undergo four one-electron oxidations was not previously reported, but presumably this reaction might also occur for (OMC)Co(PPh_3) at very positive potentials, i.e., at values of $E_{1/2}$ greater than 1.9 V vs. SCE in 0.2 M TBAP in PhCN [17]. The fourth oxidation of (OMTXPC)Co(PPh_3) was quasi-reversible for all eight compounds investigated in that study, and this reaction was not examined in detail due to its proximity to the anodic potential limit of the solvent. However, comparison of cyclic voltammograms of (OMT*p*-ClPC)Co(PPh_3) [$E_{½}$ = 0.31, 0.85, 1.45, and 1.8 V] and (T*p*-ClPP)Co(PPh_3) [$E_{½}$ = 0.30, 1.2, and 1.5 V] seemed to rule out the forth oxidation state as involving the bound phosphine ligand, since the fourth oxidation state was not present on a cyclic voltammogram of (T*p*-ClPP)Co(PPh_3). Further comparison of the (OMT*p*-ClPC)Co(PPh_3) and (T*p*-ClPP)Co(PPh_3) voltammograms showed that the first one-electron oxidation of both macrocycles occurred at virtually the same potential, i.e., + 0.31 V for the corrole and + 0.30 V for the porphyrin. The first oxidation of the neutral porphyrin corresponded to the

Co(II)/Co(III) electrode reaction, while that of the corrole was assigned to the Co(III)/Co(IV) reaction [17].

Complexes of the type [Co(CO)L(η-C_5H_5)] (where L = $P(C_6H_{11})_3$ or PPh_3) were studied by cyclic voltammetry and shown to undergo one-electron oxidation to the radical cations $[Co(CO)L(\eta\text{-}C_5H_5)]^+$. The CV of the complex [Co(CO){$P(C_5H_{11})_3$}(η-C_5H_5)] showed a reversible one-electron oxidation in CH_2Cl_2 at a platinum electrode [18]. The other compounds studied were similarly well behaved except for [Co(CO)(PPh_3)(η-C_5H_5)] which displayed a tendency to deposit a film on the platinum electrode during oxidation in CH_2Cl_2. For this compound the electrode had to be cleaned after every scan; the oxidation potential, $E°$, was estimated at 0.13 V. In THF the voltammetry was cleaner ($E°$ = 0.21 V) but the oxidation was not as chemically reversible. In addition, there was a second irreversible wave at 0.75 V, which was not present in CH_2Cl_2. Since the new wave was peculiar to THF it was believed to be due to the oxidation of the solvated radical cation $[Co(CO)(PPh_3)(THF)(\eta\text{-}C_5H_5)]^+$ to the diamagnetic dication [18].

The compound $[Co(CO)_2(\eta\text{-}C_5H_5)]$, was also studied in the presence of added $[Fe(\eta\text{-}C_5H_5)_2][PF_6]$. When $[Fe(\eta\text{-}C_5H_5)_2][PF_6]$ ($E°$ = 0.43 V) was added to $[Co(CO)_2(\eta\text{-}C_5H_5)]$ ($E°$ ~ 0.97 V) in CH_2Cl_2, no reaction occurred on the basis of $E°$ values [18]. In the presence of PPh_3, however, rapid oxidation occurred at room temperature to give $[Co(PPh_3)_2(\eta\text{-}C_5H_5)][PF_6]$. It must be noted that neither the ferricinium ion nor the dicarbonyl undergone detectable reactions with PPh_3 at room temperature. This means that the formation of $[Co(PPh_3)_2(\eta\text{-}C_5H_5)][PF_6]$ must, therefore, occur via the mechanism shown in equation 1.14 to 1.16 below [18].

$$[Co(CO)_2(\eta - C_5H_5)] + PPh_3 \leftrightarrow [Co(CO)(PPh_3)(\eta - C_5H_5)] + CO \quad (1.14)$$

$$[Co(CO)(PPh_3)(\eta - C_5H_5)] \leftrightarrow [Co(CO)(PPh_3)(\eta - C_5H_5)]^+ \quad (1.15)$$

$$[Co(CO)(PPh_3)(\eta - C_5H_5)]^+ + PPh_3 \leftrightarrow [Co(PPh_3)_2(\eta - C_5H_5)]^+ + CO \quad (1.16)$$

Electrochemical behaviour of $[\{Co(\mu\text{-}NO)(\eta\text{-}C_5H_5)\}_2][PF_6]$ was obtained in CH_2Cl_2 by cyclic voltammetry [19]. The compound was reduced to $[\{Co(\mu\text{-}NO)(\eta\text{-}C_5H_5)\}_2]$ at 0.34 V, and oxidized to $[\{Co(\mu\text{-}NO)(\eta\text{-}C_5H_5)\}_2]^{2+}$ at 1.17 V. The cyclic voltammogram also showed a second, irreversible, reduction wave at – 1.40 V. However, the peak current appeared

larger than those of the other redox processes described above, but the wave was close to that of the base electrolyte and may correspond to the initial formation of $[\{Co(\mu\text{-}NO)(\eta\text{-}C_5H_5)\}_2]^-$. In the presence of PPh_3, $[\{Co(\mu\text{-}NO)(\eta\text{-}C_5H_5)\}_2]$ was un-reactive but underwent instant metal-metal bond cleavage to give $[Co(PPh_3)(NO)(\eta\text{-}C_5H_5)]^+$. The voltammogram of $[\{Co(\mu\text{-}NO)(\eta\text{-}C_5H_5)\}_2][PF_6]$ revealed a one-electron reduction wave at 0.34 V corresponding to the couple $[\{Co(\mu\text{-}NO)(\eta\text{-}C_5H_5)\}_2]^+ - [\{Co(\mu\text{-}NO)(\eta\text{-}C_5H_5)\}_2]$. On adding one equivalent of PPh_3 a reaction occurred to give an orange-brown solution, a voltammogram showed another wave at – 0.43 V, due to the irreversible one-electron reduction to $[Co(PPh_3)(NO)(\eta\text{-}C_5H_5)]^+$ [19].

The halogen-bridged tricobalt clusters, $[Co_3Cp_3(\boldsymbol{\mu}_3\text{-}CPh)_2(\boldsymbol{\mu}\text{-}Cl)]PF_6 \cdot MeCN$ (**2**), $[Co_3Cp_3(\boldsymbol{\mu}_3\text{-}CPh)_2(\boldsymbol{\mu}\text{-}Br)]SbF_6$ (**3**), and $[Co_3Cp_3(\boldsymbol{\mu}_3\text{-}CPh)_2(\boldsymbol{\mu}\text{-}I)]SbF_6 \cdot CH_2Cl_2$ (**4**), were obtained from a reaction of a benzylidyne-capped tricobalt cluster, $[Co_3Cp_3(\boldsymbol{\mu}_3\text{-}CPh)_2]$ (**1**), with halogens ($X_2 = Cl_2$, Br_2 and I_2) in CH_2Cl_2. The compounds were characterized by X-ray diffraction, UV-Vis absorption spectra and cyclic voltammetry [20]. In a cyclic voltammogram of **1** in 0.1 M BuNCl/MeCN an oxidation wave was observed at $E_{pa} = -0.01$ V, for the oxidation of **1** to $\mathbf{1}^+$. On scan reversal an irreversible reduction wave appeared at $E_{pc} = -0.45$ V. The complexes, $\mathbf{2}^+$, $\mathbf{3}^+$, and $\mathbf{4}^+$ were studied by CV in CH_2Cl_2 with 0.1 M Bu_4NPF_6. In the oxidation of $\mathbf{2}^+$, a chemically reversible oxidation wave was observed at E_{pa} = 0.75 V versus Fc/Fc^+. Very similar oxidation waves to those of $\mathbf{2}^+$ were observed for $\mathbf{3}^+$ and $\mathbf{4}^+$. In the second scan, new redox waves were observed at $E_{pa} \sim 0.0$ V, which indicated that the oxidized species of **2** and **3** decompose slowly on a CV time-scale. In CH_3CN, $\mathbf{4}^+$ showed similar redox responses to those observed in CH_2Cl_2, but the oxidation waves of $\mathbf{2}^+$ and $\mathbf{3}^+$ were irreversible showing an E_{pa} of 0.71 and 0.72 V, respectively [20]. Reduction processes of the complexes in CH_2Cl_2 also resemble each other. An irreversible reduction wave was observed in the potential region of – 0.57 to – 0.60 V. The irreversible reduction of each complex exhibited a new chemically reversible redox couple at $E_{1/2} = -0.05$ V, which was the same as the oxidation potential of **1**. These results suggested that the reduction of the halogen-bridged complex reproduced the parent complex **1** [20].

The electrochemical properties of the redox mediator Co(III)/Co(II)$(dbbip)_2$ (dbbip = 2,6-bis(1'-butylbenzimidazol-2'-yl)pyridine) in a mixed acetonitrile/ethylene carbonate solvent have been studied by a range of techniques in order to determine the rate constants for electron transfer and the diffusion coefficients of the Co(II) and Co(III) species [21]. Cyclic

voltammogram of Co(II)$(dbbip)_2^{2+}$ in a mixture of 60 % ethylene carbonate/40 % acetonitrile at a Pt disk electrode revealed a quasi-reversible electrode process at E_p = 0.39 V, assigned to the couple Co(III)/Co(II). A plot of the peak current density, $j_{p,ox}$ versus the square root of the scan rate was used to estimate the diffusion coefficient of the Co(II) complex. The plots gave a value of 1.9×10^{-6} cm^2s^{-1} for the diffusion coefficient of the bulky Co(II)$(dbbip)_2^{2+}$ in the mixed solvent. The diffusion coefficient of Co(III) complex ion was obtained using Fick's first law and found to be equal to 1.1×10^{-6} cm^2/s^{-1} [21].

The electrochemical behaviour of monomeric [$Co_2(CO)_6$(alkyne)] derivative is well known [22]. At room temperature a one-electron diffusion controlled reduction process occurred at E_p = – 1.0 V and was followed by a fast chemical complications in CH_2Cl_2 at a Pt electrode. The chemical reversibility of the first process was enhanced by electron-withdrawing substituents (e.g. CF_3) or, to a lesser extent, by sterically demanding alkyne substituents [22]. At ambient temperatures [{$Co_2(CO)_6$}$_2$(PhC≡C–C≡CPh)] in CH_2Cl_2 the complex undergone an apparent single two-electron reduction at E_p = – 0.94 V and another ill-defined reduction wave was observed further at less negative potentials of ~ – 1.16 V. It was found that a fast chemical decomposition following the reduction prevented proper electrochemical analysis. It was also found that the two-electron peak at – 0.94 V gradually split into two one-electron peaks as the temperature was lowered. At – 80 °C both waves became reversible, as chemical complications were completely quenched, so that full chemical reversibility was achieved, as shown by the directly associated re-oxidation peaks [23].

1.3 THEORY OF ELECTROCHEMICAL FLOW CELLS

Detectors based on interactions between matter and an electrical current are another group of major detection systems in FIA [24]. Electrochemical detection relies on the transfer of electroactive species to the sensing surface. Because the sensor can only respond to species in its vicinity, their concentration should be representative of the average concentration in the bulk sample. This is strongly dependent on the characteristics of the hydrodynamic system and flow–cell used. Thus, the flow should be fully uniform, pulse–free, and the contact time of samples and standards with the sensor should be exactly the same. Kinetic

discrimination of any side reactions taking place at the sensor surface has a very favourable effect on selectivity [24].

The main assets of these detectors are their high sensitivity and selectivity which they exhibit over wide concentration ranges [24]. Unlike optical detectors, they measure no solution property, but rather respond to phenomenon occurring at the electrode surface; as a result, they are better candidates for miniaturization. Electrochemical detectors are compatible with a wide variety of cell shapes and volumes. Thus, some electrodes are embedded in the cell walls, other planar electrodes are adhered to them, and still others are of the open tubular type. Electrochemical flow cells are just as varied. They include the early cascading models, commercially available electrodes and recent designs with built–in electrodes. Also, electrodes can be placed in various positions (in the cavity, aligned with the flow direction, in combination with others such as ion–selective sensors for multi-determinations, etc.). In any case, the point measurement provided by electrodes should be representative of the mean analyte concentration in the sample [24].

The flow through electrochemical cell designed by Burguera and co-workers [25] was made from a polyethylene vial (45 cm long × 0.8 cm diameter filled with glass marbles) with an effective volume of 0.5 ml. Two parallel glassy carbon rods with a total surface of 1.5 cm^2 and of 2.0 cm^2 were used as working and counter electrodes, respectively. Between them, a 1.3 cm long Pt wire was inserted as a pseudo-reference electrode. To further reduce the inner volume of the cell to 0.5 ml, its body was filled with glass marbles of 2.0 mm of diameter [25].

A multianalyte flow electrochemical cell for boianalysis was constructed by Maestre and co-workers [26]. The upper and bottom parts of the cell were constructed from poly(methyl methacrylate), providing high-level precision for the assembly of both surfaces. The dimensions of the cell were 45 mm × 45 mm × 35 mm. A polyetheretherketone (PEEK) plastic gasket (0.10 mm thickness) between both parts determined a cell dead volume of 70 µL. The six working electrodes and the reference electrodes were located in the upper part. The inlet and the six outlets, corresponding to each working electrode, were placed in the bottom part of the cell. The radial arrangement of the working electrodes, all of which were equidistant from the inlet, guaranteed a laminar and identical hydrodynamic flow regime at the six electrodes. Next to each working electrode, but at the bottom block, the six outlets

were placed to prevent cross-talk from occurring and also to help contributing to identical hydrodynamic pressure across the electrodes. The location of the reference electrode, as well as the dimensions of the two platinum counter electrodes, prevented inadequate conductance of the cell solution. The reference electrode was an $Ag/AgCl_{sat}$ of the double liquid junction type. The refillable outer electrolyte solution served as salt bridge to prevent contamination of the reference element. This reference electrode was placed equidistantly from each working electrode [26].

A wall-jet electrochemical detector was designed and characterized by Jaenicke and co-workers [27]. The cell was manufactured from Perspex with an internal volume of ~ 4 cm^3. The working electrode was a glassy-carbon disk 3.0 mm diameter and 2.0 mm thickness (Tokai, Tokyo) which was press-fitted in a Teflon holder using an epoxy resin seal. The electrode was prepared by first polishing with abrasive paper (# 1200) followed by a final polish using 0.3 µm diamond paste until a mirror finish was obtained. A graphite disk (Johnson Matthey) with the same dimension as that of the working electrode was used as counter electrode. The reference electrode was Ag │AgCl │saturated KCl with a 'Dycor' polymer frit (Priceton Applied Research) as a liquid junction [27].

A modified Z-type flow-through cell for optical, electrochemical, and optoelectrochemical flow injection analysis measurements was designed and constructed by Haghighi and co-workers [28]. The body of the flow-through cell was machined from a block of Plexiglas. The flow cell had a 1 mm i.d. and was 20 or 10 mm long, so the volume of the cell was 16 or 8 µl, respectively. Two platinum sheets (0.1 mm thick) were placed on both ends of the flow cell. A 1 mm i.d. hole was provided in each of these platinum sheets for transmission of light. Both ends of the cell cavity were enclosed by two transparent glass windows. The two platinum sheets were used as working and auxiliary electrodes with an electrochemically active area of approximately 3 mm^2. The reference electrode, a saturated calomel electrode (SCE), was placed downstream in an overflow tube. The cell holder was made of aluminium and was designed on the basis of the shape of the cell compartments of the spectrophotometer. For spectrophotometric measurements in which organic solvent was passed through the flow cell, the body of the flow cell was machined from stainless steel [28].

The home-made electrochemical flow-through cell was designed and modified for flow injection analysis system by Masawat and co-workers [29]. The materials used were polymethylmethacrylate or Perspex (A.C.S. Xenon Company Ltd, Thailand) as a working block (19 mm thickness), stainless steel (Sahakol Machining, Chiang Mai, Thailand) as an auxiliary block, home-made poly(ethyleneterephthalate) or PET (23 – 25 µm thickness) as a spacer or gasket, 5H and 2B pencil lead (2 mm in diameter, Steadtler®) with only 5 mm each in length of pencil lead was connected with silver wire (1 mm in diameter, 5 cm in length) using conductive epoxy (Chemtronics®, USA) so that electrical contact can be made to the pencil lead working electrode, and a 1 mm in diameter, 5 cm in length of silver wire (99.9%, Prolabo, France) as a reference electrode. The Perspex body was drilled in the centre and then was inserted with a piece of pencil lead which was drilled in the small length at the other end. The silver wire was covered at one end with a small amount of conductive epoxy and was inserted immediately into the drilled hole to connect with a piece of pencil lead, then another silver wire was inserted in the drilled hole of Perspex body near the one which was inserted first [29].

A simple and versatile cell suitable for spectroscopic and spectroelectrochemical studies in the ultraviolet, visible, and infrared regions has been described [30]. Among the cell's generally beneficial traits are its continuously adjustable path length, high degree of chemical compatibility, ease of assembly and disassembly, and wide spectra range. Regarding SEC applications, the cell permits adequate control of the OTE (optically transparent working electrode) potential and exhibits a relatively short exhaustive electrolysis time. The cell body was constructed from threaded glass connectors and a Teflon stopcock assembly purchased from Ace Glass, Inc. The minimum liquid sample volume of the cell is ~10 mL when the minimum path length configuration is employed. A 10 mm × 13 mm platinum screen (Aesar, 80-mesh) welded to a Pt lead at the end of a sealed Pyrex tube was employed as the OTE in spectroelectrochemical studies. Platinum auxiliary and quasi-reference electrodes were isolated in fritted Pyrex tubes (Ace Glass, C porosity) [30].

Economou and co-workers have designed a thin layer electrochemical cell with a flow channel thickness of 0.2 mm, for the detection of Co(II) by chemiluminescence [31]. The flow cell consisted of a glassy carbon rod (3 mm in diameter) as a working electrode, a home-made Ag/AgCl as a reference electrode positioned opposite a working electrode and a

glassy carbon rod as a counter electrode was positioned downstream, near the outlet of the cell [31].

On-line electrochemistry/mass spectrometry was used to study the complex mechanism of electrochemical oxidation of N,N-dimethyl-p-phenylenediamine in aqueous electrolytes in the pH range 1.4 – 9.7 using a radial flow electrochemical cell [32]. The electrochemical flow cell consisted of two cylindrical Delrin blocks separated by a 50 µm Teflon spacer. The electrochemical flow cell consisted of a Pt disk electrode (1.6 mm diameter) as a working electrode pressed into the lower block. The electrolyte flowed in a radial, inward direction. The auxiliary and reference electrodes were both Ag | AgCl | 1 M KCl aqueous electrodes separated from the flow of the electrolyte by 2 µm PEEK frits. The volume of the compartment of the working electrode, which was the volume of electrolyte located between the working electrode and the wall of the central tube, was only 0.1 µL [32].

An electrochemical cell was developed to enable flow analysis with voltammetric detection using a hanging mercury drop electrode (HMDE) [33]. The flow cell was made from a piece of cylindrical extruded acrylic (Perpex) with a length of 2.5 cm and a diameter of 1.5 cm. The cylindrical piece was flattened at the bottom to allow the positioning of a Teflon support with a mirror for visual inspection of the mercury drop. A flow-channel was drilled through the Perpex with a diameter of 0.7 mm and a length of 1cm (volume 4 µL). The capillary of the working electrode was inserted in the flow cell from the top, perpendicular to the reference and counter electrodes. The reference electrode was a silver wire (1 cm length; 0.5 mm diameter) and the chloride in the seawater was used as a counter ion. The counter electrode was a platinum wire (1 cm length; 0.46 mm diameter). The counter electrode and reference electrode were inserted in 3 mm diameter nylon 6-6 screws and screwed into the Perpex cell with holes leading to the flow-cell [33].

The voltammetric flow cell was designed for operation in a manner compatible with FIA [34]. The flow cell was machined from a 7-mm thick Perspex plate. It had a volume of < 4 µL and accommodated three electrodes: the working electrode was a mercury hemisphere which protruded from the bottom of the flow channel; the reference electrode consisting of a Ag | AgCl wire bathed in saturated potassium chloride was placed in a Pasteur pipette with an asbestos fibre junction; the auxiliary electrode was a stainless steel syringe needle which also served as solution outlet. A suction pipette with an asbestos fibre junction; the auxiliary

electrode was held in place by a screw and silicone rubber washer. The distance between the inlet and the surface of the working electrode (*d*, ca. 3 mm) was a critical parameter and was, therefore, kept constant during all experiments [34].

Janata and co-workers have designed a flow-through cell and characterized it using the combination of FIA and cyclic voltammetry [35]. The flow cell consisted of a mercury microelectrode as a working electrode, a Ag | AgCl (in saturated KCl) as a reference electrode, a steel rod tube as an auxiliary electrode and outlet, a sample inlet, a mercury reservoir, and drop-size adjustment. The microelectrode was placed just below the orifice of the inlet tube. This arrangement ensured that any part of the sample plug comes into contact with the electrode surface only once. The replacement of the mercury drop was done by simply gently knocking off the old drop and then forming a new drop. The used up mercury was allowed to accumulate at the bottom of the cell compartment from where it was removed periodically [35].

1.4 THEORY OF ELECTRON TRANSFER CHAIN (ETC) CATALYSIS (ELECTROCATALYSIS) REACTIONS

Electrocatalysis or electron transfer chain (ETC) catalysis is the catalysis of reactions by electrons without net current flow (as opposed to redox catalysis, which means catalysis of reduction or oxidation by redox mediators, thus involving a net current flow) [36]. The theory of electrocatalysis was first applied to an organometallic system by Feldberg, who also set up the method of finite differences for the computer simulation of kinetic analysis of the electrochemical data [37].

ETC catalysis has been shown to be a very efficient way to perform organic, inorganic and organometallic reactions such as ligand exchange, isomerization, chelation, decomplexation, insertion, extrusion, and oxidative addition. The coupling of electrocatalysis with organometallic catalysis was also shown to be efficient for alkyne polymerization. The simplest organometallic reaction, ligand exchange, has been the most studied one [36].

Electrocatalysis has been efficiently practiced using either an electrode in a preparative electrolysis cell or a redox reagent as an initiator (electrocatalyst). It is thus extremely useful

to have at hand a library of redox reagents and knowledge of their redox potentials [38]. The chain induction can be affected by an oxidant (anode, 17e complex such as ferricinium, organic or inorganic oxidant) or by a reducing agent (cathode, 19e complex such as Cp_2Co or $CpFe(C_6R_6)$ (R = H or Me), or organic or inorganic reducing agent). Ligand exchange reactions have been electrocatalyzed for mono- and polynuclear complexes. Note that 19e intermediates or transition states are involved in both types of electrocatalysis induced by an oxidizing or by a reducing agent [36].

The principle of ETC catalysis involves an initiation step, which is induced by an electron or a hole of an electron [38]. This electron can be provided via an electrode or via a catalytic amount of a judiciously chosen redox couple. It is followed by the propagation step which may include many chemical steps. The cross electron transfer step closes the catalytic cycle regenerating the radical obtained at the first stage of the initiation step. Side reactions due to the high reactivity of 17- and 19-electron radicals may also disrupt the system at any stage [38].

Let us say for example, one wishes to check the electrocatalytic reaction A → B, say a ligand exchange reaction [36]. The cyclic voltammogram of a reactant A, gives a wave for A which may be reversible or not (at least a certain degree of reversibility should be observable on lowering the temperature and at high scan rate). In the presence of added ligand L^1, the CV of A will show the appearance of a new wave due to the reaction product, B ($A + L^1 \rightarrow B - L^2$). If the wave of A is a cathodic one ($A \rightarrow A^-$), setting the potential at this wave or scanning through this wave generates A^- in the vicinity of the cathode. This explains the observation of a CV wave for B. Meanwhile the wave for A is profoundly affected: since A^- reacts rapidly with L^1 to give B, its concentration in the neighbourhood of the cathode is strongly diminished and can reach zero (depending on the relative rates of the scan and of the propagation reaction of A^- with L^1). A is also consumed by the cross redox reaction ($A + B^- \rightarrow A^- + B$); hence, its intensity is also diminished. In this case the wave of B is located at a more negative potential than that of A. If a ligand exchange reaction is electrocatalyzed by a small anodic current, the CV wave normally observed in the absence of the ligand is modified in the presence of this ligand and a new wave due to the reaction product appears at a more positive potential. This behaviour is characteristic of electrocatalysis and gives an idea of the rate of both propagation steps [36].

Ligand substitution of metal carbonyls plays a key role in the catalytic sequences of a variety of important processes leading to carbon monoxide fixation. The conventional associative and dissociative mechanisms for such exchanges are usually considered to involve even-numbered, 16- and 18-electron intermediates [39]. Ligand exchange in metal carbonyls and their derivatives has received extensive mechanistic scrutiny. Electrocatalysis of ligand exchange is best illustrated by examining the effect of an extremely small anodic current upon solutions of metal carbonyls containing added nucleophiles [40].

The role of 19-electron intermediates or transition states in oxidatively induced electrocatalytic ligand exchange reactions was first demonstrated by Kochi [41], in his study of the manganese complex [$MeCpMn(CO)_2$]. The exchange of the ligands MeCN, pyridine, and THF by the less electron-releasing ligands phosphines, phosphates, and isonitriles is possible because cross ET propagation step is exergonic [41].

A cyclic voltammogram of $MeCpMn(CO)_2(MeCN)$ revealed a reversible one-electron wave at E_p = 0.22 V, in acetonitrile at a Pt microelectrode [41]. In the presence of PPh_3, a CV revealed another reversible one-electron wave at E_p = 0.55 V and the wave at E_p = 0.22 V for the reactant [R = $MeCpMn(CO)_2(MeCN)$] became irreversible. The anodic peak current for $MeCpMn(CO)_2(MeCN)$ continued to decrease in magnitude in proportion to the concentration of PPh_3, and the diffusion current fell to near zero in the presence of very high concentrations of PPh_3. It was concluded that addition of PPh_3 led to the substitution product [P = $MeCpMn(CO)_2(PPh_3)$], which occurred at E_p = 0.55 V. In other words the anodic process leading to the depletion of $MeCpMn(CO)_2(MeCN)$ away from the electrode surface, results in the concomitant formation of $MeCpMn(CO)_2(PPh_3)$. The electrochemical process involved was [41]:

$$[MeCpMn(CO)_2(MeCN)]^+ + PPh_3 \rightarrow [MeCpMn(CO)_2(PPh_3)]^+ + MeCN \qquad (1.17)$$

A cyclic voltammogram of a monopyridine complex $(py)W(CO)_5$ in acetonitrile consisted of a single irreversible wave at E_p = 1.01 V. However, after addition of 20 equivalent moles of tert-butyl isocyanide to a solution containing 1.0×10^{-3} M $(py)W(CO)_5$, a CV wave at E_p = 1.01 V disappeared and a new irreversible wave appeared at E_p = 1.18 V corresponding to a substitution product, $(t\text{-BuNC})W(CO)_5$. When smaller amounts of tert-butyl isocyanide

were employed, both waves, at E_p = 1.01 V and 1.18 V were observed on a cyclic voltammogram. The electrochemical processes involved were [42]:

$$(py)W(CO)_5 \rightarrow [(py)W(CO)_5]^+ + e^- \qquad (1.18)$$

The electrocatalytic substitution of the monopyridine and monoacetonitrile complexes of tungsten carbonyl, (py)W(CO)$_5$ (E_p = 1.01 V) and (MeCN)W(CO)$_5$ (E_p = 1.02 V), by triphenylphosphine were found to be more difficult to interpret solely on the basis of the CV experiments [42], since their anodic waves were not cleanly separated from the anodic wave of triphenylphosphine which occurred at E_p = 1.3 V. In the presence of added PPh_3, the anodic wave at E_p = 1.02 V for (MeCN)W(CO)$_5$ was absent. However, the cyclic voltammogram of (py)W(CO)$_5$ appeared to be unaffected by the presence of added triphenylphosphine. In neither case the CV wave corresponding to the product (PPh_3)W(CO)$_5$ could not be clearly discerned, owing to the presence of the phosphine wave. Nonetheless, preparative scale electrolysis demonstrated that both complexes undergo ligand substitution with PPh_3 at the electrode potentials [42].

The thermodynamic parameters governing the electron transfer chain catalyzed substitution of triphenylphosphine or iodide on CpFe(CO)$_2$I have been studied [43]. The reaction is driven by the much higher stability of the triphenylphosphine complex relative to the iodide complex, and proceeds to completion even though the electron transfer which propagates the catalytic chain is endergonic. A cyclic voltammogram of CpFe(CO)$_2$I in CH_2Cl_2 at a platinum disk electrode, revealed a chemically irreversible wave at E_p = – 1.64 V. Another irreversible wave at E_p = – 2.24 V was also observed on a CV of CpFe(CO)$_2$I, which was assigned to the formation of a dimer, [CpFe(CO)$_2$]$_2$. The chemical irreversibility of the reductions of CpFe(CO)$_2$-halide complexes was established to be the result of rapid dissociation of the halide following electron transfer. And the formation of I^- was confirmed by the observation of two oxidation peaks on the reverse CV scan at ca. 0.0 and + 0.1 V, corresponding to the two-step oxidation of iodide to triiodide and then iodide. In the presence of PPh_3, a cyclic voltammogram revealed an irreversible wave at E_p = – 1.53 V for the formation of product CpFe(CO)$_2$(PPh_3), and a wave at E_p = – 2.24 V was also observed. On scan reversal a new anodic peak, which was not present on the CV wave of CpFe(CO)$_2$I was observed at E_p = + 0.95 V and was found to match that observed for PPh_3 alone [43].

Direct electroreduction of alkyl and aryl halides is mostly performed at potentials which are more negative than – 2 V. But the picture changes radically when complexes of certain transition metals, capable of reacting with aryl- or alkyl-halides (RX) and forming more readily reducible compounds, were introduced into the electrolyte solution. The reductive dehalogenation of RX can in this case be conducted at considerably more positive potentials, most often at those of the regeneration of the metal complex active with respect to RX [44].

The complexes which are catalytically active with respect to RX can be tentatively subdivided into three groups: phosphine, tetraazamacrocyclic and polypyridyl complexes [44]. Electrochemical behaviour of solutions of NiX_2L_2 (X = Cl, Br, I; L = PPh_3) in N-methylpyrrolidinone depends on the nature and concentration of the halide ions (X^-); the concentration of L and the presence of ethylene. Reduction of the dissociated nickel (II) species leads to soluble zerovalent complexes only when Ni(II) is complexed to both phosphine and halide ions. Additions of Cl^- to solutions of $NiCl_2$ lead to formation of $NiCl_3^-$ or $NiCl_4^{2-}$, which are no longer electroactive. In the absence of ethylene the electroreduction of Ni(II) yields successfully Ni(I) and Ni(0) complexes of the type $Ni(0)L_3$. In the presence of ethylene the total reduction of NiX_2L_2 can be achieved in the absence of added L leading directly to the Ni(0) species $NiL_2C_2H_4$. The zerovalent complexes may exist in the anionic forms $Ni(0)L_3X^-$ and $Ni(0)L_2C_2H_4X^-$ depending on the nature and concentration of X [45].

Cyclic voltammetry of nickel (II) perchlorate was studied in 0.1 M TBAP in acetonitrile. In the presence of added PPh_3, it yielded an octahedral complex $[Ni^{II}(PPh_3)_2(MeCN)_4]^{2+}$, which was reduced directly in a two-electron process to $[Ni^0(PPh_3)_4]$. Another one-electron anodic peak, reversible in character, was observed on the reverse scan and was due to the oxidation of the obtained nickel(0) to $[Ni^I(PPh_3)_4]^+$ which was further oxidized at the second irreversible anodic peak, thus restoring the nickel(II) initially present. In the presence of added C_3H_5Br, three new processes appeared, one was associated with a nickel(II) cathodic peak which shifted to less negative potentials, and another two anodic peaks were due to catalytic oxidation of free bromide ions in the presence of triphenylphosphine. However, the anodic peaks relative to the stepwise oxidation of nickel(0) nearly disappeared. Further additions of C_3H_5Br only caused a progressive increase in the new cathodic peak which also took on a sigmoid shape. The overall reduction process was summarized as follows [46]:

$$[Ni^{II}(PPh_3)_2(MeCN)_4]^{2+} + 2e^- + 2PPh_3 - 4MeCN \rightarrow [Ni^0(PPh_3)_4] \quad (1.19)$$

$$[Ni^0(PPh_3)_4] + C_3H_5X - 3PPh_3 \rightarrow C_3H_5Ni^I(PPh_3)X + PPh_3 \rightarrow C_3H_5Ni^I(PPh_3)_2X \quad (1.20)$$

Cyclic voltammetry of $[Rh(PPh_3)_3]^+$ in the absence of excess PPh_3, at low scan rate (0.02 Vs^{-1}) showed two reversible one-electron reduction processes at E_p = – 1.40 V and – 1.73 V and an irreversible anodic peak was also present on scan reversal at E_p = – 0.85 V. Increasing the scan rate to 0.2 Vs^{-1}, lead to a decrease in peak current of the couple at – 1.73 V, and another reversible couple appeared at more negative potentials of – 1.90 V, and also an anodic peak at – 0.85 V decreased in magnitude [47]. At very high scan rate of 5.0 Vs^{-1}, two-well defined one-electron reversible processes appeared at – 1.40 V and – 1.90 V. Thus, it appeared that $[Rh(PPh_3)_3]^+$ was reduced in two reversible steps to $[Rh(PPh_3)_3]$ and $[Rh(PPh_3)_3]^-$, and a species, responsible for the anodic process at – 0.85 V was tentatively formulated as $[Rh(PPh_3)_2]_x$. In the presence of added free PPh_3, a rather complicated cyclic voltammogram of $[Rh(PPh_3)_3]^+$ became quite simple. $[Rh(PPh_3)_3]^+$ was reduced in two one-electron reversible steps at – 1.20 V and – 1.73 V. The second reduction potential was fixed at – 1.73 V, whilst the first one was affected by an increase in concentration of PPh_3, which made it shift positively by 60 mV per decade of concentration. This implied that the reduction process accompanied by coordination of a fourth phosphorus ligand. Since the UV-Vis spectrum of $[Rh(PPh_3)_3]^+$ was not modified by addition of PPh_3 up to 0.1 M concentration, coordination of the fourth ligand must take place after reduction of $[Rh(PPh_3)_3]^+$. The overall reduction process proposed was as follows [47]:

$$[Rh(PPh_3)]^+ + e^- \leftrightarrow Rh(PPh_3)_3 + PPh_3 \leftrightarrow Rh(PPh_3)_4 \quad (1.21)$$

The electrochemistry of (OMC)Rh(PPh_3) and (OMC)Co(PPh_3) was investigated in the presence of excess PPh_3 to determine the fate of the bound PPh_3 axial ligand after electrooxidation or electroreduction of each complex [16]. Cyclic voltammetry of (OMC)Co(PPh_3) revealed three reversible one-electron oxidation peaks in benzonitrile (PhCN) at E_p = 0.19 V, 0.76 V, and 1.54 V and two reduction waves at E_p = – 0.86 V and – 1.92 V. Both the first oxidation peak at 0.19 V and the two reduction peaks were unaffected by PPh_3 addition to solution, even after addition of 100 equivalent of PPh_3. The second oxidation peak at 0.76 V became irreversible after addition of 1.0 equivalent of PPh_3 to solution, and no further changes were observed up to addition of 500 equivalent of PPh_3, the

highest concentration investigated. The third oxidation at 1.54 V could not be investigated in the PhCN/PPh_3 mixtures due to an oxidation of PPh_3, which occurred at a more positive potential [16].

Cyclic voltammetry of (OMC)Rh(PPh_3) revealed three oxidation peaks in benzonitrile (PhCN) at E_p = 0.21 V, 0.66 V and 1.42 V and in addition two reduction peaks at E_p = – 1.27 V and – 1.34 V. Several changes were observed in the cyclic voltammograms of (OMC)Rh(PPh_3) in PhCN as PPh_3 was added to solution. The first oxidation process at 0.21 V, shifted negatively in potential while the second oxidation process at 0.66 V, became irreversible. The third oxidation at 1.42 V could not be investigated in the PhCN/PPh_3 mixtures due to an oxidation of PPh_3, which occurred at a more positive potential. Addition of PPh_3 also resulted in an increased anodic current for a reduction peak at – 1.34 V, resulting in the formation of rhodium complex $[(OMC)Rh(PPh_3)_2]^+$. The proposed electrochemical reaction was as follows [16]:

$$[(OMC)Rh^{III}(PPh_3)]^+ + PPh_3 \leftrightarrow [(OMC)Rh^{III}(PPh_3)_2]^+ \qquad (1.22)$$

The anodic peak current for the process at – 1.34 V increased with an increase in PPh_3 concentration. The ratio of anodic to cathodic peak current for process at – 1.34 V also depends upon the scan rate, which was 0.23 at 0.02 Vs^{-1} and 0.90 at 20 Vs^{-1} in the presence of 500 equivalent of PPh_3 [16].

1.5 RESEARCH AIMS AND OBJECTIVES

The overall objectives of this dissertation were as follows:

- Testing of the three flow-through cells designed and developed by Cukrowski [48] that should allow us to gain on-line, in a closed system, fundamental information about the cobalt organometallic compounds that are used as catalysts in industrial streams in non-aqueous solutions.
- Development of a method for correction of an uncompensated resistance using ferrocene as a model compound in batch solutions.
- Determine the experimental parameters to be used in each design of a flow cell (i.e., the influence of flow rate and scan rate) using ferrocene. This will enable us to

establish which flow cell will be used for fundamental studies and which for analytical purposes. Study the influence of on-line mixing on the CV curves and use the established methodologies for quantitative analysis on-line.

- Use of $CoCl_2(PPh_3)_2$ as a cobalt standard aimed to provide the quantitative information on the amount of cobalt organometallic compounds that are used as catalysts in industrial streams, since it was fairly stable. Since it is known that most cobalt catalysts are not stable under common room conditions under which the monitoring system is envisaged to operate.
- Study the electrochemical properties of $CoCl_2(PPh_3)_2$ and identify species present in solution during its oxidation, since the anodic reactions of $CoCl_2(PPh_3)_2$ were never studied using electrochemical techniques.
    - Synthesis of $CoCl_2(PPh_3)_2$ and characterisation using elemental analysis and Infrared (IR) spectroscopy.
    - Investigate the influence of a kind of working electrode material used on recorded voltammograms.
    - Establish sensitivity of voltammetric measurements towards traces of moisture present in a background solution.
    - Identify the oxidation reactions observed from the voltammograms.
    - Electrochemically monitored titration of $CoCl(PPh_3)_3$ with chloride to investigate the binding ability of chloride.
    - Electrochemically monitored titration of $CoCl_2(PPh_3)_2$ with PPh_3 using Cyclic Voltammetry (CV) to investigate the electrocatalytic properties of the complex and establish if it is possible to monitor the free PPh_3 in organic solvents in the presence of organometallic compounds containing cobalt.
    - Investigate use of ferrocene as a possible internal standard to be used during electrochemical measurements of $CoCl_2(PPh_3)_2$.
    - Determine the number of electrons involved in each electrode process observed from the voltammograms of $CoCl_2(PPh_3)_2$.
- Determine a diffusion coefficient of ferrocene in a mixture of acetonitrile and pentanol (1:1).

1.6 SUMMARY OF CHAPTERS

This dissertation contains six chapters, including the current chapter (Chapter 1). In Chapter 1 (Introduction) a detailed literature review and the aims and objectives of this research project were presented.

In Chapter 2 the theory associated with the electrochemical techniques employed in the dissertation were discussed in detail.

In Chapter 3 the experimental procedures employed for each electrochemical technique and the types of instruments used including the instrumental parameters were presented. The reagents and electrodes used were also listed.

Chapters 4 and 5 contain results and discussion regarding the preliminary studies using ferrocene and the electrochemical properties of dichlorobis(triphenylphosphine)cobalt(II), $CoCl_2(PPh_3)_2$.

Chapter 6 contains the conclusions achieved from the results obtained.

Other results were also presented in an Appendix section A and B whilst references were provided at the end of the dissertation.

CHAPTER 2 THEORY OF EXPERIMENTAL TECHNIQUES EMPLOYED

In this chapter, a theory of the basic concepts of electrochemical techniques employed in this work is reviewed. The interest in characterization of electrode mechanisms has motivated the development of a multitude of electrochemical techniques. These techniques enable the sequence of reactions to be determined and the rate constant(s) of the homogeneous chemical reactions to be measured. Such information is deduced from the effect of the coupled chemical reactions on the response signal to a particular excitation signal that is impressed on the electrode. Spectroscopic techniques (UV-visible, IR, NMR and ESR) have been effectively coupled with electrochemistry to enable monitoring of homogeneous chemical reactions. Intermediates and products can sometimes be identified from their spectra [2].

Electrochemistry has proven to be a valuable technique for generating reactive oxidation states and studying the attendant solution chemistry of such electrogenerated species. The ease of oxygen removal from electrochemical cells greatly facilitates the study of oxygen-sensitive species which are electrogenerated. Small quantities of valuable materials can be studied with ease. Very rapid reactions can be monitored since some electrochemical techniques are capable of measuring reactions up to the limit of diffusion-controlled rates. Electrochemistry often has an additional advantage over traditional chemical approaches in that the solution is not complicated by a reagent added to generate the redox state of interest [2].

2.1 CYCLIC VOLTAMMETRY (CV)

Cyclic Voltammetry (CV) is perhaps the most effective and versatile electroanalytical technique available for the mechanistic study of redox systems [2]. It enables the electrode potential to be rapidly scanned in search of redox couples. Once located, a couple can then be characterized from the potentials of peaks on the cyclic voltammogram and from changes caused by variation of the scan rate. CV is often the first experiment performed in an electrochemical study. The repetitive triangular potential excitation signal for CV causes the

potential of the working electrode to sweep back and forth between two designated values (the switching potentials). Although the potential scan is frequently terminated at the end of the first cycle, it can be continued for any number of cycles, hence the terminology cyclic voltammetry. A scan in which the potential is becoming increasingly positive is termed a positive scan and a scan in which the potential is becoming increasingly negative is a negative (even though the potential may actually be positive). The scan profile used in a particular experiment is generally determined by the location of the redox couple of interest [2].

CV has the further attraction of providing information not only on the thermodynamics of redox processes but also on the kinetics of heterogeneous electron-transfer reactions and coupled chemical reactions. The characteristic shapes of the voltammetric waves and their unequivocal position on the potential scale virtually fingerprint the individual electrochemical properties of redox systems. For this reason the method has been labelled "electrochemical spectroscopy" [49].

The cells for voltammetric experiments usually comprise a three-electrode arrangement, with working and counter-electrodes sufficiently spaced, while the reference electrode is brought close to the working electrode surface with a Haber-Luggin capillary to minimize IR loss. In particular, in case of organic solvents and high scan rates, uncompensated resistance with the resulting IR drop and double layer effects may affect the voltammograms. The IR drop distorts the linear *E/t* curve, usually assumed in CV. Of course, in turn, the current is affected. Thus, the IR compensation or correction is strongly recommended [50].

The IR correction is then the potential drop between electrode and the capillary tip from the salt bridge (note that there is no potential drop between the capillary tip and the reference electrode itself, since only minute ($< 10^{-12}$ A) currents flow in the reference electrode circuit) [51]. It is obviously essential that the electrolyte conductivity should not vary with capillary position, that the current flow should be uniform and that no substantial electrolyte concentration profile should be set up in the diffusion layer, which can best be achieved with highly conductive concentrated electrolyte. Experimental determination of the IR drop is always possible. Earlier work involved the systematic variation of tip-electrode distance and extrapolated the resultant measurement to zero separation, but nowadays the current-

interrupt method is most commonly employed. This exploits the fact that, on interrupting the current, the IR contribution to the potential drops immediately to zero, whereas the electrode potential falls only relatively slowly (in the order of ms) owing to the large double-layer capacitance. The potential change can be measured with a storage oscilloscope or by utilizing an appropriate electronic circuit within the potentiostat; IR compensation can be built into the potential control by a variety of means, yielding automatically corrected values of the electrode potential [51].

Another significant problem in cyclic voltammetry is the possibility of dissolution of the counter electrode [51]. The potentiostat will force an equal and opposite current through the counter electrode as the working electrode, and a small amount of metal at the counter electrode may dissolve and re-deposit on the working electrode. For this reason, a counter electrode of the same material as the working electrode is usually employed during electrochemical investigations on gold, platinum etc. Cyclic voltammograms of a much more complex form are found for more complex electrochemical processes such as the oxidation of organic substances, especially in cases where the solution is unstirred, and the CV shows a sensitive dependence on the type of electroactive substance in the electrolyte, the electrolyte itself, and the electrode material. The existence of multiple peaks often reflects the build-up and dissolution of chemisorbed inhibitor layers on the electrode surface, for example, the inhibiting effect of a build-up of oxide layer on platinum on the oxidation of small organic molecules [51].

Applicability of voltammetric techniques is in some cases limited due to several factors. In a background electrolyte solution, we will observe oxidation or reduction of electrolyte components, the electrode material itself, or impurities in the electrolyte at certain potentials. These processes define the *accessible potential window*, and the observable electrode reactions should yield voltammetric signals well inside this window to allow analysis without interferences of background contributions [50].

If voltammetry is used for analytical purposes, an extremely large electrode area or volume ratio is often chosen to increase sensitivity, e.g., in inverse voltammetry or when working with thin-layer cells. Under these conditions, diffusion is no longer semi-infinite but finite, i.e., the thickness of the diffusion layer is limited by the volume, and this changes the characteristics of the diffusion gradient. In a voltammetric experiments the measurable

current at the working electrode has two components; one for the heterogeneous charge transfer and one for the mass transport. However, there are two exceptions: the reversible and the irreversible case [49].

❖ **Reversible System.**

An example of an electrochemical reversible system is the simplest possible one-electron oxidation or reduction of a chemical species in solution at the working electrode (WE). The rate of heterogeneous charge transfer is so high that a dynamic equilibrium is established at the phase boundary. The Butler-Volmer equation [eq. (2.1)] is reduced to the Nernst equation [eq. (2.2)], i.e., the surface concentrations depend only on the actual electrode potential and are no longer influenced by heterogeneous kinetic effects. The current, as a measurable quantity for the charge flux at the electrode surface, is influenced solely by mass transport, the slowest step (diffusion control). The characteristic shape of the cyclic voltammogram is a result of the potential-dependent changes in the surface concentrations of the redox system and the simultaneous diffusion processes [49].

$$j_A(0,t) = \frac{i}{nFA}$$
$$= C_A(0,t)k^o \exp[-\alpha nF/RT(E - E^o)] - C_B(0,t)k^o \exp[(1-\alpha)\, nF/RT\,(E - E^o)] \quad (2.1)$$

$$E = E^o - \frac{RT}{nF} \ln Q \quad (2.2)$$

where, j_A is a flux of species A (mol $s^{-1}cm^{-2}$); k° is a standard heterogeneous rate constant (cm/s); α is a cathodic transfer coefficient, $1 - \alpha$ is an anodic transfer coefficient, and Q is a reaction quotient. The other variables were defined in the previous chapter and in the list of symbols.

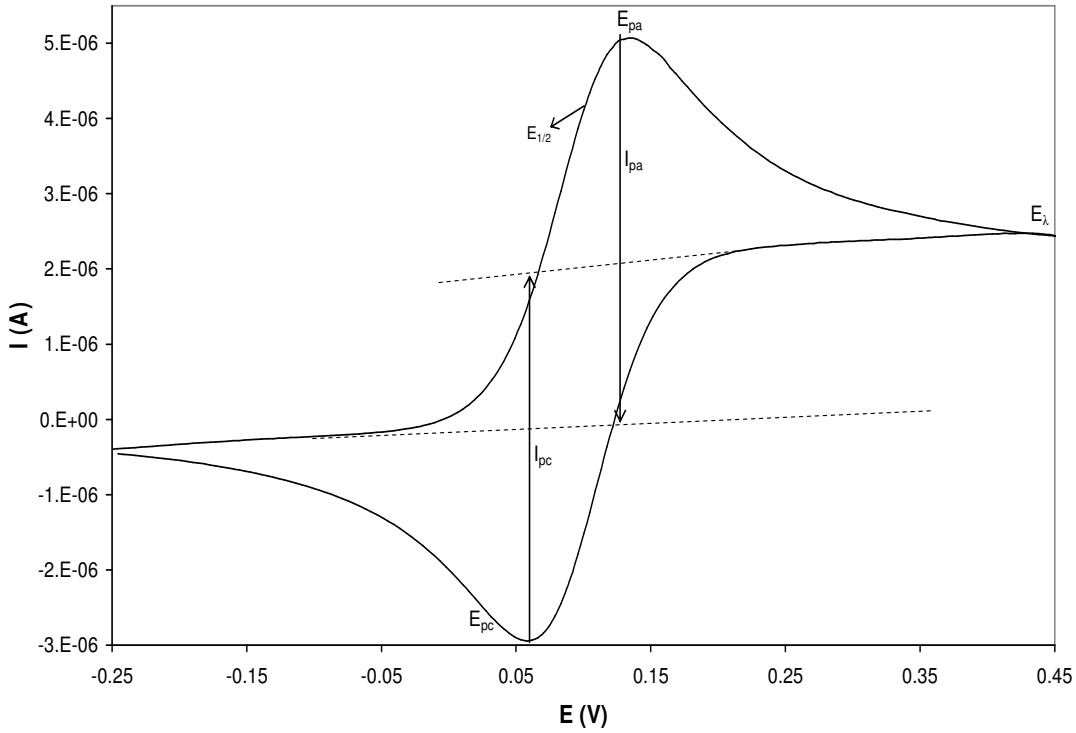

Figure 2.1 Cyclic voltammetric curve of a reversible charge transfer obtained to show how the CV parameters were evaluated. E_λ = switching potential, $E_{1/2}$ = half-wave potential, E_{pa} and E_{pc} = anodic and cathodic peak potential, I_{pa} and I_{pc} = anodic and cathodic peak current.

The most important parameters are the two peak potentials E_{pa} and E_{pc} as well as the peak currents I_{pa} and I_{pc} (Fig. 2.1). For reversible charge transfer (α = 0.5) without coupled chemical reactions, $I_{pa}/I_{pc} = 1$ and $\Delta E_p = 59 / n$ mV (at 25 °C) [49].

The peak current for a reversible electron transfer is given by the Randles-Sevčik equation (at 25 °C):

$$i_p = 2.686 \times 10^5 \; n^{3/2} C D^{1/2} v^{1/2} A \qquad (2.3)$$

where, n = number of moles (mol^{-1}); C = concentration of the oxidized or reduced species in a bulk solution (mol cm^{-3}); D = diffusion coefficient (cm^2 s^{-1}); v = scan rate (V s^{-1}) and A = area of the WE electrode (cm^2). The peak current is proportional to the square root of the scan rate.

❖ **Irreversible System**

Charge transfer at the electrode is extremely slow. Depending on the potential, only one of the cathodic or anodic heterogeneous reactions has a measurable rate. Thus, the current is largely controlled by the rate of the charge-transfer reaction (charge-transfer control). Since the surface concentrations at the electrode are dependent on the heterogeneous reaction and are far removed from thermodynamic equilibrium, one speaks of an irreversible process. Under such conditions, the Nernst equation does not apply. Furthermore, this means that the measured potential values cannot be compared with thermodynamic equilibrium potentials [49].

❖ **Quasi-reversible System.**

Both the charge transfer and the mass transport determine the current. The Nernst equation is only approximately satisfied. The charge transfer is therefore termed quasi-reversible [49].

❖ **Multielectron Transfer Processes.**

Multielectron transfer usually takes place in separate steps. Depending on the separation between the theoretical potentials of the redox reactions, several cases have to be distinguished. If the separation of the potentials between redox transfers is large, the resulting cyclic voltammogram consists of two typical, additively superimposed, one-electron transfer waves [49]. Also, the second electron transfer might take place at potentials negative to the first, giving rise to two overlapped one-electron peaks. Often there is a chemical reaction upon reduction or oxidation, giving rise to an ECE process with an apparent multielectron transfer [52].

Figure 2.2 presents a typical example of a two-step redox process of cobalt-tetra-{2-(2-thienyl)ethoxy}phthalocyanine [CoTETPc]. The first wave corresponds to oxidation of Co^{II}TETPc to Co^{III}TETPc which was followed by complex oxidation, Co^{III}TETPc to $[Co^{III}TETPc]^{+}$. In this Figure a multielectron overall response arises. The product of the first electron-transfer reaction (process I) undergoes a second electron-transfer step (process II) at potentials more positive than that for the first step [4].

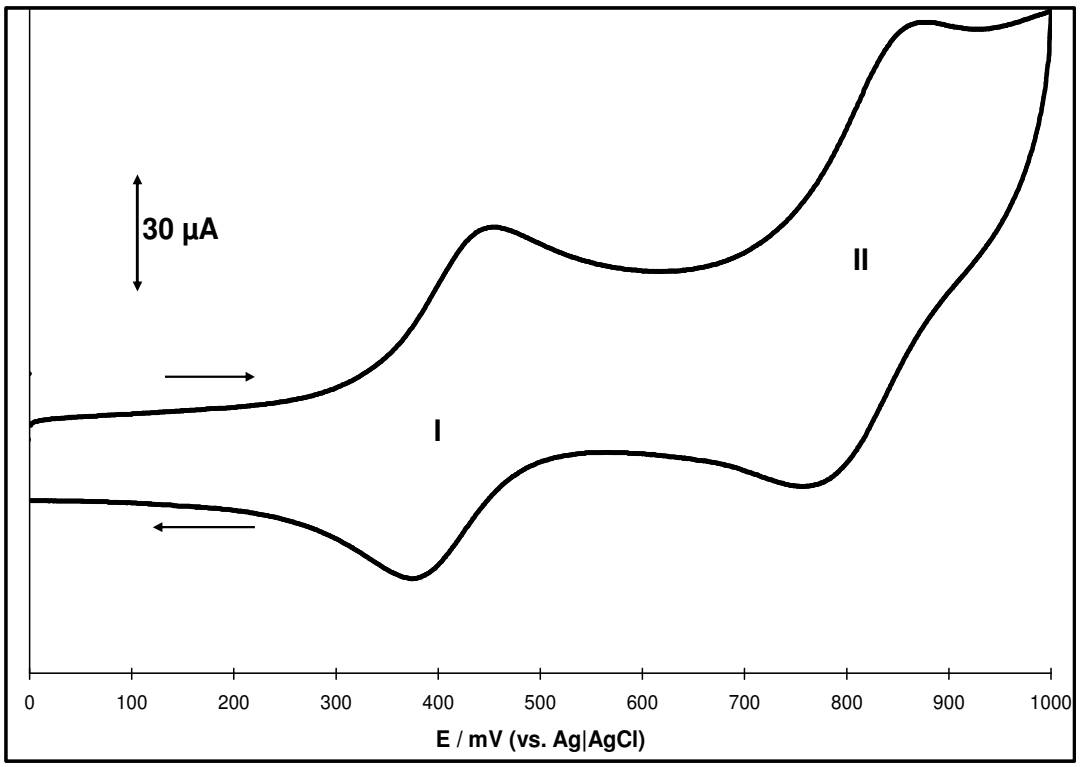

Figure 2.2 Cyclic voltammogram of two-electron transfer process obtained using 5 mM CoTETPc; in DMF containing 0.1 M $TBABF_4$, at a scan rate of 100 mV/s, obtained from Ref [53].

❖ **Electron Transfer with Coupled Chemical Reactions**

One of the most intriguing aspects of electrochemistry involves the homogeneous chemical reactions that often accompany heterogeneous electron-transfer processes occurring at the electrode-solution interface. The addition or removal of an electron from a molecule generates a new redox state, which can be chemically reactive. A variety of mechanisms, some of which involve complicated sequences of electrode and chemical reactions, have been characterized [2].

2.2 CHRONOAMPEROMETRY

In Chronoamperometry a current through a working electrode is recorded as a function of time, while the constant potential is applied to this electrode. During the experiment the electrode is stationary and usually the electrolyte is not agitated, but is at rest. The derivation of the response began at a potential step from a value at which no current flows, to one at which the diffusion-limited current passes [50]. The response of the current to this

perturbation will be a sharp change from zero current followed by relaxation to a value close to zero, the final steady state magnitude that is determined by the flow of species to the electrode surface (Figure 2.3). Hence this varies according to electrode geometry and solution convection [50].

For a uniformly accessible planar electrode, the diffusion process is known as semi-infinite linear diffusion, since it can be assumed to occur only in one dimension perpendicular to the electrode surface. The observed current depends directly on the observed concentration gradient at the electrode surface [50].

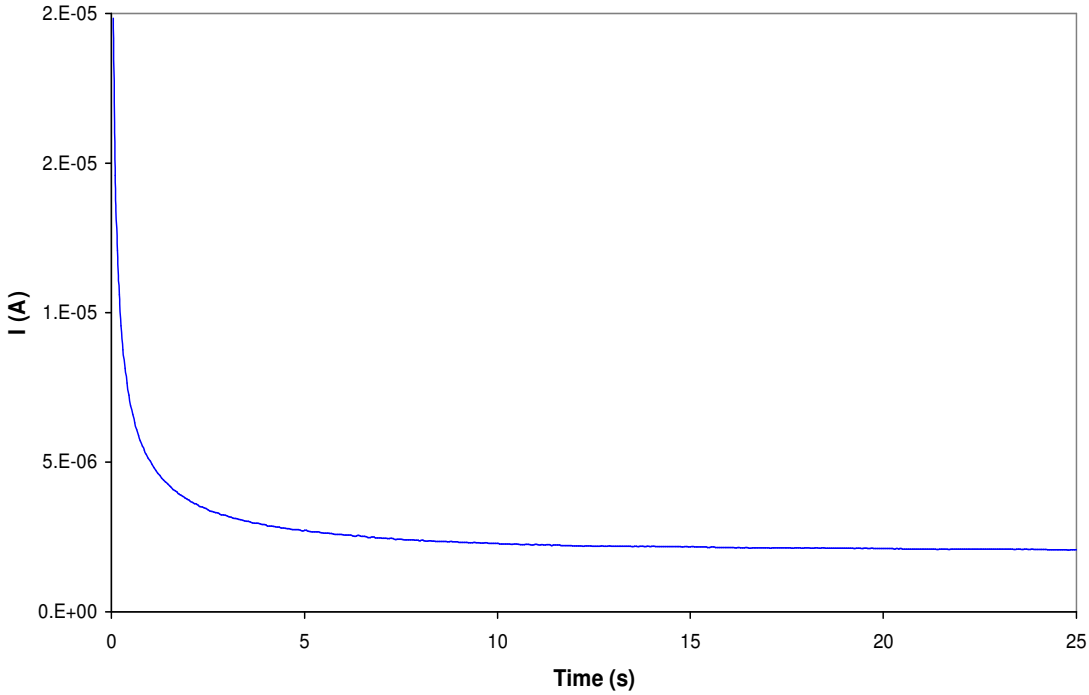

Figure 2.3 Potential step chronoamperometric response of a 7.7×10^{-4} mol/l ferrocene solution in 0.05 M TBAHFP in acetonitrile.

In fact, the current decays smoothly from an initial value at $t = 0$ and approaches zero with increasing the time as described by the Cottrell equation for a planar electrode [2]:

$$i_t = \frac{nFACD^{1/2}}{\pi^{1/2} t^{1/2}} \tag{2.4}$$

where, i_t = current of time (t), A

n = number of electrons, mol^{-1}

F = Faraday's constant, 96485 A.s

A = electrode area, cm^2

C = concentration of electroactive species, mol/cm^3

D = diffusion coefficient of electroactive species, cm^2/s

Hence, the current is inversely proportional to the square root of time. The Cottrell equation states that the product $it^{1/2}$ should be a constant for a diffusion-controlled reaction at a planar electrode. Deviation from this constancy can be caused by a number of situations, including nonplanar diffusion, convection in the cell, slow charging of the electrode during the potential step, and coupled chemical reactions. For each of these cases the variation of $it^{1/2}$, when plotted against t, is somewhat characteristic [2].

Chronoamperometry has proven useful for the measurement of diffusion coefficients of electroactive species. An average value of $it^{1/2}$ over a range of time is determined at an electrode the area of which is accurately known and with a solution of known concentration. The diffusion coefficient can then be calculated from $it^{1/2}$ via the Cottrell equation. Although the electrode area can be physically measured, a common practice is to measure it electrochemically by performing the chronoamperometric experiment on a redox species whose diffusion coefficient is known. The value of A is then calculated from $it^{1/2}$. Such an electrochemically measured surface area takes into account any unusual surface geometry that may be difficult to measure geometrically [2].

If the heterogeneous electron transfer of the redox species with the electrode itself is slow, the current after the potential step is necessarily less than in a system in which the electron transfer is rapid. This aspect of electrochemistry has been used for the measurement of heterogeneous rate constants. The behaviour of $it^{1/2}$ as a function of time can be influenced substantially by the presence of chemical reactions that are coupled to the electrode process. Consequently, characteristic variations of $it^{1/2}$ vs. t have been effectively utilized for the quantitative study of such homogeneous chemical reactions [2].

2.3 FLOW INJECTION ANALYSIS (FIA)

Years ago scientists involved with making analytical measurements had very limited and primitive equipment at their disposal. Light sources were flames and the sun. Most wavelength dispersions or discrimination were performed using filters or prisms. The detectors, in many cases, were the eyes or eventually photographic films. The readout devise was a person capable of evaluating the observed signals. Data evaluation was again a person. The sample was collected by a person and filtered, diluted, and in general handled by a person using volumetric glassware, like pipettes and volumetric flasks. All measurements were slow, tedious, and required a great deal of skill on the part of the analysts in order to ensure precise and accurate results [54].

Any measurement in a chemical laboratory involving liquid materials comprises the following operations: solution handling, analyte detection, data collection and computation of results. Nowadays, there is no shortage of computers and sophisticated detectors to aid chemists in performing data collection and computation of results, but solution handling requires an arsenal of skills, which a practicing chemist has to master, since mixing, decanting, pipetting, and other volumetric operations are still performed manually, even in the most advanced laboratories, using tools that were designed more than 200 years ago [55]. It might seem that robots would be suitable tools for automation of such manual tasks; but, it is likely that their impact will remain limited to repetitive operations like weighing of pulverized materials, mechanization of sample injection into chromatographic columns, handling of radioactive materials, or sample preparation. Because manual handling using robots requires extensive programming and active feedback control, the use of robots is justified only if large series of repetitive operations is to be handled over prolonged periods [55].

Truly, there seems to be no way of resolving the problem of automated solution handling other than by manual operations, as long as we think in terms of batch operations, a concept in which generations of chemists have been trained. Therefore, in freshmen courses, as well as in advanced research laboratories, beakers, flasks, and volumetric glassware are still the standard tools of the trade, coexisting with the electronics of advanced detectors and computers [55].

In flow injection analysis (FIA) the sample is injected directly into a moving stream without the addition of air (Fig. 2.4). The sample-reagent zone mixes and reacts as it moves downstream towards the detector; the degree of dispersion is controlled by a variety of factors, their impact being specific to the analytical system in use. It is the control of this dispersion which is at the heart of the technique and coupled with short, highly reproducible retention times and provides the potential for sampling rates up to 200 per hour [24]. Figure 2.5 below shows an amperometric response obtained from multiple injections of various concentrations of ferrocene solution in the flow cell using FIA system, using a continuous-flow method.

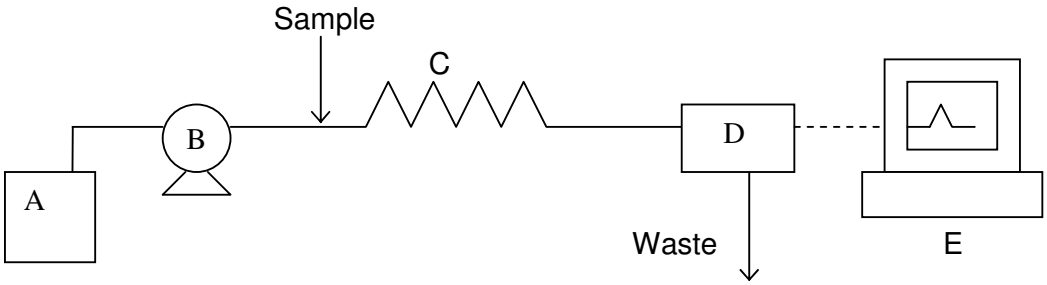

Figure 2.4 Schematic representation of a typical flow injection analysis system. A = background electrolyte solution, B = Pump, C = mixing coil, D = detector and E = computer.

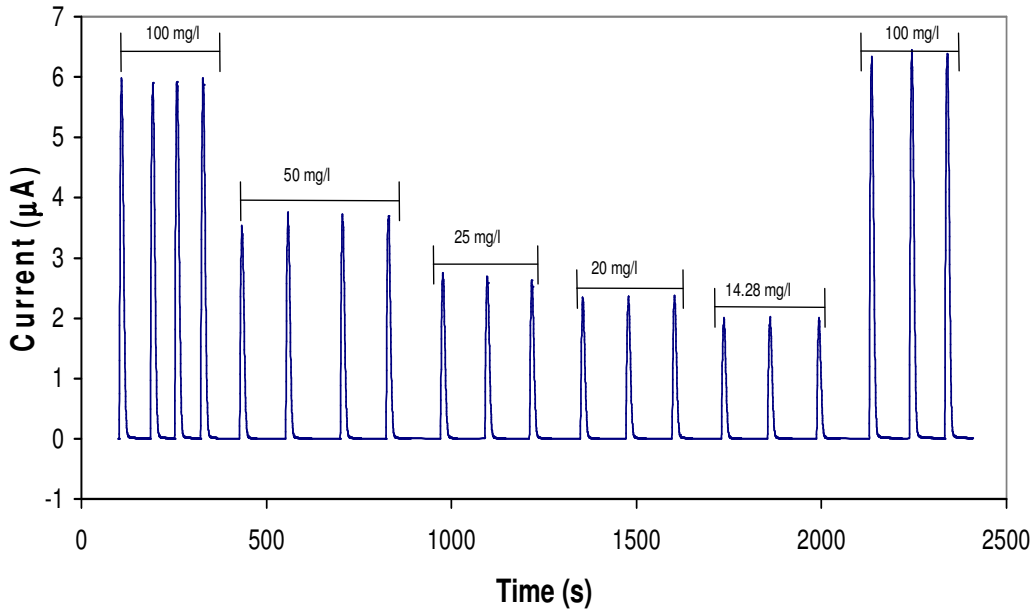

Figure 2.5 Typical detector output of an FIA system into which a ferrocene solution of various concentrations is repeatedly injected.

According to the type of flow used, flow methods can be classified as: (i) segmented-flow, (ii) continuous-flow, and (iii) stopped-flow methods [56]. The term 'stopped-flow methods' is applied to kinetic methods involving mixing of the sample and the reagents in the detector cell in order to perform periodic measurements for monitoring reaction development. This type of method is rarely considered to be of the automatic type. We should note that the 'continuous-flow' concept does not exclude occasionally stopping the flow (for example, to allow the reaction to proceed without increasing sample dispersion in the carrier). Continuous-flow methods are also kinetic methods: measurements are performed during the course of the reaction without the need to wait for equilibrium to be reached. Therefore, some continuous-flow methods frequently include halting of the flow. In segmented-flow methods the flowing stream is segmented by air bubbles that are primarily intended to avoid carry-over between successively processed samples [56].

The three basics of FIA, as defined by Růžička and Hansen, are reproducible timing (which leads to the reproducible physical conditions), sample injection and controlled dispersion. Dispersion is described as the amount that the chemical signal is reduced by injecting a sample plug into an FIA system [54]. This is represented mathematically by

$$D^{*} = C^{\circ} / C^{\max} \tag{2.5}$$

where D^{*} is the dispersion coefficient at the peak maximum produced by the ratio between C°, the concentration of a pure dye, and $C^{\max}$, the concentration of that same injected dye as it passes through the detector [54].

The experimental conditions usually involved in FIA result in incomplete mixing of the injected sample plug with the carrier stream, with two important consequences, (i) mixing is time-dependent, and therefore occurs to different extents at different points along the flow-line, (ii) the extent of mixing is highly reproducible from sample to sample. Thus, the technique gives rise to the creation of a time-dependent concentration gradient of sample within the carrier streams. The physical foundations of FIA are related to dispersion, which is defined as the dilution undergone by a sample volume injected into the flowing stream. The dispersion is characterized by the concentration profile adopted by a zone or plug inserted at a given point in the system without stopping the flow [57].

There are two mechanisms contributing to the dispersion of the injected sample,

(i) Convective transport, occurring under laminar flow conditions (Fig. 2.6). This yields a parabolic velocity profile with sample molecules at the tube walls having zero linear velocity and those at the centre of the tube having twice the average velocity [57].

(ii) Diffusional transport, due to the presence of concentration gradients in the convective transport regime, gives rise to axial and radial diffusion (Fig. 2.6). The former, due to horizontal concentration gradients at the leading and trailing edges of the injected sample zone contributes insignificantly to the overall dispersion, whereas the latter, resulting from concentration differences perpendicular to the direction of the flow makes an important contribution to the overall dispersion. If the flow is considered to be made up of a large number of superimposed fluid cylinders travelling convectively at different speeds, radial diffusion tends to balance concentrations in such a manner that the molecules located at the tube walls tend to move to the centre, whereas those at the centre travel outwards. This process is of transcendental importance in accounting for the fact that every sample injected maintains its integrity. Indeed, this motion slows down convective transport, thus hindering progressive dilution of the zone in the carrier stream [57].

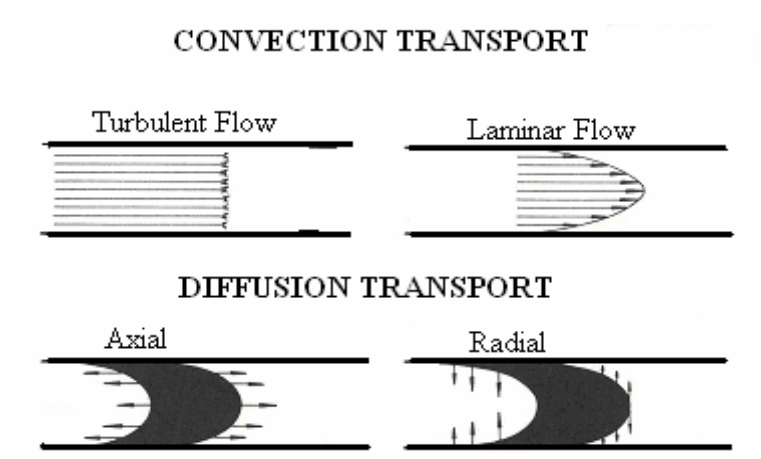

Figure 2.6 Types of transport mechanisms present in a closed system.

Flow operations are much easier to automate, since they replace the mechanical handling of oddly shaped (and often fragile) containers by sequential movements of liquids in tubes.

Flow operations are much easier to miniaturize by using small bore tubing, and the micro volumes are conveniently manipulated and metered by pumping devices, which (unlike pipettes) are not affected by surface tension (or by shaking hands) [55]. Flow operations are much easier to control in space and time, since using closed tubing avoids evaporation of liquids, provides exactly repeatable path(s) through which measured solutions move, and provides an environment for a highly reproducible mixing of components and formation of reaction products. Flow operations are very versatile, since flows can be mixed, stopped, restarted, reversed, split, recombined, and sampled, while contact times with selected sections of reactive or sensing surfaces can be precisely controlled. Finally, flow operations allow most detectors and sensors to be used in a more reproducible manner than when used in batch operations and by hand-as is obvious to anyone who has used both conventional and flow-through cuvettes [55].

While many of the advantages of flow operations have been exploited in chromatography, why has the batch approach not yet been replaced by flow systems in all areas of laboratory practice? The reason must be tradition, and the fact that most chemists are used to thinking in terms to batch operations, where homogeneous mixing is thought to be the only reproducible way to bring reactants together and where the homogeneously mixed solution is regarded as the only suitable form in which a reproducible measurement can be taken [55].

FIA technique can be applied to agriculture, water and soil analysis, environmental laboratories, biochemistry, biotechnology, pharmaceuticals, clinical laboratories and in food and feed, and in process and quality control [54]. Predominantly FIA has been applied to colorimetric methods using well established chemistries also found on both air segmented and discrete analysis systems. Such analysis can be simple involving no more than the addition of the sample to the moving reagent/carrier stream or involve dialysis; solvent extraction; multiple reagent addition as intermediate steps. Improved sensitivity can be achieved from a stopped flow technique, on line pretreatment etc, but at the expense of sampling rate. FIA can also be applied to other detection systems e.g. ion selective electrodes or as a means of sample introduction to Atomic Absorption Spectrophotometry [24].

Modern electrochemistry offers a wide range of methods that can be used for continuous or discrete measurements in flowing liquids. The combination of flow injection analysis and cyclic voltammetry is attractive because of the flexibility of the former and the diagnostic power of the latter. Recently developed flow injection techniques with controlled dispersion offer a unique possibility to prepare solutions under controlled conditions in flowing systems [58]. Two classes of electrochemical measurement are employed in flow detection: one class is based on charge transfer between a liquid or gaseous phase containing the analytes and a solid or immiscible liquid phase that is electrically conductive or semi conductive, and includes the most common potentiometric, voltammetric and coulometric detection techniques, and the other class involves the measurement of the electrical properties of liquids, i.e. the electrical conductivity and relative permissivity [58].

There are many designs of flow-through detectors described in the literature, mainly for continuous, on-line monitoring and for chromatographic applications [58]. The best design for both solid-state and polarographic detectors involves a geometry in which the fluid stream points at a right angle to the electrode surface or a disk upon which the fluid system stream impinges perpendicularly. For the polarographic detectors, the best geometry is that the fluid and mercury streams are at right angle to each other. The two kinds of detectors then perform equally well [59]. Figure 2.7, shows an example of a cyclic voltammetric curve of ferrocene solution in a flowing solution, using a kind of detector cell where the fluid stream points at a right angle to the electrode surface.

Flowers and Callender, designed and characterized a transmittance cell (volume 10 ml) for ultraviolet, visible, and infrared spectroscopy and spectroelectrochemistry [30]. Cyclic voltammograms were measured at various scan rates for ~ 1.5 mM ferricyanide in 0.1 M KNO_3. A rather severe edge effect manifested the voltammograms due to exposure of the thin layer to the bulk solution about its entire perimeter. Separation of the cathodic and anodic peaks was observed to increase from ~ 50 to 100 mV as the scan rate was increased from 1 to 4 mV/s. This was likely a result of ohmic drop across the optically transparent working electrode due to the resistance of the thin layer solution. Despite these shortcomings, the quality of the voltammograms indicated that the cell design permitted reasonably accurate control of the optically transparent working electrode [30].

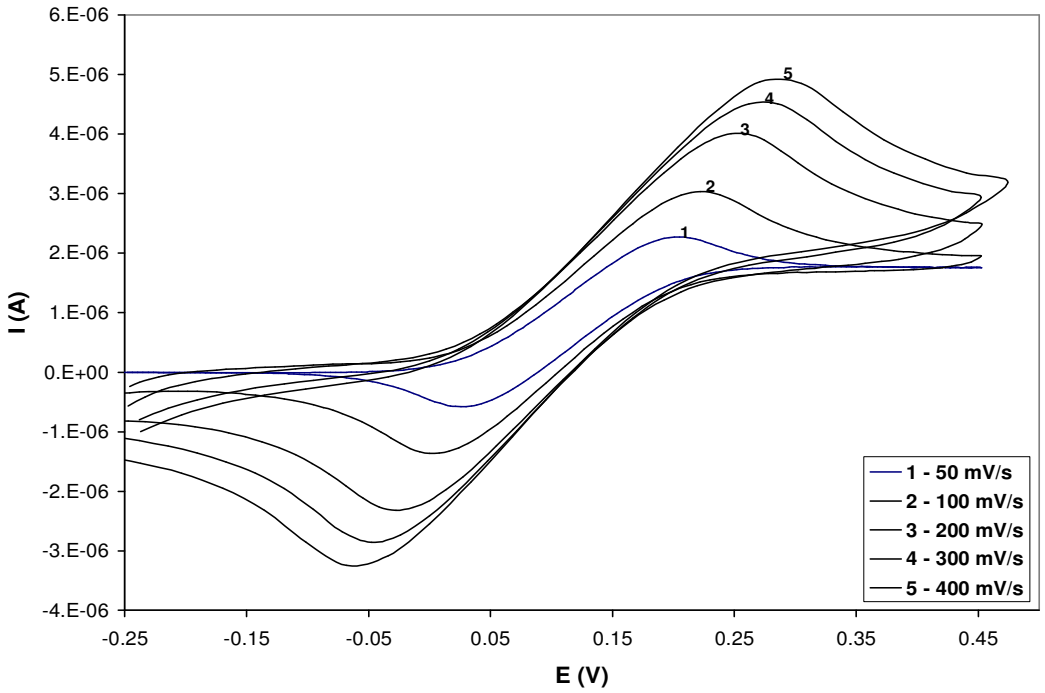

Figure 2.7 Cyclic Voltammograms of a 50 mg/l Ferrocene in 0.01 M TBAHFP in acetonitrile on a Pt disk electrode at various scan rates, using a flow-through cell, at a flow rate of 1 ml/min.

Chen and Long designed a flow micro-cell (volume 5 µL) and characterized it using cyclic voltammetry of potassium hexacyanoferrate(III) at various scan rates [60]. A separation of the cathodic and anodic peaks from 26 to 89 mV was observed, when the scan rate was increased from 2 to 18 mV/s. They found that the edge effect of the flow micro-cell was less than that previously reported by Flowers and Callender [30], the symmetry of the cyclic voltammogram for this thin layer cell was improved and the IR drop was decreased. The quality of the data demonstrated that the flow microcell can be successfully used for electrochemical studies [60].

CHAPTER 3 EXPERIMENTAL

This chapter describes in general the experimental procedures employed for each electrochemical technique and the types of instruments used including the instrumental parameters. The description of the three flow cells is included, the reagents and types of electrodes used. The synthetic procedure of the two cobalt organometallic complexes is also presented.

3.1 REAGENTS AND ELECTRODES

3.1.1 Reagents

- Tetrabutyl ammonium hexaflourophosphate ($TBAPF_6$), and ferrocene were purchased from Fluka and used without further purification.
- Acetonitrile C.P (99 %) was purchased from Sigma-Aldrich and purified by distillation over P_2O_5 (98 %, from Riedel-deHaën).
- Pentanol (99 %) was purchased from Fluka and purified by distillation over dried potassium carbonate (99.85 %, from Ssangyong) (dried at 125 °C).
- Acetone A.R (99.8 %), from Promark Chemicals was used as received.
- Methanol A.R (99.5 %) and Hexane C.P (96 %) were purchased from Radchem Laboratory Supplies and used as received.
- Tetrahydrofuran A.R (99.8 %), from Lab-Scan Analytical Sciences was use as received.
- Ethanol (99.5 %), from Merck was used as received.
- Ethyl acetate, ACS reagent (99.5 %); petroleum ether; Hydranal-Coulomat AD (reagent for coulometric Karl Fischer titration for cells without diaphragm), were purchased from Riedel-deHaën and used as received.
- Cobalt (II) chloride hexahydrate ($CoCl_2.6H_2O$) was purchased from Riedel-deHaën and dried in an oven to a blue color before use.
- Nitric acid C.P (HNO_3, 55 %), from Bio-zone chemicals was used as received.
- Sodium tetrahydroborate ($NaBH_4$, 98 %), and $AgNO_3$ were purchased from Saarchem and used as received.
- Triphenylphosphine was purchased from Sigma-Aldrich and used as received.

- Bis-(triphenylphosphine)dichlorocobalt(II) $[CoCl_2(PPh_3)_2]$ and chlorotris-(triphenylphosphine)cobalt(I) $[CoCl(PPh_3)_3]$ were synthesized using the literature method [61 – 62].

3.1.2 Electrodes

- Platinum disk, glassy carbon, silver disk, and gold disk electrodes, each 2 mm in diameter, were purchased from Metrohm, Switzerland.
- Steel rod tube outlet (1/16 x 0.040 x 5 cm), from Upchurch Scientific, Anatech.
- Platinum sheet electrode was from Metrohm, Switzerland.
- Autolab dummy Cell, from Echo Chemie, Netherlands.

3.2 APPARATUS

3.2.1 Flow Injection Analysis

The flow injection apparatus consisted of two Dosimats (Metrohm), with a 10 and a 5 ml exchange units, a PEEK mixing tee (25 x 23 x 20 mm in size), a six-port Hamilton injection valve, and a flow cell. The tube length between the injectors and the mixing tee was 40 cm Teflon tubing (2 mm ID, Metrohm). The tube length between the mixing tee and the manifold and the manifold and the detector were both 15 cm Teflon tubing (2 mm ID, Metrohm). The solutions were degassed by bubbling with argon before pumping through the flow injection analysis system. The descriptions of the three flow cells designed by Cukrowski [48] are as follows:

- **Flow Cell 1**

The flow–by electrochemical cell body was made of a rectangular piece of PEEK (49 x 32 x 25 mm in size). The flow cell consisted of a platinum disk electrode (2 mm diameter) as a working electrode, a gold disk electrode (2 mm diameter) as a counter electrode and a $Ag \mid AgNO_3$ (0.01 M) in acetonitrile as a reference electrode, connected to a frit as a liquid junction, and two bores (inlet and outlet) and a spacer. In this flow cell, the working electrode was positioned in such a way that the fluid stream points at a right angle to the electrode surface. The counter and the reference electrode were facing each other at opposite

positions. The working electrode and the spacer were also facing each other, and the spacer was used to vary the flow cell volume.

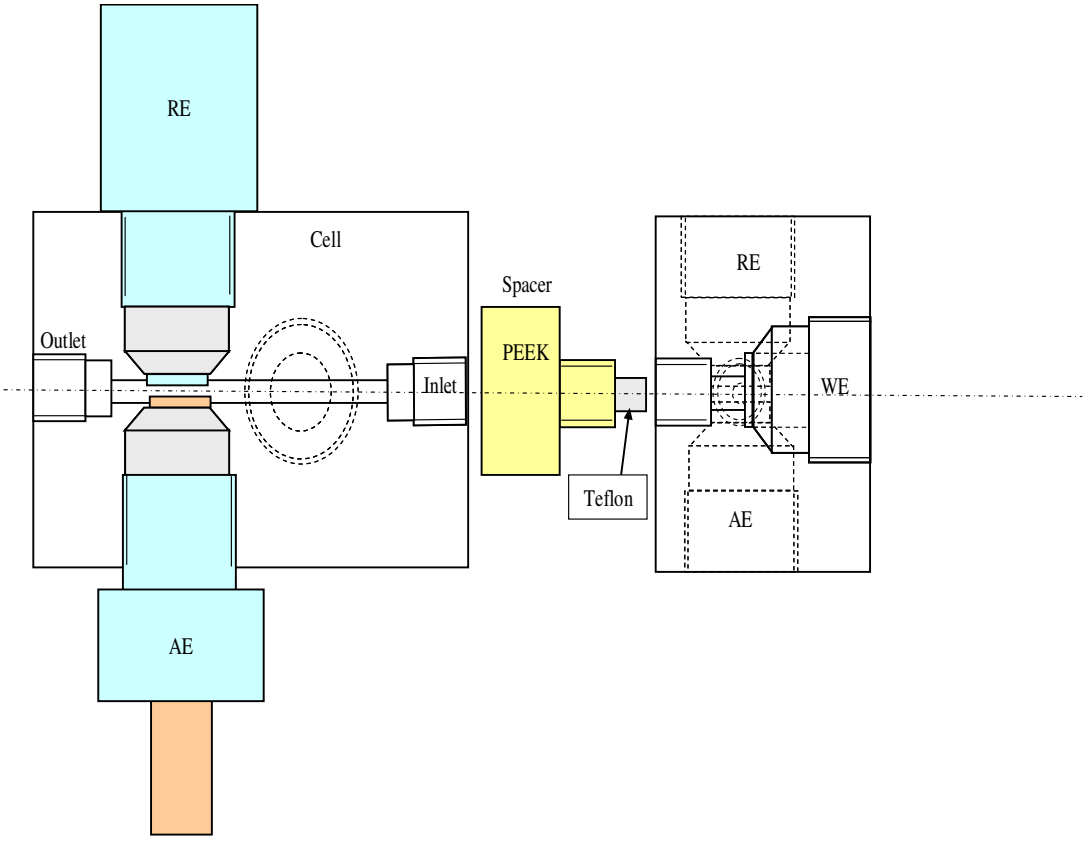

Figure 3.1 Diagram of the representative electrochemical flow–by cell 1, where WE = working electrode, RE = reference electrode and AE = auxiliary electrode.

- **Flow Cell 2**

The electrochemical flow cell was a wall-jet type. The cell body was made of a rectangular piece of PEEK (42 x 32 x 25 mm in size). The flow cell consisted of the same electrodes as those described in flow cell 1. The only difference between the two flow cells was the position of the inlet tube with respect to the working electrode. In this flow cell the working electrode was facing the inlet tube. This arrangement ensures that any part of the sample plug comes into contact with the working electrode surface only once. And also an inlet tube was incorporated inside a spacer.

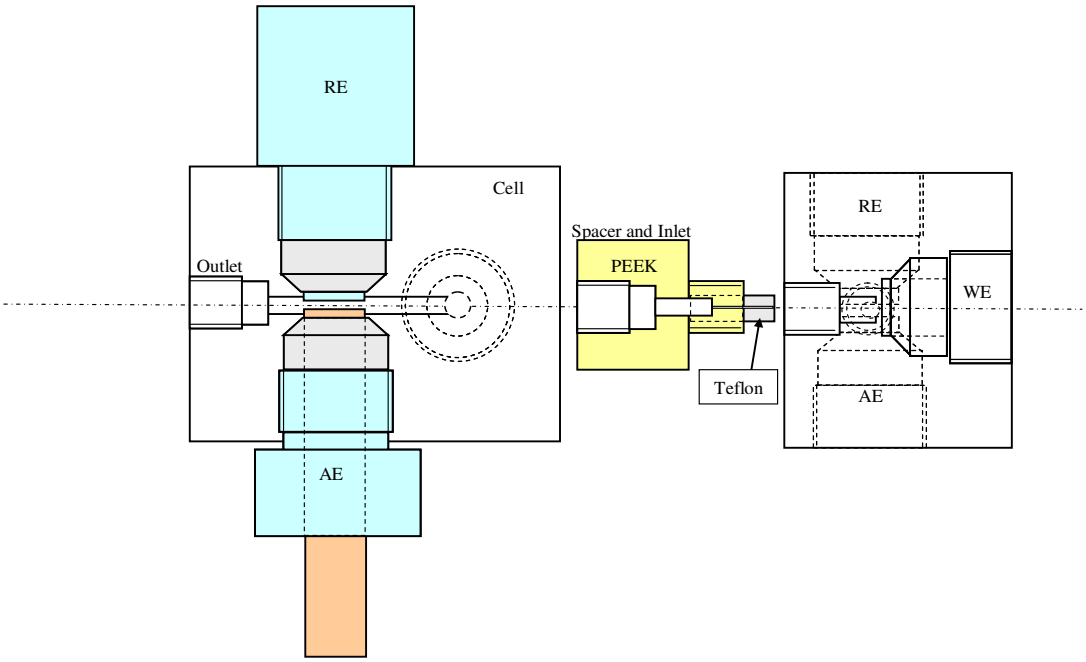

Figure 3.2 Diagram of the electrochemical wall–jet cell 2, with a gold disk as a counter electrode.

Flow Cell 3

The electrochemical flow cell was a wall-jet type. The cell body was made of a rectangular piece of PEEK (42 x 27 x 25 mm in size). The position and type of the counter electrode in this flow cell differs from that of flow cell 2. The counter electrode was a steel rod tube and it was positioned perpendicular to the reference electrode, and it served as a solution.

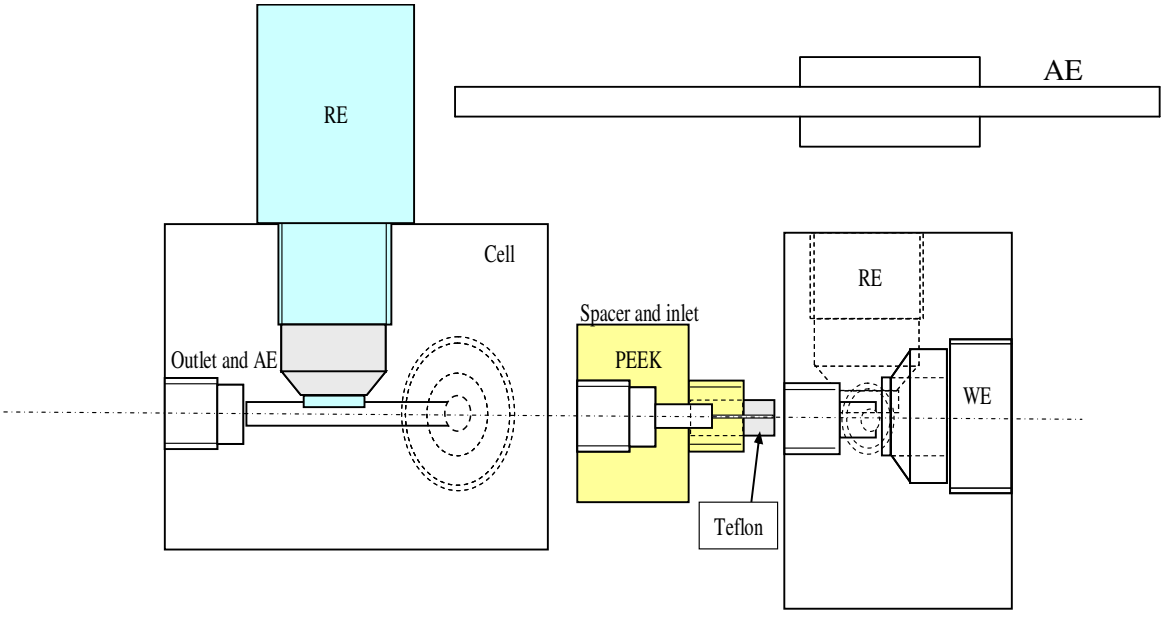

Figure 3.3 Diagram of the electrochemical wall–jet cell 3, with the steel rod tube as a counter electrode.

3.2.2 Cyclic Voltammetry (CV) and Chronoamperometry

An Autolab Type II system (Eco Chemie, Utrech, Netherlands) connected to a model VA Stand 663 (Metrohm, Herisau, Switzerland) was used for all experiments. The instrument was controlled by PC via GEPS version 4.8 software. All electrochemical experiments were carried out at room temperature using a three-electrode cell. The working electrodes were either a Pt disk; gold disk or a glassy carbon disk (all from Metrohm, each with diameter of 2 mm). The counter electrode was a Pt sheet. The reference electrode consisted of a silver wire immersed in a solution of silver nitrate (0.01 M) in acetonitrile. The reference electrode was immersed in a Luggin capillary salt bridge containing 0.1 M TBAHFP dissolved in a desired background solvent. The distance between the Pt disk working electrode and the tip of the salt bridge was ~ 1 mm to minimize ohmic drop. The stability of the reference electrode was checked periodically against a 0.77 mM ferrocene solution in the solvent of interest by measuring the change in peak potential, ΔE_p, of $Fe^{2+}Cp_2/Fe^{3+}Cp_2$ after measurement of the current-potential curve of the investigated compound. All potentials have been referenced to the $Fe^{2+}Cp_2/Fe^{3+}Cp_2$ couple. The standard IR drop correction facility of the instrument was used to minimize the effects of resistance in the electrolyte, using the resistance value obtained with ferrocene.

3.2.3 Digital Fitting and Simulation

Theoretical cyclic voltammograms were fitted using the Fit and Simulation option located in the Analysis menu of the Data Presentation window obtained from a GPES version 4.8 software. A reversible model was selected and a model name was set to Fit. The number of exchanged electrons was set to 1, temperature to 298 K and the initial guesses of the parameters were obtained. The Full Fit control parameter was selected followed by a Fast Fit and the fitted curve was saved.

3.2.4 Karl Fischer Titration

A Hydranal-Coulomat AD reagent for coulometric titration for cells without diaphragm was used. The reagent contains methanol, imidazole, sulfur dioxide and diethanolamine. The instrument used for moisture determination was 831 KF Coulometer (Metrohm), and a 728 magnetic stirrer (Metrohm). This instrument consisted of a generator electrode, a platinum wire electrode (with two wires), a 300 ml titration vessel, a stirrer bar and a keyboard.

3.2.5 UV-Visible Spectroscopy

A Perkin Elmer UV-Vis (Lambda E2 201) spectrometer was used. The experimental parameters were as follows: scan speed = 400 nm/min; path length = 10 mm; response = medium and data range = 190 – 800 or 500 – 800 nm.

3.2.6 Infrared Spectrum

The IR spectra were obtained from KBr disks. The disks were run on the Perkin Elmer (RX 1 FT-IR system) spectrum using 32 scans at 2.0 cm^{-1} resolution and in the region 400 to 4000 cm^{-1}.

3.2.7 Nuclear Magnetic Resonance (NMR) Spectroscopy

Room-temperature ^{31}P NMR measurements of the free ligand, and complex were performed on a Bruker ARX 300. H_3PO_4 ($\delta = 0$) was used as an internal standard for ^{31}P spectrum.

3.2.8 Other Equipment

- Hyprez Five-Star 1µm synthetic diamond paste for use on IMP cloth was purchased from IMP Sampling Analysis.
- Diamond extender blue, used as a lubricant with synthetic diamond paste was purchased from IMP Sampling Analysis.
- An IMP polishing cloth was purchased from IMP Sampling Analysis.
- A DPA-2 polishing wheel was from Struers.
- Whatman filter paper (44 Ashless Circles 110 mm diameter), from Sigma-Aldrich.
- Magnetic stirrer hot plate was purchased from Metrohm.
- A PTFE magnetic stirrer bar.
- A PTFE magnetic retriever rod.
- Drying Oven Series 2000, with a maximum temperature of 250 °C was purchased from Apollo Scientific.
- Precision balance (Mettler Toledo, 4 decimal places in grams), was purchased from Microsep, Switzerland.
- 763 Dosimats and exchange units were purchased from Metrohm, Switzerland.
- A six port distribution valve (model-R77810) and valve head (model-R36719) were purchased from Hamilton, Switzerland.

- PEEK material was purchased from Metrohm, Switzerland.
- Teflon tubing's were purchased from Metrohm, Switzerland.
- Millipore (Milli-Q Synergy), water supply system capable of producing ultra pure water with a resistivity of 18.2 M Ω cm was purchased from Microsep.
- Argon UHP gas (minimum purity 99.999 %), from Afrox Scientific.

3.3 SYNTHESIS

3.3.1 Synthesis of Bis-(triphenylphosphine)-dichlorocobalt(II) [$CoCl_2(PPh_3)_2$]

$CoCl_2(PPh_3)_2$ solid was prepared by dissolving 2.4007 g of dried $CoCl_2$ in 60 ml of ethanol and heated at 60–70 °C. 8.0003 g of triphenylphosphine was also dissolved in 60 ml of ethanol and heated at 60–70 °C. The hot ethanol solutions of $CoCl_2$ and triphenylphosphine were mixed slowly. The complexes began to precipitate before the mixing was complete. After complete mixing the hot solution was allowed to cool for about 2 minutes, filtered using canular technique while still warm, and the crystalline products were washed several times with ethanol and finally with ethyl acetate. The products were then dried in vacuum [61 – 62]. The solid product was blue and it was stored in a desiccator over $CoCl_2$. Yield = 4.4 g (66 %). Anal. Calcd for $CoCl_2(PPh_3)_2$ ($CoC_{12}H_{10}P_2Cl_2$): C, 66.06; H, 4.62; Found: C, 65.80; H, 4.60. IR (KBr) v/cm^{-1}: 3364m, 3047s [ν(C–H)], 1658mw, 1480s [m ν(C–C)], 1434vs [n ν(C–C)], 1303m, 1181vs, 1164s [c δ(C–H) ip], 1096s [q X-sens], 1070s [d δ(C–H) ip], 1028m [b δ(C–H) ip], 997s [p ring], 920 m [l δ(C–H) oop], 843m [g δ(C–H) oop], 744s [f δ(C–H) oop], 708vs [v δ(C–C) oop], 520s [y X-sens], 498s [y X-sens], 456m, 439m [t X-sens], 420w [[t X-sens]. UV-Vis [acenonitrile/pentanol (1:1)] λ_{max}/nm: 297, 591, 678 nm.

3.3.2 Synthesis of chlorotris(triphenylphosphine)cobalt(I) [$CoCl(PPh_3)_3$]

Cobalt (II) chloride hexahydrate (2.4006 g) and triphenylphosphine (8.0004 g) were added to ethanol (60 ml), and the mixture was vigorously stirred at 60–70 °C for 30 min to form blue $CoCl_2(PPh_3)_2$. The mixture was cooled to 30 °C, and sodium tetrahydridoborate was added (total of 0.3206 g, added in 10 small portions) over ca. 10 min. The reaction mixture turned dark-green, and finally minute brown crystals were formed. The crystals of

chlorotris(triphenylphosphine)cobalt(I) were vacuum-filtered under argon, washed with ethanol, water, ethanol, and petroleum ether, and dried under vacuum [62]. Yield = 5.1 g (57 %). Anal. Calcd for $CoCl(PPh_3)_3$ ($CoC_{54}H_{45}P_3Cl$): C, 73.59; H, 5.15; Found: C, 68.17; H, 4.75. IR (KBr) v/cm^{-1}: 3542m, 3418m, 3047s [*v*(C–H)], 1974mw, 1811mw, 1583m [k *v*(C–C)], 1479s [m v(C–C)], 1434vs [n v[C–C], 1307m, 1282mw, 1189vs, 1154s [c *δ*(C–H)], 1119vs, 1090s [q X-sens], 1070s [d *δ*(C–H) ip], 1025m [b *δ*(C–H) ip], 997s [p ring], 918m [l *δ*(C–H) oop], 852m [g *δ*(C–H) oop], 742s [f *δ*(C–H) oop], 722vs, 693vs [v *δ*(C–C) oop], 618w [s *δ*(C–C) ip], 541vs, 507m [y X-sens], 484s [y X-sens], 406m [w *δ*(C–C) oop].

3.4 SOLUTION PREPARATION

3.4.1 Background Electrolyte Solution

- 0.3874 g (1 mmol) TBAHFP salt was weighed and transferred into a 20 ml volumetric flask. 10 ml of acetonitrile was added to the flask to dissolve the salt. Pentanol was later added to the mark to make up a 20 ml background electrolyte solution.

3.4.2 Salt Bridge Solution

- A 0.3874 g (1 mmol) of TBAHFP salt was weighed and transferred into a 10 ml volumetric flask. 5 ml of acetonitrile was added to the flask to dissolve the salt. Pentanol was later added to the flask to the mark to make up a 10 ml solution.

3.4.3 Reference Electrode Solution

- A 0.0425 g (0.25 mmol) of $AgNO_3$ salt was weighed and transferred into a 25 ml volumetric flask. Acetonitrile was added to dissolve the salt. Once dissolution was complete, the flask was filled to the mark with acetonitrile, to make up a 0.01 M solution. The reference electrode solution was prepared weekly. The reference electrode was stored in a 0.01 M $AgNO_3$ solution in acetonitrile (solution was changed weekly).

3.4.4 Analyte (i.e. Ferrocene, $CoCl_2$, etc.) Solution

- For example, a 0.05×10^{-3} mol/l analyte stock solution was prepared by weighing a required mass of solid and transferring it into a 20 ml volumetric flask and diluting it with the background solvent (i.e. mixture of acetonitrile and pentanol (1:1)) containing the supporting electrolyte.

3.5 PROCEDURE

3.5.1 Cleaning of Electrodes and Cells

- A titration vessel and a Luggin-capillary salt bridge were rinsed first with deionised water, followed by nitric acid (0.5 M), then rinsed with deionized water and finally dried by rinsing with acetone (three times), wiped with a filter paper. During repeats of experiments the cell was rinsed with a background solvent and dried with acetone.
- The flow cells were rinsed first with deionized water, followed by rinsing quickly with nitric acid (0.5 M) (to avoid swelling of the cells, since they were made of PEEK material), then rinsed thoroughly with deionized water and finally dried by rinsing with acetone (three times). During repeats of experiments, the cell was cleaned by passing the background electrolyte solution into the cell, and scanning the CV at the same potential range, until no redox features indicating the presence of the studied electroactive species can be detected.
- A Pt sheet auxiliary electrode was cleaned in the similar manner as the salt bridge.
- The reference electrode was rinsed with acetone and wiped with a filter paper.
- The Pt disk working electrode was cleaned by polishing with a 1 µm diamond paste mixed with diamond extender blue, using a polishing cloth. The disk electrode was mantled on a polishing wheel and rolled for several minutes over a wet polishing cloth, until it was shiny. It was then rinsed with deionized water, followed by a 0.5 M HNO_3 acid, deionized water, and finally rinsed with acetone (three times) and wiped with a filter paper.
- During repeats of experiments, the electrodes were removed from the solution, carefully rinsed with a background solvent, dried with acetone and scanned over the

same potential range in the same background electrolyte solution, until no redox features indicating the presence of the studied electroactive species were detected.

3.5.2 Karl Fischer Titration

- A 5 ml syringe was used to suck the distilled solvent from the flask.
- The syringe was weighed.
- The start button form the KF instrument was pressed, and 2 ml of the solvent in a syringe was added into the KF cell, the syringe was weighed again and the obtained mass (i.e. the mass of a 2 ml solution) was entered into the KF parameters using a keyboard.
- The enter button was pressed to resume the titration and the results were recorded on the KF screen.

3.5.3 CV in Stationary Solution

- An electrochemical cell was filled with 20 ml of a background electrolyte solution.
- The cell was equipped with all the electrodes. All necessary electrical connections between the electrodes and the potentiostat were made.
- The solution was purged, by bubbling with argon for approximately 10 minutes. The argon was turned off during measurement, but a blanket of argon was maintained over a solution.
- The CV parameters were set as follows.

  (a) Ferrocene:

  - $E_{start} = -0.25$ V
  - $E_{sweep} = +0.45$ V
  - $E_{final} = -0.25$ V
  - E_{step} and Scan Rate = 0.004 V (50 mV/s).

  (b) $CoCl_2(PPh_3)_2$:

  - $E_{start} = 0$ V
  - $E_{sweep} = +1.8$ V
  - $E_{final} = 0$ V
  - E_{step} and Scan Rate = 0.004 V (50 mV/s).

- Before adding the analyte to the background solution, the background curves were recorded. These curves were subtracted later from the curves in the presence of the analyte.
- The background electrolyte solution was stirred between measurements in order to restore initial conditions, but it was not stirred during the experiment.
- A desired amount of the analyte was injected into the cell and the CV for the redox couple was recorded.
- The solution was purged between measurements.

3.5.4 Chronoamperometry in Stationary Solution

- Chronoamperometric curves were recorded immediately after recording a cyclic voltammogram (i.e. from the same solution).
- Before measurement of any chronoamperometric curves, each compound was first evaluated using cyclic voltammetry; the potentials determined by CV were used to set the potential limits for the chronoamperometry experiments.
- Example of the chronoamperometric experiment:
    - The background current of the electrode was recorded in 0.05 M TBAHFP in acetonitrile (20 ml), applying the constant potential.
    - The potential was stepped from –0.2 to 0.2 V.
    - A desired amount of ferrocene was injected into the cell, and current was recorded as a function of time at an appropriate potential.
    - The background curve was subtracted from the ferrocene curve.
    - The Cottrell plot of current versus the square root of time was constructed, and the slope was determined using linear regression analysis.
    - The electrochemically active area of the electrode was determined from the slope and the diffusion coefficient for ferrocene obtained from the literature (D = 2.37 x 10^{-5} cm^2/s, at 24 °C [63]).
    - After the determination of the electrode area, the cell and electrodes were cleaned as described in section 3.3, and the same procedure as above was repeated to determine the diffusion coefficients of the other compounds.
    - Chronoamperometric parameters in mixture of acetonitrile and pentanol (1:1) were set as follows:

(a) Ferrocene:

- Standby Potential = – 0.2 V
- Number of Potential Steps = 1
- Applied Potential = 0.25 V
- Duration Time = 25 s
- Sample Time = 0.01 s

(b) $CoCl_2$:

- Standby Potential = 0.2 V
- Number of Potential Steps = 1
- Applied Potential = 1.0 V
- Duration Time = 25 s
- Sample Time = 0.01 s

(c) $CoCl_2(PPh_3)_2$:

- Standby Potential = 0.2 V
- Number of Potential Steps = 1
- Applied Potential = 1.1 V
- Duration Time = 25 s
- Sample Time = 0.01 s

3.5.5 Combination of FIA and CV.

- 200 ml of a background electrolyte solution was added into a 250 ml bottle and connected to a dosimat (with a 10 ml exchange unit).
- A 100 ml solution of an analyte was added into another 250ml bottle and connected to another dosimat (with a 5 ml exchange unit).
- The two solutions were degassed by bubbling with argon before pumping through the flow injection analysis system.
- Then the background solution was pumped through the cell at a flow rate of 1 ml min^{-1} and the CV obtained.
- Both the background solution and the sample solution were pumped at a flow rate of 4 ml min^{-1} each to afford a total flow rate of 8 ml min^{-1}, to the mixing tee where they were mixed.
- After leaving the mixing tee, the mixed sample and background solution passed through a length of tubing and went to waste.

- They were then pumped at a flow rate of 0.5 ml min^{-1} each to afford a total flow rate of 1 ml min^{-1}, to the detector.
- The analyte was oxidized at the platinum disk working electrode in the flow cell. After travelling through the flow cell, the stream exited the cell, flowed past a reference and counter electrode, and then was delivered to waste.
- The CV was then obtained on a flowing solution.
- The flow was then stopped for a few seconds and the CV was obtained in a stopped flowing solution.

3.6 ELECTROCHEMICAL DATA ANALYSIS

- Peak current ratios for peaks of nearly reversible redox couples, where obtained from:

  i_{pa} / i_{pc} (3.1)

- For the evaluation of the separation of peak potentials the equation below was used,

  $\Delta E_p = E_{pa} - E_{pc}$ (3.2)

- ΔE_p was also used for the measurement of the reversibility of the charge transfer. For a fully reversible system, it was given by,

  $\Delta E_p = 2.3RT/nF = 59/n$ mV (25 °C) (3.3)

- The half-wave potential was determined from the following equation,

  $E_{1/2} = E_{pa} - \Delta E_p/2 = (E_{pa} + E_{pc})/2$ (3.4)

- Analysis of the chronoamperometry data was done by fitting the current-time data to the Cottrell equation (eq. 2.4) using i versus $t^{-1/2}$ graph.
- The slope of this plot was obtained.
- The active electrode area was calculated by substituting the value of $it^{1/2}$ into the Cottrell equation.
- The same working electrode was immediately used to determine the diffusion coefficient of ferrocene (in another solvent) and that of cobalt compounds studied.
- The values of $it^{1/2}$ and the active electrode area were then substituted into the Cottrell equation and the diffusion coefficient was calculated.
- The number of electrons involved was determined from the slope of a Cottrell plot of $i\pi^{1/2}/FACD^{1/2}$ vs. $t^{-1/2}$.

CHAPTER 4 PRELIMINARY STUDIES INVOLVING FERROCENE

This chapter will focus on the preliminary studies involving ferrocene as a model compound using electrochemical techniques. Ferrocene/ferrocinium couple will be used as a reference electrode potential during the studies involving cobalt organometallic compounds. In this chapter the value of resistance present in solvent mixtures that will be used in the study of cobalt organometallic compounds will be measured using ferrocene as an electroactive species. This value will then be used to correct the IR voltage drop present in solutions when studying the electrochemical properties of cobalt organometallic compounds. The effect of electrolyte concentration on the peak potential separation value will also be evaluated in this chapter. The effect that electrode positioning has on the cyclic voltammogram will also be evaluated in a flowing solution using three different types of electrochemical flow cells designed by Cukrowski [48] during the course of this project. This was done by investigating the influence of solution flow-rate and scan rate on the appearance of the voltammogram and also investigating the possibility of sample/reagent mixing on-line.

Typical experimental conditions of CV were as follows, unless otherwise stated:

- Platinum (Pt) disk was used as a working electrode (WE).
- Acetonitrile was used as a background solvent.
- Tetrabutyl ammonium hexafluorophospate ($TBAPF_6$) was used as a supporting electrolyte.
- An analyte concentration of 7.7×10^{-4} mol/l was employed.
- A scan rate was 50 mV/s.
- Only the third (or last) CV scan was used for analysis.
- All measurements were made at room temperature.

4.1 A MEASUREMENT OF UNCOMPENSATED RESISTANCE PRESENT IN VOLTAMMOGRAMS OF FERROCENE

The oxidation of ferrocene is widely used in cyclic voltammetric studies in highly resistive organic solvents as a means of reference electrode potential calibration, because of its presumed ideal reversible behaviour [64]. It has become common procedure to add ferrocene, typically in the range 0.5-1.0 mM concentration, to the electrolyte solution when cyclic voltammetry is practised in non-aqueous solvents. The main purpose of this preliminary work is to make use of the resistive distortion present in the ferrocene voltammogram to determine a reliable value of the uncompensated resistance, which in turn will be used to correct for IR voltage drop present in the voltammogram of the compound of interest. This was done by introducing increasing amounts of resistance into the cyclic voltammetric program until a good match was found between the theoretical and the experimental voltammogram. This method can also be used to confirm that the ferrocene process is indeed behaving in the ideal manner required for both reference potential and resistance calibration procedures to be valid. The uncompensated resistance in a cell is that resistance which, when multiplied by the total cell current, gives the difference in potential between the solution at the surface of the working electrode (but outside the electrical double layer) and the solution at the tip of the reference electrode probe [65].

In this work ferrocene is investigated over the appropriate range of scan rate and at various concentrations. IR drop correction was applied until the properties of the cyclic voltammograms adhere to the criteria for reversibility: difference between half-peak and peak potentials ($E_{pa} - E_p/2$) equalling 56.5 mV, difference between the anodic and cathodic peak potentials ($E_{pa} - E_{pc} = \Delta E_p$) of about 59 mV (with some dependence on switching potential), peak potentials that are independent of scan rate (numerical criteria are for a one-electron reaction at 298 K) [65], the peak current that is directly proportional to the square root of scan rate ($I_p/v^{1/2} = k$) and the ratio between anodic and cathodic peak current (I_{pa}/I_{pc}) must be equal to one. The solvent used in this experiment is a mixture of acetonitrile and pentanol (1:1 volume ratio), with 0.05 M tetrabutyl ammonium hexaflourophosphate ($TBAPF_6$) as supporting electrolyte.

A typical cyclic voltammogram with resistance compensation for the oxidation of ferrocene is given in Figure 4.1 below. The diamonds curve is the theoretical current-potential curve

for a reversible one-electron process whilst the bold line is the experimental current-potential curve obtained using Ferrocene after IR voltage drop correction. The theoretical CV curve was obtained using a digital fitting and simulation method (the procedure is given in the experimental section chapter 3). The resistance compensation was adjusted in this case by using the method described in the above paragraph. The agreement between experiment and theory indicates that the instrumental compensation has introduced no significant distortion in the data.

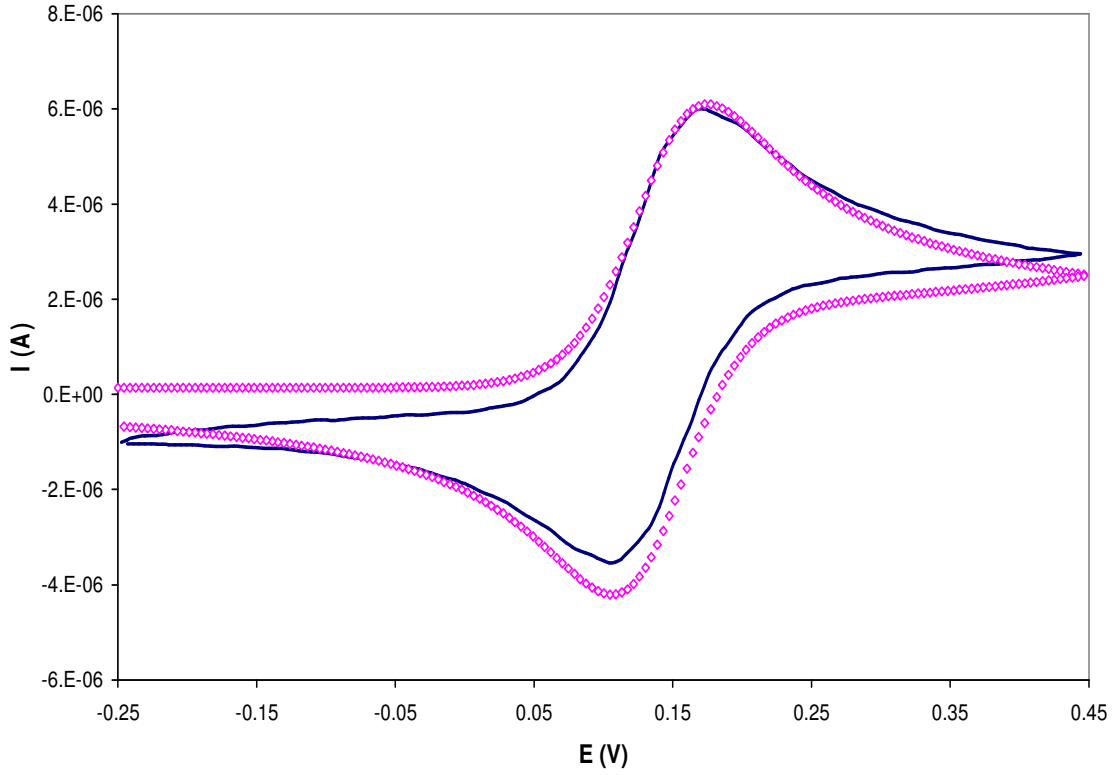

Figure 4.1 Comparison of a theoretical (diamonds) and experimental (solid line) corrected for IR with, R = 2200 Ω) CV curves of ferrocene.

Under the same conditions with no compensation, the curve resulted in large ΔE_p of about 86 mV at low scan rates of 100 mV/s (Figure 4.2). Data from 8 experiments for scan rates between 0.05 and 0.5 V/s were analysed and several important parameters describing the shape of the voltammograms were obtained. The data is summarised in Table 4.1 and 4.2.

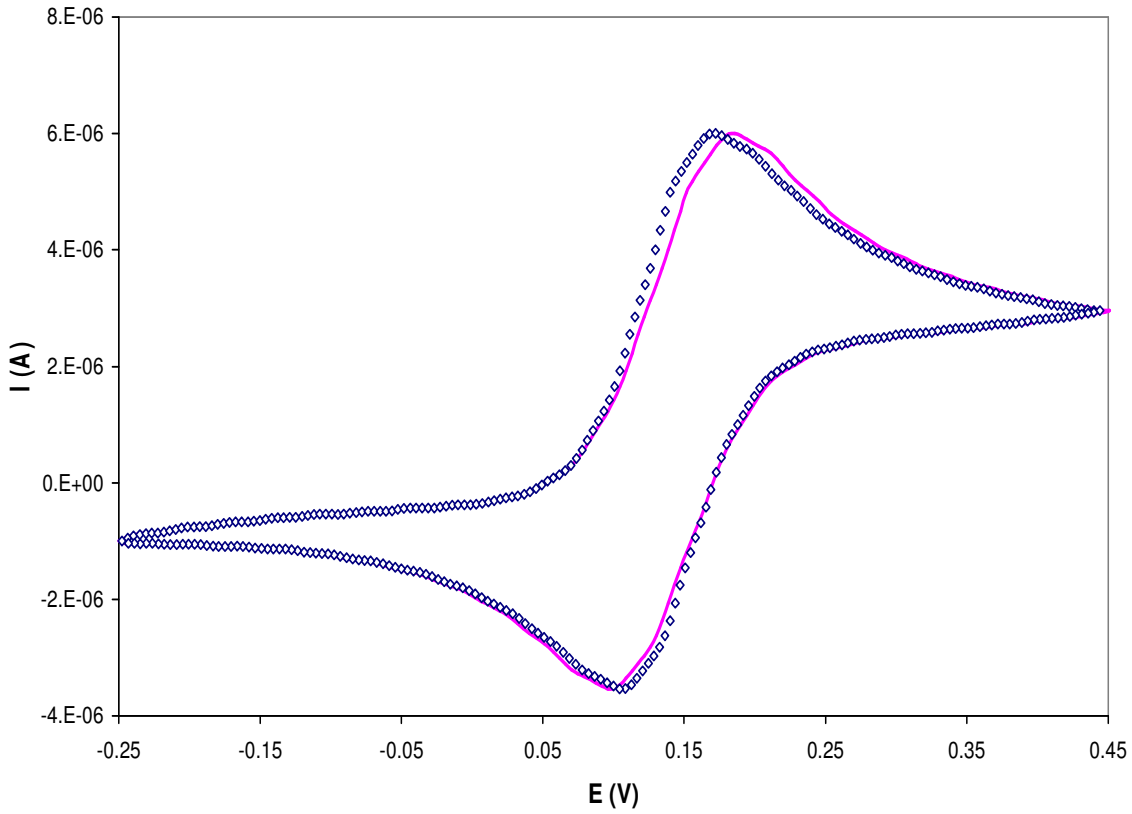

Figure 4.2 Comparison of an experimental uncorrected (solid line) and corrected for IR with R = 2200 Ω (diamonds) CV curves of ferrocene.

ΔE_p remains constant up to scan rates of 500 mV/s, a fact attesting to the accuracy of the compensation (Table 4.2). Uncompensated voltammograms obtained under the same conditions showed peak potential shifts of 8 mV at 500 mV/s (Table 4.1). $E_{pa} - E_p/2$, I_{pa}/I_{pc}, and ΔE_p values are all in accord with theory. Anodic peak current over square root of scan rate ($I_{pa}/v^{1/2}$) remained constant regardless of scan rate, which is ideal for a reversible one-electron transfer process.

Table 4.1 Analysis of data obtained from CV curves of ferrocene after background subtraction.

Scan rate, v (V/s)	E_{pa} (V)	E_{pc} (V)	ΔE_p (mV)	I_{pa} (A)	I_{pc} (A)	I_{pa}/I_{pc}	$I_{pa}/v^{1/2}$ [A/(V/s)$^{1/2}$]	$E_{pa}-E_p/2$ (mV)
0.05	0.182	0.100	82	3.60×10^{-6}	3.58×10^{-6}	1.00	1.6×10^{-5}	57
0.075	0.186	0.100	86	4.50×10^{-6}	4.48×10^{-6}	1.00	1.6×10^{-5}	60
0.100	0.186	0.100	86	5.22×10^{-6}	5.19×10^{-6}	1.00	1.6×10^{-5}	60
0.150	0.186	0.100	86	6.38×10^{-6}	6.36×10^{-6}	1.00	1.6×10^{-5}	60
0.200	0.190	0.100	90	7.37×10^{-6}	7.34×10^{-6}	1.00	1.6×10^{-5}	62
0.250	0.190	0.100	90	8.25×10^{-6}	8.25×10^{-6}	1.00	1.6×10^{-5}	63
0.400	0.190	0.100	90	1.04×10^{-5}	1.09×10^{-5}	0.95	1.6×10^{-5}	63
0.500	0.190	0.100	90	1.16×10^{-5}	1.20×10^{-5}	0.97	1.6×10^{-5}	63

Table 4.2 Analysis of data obtained from CV curves of ferrocene after background subtraction and after correction of IR voltage drop using an R value of 2200 Ω.

v (V/s)	E_{pa} (V)	E_{pc} (V)	ΔE_p (mV)	I_{pa} (A)	I_{pc} (A)	I_{pa}/I_{pc}	$I_{pa}/v^{1/2}$ [A/(V/s)$^{1/2}$]	$E_{pa}-E_p/2$ (mV)
0.05	0.173	0.113	60	3.60×10^{-6}	3.58×10^{-6}	1.00	1.6×10^{-5}	54
0.075	0.173	0.113	60	4.50×10^{-6}	4.48×10^{-6}	1.00	1.6×10^{-5}	54
0.100	0.173	0.113	60	5.22×10^{-6}	5.19×10^{-6}	1.00	1.6×10^{-5}	54
0.150	0.173	0.113	60	6.38×10^{-6}	6.36×10^{-6}	1.00	1.6×10^{-5}	54
0.200	0.173	0.113	60	7.37×10^{-6}	7.34×10^{-6}	1.00	1.6×10^{-5}	54
0.250	0.173	0.113	60	8.25×10^{-6}	8.25×10^{-6}	1.00	1.6×10^{-5}	54
0.400	0.173	0.113	60	1.04×10^{-5}	1.09×10^{-5}	0.95	1.6×10^{-5}	54
0.500	0.173	0.113	60	1.16×10^{-5}	1.20×10^{-5}	0.97	1.6×10^{-5}	54

4.2 CV OF FERROCENE IN A FLOWING SOLUTION

We needed to analyse the compounds of interest in a closed system by combining flow injection analysis and cyclic voltammetry technique. Combination of flow injection analysis and cyclic voltammetry is attractive because of the flexibility of the former and the diagnostic power of the latter [35]. In order to do this we first determined the suitable flow rate, scan rate, and a type of flow cell to use in order to obtain important parameters from a CV curve. Ferrocene was used as a model compound for this study since it is a well-studied compound that behaves reversibly. The flow rate and the scan rate are the two important parameters. Their influence on the appearance of the voltammogram is examined in detail using the three flow cells designed in our group by Cukrowski [48]. Full descriptions of the

cell designs are presented in the experimental section (Chapter 3). CV's of ferrocene were obtained first in a stationary solution before obtaining them in a flowing solution.

The effect of concentration of the supporting electrolyte was evaluated in order to make an educated decision on which concentration to use in a flowing solution. This was done with the aim of minimizing the cost of an electrolyte since high concentrations of background electrolyte will demand huge amounts of supporting electrolytes (bearing in mind that large amounts of electrolytes will be consumed daily during monitoring). Ferrocene was also investigated in this solvent over a wide range of scan rates and at various concentrations and IR drop correction was applied until the properties of the cyclic voltammograms adhere to the criteria for reversibility.

4.2.1 Studies in a Stationary Solution.

First we looked at the effect of supporting electrolyte concentration to determine a suitable concentration to be used for the preliminary studies of ferrocene in a flowing solution; the electrolyte concentrations investigated were 0.01 M and 0.05 M. Table 4.3 and 4.4 present tabulated results of the peak current separations before and after IR drop correction with R = 6200 Ω over a wide range of scan rates and on samples containing 50 and 100 mg/l concentration of ferrocene using 0.01 M $TBAPF_6$ as supporting electrolyte concentration.

Data from 9 experiments for scan rates between 0.05 and 0.5 V/s were analysed and several important parameters describing the shape of the voltammograms were obtained (Table 4.3 and 4.4). From Table 4.3 before IR voltage drop correction, ΔE_p increases with increase in scan rate and concentration of ferrocene at high scan rates (300 mV/s). At low scan rates of up to 200 mV/s and at a concentration of 50 mg/l, ΔE_p remains constant but is above 59 mV. $E_{pa} - E_p/2$ is 55 mV, I_{pa}/I_{pc} ratio is close to one and $I_{pa}/v^{1/2}$ remained constant. Increasing the scan rate to above 200 mV/s resulted in an increase in ΔE_p, $E_{pa} - E_p/2$ and decrease in $I_{pa}/v^{1/2}$ values. Increasing the concentration to 100 mg/l resulted in a huge increase in ΔE_p, $E_{pa} - E_p/2$ and decrease in $I_{pa}/v^{1/2}$ values at all studied scan rates. The ratio between anodic and cathodic peak current is far from unity.

Table 4.3 Analysis of data obtained from CV curves of ferrocene in acetonitrile containing 0.01 M $TBAPF_6$ after background subtraction.

Conc. (mg/l)	v (V/s)	E_{pa} (V)	E_{pc} (V)	ΔE_p (mV)	I_{pa} (A)	I_{pc} (A)	I_{pa}/I_{pc}	$I_{pa}/v^{1/2}$ [A/(V/s)$^{1/2}$]	$E_{pa}-E_p/2$ (mV)
50	0.05	0.135	0.053	82	1.80×10^{-6}	1.75×10^{-6}	1.03	8.0×10^{-6}	55
	0.075	0.135	0.053	82	2.20×10^{-6}	2.18×10^{-6}	1.01	8.0×10^{-6}	55
	0.100	0.135	0.053	82	2.53×10^{-6}	2.50×10^{-6}	1.01	8.0×10^{-6}	55
	0.125	0.135	0.053	82	2.84×10^{-6}	2.79×10^{-6}	1.02	8.0×10^{-6}	55
	0.150	0.135	0.053	82	3.10×10^{-6}	3.04×10^{-6}	1.02	8.0×10^{-6}	55
	0.200	0.135	0.053	82	3.60×10^{-6}	3.55×10^{-6}	1.01	8.0×10^{-6}	55
	0.300	0.139	0.053	86	4.20×10^{-6}	4.18×10^{-6}	1.00	7.7×10^{-6}	57
	0.400	0.143	0.045	98	4.77×10^{-6}	4.73×10^{-6}	1.00	7.5×10^{-6}	62
	0.500	0.143	0.045	98	5.26×10^{-6}	5.24×10^{-6}	1.00	7.4×10^{-6}	62
100	0.050	0.147	0.049	98	3.49×10^{-6}	3.08×10^{-6}	1.13	1.6×10^{-5}	63
	0.075	0.156	0.045	111	4.10×10^{-6}	3.38×10^{-6}	1.21	1.5×10^{-5}	66
	0.100	0.160	0.045	115	4.63×10^{-6}	3.84×10^{-6}	1.21	1.5×10^{-5}	68
	0.125	0.160	0.045	115	5.00×10^{-6}	4.15×10^{-6}	1.21	1.4×10^{-5}	68
	0.150	0.164	0.041	123	5.35×10^{-6}	4.44×10^{-6}	1.21	1.4×10^{-5}	70
	0.200	0.169	0.041	128	5.95×10^{-6}	4.98×10^{-6}	1.20	1.3×10^{-5}	72
	0.300	0.173	0.036	137	6.97×10^{-6}	5.92×10^{-6}	1.18	1.3×10^{-5}	74
	0.400	0.177	0.032	145	7.73×10^{-6}	6.73×10^{-6}	1.15	1.2×10^{-5}	76
	0.500	0.182	0.032	150	8.27×10^{-6}	7.18×10^{-6}	1.15	1.2×10^{-5}	80

Introduction of IR drop correction only improved the ΔE_p value, which remained constant with increase in scan rate with a value of 60 mV (Table 4.4). The $E_{pa} - E_p/2$ deviated from a theoretical value by about 5 mV at all studied scan rates at a concentration of 50 mg/l and deviated by 4 mV at a concentration of 100 mg/l. The deviation in a ($E_{pa} - E_p/2$) value from 56 mV predicted for the process controlled only by diffusion, may be due to overcompensation resulting in a steep curve. The peak current ratio remained unchanged after compensation, so was the value of $I_{pa}/v^{1/2}$.

Table 4.4 Analysis of data in Table 4.3, obtained from CV curves of ferrocene after correction of IR voltage drop using an R value of 6200 Ω.

Conc. (mg/l)	v (V/s)	E_{pa} (V)	E_{pc} (V)	ΔE_p (mV)	I_{pa} (A)	I_{pc} (A)	I_{pa}/I_{pc}	$I_{pa}/v^{1/2}$ [A/(V/s)$^{1/2}$]	$E_{pa}-E_p/2$ (mV)
50	0.050	0.120	0.060	60	1.80×10^{-6}	1.75×10^{-6}	1.03	8.0×10^{-6}	51
	0.075	0.120	0.060	60	2.20×10^{-6}	2.18×10^{-6}	1.01	8.0×10^{-6}	51
	0.100	0.120	0.060	60	2.53×10^{-6}	2.50×10^{-6}	1.01	8.0×10^{-6}	51
	0.125	0.120	0.060	60	2.84×10^{-6}	2.79×10^{-6}	1.02	8.0×10^{-6}	51
	0.150	0.120	0.060	60	3.10×10^{-6}	3.04×10^{-6}	1.02	8.0×10^{-6}	51
	0.200	0.120	0.060	60	3.60×10^{-6}	3.55×10^{-6}	1.01	8.0×10^{-6}	51
	0.300	0.120	0.060	60	4.20×10^{-6}	4.18×10^{-6}	1.00	7.7×10^{-6}	51
	0.400	0.120	0.060	60	4.77×10^{-6}	4.73×10^{-6}	1.00	7.5×10^{-6}	51
	0.500	0.120	0.060	60	5.26×10^{-6}	5.24×10^{-6}	1.00	7.4×10^{-6}	51
100	0.050	0.122	0.062	60	3.49×10^{-6}	3.08×10^{-6}	1.13	1.6×10^{-5}	52
	0.075	0.122	0.062	60	4.10×10^{-6}	3.38×10^{-6}	1.21	1.5×10^{-5}	52
	0.100	0.122	0.062	60	4.63×10^{-6}	3.84×10^{-6}	1.21	1.5×10^{-5}	52
	0.125	0.122	0.062	60	5.00×10^{-6}	4.15×10^{-6}	1.21	1.4×10^{-5}	52
	0.150	0.122	0.062	60	5.35×10^{-6}	4.44×10^{-6}	1.21	1.4×10^{-5}	52
	0.200	0.122	0.062	60	5.95×10^{-6}	4.98×10^{-6}	1.20	1.3×10^{-5}	52
	0.300	0.122	0.062	60	6.97×10^{-6}	5.92×10^{-6}	1.18	1.3×10^{-5}	52
	0.400	0.122	0.062	60	7.73×10^{-6}	6.73×10^{-6}	1.15	1.2×10^{-5}	52
	0.500	0.122	0.062	60	8.27×10^{-6}	7.18×10^{-6}	1.15	1.2×10^{-5}	52

Increasing the electrolyte solution concentration to 0.05 M, results in improved results. Table 4.5 presents data before IR voltage drop correction for scan rates between 0.05 and 0.5 V/s; ΔE_p remains constant but is above 59 mV. The $E_{pa} - E_p/2$ value is 55 mV and I_{pa}/I_{pc} is close to one; this is all in accord with theory at all studied scan rates and concentrations.

Table 4.5 Analysis of data obtained from CV curves of ferrocene in acetonitrile containing 0.05 M $TBAPF_6$ after background subtraction.

Conc. (mg/l)	v (V/s)	E_{pa} (V)	E_{pc} (V)	ΔE_p (mV)	I_{pa} (A)	I_{pc} (A)	I_{pa}/I_{pc}	$I_{pa}/v^{1/2}$ [A/(V/s)$^{1/2}$]	$E_{pa}-E_p/2$ (mV)
50	0.050	0.130	0.062	68	1.80×10^{-6}	1.82×10^{-6}	0.99	8.0×10^{-6}	55
	0.075	0.130	0.062	68	2.20×10^{-6}	2.20×10^{-6}	1.00	8.0×10^{-6}	55
	0.100	0.130	0.062	68	2.55×10^{-6}	2.62×10^{-6}	0.97	8.0×10^{-6}	55
	0.125	0.130	0.062	68	2.85×10^{-6}	2.83×10^{-6}	1.00	8.0×10^{-6}	55
	0.150	0.130	0.062	68	3.10×10^{-6}	3.12×10^{-6}	0.99	8.0×10^{-6}	55
	0.175	0.130	0.062	68	3.36×10^{-6}	3.31×10^{-6}	1.01	8.0×10^{-6}	55
	0.200	0.130	0.062	68	3.60×10^{-6}	3.55×10^{-6}	1.01	8.0×10^{-6}	55
	0.300	0.130	0.062	68	4.41×10^{-6}	4.37×10^{-6}	1.01	8.0×10^{-6}	55
	0.400	0.130	0.062	68	5.09×10^{-6}	5.05×10^{-6}	1.01	8.0×10^{-6}	55
	0.500	0.130	0.062	68	5.66×10^{-6}	5.54×10^{-6}	1.02	8.0×10^{-6}	55
100	0.050	0.130	0.062	68	3.61×10^{-6}	3.58×10^{-6}	1.00	1.6×10^{-5}	55
	0.075	0.130	0.062	68	4.41×10^{-6}	4.42×10^{-6}	1.00	1.6×10^{-5}	55
	0.100	0.130	0.062	68	5.08×10^{-6}	5.05×10^{-6}	1.00	1.6×10^{-5}	55
	0.125	0.130	0.062	68	5.65×10^{-6}	5.66×10^{-6}	1.00	1.6×10^{-5}	55
	0.150	0.130	0.062	68	6.10×10^{-6}	6.05×10^{-6}	1.00	1.6×10^{-5}	55
	0.200	0.130	0.062	68	7.00×10^{-6}	6.96×10^{-6}	1.00	1.6×10^{-5}	55
	0.300	0.130	0.062	68	8.52×10^{-6}	8.50×10^{-6}	1.00	1.6×10^{-5}	55
	0.400	0.130	0.062	68	9.96×10^{-6}	9.94×10^{-6}	1.00	1.6×10^{-5}	55
	0.500	0.130	0.062	68	1.15×10^{-5}	1.14×10^{-5}	1.00	1.6×10^{-5}	55
200	0.050	0.130	0.062	68	6.88×10^{-6}	7.04×10^{-6}	0.98	3.1×10^{-5}	55
	0.075	0.130	0.062	68	8.56×10^{-6}	8.66×10^{-6}	0.99	3.1×10^{-5}	55
	0.100	0.130	0.062	68	9.93×10^{-6}	1.00×10^{-5}	0.99	3.1×10^{-5}	55
	0.125	0.130	0.062	68	1.11×10^{-5}	1.12×10^{-5}	0.99	3.1×10^{-5}	55
	0.150	0.130	0.062	68	1.21×10^{-5}	1.22×10^{-5}	0.99	3.1×10^{-5}	55
	0.200	0.130	0.062	68	1.40×10^{-5}	1.40×10^{-5}	1.00	3.1×10^{-5}	55
	0.300	0.130	0.062	68	1.69×10^{-5}	1.69×10^{-5}	1.00	3.1×10^{-5}	55
	0.400	0.130	0.062	68	1.95×10^{-5}	1.94×10^{-5}	1.00	3.1×10^{-5}	55
	0.500	0.130	0.062	68	2.19×10^{-5}	2.16×10^{-5}	1.00	3.1×10^{-5}	55

Correction of IR drop only improved the ΔE_p value, which remained constant with increase in scan rate and concentration and had a value of 60 mV (Table 4.6 and 4.7). The $E_{pa} - E_p/2$ deviated from a theoretical value of 56 mV by about 3 mV at all studied concentrations.

Table 4.6 Analysis of data in Table 4.5 obtained from CV curves of ferrocene after correction of IR voltage drop using an R value of 3000 Ω.

Conc. (mg/l)	v (V/s)	E_{pa} (V)	E_{pc} (V)	ΔE_p (mV)	I_{pa} (A)	I_{pc} (A)	I_{pa}/I_{pc}	$I_{pa}/v^{1/2}$ [A/ (V/s)$^{1/2}$]	$E_{pa}-E_p/2$ (mV)
50	0.050	0.126	0.066	60	1.80×10^{-6}	1.82×10^{-6}	0.99	8.0×10^{-6}	53
	0.075	0.126	0.066	60	2.20×10^{-6}	2.20×10^{-6}	1.00	8.0×10^{-6}	53
	0.100	0.126	0.066	60	2.55×10^{-6}	2.62×10^{-6}	0.97	8.0×10^{-6}	53
	0.125	0.126	0.066	60	2.85×10^{-6}	2.83×10^{-6}	1.00	8.0×10^{-6}	53
	0.150	0.126	0.066	60	3.10×10^{-6}	3.12×10^{-6}	0.99	8.0×10^{-6}	53
	0.175	0.126	0.066	60	3.36×10^{-6}	3.31×10^{-6}	1.01	8.0×10^{-6}	53
	0.200	0.126	0.066	60	3.60×10^{-6}	3.55×10^{-6}	1.01	8.0×10^{-6}	53
	0.300	0.126	0.066	60	4.41×10^{-6}	4.37×10^{-6}	1.01	8.0×10^{-6}	53
	0.400	0.126	0.066	60	5.09×10^{-6}	5.05×10^{-6}	1.01	8.0×10^{-6}	53
	0.500	0.126	0.066	60	5.66×10^{-6}	5.54×10^{-6}	1.02	8.0×10^{-6}	53
100	0.050	0.126	0.066	60	3.61×10^{-6}	3.58×10^{-6}	1.00	1.6×10^{-5}	53
	0.075	0.126	0.066	60	4.41×10^{-6}	4.42×10^{-6}	1.00	1.6×10^{-5}	53
	0.100	0.126	0.066	60	5.08×10^{-6}	5.05×10^{-6}	1.00	1.6×10^{-5}	53
	0.125	0.126	0.066	60	5.65×10^{-6}	5.66×10^{-6}	1.00	1.6×10^{-5}	53
	0.150	0.126	0.066	60	6.10×10^{-6}	6.05×10^{-6}	1.00	1.6×10^{-5}	53
	0.200	0.126	0.066	60	7.00×10^{-6}	6.96×10^{-6}	1.00	1.6×10^{-5}	53
	0.300	0.126	0.066	60	8.52×10^{-6}	8.50×10^{-6}	1.00	1.6×10^{-5}	53
	0.400	0.126	0.066	60	9.96×10^{-6}	9.94×10^{-6}	1.00	1.6×10^{-5}	53
	0.500	0.126	0.066	60	1.15×10^{-5}	1.14×10^{-5}	1.00	1.6×10^{-5}	53

Table 4.7 Analysis of data obtained from CV curves of ferrocene after background subtraction and after correction of IR voltage drop using an R value of 1000 Ω.

Conc. (mg/l)	v (V/s)	E_{pa} (V)	E_{pc} (V)	ΔE_p (mV)	I_{pa} (A)	I_{pc} (A)	I_{pa}/I_{pc}	$I_{pa}/v^{1/2}$ [A/ (V/s)$^{1/2}$]	$E_{pa}-E_p/2$ (mV)
200	0.050	0.122	0.062	60	6.88×10^{-6}	7.04×10^{-6}	0.98	3.1×10^{-5}	53
	0.075	0.122	0.062	60	8.56×10^{-6}	8.66×10^{-6}	0.99	3.1×10^{-5}	53
	0.100	0.122	0.062	60	9.93×10^{-6}	1.00×10^{-5}	0.99	3.1×10^{-5}	53
	0.125	0.122	0.062	60	1.11×10^{-5}	1.12×10^{-5}	0.99	3.1×10^{-5}	53
	0.150	0.122	0.062	60	1.21×10^{-5}	1.22×10^{-5}	0.99	3.1×10^{-5}	53
	0.200	0.122	0.062	60	1.40×10^{-5}	1.40×10^{-5}	1.00	3.1×10^{-5}	53
	0.300	0.122	0.062	60	1.69×10^{-5}	1.69×10^{-5}	1.00	3.1×10^{-5}	53
	0.400	0.122	0.062	60	1.95×10^{-5}	1.94×10^{-5}	1.00	3.1×10^{-5}	53
	0.500	0.122	0.062	60	2.19×10^{-5}	2.16×10^{-5}	1.00	3.1×10^{-5}	53

The amount of resistance required for compensation of curves at high concentrations of ferrocene (200 mg/l) was smaller than the amount required for low concentrations. The

resistance amount required for compensation was only 1000 Ohm. This shows that analyte made significant contribution to the overall conductivity of solution that most likely resulted in migration current. Therefore, for any rigorous studies involving e.g. mechanisms of electrochemical reaction, either the concentration of the supporting electrolyte would have to be increased or concentration of the analyte (i.e. ferrocene) would have to be decreased.

4.2.2 Studies in a Flowing Solution.

Here we investigated the effect of scan rate and flow rate on the appearance of a cyclic voltammogram using different flow cells. The main difference in these flow cells was positioning of electrodes. The performances of the flow through cells were evaluated by cyclic voltammetry using ferrocene as an analyte. First we analysed the CV curves obtained using the so-called flow-by cell, whereby the background electrolyte solution is flowing along the working electrode. The reference and counter electrodes were facing each other and so were the outlet and inlet tubes.

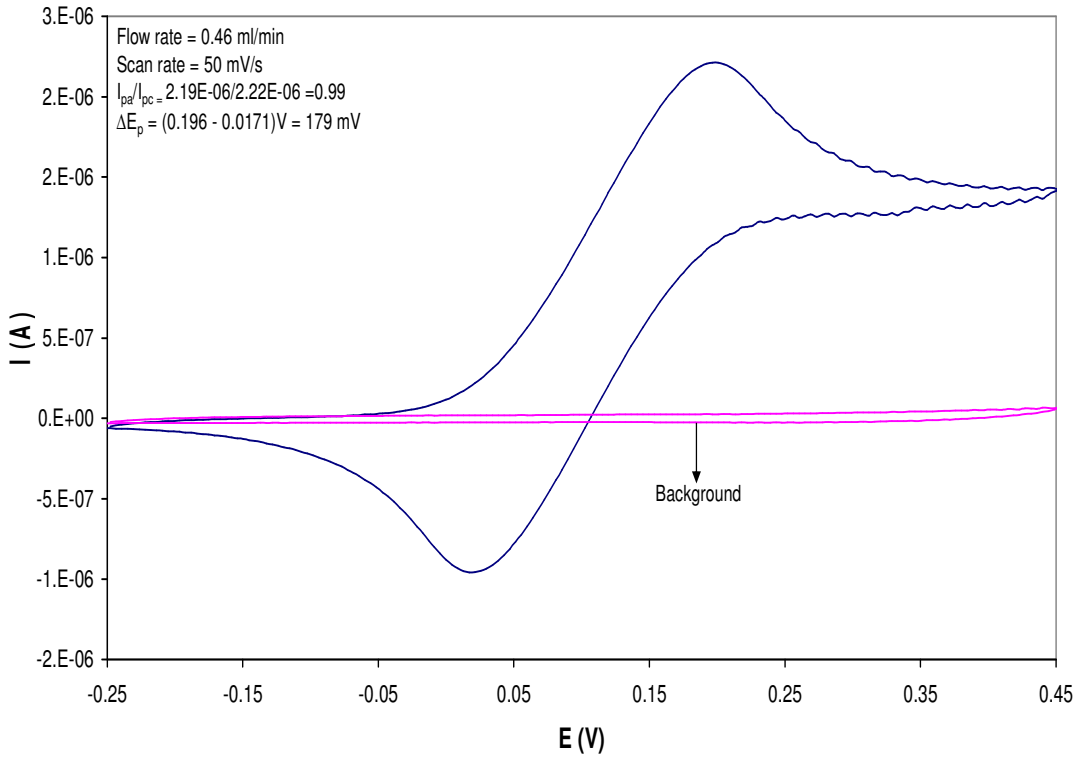

Figure 4.3 CV curve of a 50 mg/l ferrocene obtained using a flow-by electrochemical cell, flow rate = 0.46 ml min^{-1}.

The employed concentration of the supporting electrolyte ($TBAPF_6$) was 0.01 M. A low concentration of electrolyte solutions was used to minimize cost and because the amount of resistance introduced could be corrected for. Figure 4.3 shows a cyclic voltammogram of ferrocene at a scan rate of 50 mV/s and a flow rate of 0.46 ml min^{-1}. Well-defined anodic and cathodic peaks were observed from the CV curve. The anodic wave represents the oxidation of $Fe^{2+}Cp_2$ to $Fe^{3+}Cp_2$, while the cathodic wave represents the reduction of $Fe^{3+}Cp_2$ to $Fe^{2+}Cp_2$ (the reverse reaction).

Table 4.8 Data of peak potential separations and peak current ratio obtained from a 50 mg/l ferrocene stock solution at different scan rates and flow rates using a flow-by cell 1.

		Before IR drop correction				After IR drop correction		
Flow rate (ml min^{-1})	v (V s^{-1})	E_{pa} (V)	E_{pc} (V)	ΔE_p (mV)	I_{pa}/I_{pc}	E_{pa} (V)	E_{pc} (V)	ΔE_p (mV) [R = 34000 Ω]
0.00	0.050	0.183	0.00427	178	0.99	0.120	0.060	60
	0.100	0.206	0.0159	190	0.99	0.120	0.060	60
	0.200	0.233	0.0412	192	0.99	0.120	0.060	60
	0.300	0.262	0.062	200	0.98	0.120	0.060	60
	0.400	0.271	0.0677	203	0.98	0.120	0.060	60
0.46	0.050	0.196	0.0171	179	0.99	0.120	0.060	60
	0.100	0.214	0.0275	186	0.96	0.120	0.060	60
	0.200	0.247	0.0412	206	0.91	0.120	0.060	60
	0.300	0.262	0.0476	214	0.86	0.120	0.060	60
	0.400	0.271	0.0510	220	0.85	0.120	0.060	60
0.98	0.050	0.201	0.0256	175	0.99	0.120	0.060	60
	0.100	0.222	0.0159	206	0.99	0.120	0.060	60
	0.200	0.247	0.0275	219	0.98	0.120	0.060	60
	0.300	0.286	0.0476	238	0.94	0.120	0.060	60
	0.400	0.305	0.0577	247	0.89	0.120	0.060	60
1.52	0.050	0.214	0.0299	184	0.98	0.120	0.060	60
	0.100	0.230	0.0159	214	0.97	0.120	0.060	60
	0.200	0.247	0.0137	233	0.95	0.120	0.060	60
	0.300	0.284	0.0473	237	0.93	0.120	0.060	60
	0.400	0.304	0.0550	249	0.93	0.120	0.060	60

The CV curves obtained with increase in scan rate are presented in Appendix A (Figure A1 – A4). Increasing the flow rate and scan rate result in large potential separation between the anodic and cathodic peaks which can be interpreted in terms of IR drop due to the working

electrode and the reference electrode being far apart (Table 4.8). It is interesting to see that after IR drop correction (R = 34000 Ω) the ΔE_p value approached 60 mV for all studied scan rates as predicted for one-electron reversible charge transfer.

Figures 4.4 to 4.6 present comparisons of the CV curves of ferrocene obtained in a flowing solution, non-flowing solution in a flow cell and bulk solution in an open cell before and after IR voltage drop correction. This was done to see how the peak potential separation value vary in different solution types and how much resistance would be required in each CV to bring the peaks closer together (to ~ 60 mV). The amount of resistance used to bring the peak separation value to 60 mV was 34000 Ω in both the flowing and non-flowing solution and 6200 Ω in a bulk solution. The difference in IR is due to the geometry of the cells, namely the distance between the reference and the working electrode.

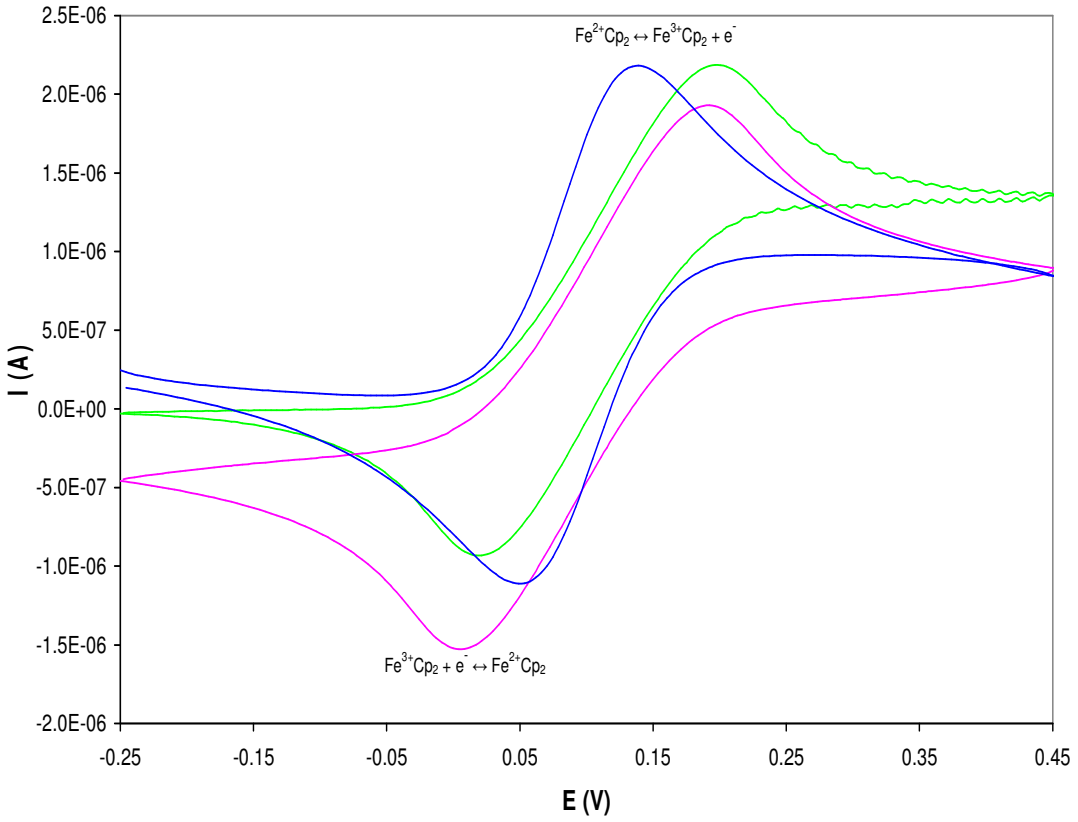

Figure 4.4 Comparison of the CV curves of a 50 mg/l ferrocene in a flowing (— 0.46 ml min^{-1}) and non-flowing (—) solution using a flow-by electrochemical cell and in a bulk solution (—) using an open cell.

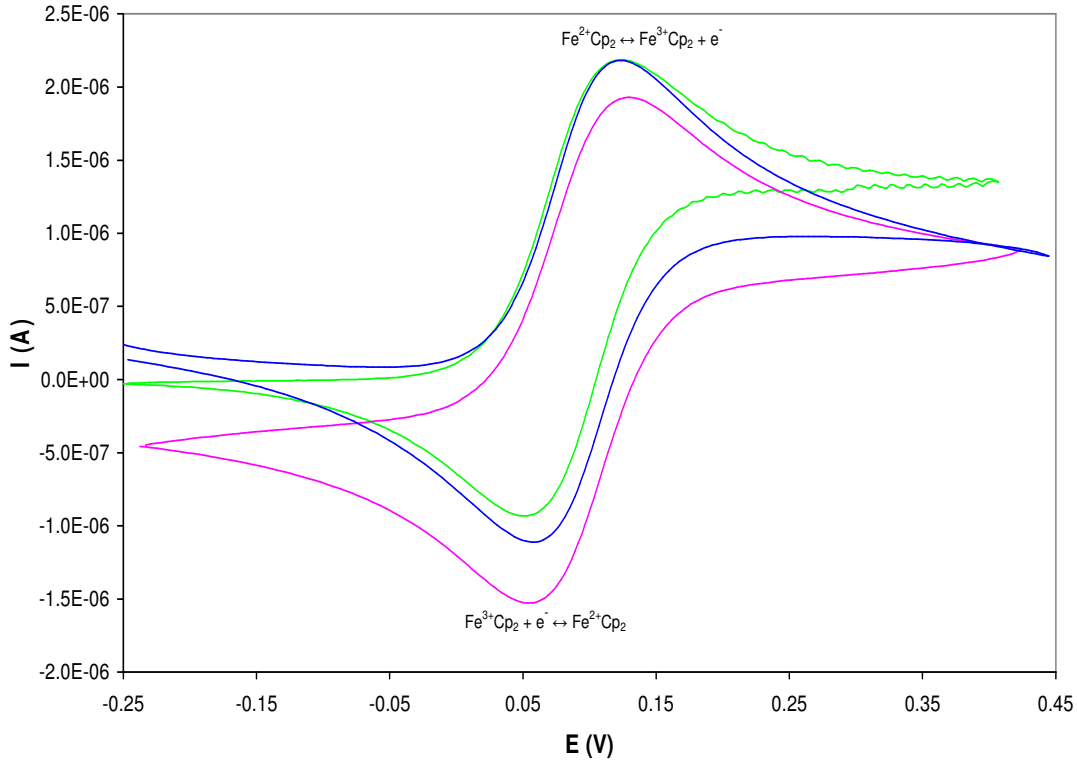

Figure 4.5 Comparison of the CV curves of ferrocene shown in Figure 4.4 after IR voltage drop correction.

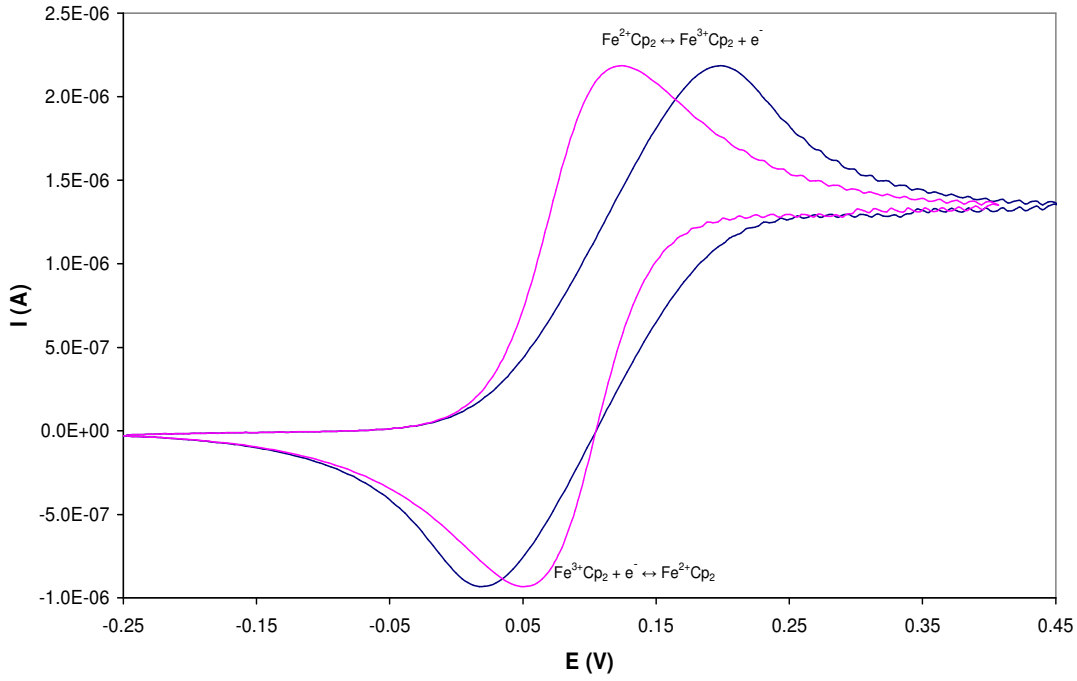

Figure 4.6 Comparison of CV curves of a 50 mg/l ferrocene in a flowing solution before (—) and after (—) IR voltage drop correction (R = 34000 Ω), flow rate = 0.46 ml min^{-1}.

Next, we repeated the above experiments of ferrocene in a flowing solution using a wall-jet type of a flow cell whereby the solution is flowing perpendicularly towards the working electrode. Two types of wall-jet flow cells were used in this study, with the main difference being a type of the auxiliary electrode used and its position in a flow cell as described in the experimental section chapter 3. Figures 4.7 and 4.8 show CV's of ferrocene in a flowing solution using two wall-jet flow cells at a flow rate 0.46 ml min^{-1}. CV exhibits a characteristic polarogram-like shape at slow scan rate (50 mV/s) and the reverse trace is almost superimposable on the forward trace, hence no peak-like responses are observed. In this respect the reverse trace yield no useful information as oxidized products are swept away from the electrode before they could eventually be reduced. This behaviour arises because in wall-jet cells a thin layer of stagnant solution is present adjacent to the electrode surface and flow is away from the electrode ensuring that a fresh solution is effectively brought to the electrode surface. Under such hydrodynamic conditions, the electrochemical process is controlled by both convection and diffusion.

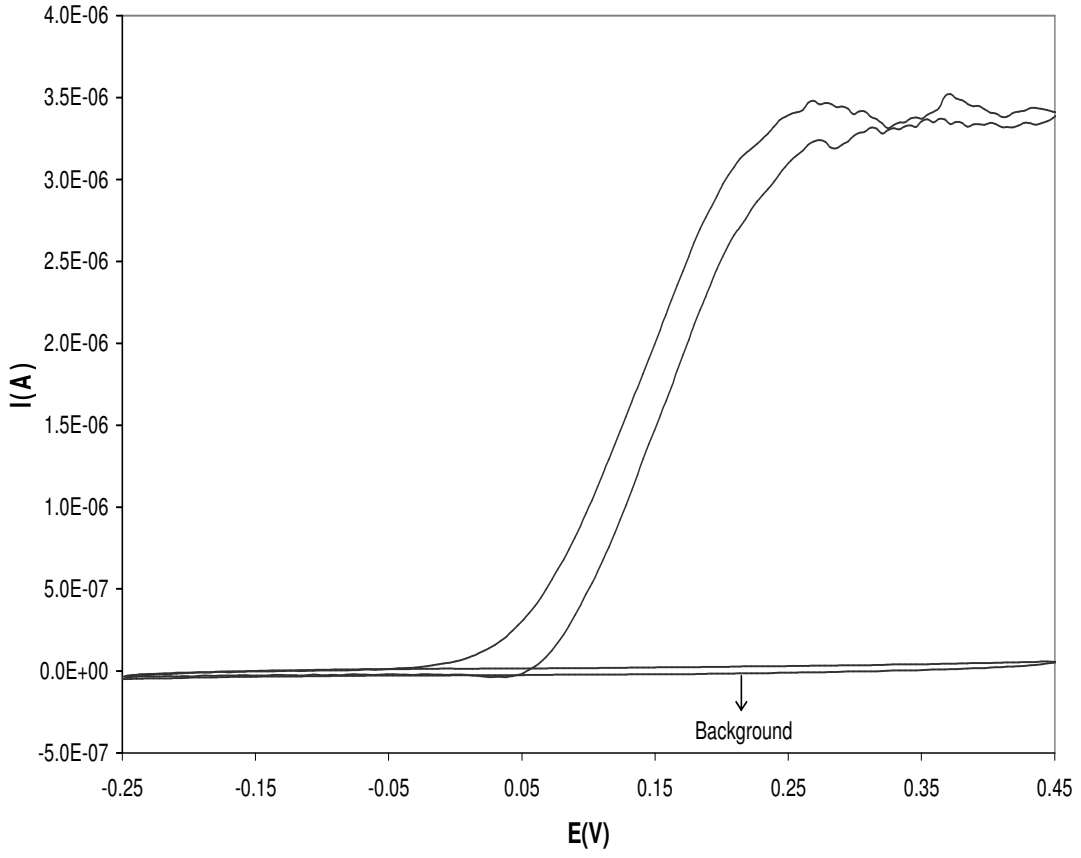

Figure 4.7 CV curves of a 50 mg/l ferrocene in a flowing solution using a wall-jet electrochemical cell with a gold-disk auxiliary electrode, flow rate = 0.46 ml min^{-1}.

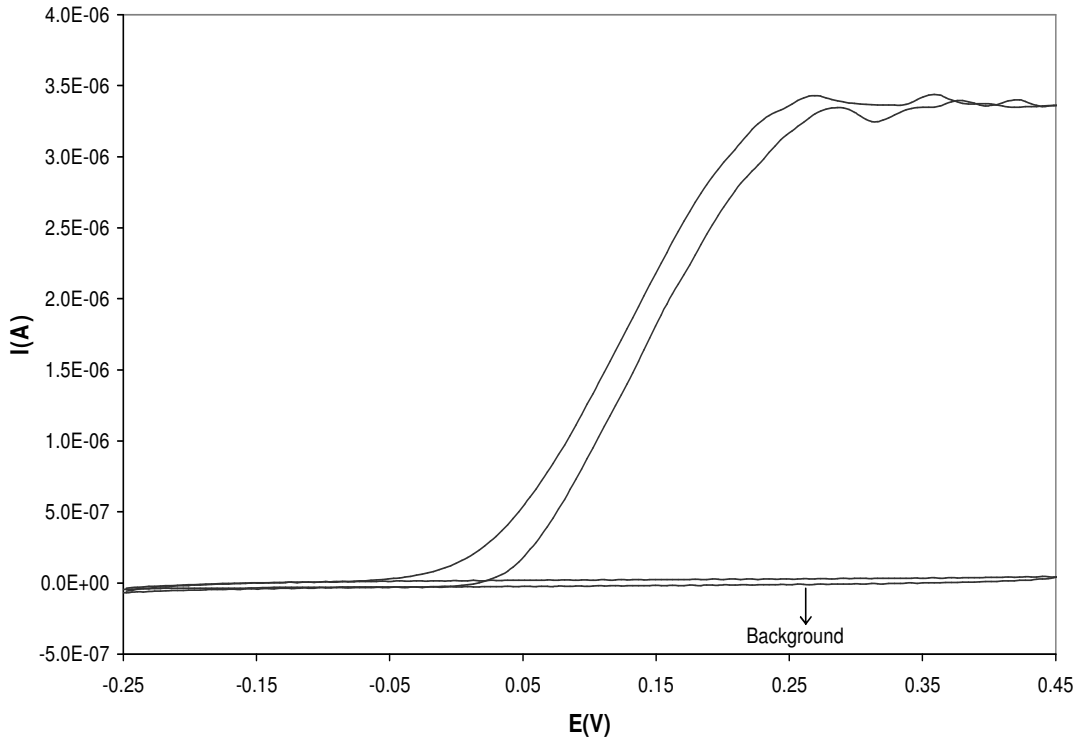

Figure 4.8 CV curves of a 50 mg/l ferrocene in a flowing solution using a wall-jet electrochemical cell with a steel rod tube auxiliary electrode and outlet, flow rate = 0.46 ml min^{-1}.

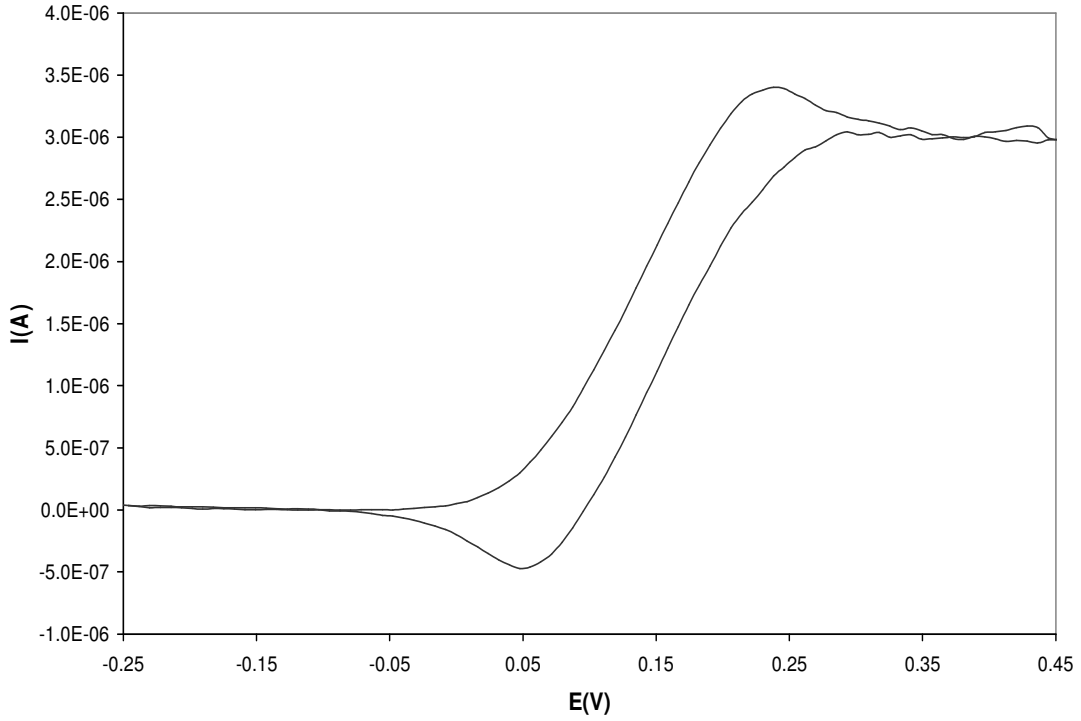

Figure 4.9 CV curves of a 50 mg/l ferrocene in a flowing solution using a wall-jet electrochemical cell with a gold-disk auxiliary electrode, flow rate = 0.46 ml min^{-1} and v = 100 mV/s.

As scan rate is increased to 100 mV/s, the voltammograms deviates a little from the typical polarogram shape, as a small peak component is present at the onset of the limiting current plateau (Figure 4.9).

Figure 4.10 shows the effect of increased scan rate on the cyclic voltammogram of ferrocene. As the scan rate is increased to above 100 $mV.s^{-1}$, the voltammograms deviate from a convection/diffusion-controlled polarogram shaped curve to nearly diffusion controlled peak-shaped curves. The peak intensity increased with increasing scan rate, while the anodic peak shifts towards higher potentials as expected due to IR drop. The oxidized compound will still be present in the stagnant layer attached to the electrode surface during the reverse scan, and the reversibly oxidized ferrocene clearly shows a reduction wave since increasing the scan rate results in a decrease of the diffusion layer thickness. There seems to be no significant difference between curves obtained in the two wall-jet flow cells, which confirms that the type and position of the auxiliary electrode does not play a significant role. The CV data obtained for the peak potential separations are summarised in Tables 4.9 and 4.10.

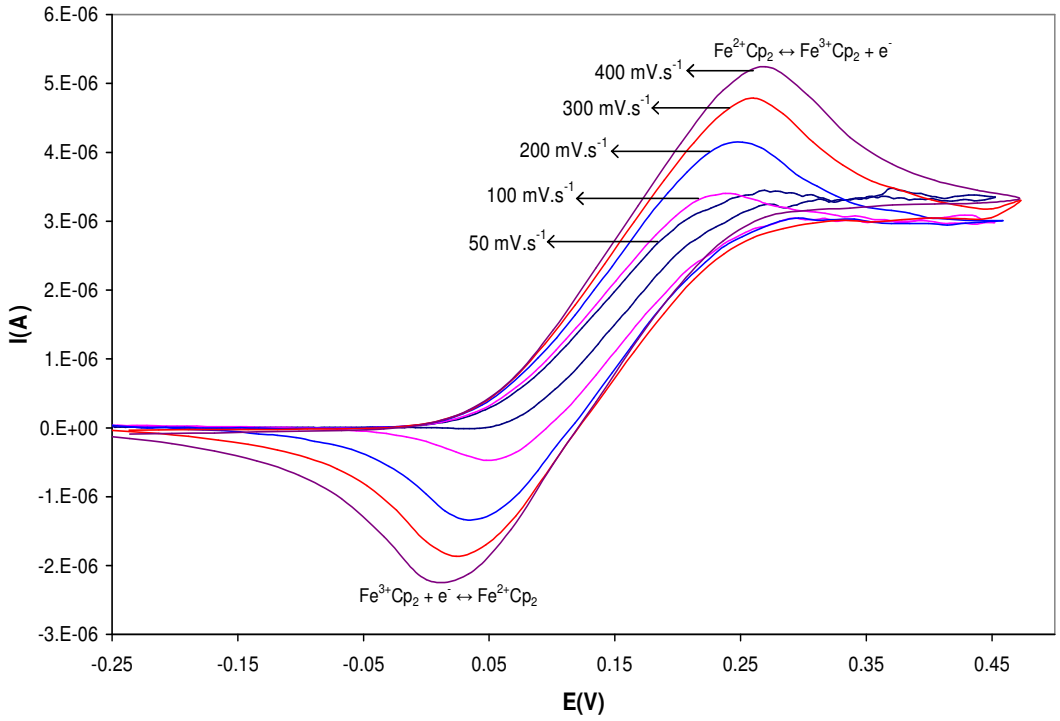

Figure 4.10 CV curves of a 50 mg/l ferrocene after background subtraction at different scan rates and a flow rate of 0.46 ml/min using a wall-jet electrochemical cell with a gold-disk auxiliary electrode.

Table 4.9 Data of peak potential separations and peak current ratio obtained from a ferrocene solution using a wall-jet flow cell with a gold disk auxiliary electrode.

Flow rate (ml min^{-1})	v (V s^{-1})	E_{pa} (V)	E_{pc} (V)	ΔE_p (mV)	I_{pa}/I_{pc}
0.46	0.050	–	–	–	–
	0.100	0.230	0.0476	182	0.97
	0.200	0.252	0.0296	222	0.97
	0.300	0.260	0.0237	236	0.97
	0.400	0.270	0.0000	270	0.99
0.98	0.050	–	–	–	–
	0.100	–	–	–	–
	0.200	–	–	–	–
	0.300	0.286	0.0238	262	1.03
	0.400	0.305	0.0000	305	0.99

– = *no peak was observed*

Table 4.10 Data of peak potential separations and peak current ratio obtained from ferrocene solution using a wall-jet flow cell with a steel rod tube auxiliary electrode.

Flow rate (ml min^{-1})	v (V s^{-1})	E_{pa} (V)	E_{pc} (V)	ΔE_p (mV)	I_{pa}/I_{pc}
0.46	0.050	–	–	–	–
	0.100	0.230	0.0159	214	1.0
	0.200	0.237	0.0148	222	1.0
	0.300	0.262	0.0238	238	0.99
	0.400	0.271	0.0310	240	0.99
0.98	0.050	–	–	–	–
	0.100	–	–	–	–
	0.200	–	–	–	–
	0.300	0.286	0.000	286	1.0
	0.400	0.305	0.000	305	1.0

– = *no peak was observed*

We arrived at the following conclusions from the above data:

- With all the flow cells it is possible to choose the experimental conditions that favour convection/diffusion-controlled (polarogram-shaped) voltammograms or diffusion-controlled (peak-shaped) voltammograms.
- The main distinguishing factor between the three home-made designs of the flow cells is that with the flow–by electrochemical cell 1, there is no convection, so

processes are controlled only by diffusion and results are very much similar to those obtained in the bulk solution in an open cell. It is obvious that diffusion-controlled electrochemical processes recorded here might change to mixed mode (convection and diffusion) at slow scan rates and increased flow rates. Flow-by cell is by far more versatile as it can be recommended for fundamental, mechanisms, speciation, quantitative and qualitative studies performed on-line.

- The wall-jet cells should be recommended for quantitative analysis as it generates significantly higher analytical signal when compared with the flow-by cell.

4.2.3 Investigations of the Possibility of Sample/Reagent Mixing On-Line Using Ferrocene in Acetonitrile Containing 0.01 M $TBAPF_6$.

The above flow injection analysis experiments were performed in solutions that were prepared in batch. We attempted to mix the electrolyte and sample solution on-line by incorporating a mixing T-piece onto our FIA system. During on-line mixing the mixing T-piece originated a reaction (mixing) zone that was subsequently carried through a six port manifold into the detector. The efficiency of the mixing approach is of importance for convenient reaction development, to improve the analytical signal and reproducibility. Before analysis, we performed an experiment over a range of resultant flow rates to see its effect on the anodic peak height. The resultant mixing flow rate is the total flow rate of the background electrolyte and the sample solution.

For example, if one desires to measure a CV curve of a 50 mg/l ferrocene solution from a 100 mg/l ferrocene stock solution on-line one will pump both the background and sample solution at a flow rate of 4 ml/min resulting in a mixed solution with a total flow of 8 ml/min to the cell.

$$Q/q = C/c$$

Where Q = is the total or resultant flow rate to the cell

q = is the sample solution flow rate to the mixing T-piece

C = is the concentration of the stock solution

c = is the concentration of the sample solution to the cell

Therefore: $q = Qc/C$

$$q = \frac{(8\ ml/\min) \times (50\ mg/l)}{100\ mg/l}$$

$$q = 4\ ml/\min$$

$$\therefore Background\ \ flow\ rate\ to\ the\ mixing\ T-piece = Q - q$$

$$= 8\ ml/\min - 4\ ml/\min$$

$$= 4\ ml/\min$$

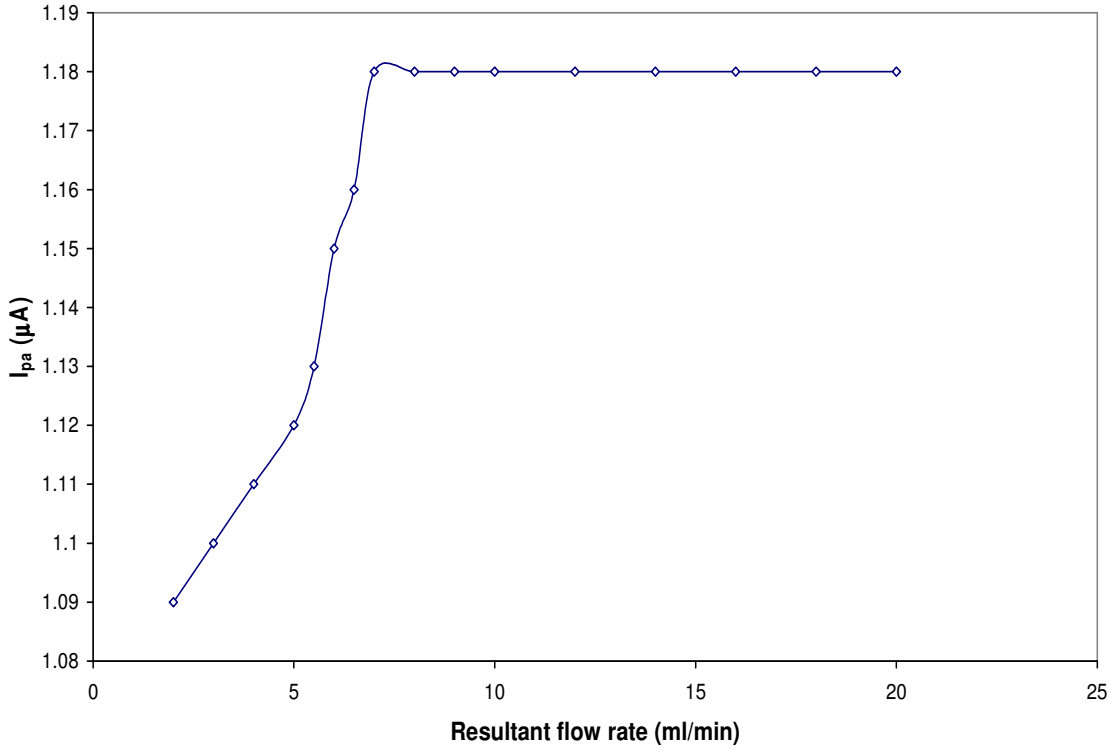

Figure 4.11 Plot of resultant flow rate vs. anodic peak current of ferrocene, v = 100 mV/s.

Figure 4.11 shows a plot of resultant mixing flow rate versus anodic peak current obtained in a ferrocene solution. The anodic peak current increased with an increase in mixing flow rate from 2 ml min^{-1} to 7 ml min^{-1} and remained constant from 7 ml min^{-1} to 20 ml min^{-1} (the highest studied mixing flow rate). It appears that from the resultant flow rate of 7 ml/min the stagnant layer remains constant as it has reached the smallest thickness, hence the signal does not increase further. From this data we decided to use 10 ml min^{-1} as the mixing flow rate in all experiments performed with on-line mixing.

The influence of on-line mixing on the CV curves of ferrocene was demonstrated by comparing the curve obtained with manual mixing to the one obtained with on-line mixing

(Figure 4.12). The peaks were enhanced when CV curves were recorded during on-line mixing and the analytical signal was improved. This behaviour arises because the solutions were prepared under controlled conditions with exclusion of moisture and any other particulate matters that can lead to contamination of solution. Comparison with a voltammogram obtained in a bulk solution (Figure 4.12, dotted curve) showed that the situation in a bulk solution approaches that in a flowing solution, when the analysed concentration of an analyte is prepared by hand using a syringe, in terms of signal intensity. It was not clear at this stage why the curve measured using an on-line mixing method was much higher or led to greater sensitivity as compared to those prepared in batch.

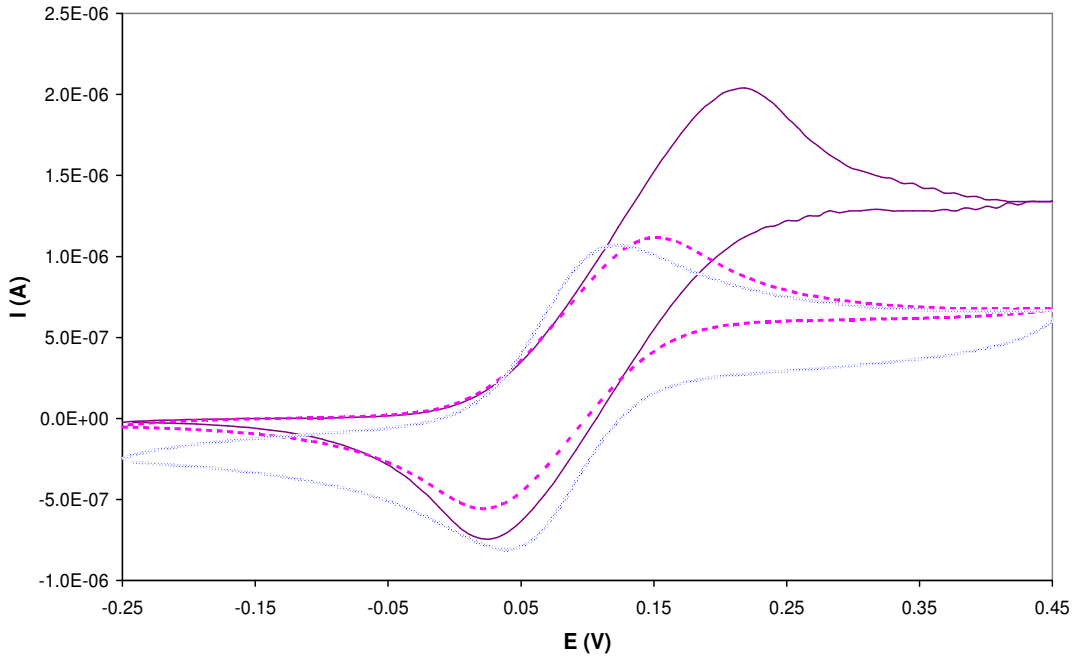

Figure 4.12 Comparison of the CV curves of a 20 mg/l ferrocene obtained in a flowing solution when the stock solution was prepared by hand (---) and using on-line (—) mixing technique, flow rate = 0.98 ml min^{-1} and v = 100 mV/s. The CV curve of 20 mg/l ferrocene obtained in a bulk solution (….) using an open cell at the same scan rate is also overlaid for comparison.

Quantitative analysis test of ferrocene at different concentrations was performed using on-line mixing approach. It must be noted that, one can prepare solutions of different concentrations by varying the flow rates of both the background and the sample solution.

Figures 4.13 and 4.14 shows CV curves obtained in different concentrations of ferrocene in a flowing solution with on-line mixing using a flow-by electrochemical cell. The peak intensity increases and the anodic peak shifts to higher potentials with an increase in

concentration. As a result the peak potential separation increased with an increase in concentration. This behaviour arises due to large IR voltage drop present in solution, which becomes significant in flowing solutions. Linearity was observed from a calibration curve constructed from CV curves obtained after background subtraction (Figure 4.15).

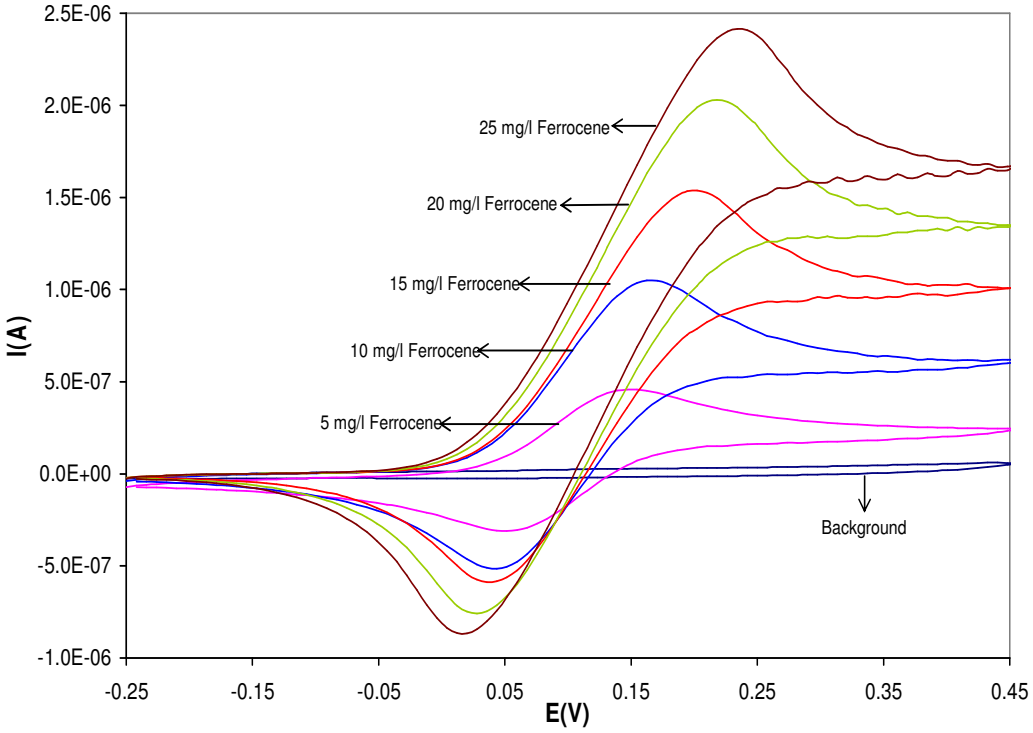

Figure 4.13 CV curves obtained from various concentrations of ferrocene in a flowing solution, flow rate = 0.98 ml min^{-1}, mixing rate = 10 ml min^{-1} and v = 100 mV/s.

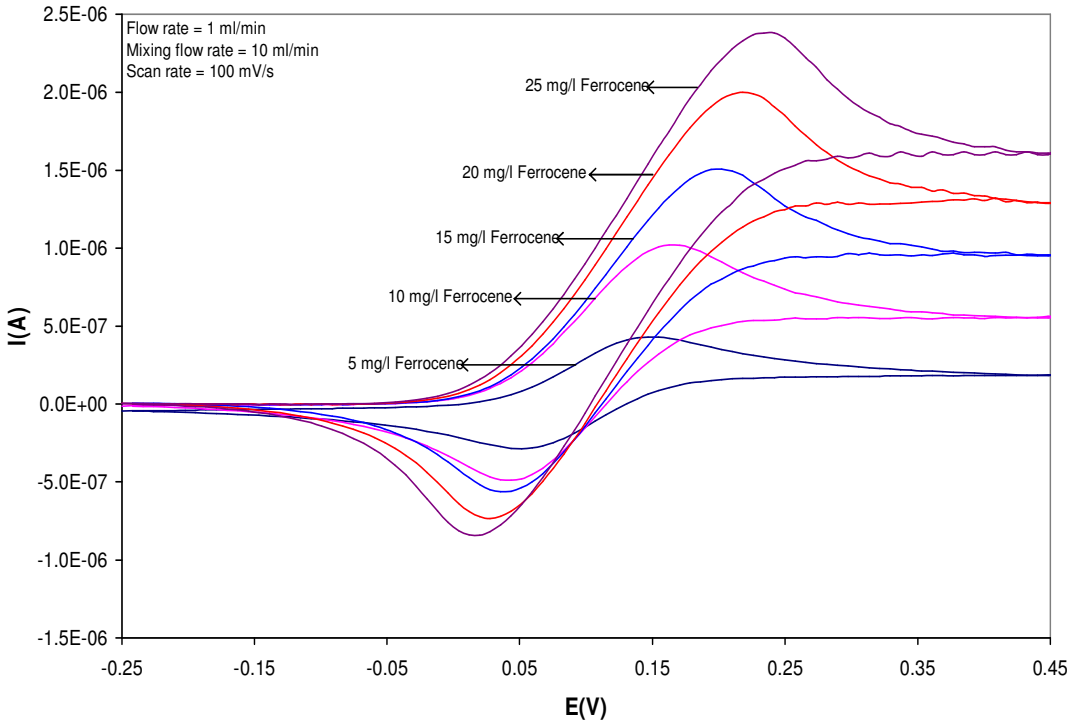

Figure 4.14 CV curves obtained in Figure 4.13 after background subtraction.

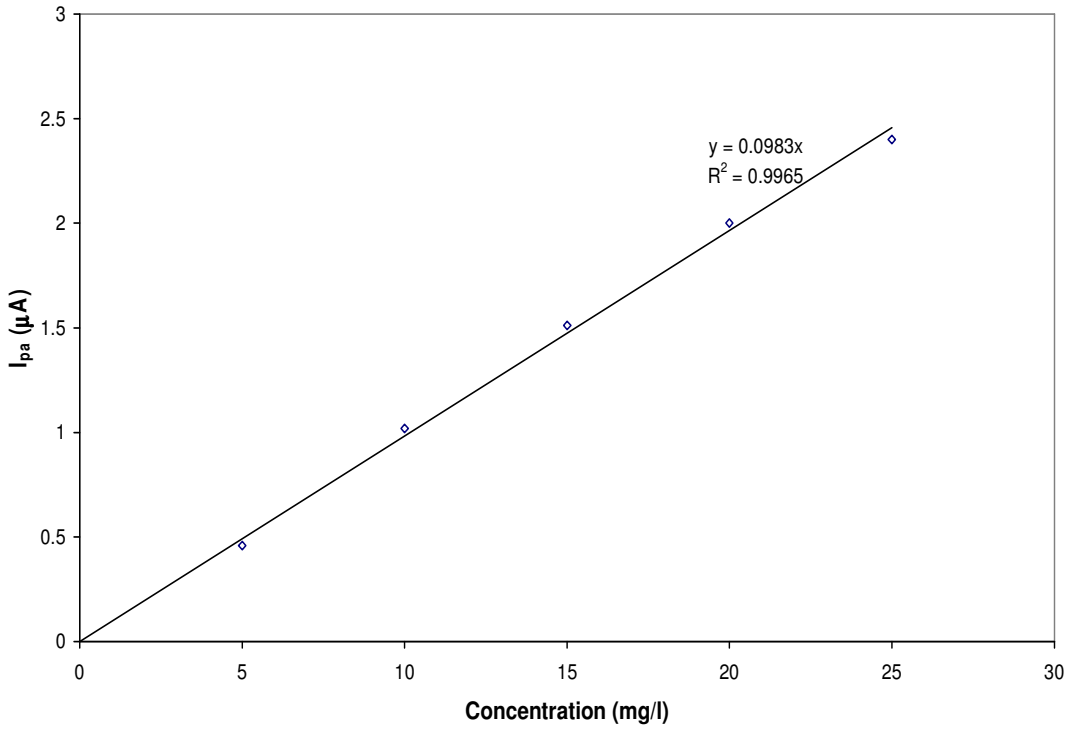

Figure 4.15 Calibration plot for data presented in Figure 4.14.

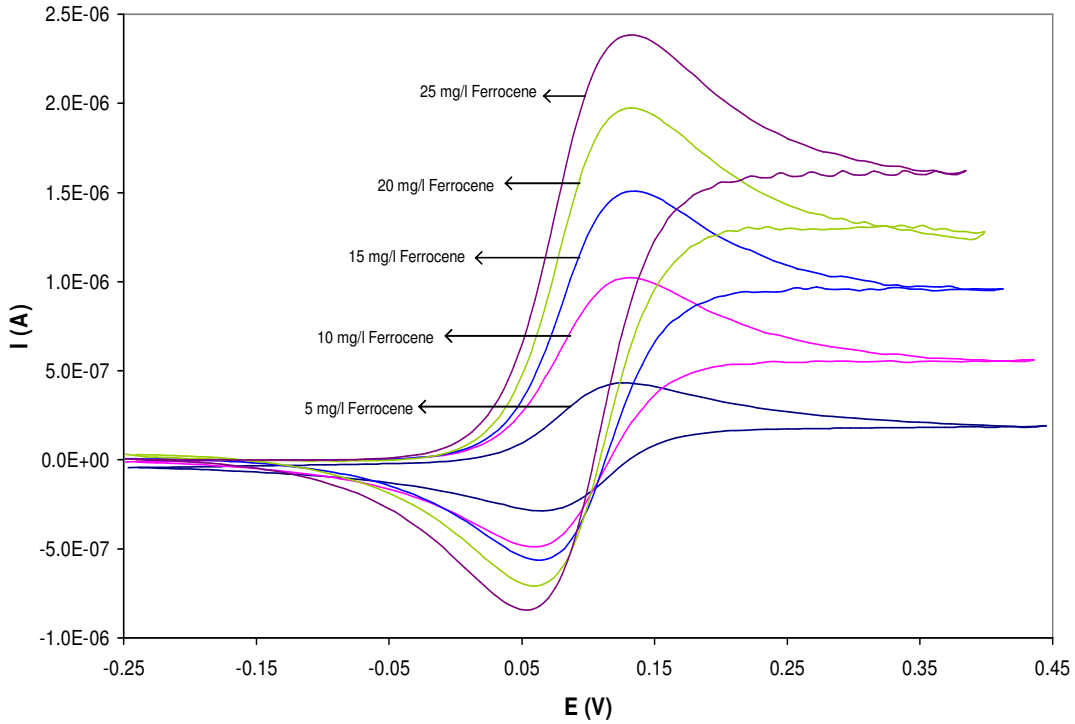

Figure 4.16 CV curves obtained in Figure 4.14 after IR voltage drop correction.

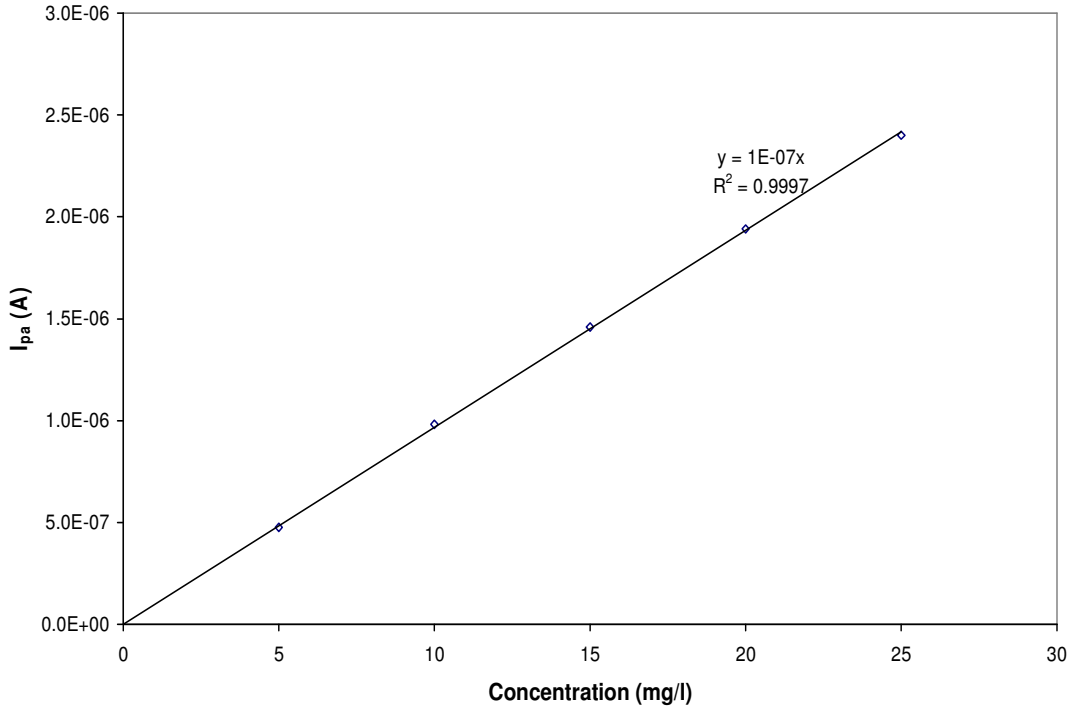

Figure 4.17 Calibration plot for data presented in Figure 4.16.

The CV curves obtained at different concentrations of ferrocene in Figure 4.14 where corrected for IR voltage drop with R = 34000 Ω and the new calibration plot was constructed. Figure 4.16 shows the CV curves obtained at different concentrations of ferrocene after IR voltage drop correction. The peak potential separation remained constant with increase in concentration. The calibration plot gave a linear relationship with concentration (Figure 4.17). IR voltage drop correction improved a calibration plot of ferrocene – almost a perfect straight line was obtained.

Most importantly, the anodic peak potential (E_{pa}) remained independent on the analyte concentration. This would allow applying constant potential, e.g. between 0.15 and 0.20 V for quantitative monitoring of the analyte. Without IR correction, it would be required to apply a large positive potential, which will vary with concentration of the analyte and might result in interferences from other oxidizable materials in cases where more than one compound is analysed or electroactive. It follows that IR drop plays a major role so one should redesign the cells to bring the reference electrode much closer to the working electrode to minimize IR drop and this can be achieved when using flow-by cell.

CHAPTER 5 ELECTROCHEMICAL PROPERTIES OF $CoCl_2(PPh_3)_2$

This chapter dwells on characterization of the synthesized $CoCl_2(PPh_3)_2$ in a mixture of acetonitrile and pentanol (1:1), using both electrochemical (cyclic voltammetry (CV) and chronoamperometry) and spectroscopic (UV-Vis and NMR spectroscopy) techniques. CV was used to identify different species formed in solution, to investigate the electrocatalytic properties of the complex $CoCl_2(PPh_3)_2$ by titration with PPh_3, for quantitative analysis, and development of internal standards. Chronoamperometry was used to determine number of electrons and physical parameters (i.e. electrochemical surface area (A) of the working electrode and diffusion coefficient of ferrocene in a mixture of acetonitrile and pentanol (1:1)). UV-Vis and NMR spectroscopy were used to characterize and investigate the electrocatalytic properties of the complex $CoCl_2(PPh_3)_2$ by titrating with PPh_3.

Typical experimental conditions of CV were as follows, unless otherwise stated:

- Platinum (Pt) and glassy carbon (GC) disks were used as working electrodes (WE).
- A mixture of acetonitrile and pentanol in a 1:1 volume ratio was used as a background solvent.
- Tetrabutyl ammonium hexafluorophospate ($TBAPF_6$) was used as a supporting electrolyte at a concentration of 0.05 M.
- An analyte concentration of 7.7×10^{-4} mol/l was employed.
- The scan rate was 50 mV/s.
- CV's were recorded starting from 0 to more positive potentials.
- Only the third (or last) CV scan was used for analysis.
- All measurements were made at room temperature.

5.1 ANODIC VOLTAMMETRIC STUDIES OF $CoCl_2(PPh_3)$

The main aim of the research project was towards on-line monitoring of cobalt organometallic compounds, using electrochemical techniques in non-aqueous solutions. Most of this organometallic compounds are very sensitive to air and moisture. First, we had to understand their electrochemical behaviour by conducting experiments in an open cell. In order to do this a cobalt organometallic compound that was stable to some extend when exposed to moisture was chosen as a model compound. $CoCl_2(PPh_3)_2$ complex was found to satisfy the above criteria. The anodic electrochemical behaviour of $CoCl_2(PPh_3)_2$ was never studied before using electrochemical techniques. Most work on this compound involved studies by polarography and inorganic techniques. A thorough study was conducted to determine the electrochemical properties of $CoCl_2(PPh_3)_2$ in batch solutions to identify species present in solution during its oxidation. We synthesized this compound and characterized it using elemental analysis and infrared spectroscopy (the results obtained are presented in Experimental Section, Chapter 3).

The anodic voltammetric study of $CoCl_2(Ph_3)_2$ was conducted in a mixture of acetonitrile and pentanol (1:1). Most electrochemical measurements are performed in non-aqueous solvents like acetonitrile, CH_2Cl_2, THF, DMF, etc. They are not normally conducted in alcohols because supporting electrolytes cannot dissolve in alcohols. Pentanol, as an alcohol, was added as one of the background solvents because there was a need to work in the presence of alcohols to become closer to industrial samples that contained alcohols. Electron transfer processes of a certain compound may differ depending on the type of working electrode (WE) material used. First we had to search for an electrode material which would allow the study of electrochemical oxidation of $CoCl_2(PPh_3)_2$ free of complications from surface interactions.

5.1.1 Examination of Different Working Electrode Materials That Could be Used for Anodic Voltammetric Studies of $CoCl_2(PPh_3)_2$

Platinum (Pt) and glassy carbon (GC) disks WE were chosen since they were the most useful and convenient materials for anodic studies. Their influence on the background current curves obtained in a mixture of acetonitrile and pentanol (1:1) were evaluated using cyclic voltammetry (CV) [Figure 5.1]. This experiment allowed us to identify any impurities present in solution, i.e. oxidation or reduction of electrolyte components or the electrode

material itself, as this can cause havoc in the interpretation of results obtained in the presence of an electroactive species. The experiment then defined the accessible potential window, in which the observable electrode reactions should yield voltammetric signals to allow analysis without interference of background contributions.

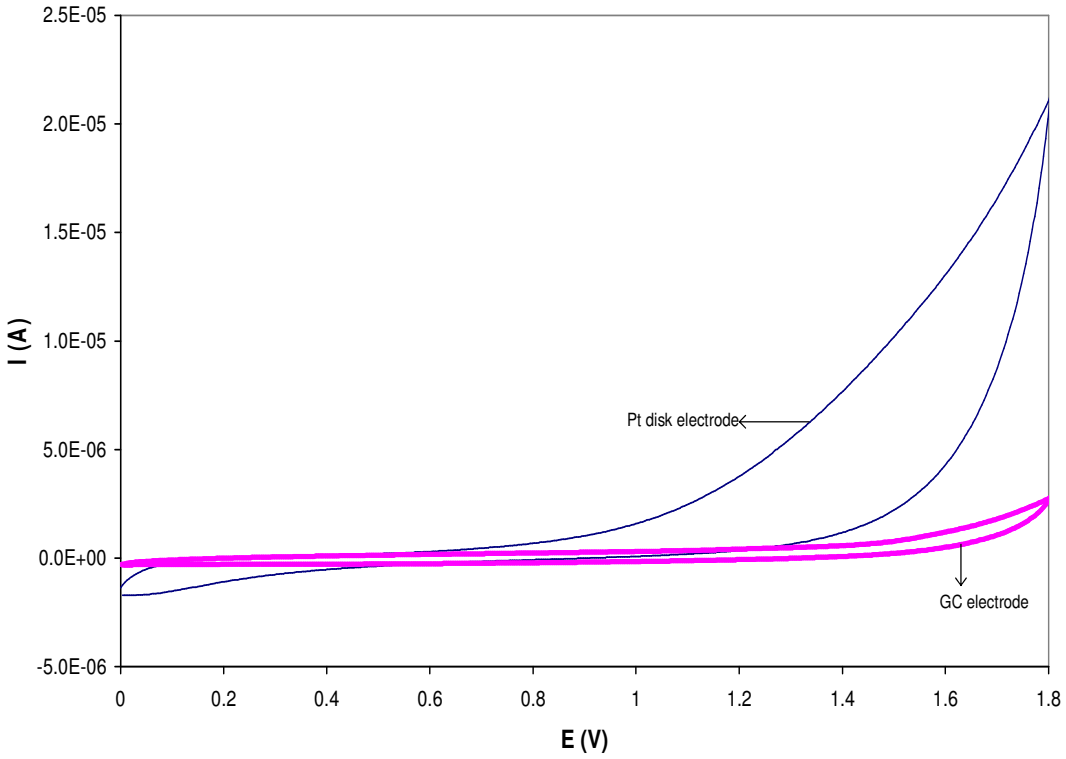

Figure 5.1 Influence of Pt and GC disk WE on the background current CV curve that defines the accessible potential window in a mixture of acetonitrile and pentanol.

The background current curve obtained at a Pt disk WE showed electrochemical activity at E above 1.2 V (Figure 5.1). An increase in background current could have arisen due to oxidation of either the solvent or the anion of the supporting electrolyte (or both) resulting in formation of one or several new compounds. $TBAPF_6$ has been used widely as a supporting electrolyte for the electrochemical studies at a Pt disk WE and it was not oxidized in various non-aqueous solvents, including acetonitrile and alcohols. This then leaves the background solvent as a possible cause of an increase in background current at high potentials above 1.2 V.

Acetonitrile (with $TBAPF_6$) undergoes electrochemical oxidation at E_p = 3.6 V (versus saturated calomel electrode (SCE)), whilst alcohols undergoes electrochemical oxidation at E_p = > 2.5 V in acetonitrile at a Pt electrode [66]. In this study a current increase was observed very early inside the potential window of the two solvents used. It must be noted that the potential window for non-aqueous solvents depends on the solvent purity and especially on the amount of traces of water [1]. It is well-known that water is the most common impurity or contaminant in non-aqueous solvents. Therefore, an increase in background current at potentials above 1.2 V might have arisen due to oxygen evolution from traces of water present. Traces of water were always present in the solvents used even after purification since a simple distillation procedure was conducted (see Experimental Section, Chapter 3).

Gold [66] demonstrated that on raising the potential in solutions containing acetate in aqueous solutions on a Pt electrode, PtO and adsorbed oxygen began to cover the surface and oxygen evolution took place in the range between 1.2 – 1.8 V. A further increase in the potential brought about a change in the oxide composition to a higher oxide (PtO_2) [66]. He also found that a similar surface modification of platinum took place in non-aqueous solvents that favour surface oxide formation, considering the fact that water is easily present at the 1 mM level in such solvents [66]. Therefore, the accessible potential window in this study, in a mixture of acetonitrile and pentanol (1:1) at a Pt disk WE was determined in the positive potential to be from 0 to + 1.2 V.

To prove that an increase in background current at more positive potentials arisen due to traces of moisture present in the background solvents, we compared the background curves that contained different amounts of water after distillation (Figure 5.2). We found the shape and the increase in current of the background curves to depend on the amount of water present.

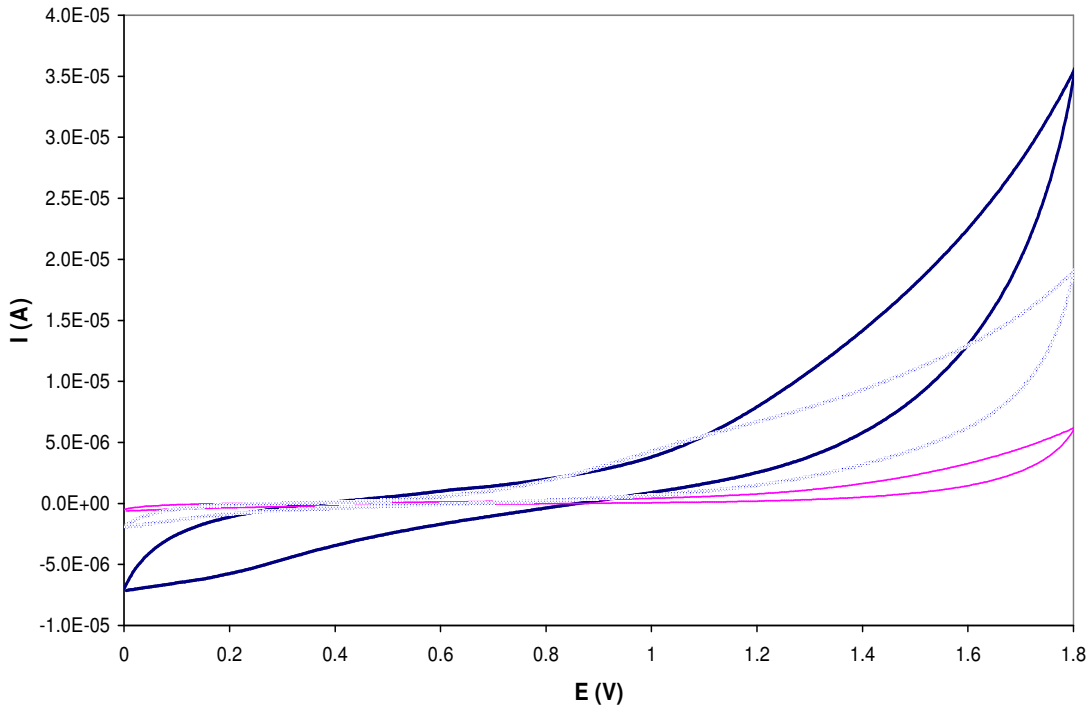

Figure 5.2 Influence of moisture on the background current CV curves obtained at a Pt disk WE. The amounts of water present were as follows: 210 (—), 455.5 (….) and 895.3 (—) ppm.

The background curve obtained at a GC disk WE on the other hand displayed a wide region (between 0 and + 1.8 V) in which 'no' current flowed through the electrolyte solution, except for a very minute residual current due mostly to non-faradaic processes (i.e. processes not involving electrochemical transformations) [Figure 5.1]. This means none of the possible reactants in the system, i.e. the solvent molecule or the anion of the supporting electrolyte is electroactive at this potential range. From these results we decided that GC disk will be a suitable WE material to be used for the analysis of $CoCl_2(PPh_3)_2$ in a mixture of acetonitrile and pentanol (1:1) that contained traces of water.

CV of $CoCl_2(PPh_3)_2$ at a GC disk WE is shown in Figure 5.3. CV of $CoCl_2(PPh_3)_2$ revealed two well-defined oxidation peaks labelled peak 1(a) at E_p = 0.85 V and peak 2(a) at E_p = 1.20 V which had a coupled reduction peak 3(a) at E_p = 1.0 V in the reverse scan, when the potential is switched at 1.5 V (Figure 5.3, dotted-line curve). On repeating the scan and increasing the switching potential to more positive (E_λ = 1.9 V), oxidation peak 1(a) shifted to more positive potential (peak 1(b)), peak 2(a) flattened, and the overall background current increased tremendously at more positive potentials (Figure 5.3, solid-line curve).

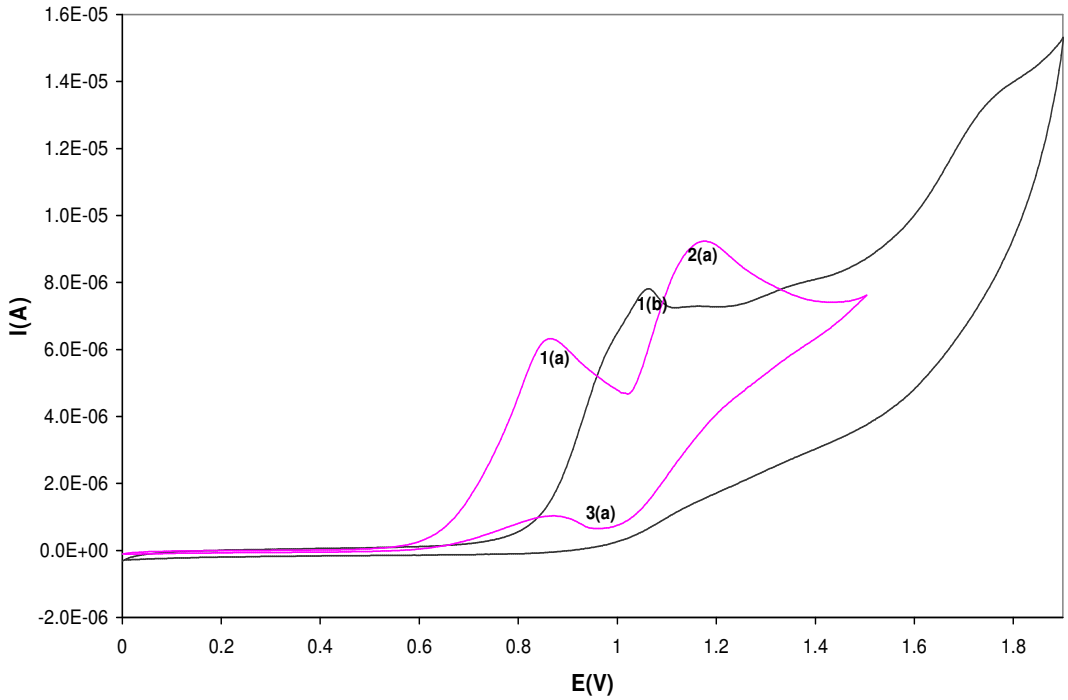

Figure 5.3 CV curves obtained in solutions containing $CoCl_2(PPh_3)_2$ at a GC disk WE at a potential range (a) 0 to 1.15 V (—) and (b) 0 to 1.9 V (—).

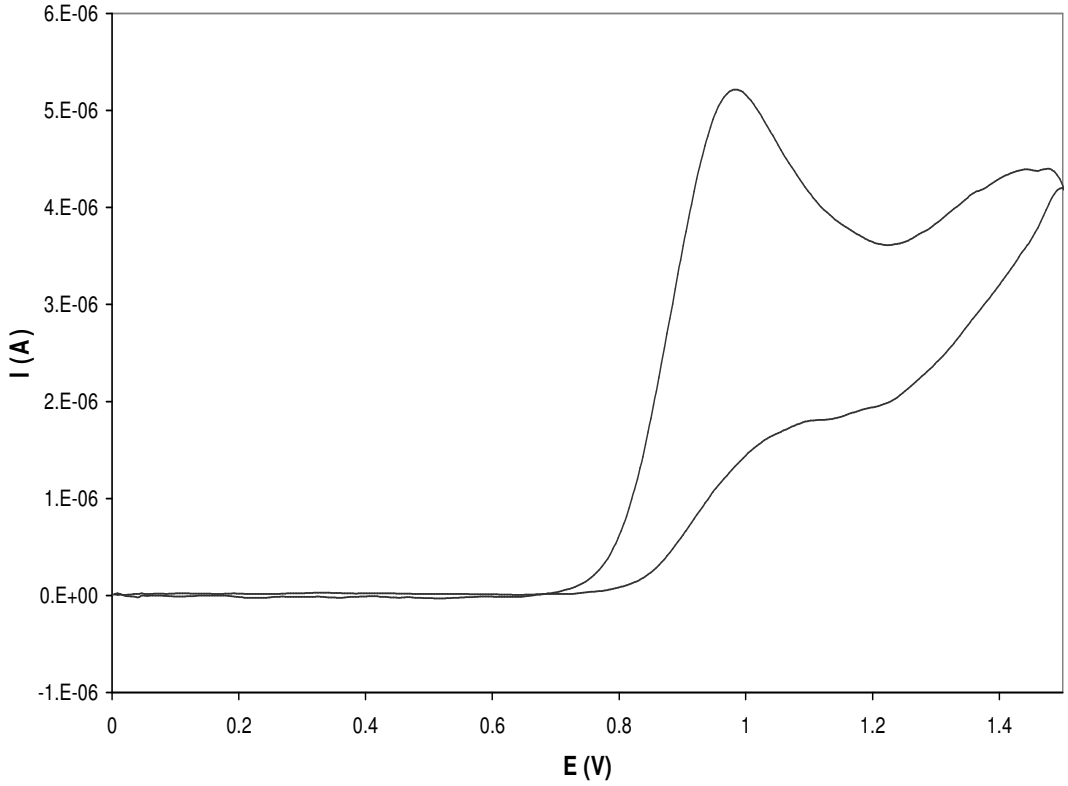

Figure 5.4 CV curve of $CoCl_2(PPh_3)_2$ obtained after 1 minute of recording CV in Fig. 5.3 using the same solution.

Unfortunately the activity of the WE could not be maintained for more than a few CV cycles in solutions containing $CoCl_2(PPh_3)_2$ as shown in Figure 5.3 (potentials range up to 1.9 V). The measurement was repeated in the same solution for a shorter potential range; the oxidation peak 2 and its coupled reduction peak 3 disappeared (Figure 5.4). A decrease in peak current for the oxidation process at more positive potentials (~ 1.2 V) was attributed to deactivation of the GC disk WE surface, probably by oxidation or by surface interaction with other species in solution.

CV was also recorded using $CoCl_2$ as an electroactive species at a GC disk WE (Figure 5.5), since it was one of the starting materials used during synthesis of $CoCl_2(PPh_3)_2$. CV of $CoCl_2$ showed two overlapping ill-defined oxidation peaks at E_p ~ 1.10 and 1.25 V. On extending the potential to more positive, the oxidation peaks shifted to more positive potentials and the overall background current at higher potentials increased.

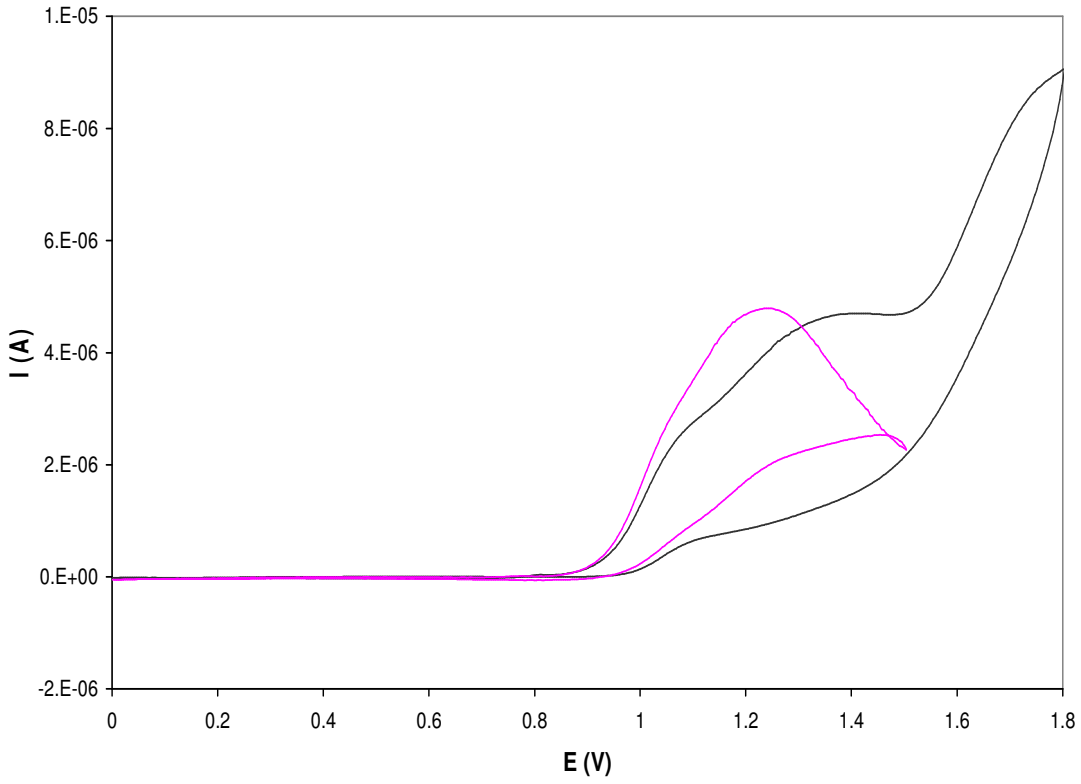

Figure 5.5 CV curves obtained in solutions containing $CoCl_2$ at a GC disk WE at a potential range (a) 0 to 1.15 V (—) and (b) 0 to 1.8 V (—).

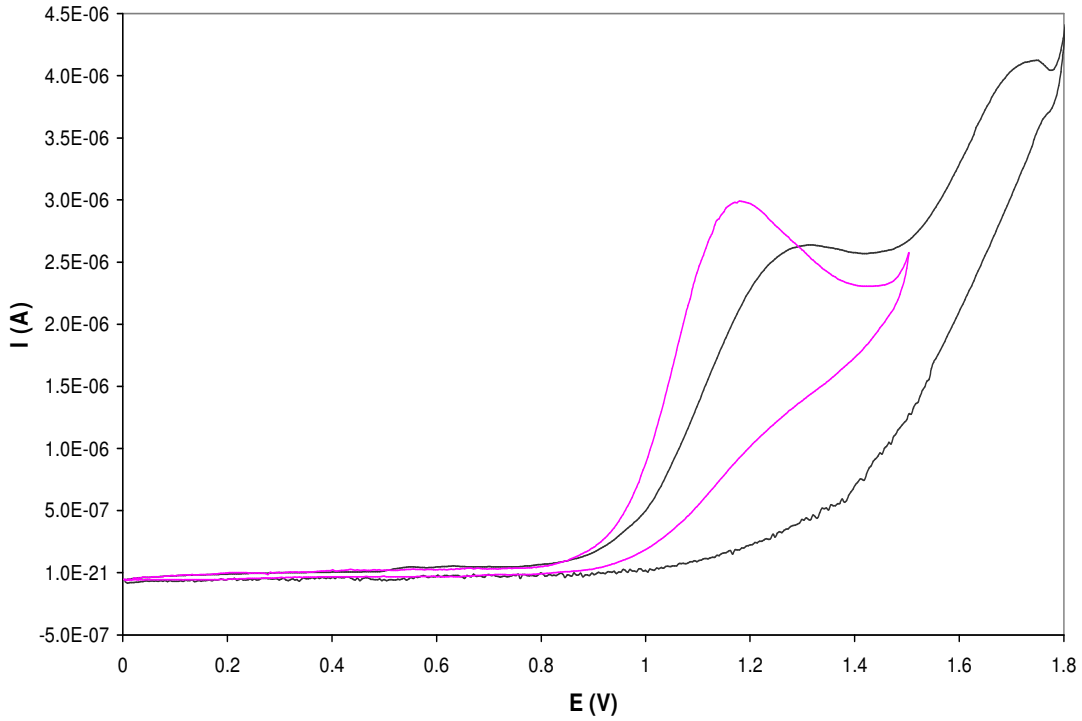

Figure 5.6 CV curves obtained in solutions containing TEACl at a GC disk WE at a potential range (a) 0 to 1.15 V (—) and (b) 0 to 1.8 V (—).

The same experiment was also performed using tetraethyl ammonium chloride (TEACl) at a GC disk WE (Figure 5.6), since it contained chloride as the only electroactive species present to see the effect of chloride on GC electrode. CV of TEACl showed a well-defined diffusion controlled oxidation peak at E_p = 1.10 V, which shifted to more positive potentials and became broad when the GC WE was exposed to higher potential of 1.8 V and the overall background current at higher potentials increased.

CV was also recorded using PPh_3 as an electroactive species at a GC disk WE (Figure 5.7), since it was one of the starting materials used during synthesis of $CoCl_2(PPh_3)_2$. The CV of PPh_3 showed one diffusion controlled oxidation peak at E_p = 0.90 V and no shift in potential was observed when the switching potential was extended to 1.8 V. No increase in current was observed at high potentials when the potential was scanned to 1.8 V. The oxidation peak at 0.90 V in PPh_3 solutions was identical to the one at 0.85 V obtained in $CoCl_2(PPh_3)_2$ solutions. Since in both solutions this oxidation peak was not affected by an increase in potential, it was related to either oxidation of cobalt or PPh_3 from the complex.

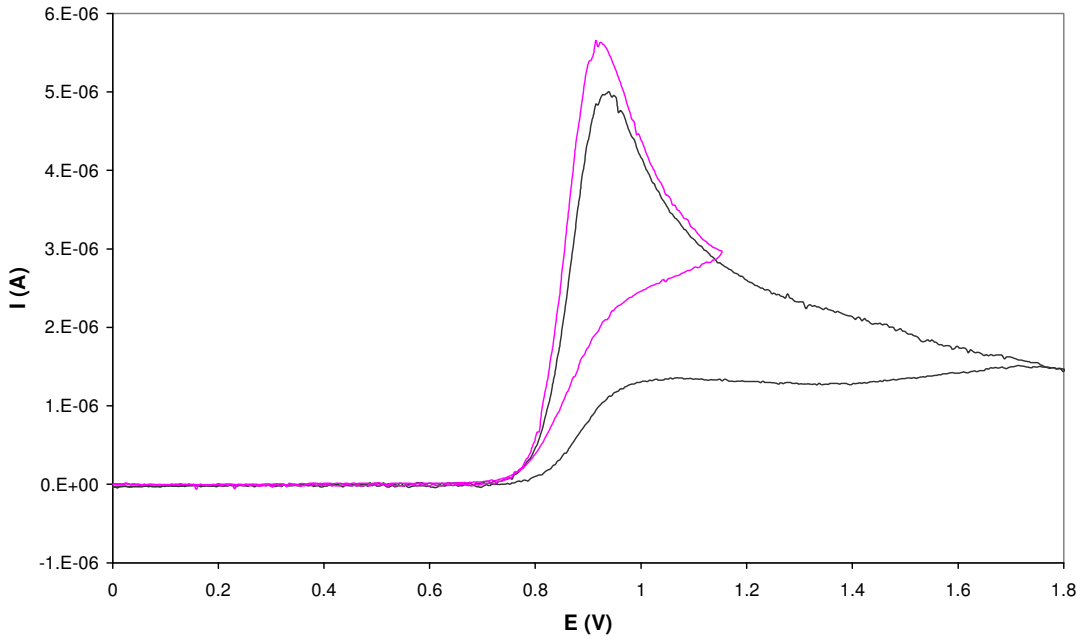

Figure 5.7 CV curves obtained in solutions containing PPh_3 at a GC disk WE at a potential range (a) 0 to 1.15 V (—) and (b) 0 to 1.8 V (—).

From the above results we attributed an overall increase in background current observed in solutions containing $CoCl_2(PPh_3)_2$, $CoCl_2$ or TEACl to generation of chlorine at the GC WE surface. The oxidized chloride in turn modified the GC disk WE surface. However, PPh_3 generated a good irreversible diffusion controlled signal at a GC disk WE, as it did not contain chloride ions.

In conclusion, it appears that a decrease in activity of GC WE shown from voltammograms of $CoCl_2(PPh_3)_2$ was due to the adsorption of a chloride ion or of small amounts of unknown side products produced during oxidation of $CoCl_2(PPh_3)_2$ at the WE surface. However, from the CV's measured in solutions containing PPh_3, the peak heights were reproducible from run to run for several cycles without loss of a GC WE activity. It appears that one will not be able to use GC disk WE for monitoring or studying the electrochemistry of compounds that contains chloride, because chloride modified the GC WE surface. However, GC WE can be recommended for monitoring of compounds that do not oxidize it, for example PPh_3. Moreover, the use of GC WE in chloride containing medium, i.e. in solutions containing $CoCl_2(PPh_3)_2$ at potentials below chloride oxidation (i.e. below, 1.2 V) should be considered. GC appeared to be an excellent WE to use for electrochemical studies in non-

aqueous solutions containing traces of water since it had the largest available potential window in comparison to Pt WE.

Gold disk electrode was also examined as a possible WE material to be used for the anodic voltammetric studies of $CoCl_2(PPh_3)_2$. A background current curve obtained at a gold disk WE is shown in Figure 5.8. A diffusion controlled peak was observed at E_p = 1.20 V, which might have arisen due to oxidation of aldehydes formed from a reaction of an oxygen radical generated from H_2O with pentanol or simply due to formation of gold oxide. The above suggestion was not confirmed since any literature on oxidation of aldehydes or of gold oxide was not conducted to check at which potential were they oxidized. Since $CoCl_2(PPh_3)_2$ showed oxidation peaks at potentials below and around 1.2 V at a GC disk WE, it follows that it might not be possible to study the electrochemical behaviour of this complex using gold disk as a WE.

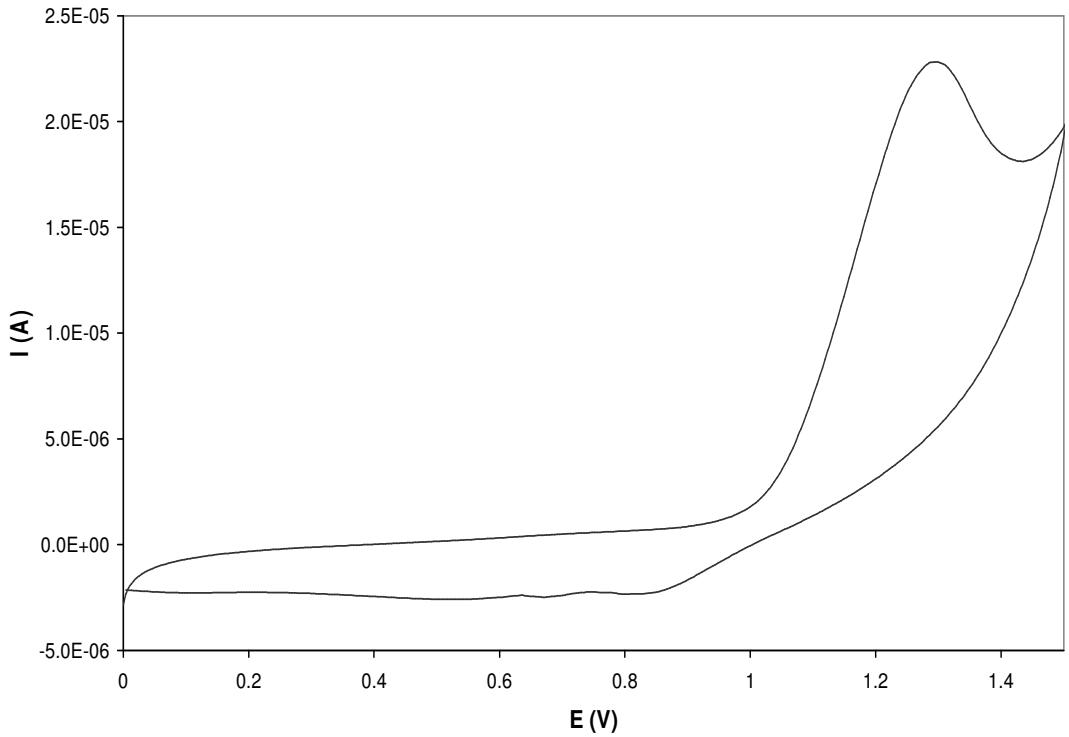

Figure 5.8 Background current CV curve that defines the accessible potential window at a gold disk WE.

In order to prove the above statement we recorded a CV curve of $CoCl_2(PPh_3)_2$ at a gold disk WE (Figure 5.9). There was a tremendous increase of background current at potentials

above 1.2 V and the oxidation peak observed from the CV of the background current curve disappeared. In conclusion, gold disk cannot be used as a WE for studying the electrochemical behaviour of compounds that are oxidized at more positive potentials than 1.20 V in a mixture of acetonitrile and pentanol.

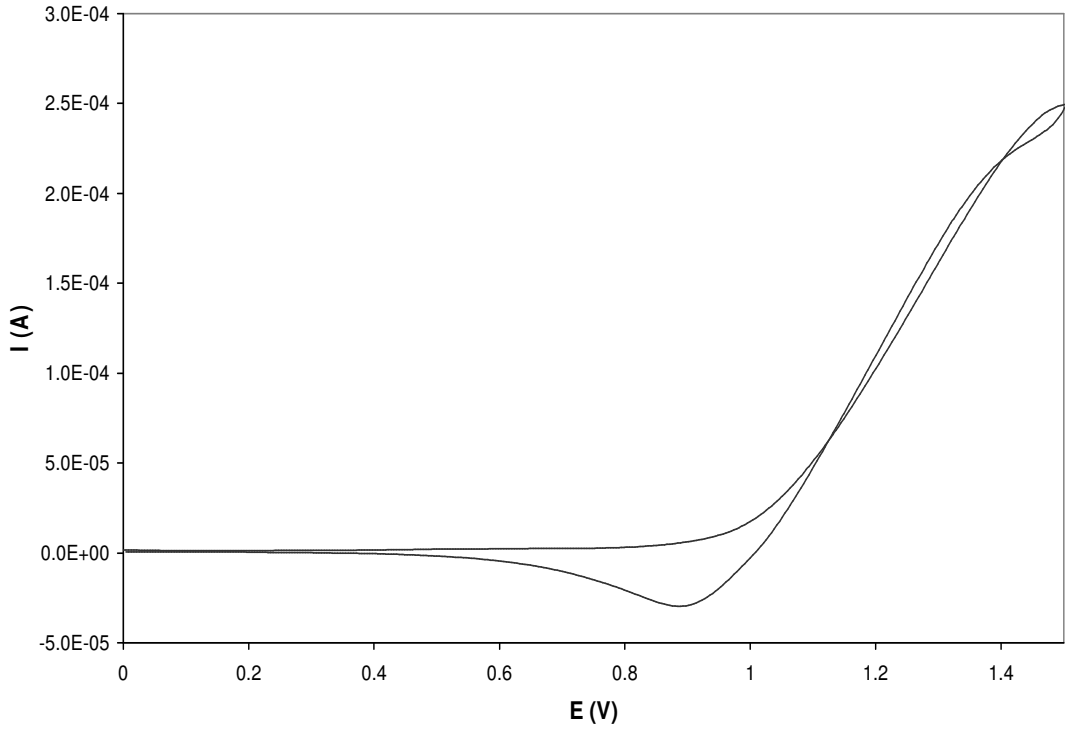

Figure 5.9 CV curves obtained in solutions containing $CoCl_2(PPh_3)_2$ at a gold disk WE.

Since we exhausted all the electrode materials that we had, we decided to go back to examine the anodic voltammetric behaviour of $CoCl_2(PPh_3)_2$ in a mixture of acetonitrile and pentanol (1:1) at a Pt disk WE (Figure 5.10). CV of $CoCl_2(PPh_3)_2$ showed two well-defined oxidation peaks labelled peak 1 and 2 when the potential was scanned up to 1.15 V (insert in Figure 5.10). On scanning to more positive potential of 1.8 V, another irreversible oxidation peak labelled peak 4 was observed with a very large current (Figure 5.10). A large peak current observed from oxidation peak 4 might have arisen due to a catalytic reaction of some species present in $CoCl_2(PPh_3)_2$ solution with traces of water present in the background solvents. The oxidation peaks 1 and 2 were reproducible and well-defined, only the oxidation peak 4 varied slightly from different experiments due to different amounts of water present.

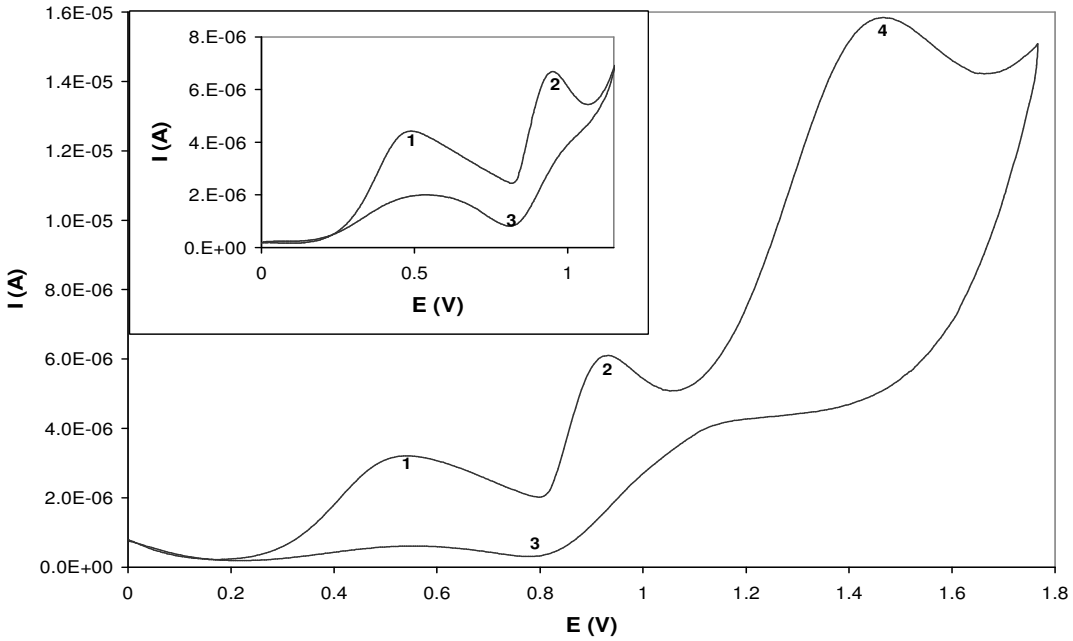

Figure 5.10 CV curves obtained in solutions containing $CoCl_2(PPh_3)_2$ at a Pt disk WE. CV curve obtained at short potential range up to 1.15 V is shown as an insert.

From these results we decided to use Pt disk WE for studying the anodic voltammetric behaviour of $CoCl_2(PPh_3)_2$ even if the background current curve showed electrochemical activity at potentials above 1.2 V because of traces of H_2O present. From the CV curve of $CoCl_2(PPh_3)_2$ shown in Figure 5.10 it appeared that we can still analyse its electrochemical properties at a Pt disk WE even in the presence of traces of H_2O.

5.1.2 Identification of Redox Peaks Observed From CV Curves of $CoCl_2(PPh_3)_2$

This section deals with assignment of the three oxidation peaks observed from the CV curve of $CoCl_2(PPh_3)_2$ at a Pt disk WE. In order to do this we examined the CV curve of $CoCl_2$ and that of PPh_3 individually and added together, as they were the starting materials during synthesis of this complex, $CoCl_2(PPh_3)_2$.

CV curves of $CoCl_2$ in Figure 5.11 revealed an irreversible diffusion controlled oxidation peak labelled peak 1 at E_p = 0.95 V, with the corresponding reduction peak labelled peak 1' at E_p = 0.70 V and an oxidation peak 2 which had a very large current (about 5 times higher than current of peak 1) at E_p = 1.50 V.

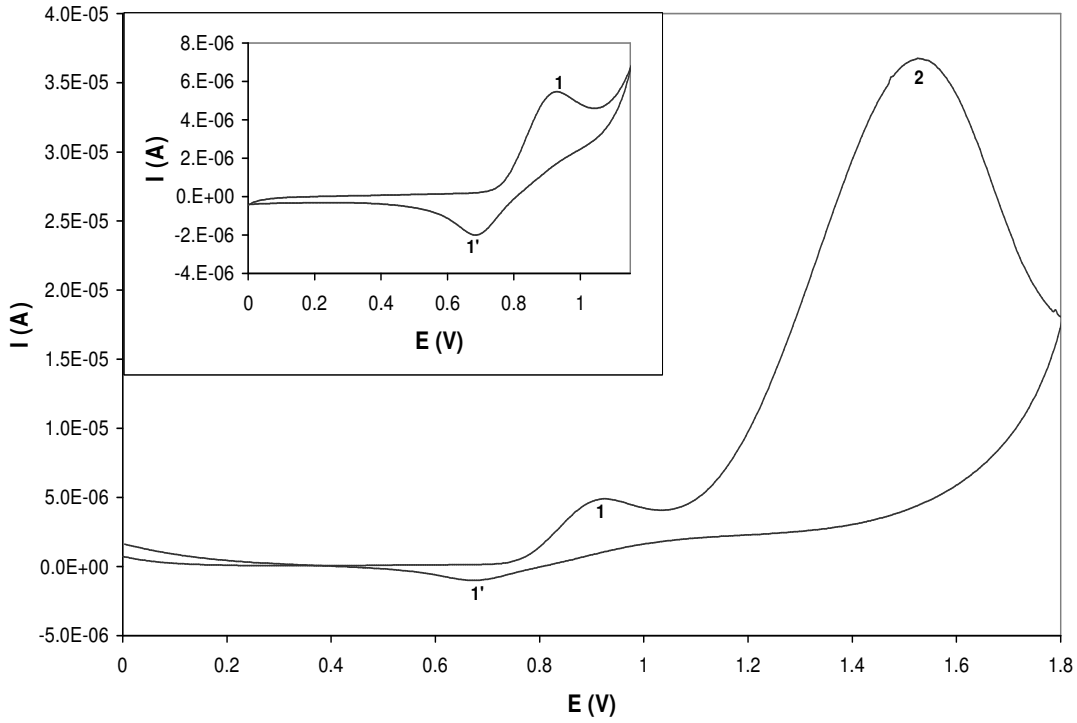

Figure 5.11 CV curves obtained in solutions containing $CoCl_2$ at a Pt disk WE. CV curve obtained at short potential range up to 1.15 V is shown as an insert.

The oxidation peak 2 and 4 of $CoCl_2(PPh_3)_2$ (Figure 5.10) and oxidation peak 1 and 2 of $CoCl_2$ (seen in Figure 5.11) were observed at similar positions and had similar shapes. The current of the oxidation peak 2 obtained from $CoCl_2$ solutions was much higher and shifted to more positive potentials as compared to that of oxidation peak 4 obtained from $CoCl_2(PPh_3)_2$ solutions. The shift may be due to a greater degree of solvation of the chloride ions when different amounts of water are present in the background solutions, or due to the fact that the catalytic reaction of chloride takes place more rapidly with increase in amount of water.

The two background curves obtained before measurement of the CV curve of $CoCl_2(PPh_3)_2$ and that of $CoCl_2$ are shown for comparison in Figure 5.12 to confirm the above point that the increase in current for the oxidation peak at E_p ~ 1.40 V arisen due to different amounts of water present in the background solutions. The background solvent used during measurement of $CoCl_2$ contained more moisture as the solvents were exposed to moisture when they were added to the cell before measurement. Whilst with $CoCl_2(PPh_3)_2$ the solvents were collected under argon using schlenk tubes. A background current obtained

before measurement of $CoCl_2$ was higher than the one obtained before measurement of $CoCl_2(PPh_3)_2$ at potentials above 1.2 V.

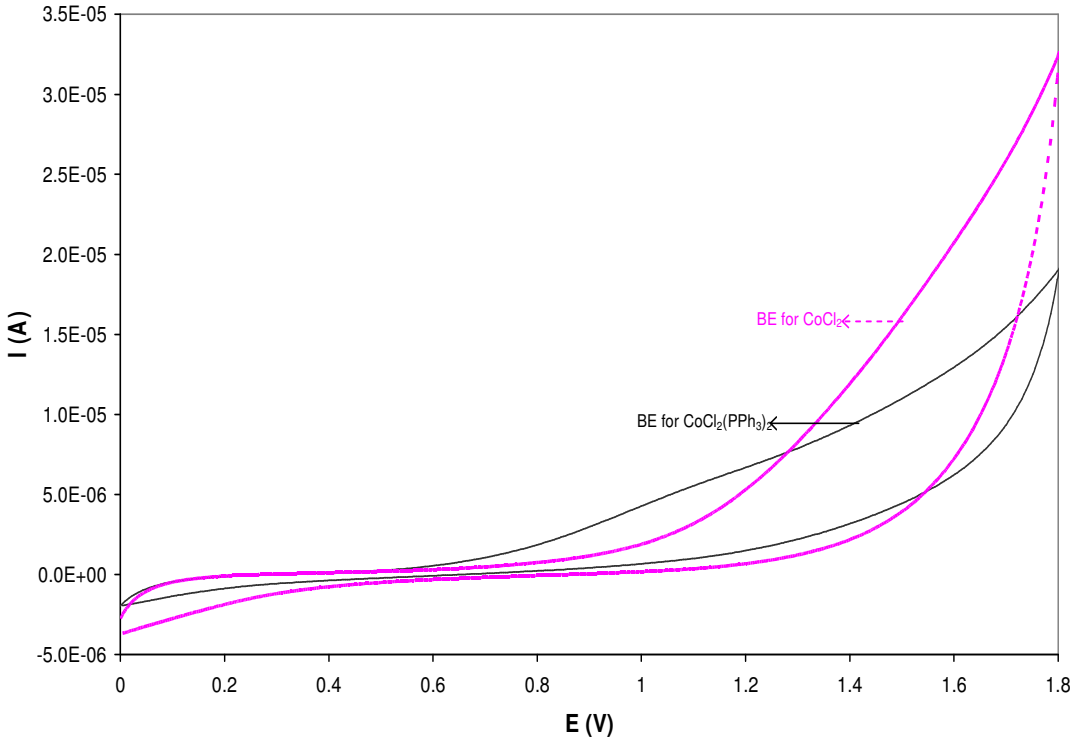

Figure 5.12 Influence of water on the background current CV curves obtained before CV measurements of $CoCl_2(PPh_3)_2$ and $CoCl_2$ at a Pt disk WE.

These show that the current of an oxidation peak 2 was enhanced by an increased amount of water in the background solutions. From these data we concluded that the oxidation peak 2 (from a CV of $CoCl_2$) and 4 (from a CV of $CoCl_2(PPh_3)_2$) arisen due to a catalytic reaction of chloride with water present in the background solvent. Therefore, the peak intensity depends on the amount of water present.

CV curves of PPh_3 are shown in Figures 5.13 and they revealed only one oxidation peak labelled peak 1 at E_p = 1.05 V. No coupled reduction peak was observed from the voltammograms and no further oxidation peaks were observed on scanning to more positive potentials. CV of PPh_3 was also reported by Hershberger and co-workers [42] who found PPh_3 to be oxidized irreversibly with one-electron transfer to PPh_3^+ at ~ 1.3 V in acetonitrile.

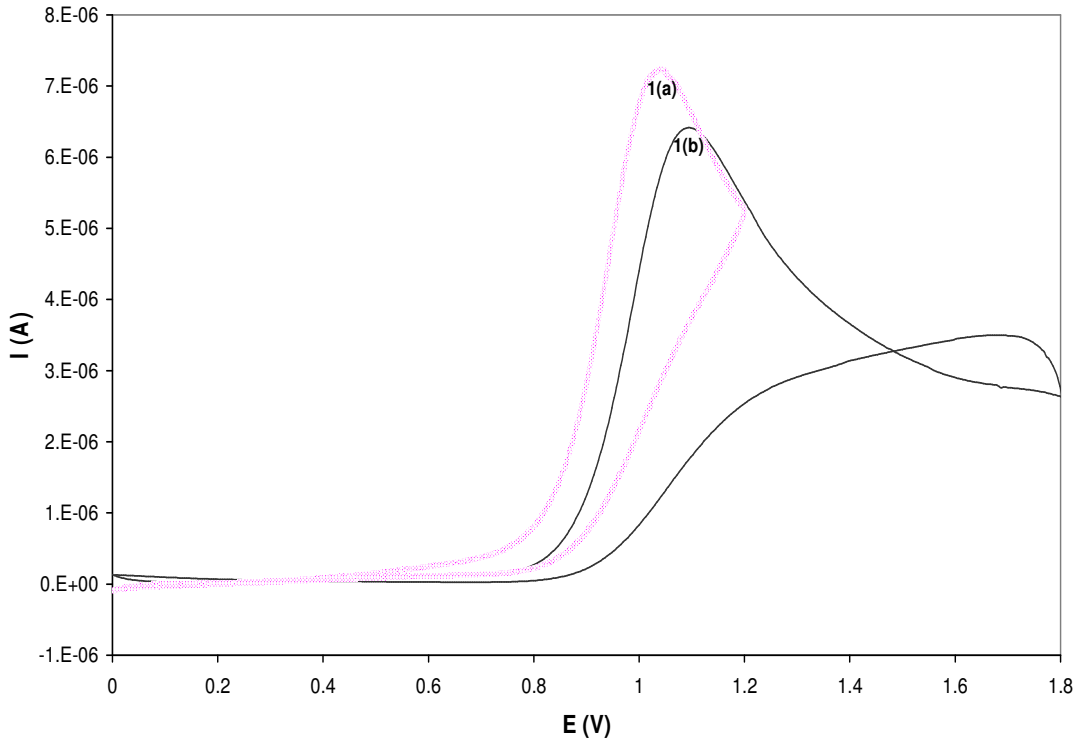

Figure 5.13 CV curves obtained in solutions containing 1.54×10^{-3} mol/l PPh_3 at a Pt disk WE at a potential range (a) 0 to 1.15 V (….) and (b) 0 to 1.8 V (—).

In the absence of chloride ions, a large oxidation peak at ~ 1.40 V was not observed and there was no enhancement of current at more positive potentials, which showed the absence of a catalytic effect. This proves that the oxidation peak observed at E_p ~ 1.40 V observed from the CV's of $CoCl_2$ and $CoCl_2(PPh_3)_2$ arisen due to a catalytic reaction of chloride with water present in the background solvent, as it was only observed from CV's of the compounds containing chloride.

In order to assign the oxidation peak 1 of the complex $CoCl_2(PPh_3)_2$, we synthesized the complex electrochemically by first recording the CV with only $CoCl_2$ present in solution and then adding two equivalent moles of PPh_3. CV curve of $CoCl_2$ is shown in Figure 5.14 (solid-line curve) and reveals the presence of one oxidation peak at $E_p = 0.95$ V, which has a coupled reduction peak at $E_p = 0.70$ V when the scan is reversed at 1.15 V.

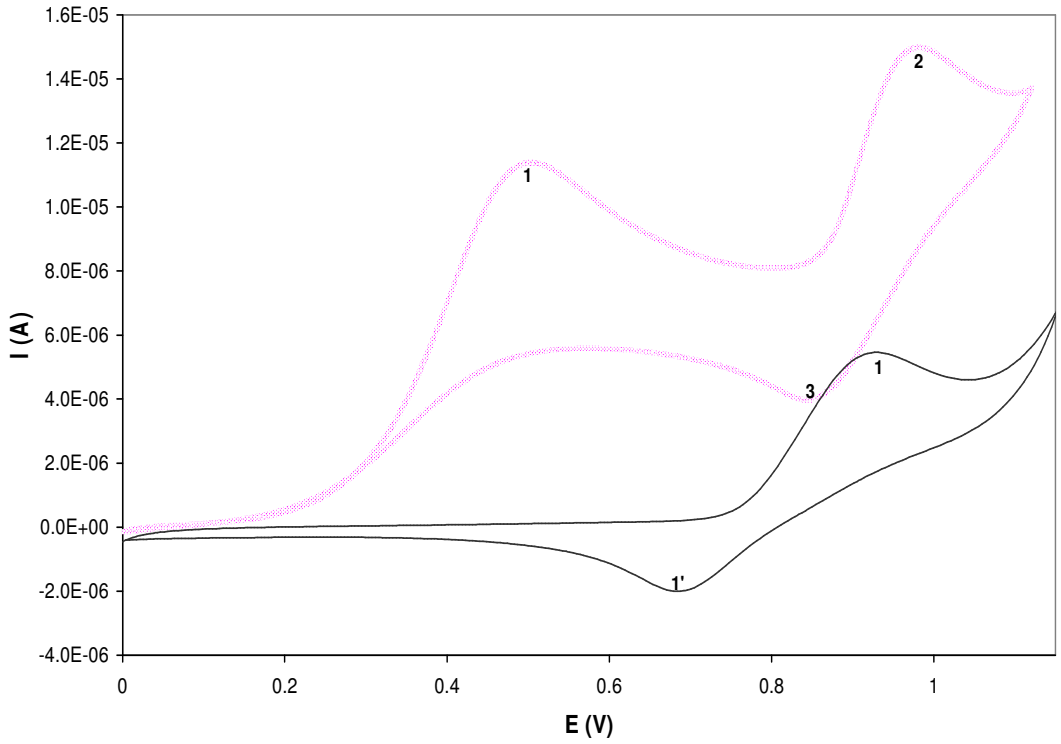

Figure 5.14 Effect of added PPh_3 on the CV curve of $CoCl_2$. CV curves of a 7.7×10^{-4} mol/l $CoCl_2$ before (—) and after (....) addition of 1.54×10^{-3} mol/l (2 equiv) of PPh_3 in a mixture of acetonitrile and pentanol (1:1) are presented.

Addition of two equivalent moles of PPh_3 resulted in an appearance of another irreversible oxidation peak labelled peak 1 at a less positive potential of ~ 0.50 V (Figure 5.14, dotted-line curve). This peak was not observed before from the CV curve of a free PPh_3, or that of $CoCl_2$. Since it only appeared after mixing of the two starting materials, it was assigned to oxidation of Co^{II} to Co^{III} from the complex, $CoCl_2(PPh_3)_2$. It can be seen from Figure 5.14 that peak 1 observed from the CV of $CoCl_2$ remained at the same position after addition of PPh_3 (now labelled peak 2, on the dotted-line curve). Its coupled reduction peak 1' shifted to more positive potentials (now labelled peak 3) and the electrode process at E_p = 0.95 V became partially reversible. The above results showed that the CV peak of $CoCl_2$ observed in the absence of a PPh_3 ligand was modified in the presence of this ligand and a new peak due to the reaction product (i.e. $CoCl_2(PPh_3)_2$) appeared at a more positive potential. This behaviour is characteristic of electrocatalysis as discussed in Chapter 1 section 1.4 that the CV wave normally observed in the absence of the ligand (i.e. PPh_3 in this case) can be modified in the presence of this ligand and a new wave due to the reaction product will appear.

At this stage we managed to assign the oxidation peak 1 and 4 observed from the CV of $CoCl_2(PPh_3)_2$. Assignment of the oxidation peak 2 was a bit difficult since the CV curves of both $CoCl_2$ and PPh_3 showed an oxidation peak around the same potential (~ 1.0 V). But from analysis of the CV curves of $CoCl_2$ before and after addition of PPh_3 it was shown that PPh_3 reacted completely with $CoCl_2$ to form a complex $CoCl_2(PPh_3)_2$. From this result we immediately assumed that the oxidation peak 2 of $CoCl_2(PPh_3)_2$ did not arise from PPh_3 oxidation but rather from oxidation of a chloride ligand present in the complex. Firstly we attempted to assign an oxidation peak 1 observed from a CV curve of $CoCl_2$. To our knowledge there was no literature available on anodic voltammetric studies of $CoCl_2$, so we looked at some literature on anodic voltammetric studies of chloride and compared the results with those obtained from CV of $CoCl_2$.

The electrochemical behaviour of the chloride/chlorine system has been previously studied at the rotated platinum microelectrodes in acetonitrile solutions using LiCl as a chloride source [67]. Voltammetric studies demonstrated that the electrode reaction gave two anodic waves, at 1.1 V and 1.7 V. The following overall reactions were postulated, $3Cl^- \leftrightarrow Cl_3^- + 2e^-$ and $2Cl_3^- \leftrightarrow 3Cl_2 + 2e^-$, for the first and second wave, respectively. The Cl^-/Cl_2 couple was also studied in acetone and nitromethane and only one anodic and one cathodic wave was found and the total electrochemical reaction was given as $2Cl^- \leftrightarrow Cl_2 + 2e^-$ [68]. The second anodic wave occurred at 1.9 V in nitromethane and at 1.8 V in acetone. It was attributed to oxidation of the background current.

Chloride oxidation was also reported to occur as a one-step process in dimethylformamide (DMF) [69] and dimethylsulphoxide (DMSO) [70]. Sereno et al [71] decided to investigate this electrode reaction thoroughly in acetonitrile. Since acetonitrile can be considered as an aprotic solvent with similar properties to nitromethane and DMF, there was no valid reason to justify a different behaviour for its electrode process [71]. They found that chloride undergone a two-electron exchange per mol to chlorine and only one anodic and one cathodic wave was found using LiCl as a chloride source at a platinum rotating disk electrode.

From the above results we decided to investigate first the electrochemical behaviour of $CoCl_2$ at a Pt disk WE in acetonitrile. A CV curve of $CoCl_2$ in acetonitrile is shown in Figure 5.15. The voltammogram revealed only one broad oxidation peak at E_p = 1.1 V and

one reduction peak at E_p = 0.65 V. No additional oxidation or reduction peaks were observed when scanning to more positive or less negative potentials.

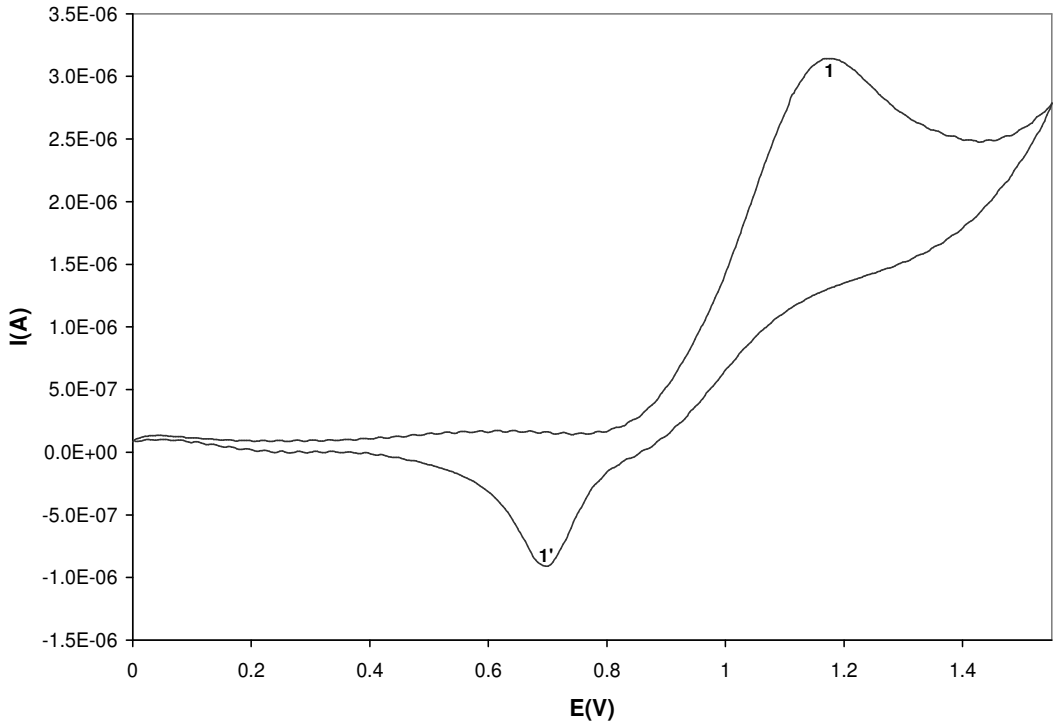

Figure 5.15 CV curves obtained in solutions containing $CoCl_2$ in acetonitrile at a Pt disk WE.

From these results we suggested that the oxidation peak 1(a) obtained from the CV of $CoCl_2$ (Figure 5.15) in acetonitrile arose due to overlap between cobalt and chloride oxidation. This result was related to some literature studies on reduction of cobalt bromide, where Co^{II} and bromide were found to be reduced at the same potential giving rise to one reduction peak [14]. Furthermore, the oxidation peak 2 at 1.5 V obtained from CV of $CoCl_2$ in a mixture of acetonitrile and pentanol (1:1) was not observed in acetonitrile even when the potential was scanned further to 1.8 V. This might have arisen due to the fact that most of the water that was responsible for an increase in current of the background current curves at potentials above 1.2 V, in a mixture of acetonitrile and pentanol was from pentanol. It appeared that it was more difficult to remove traces of water from pentanol than from acetonitrile. When the amount of water was measured individually, pentanol after distillation still contained about 1500 ppm of water whilst acetonitrile after distillation contained only about 200 ppm of water. This proves the above suggestion that most of the

water came from pentanol and maybe pentanol in the presence of water undergone oxidation easier.

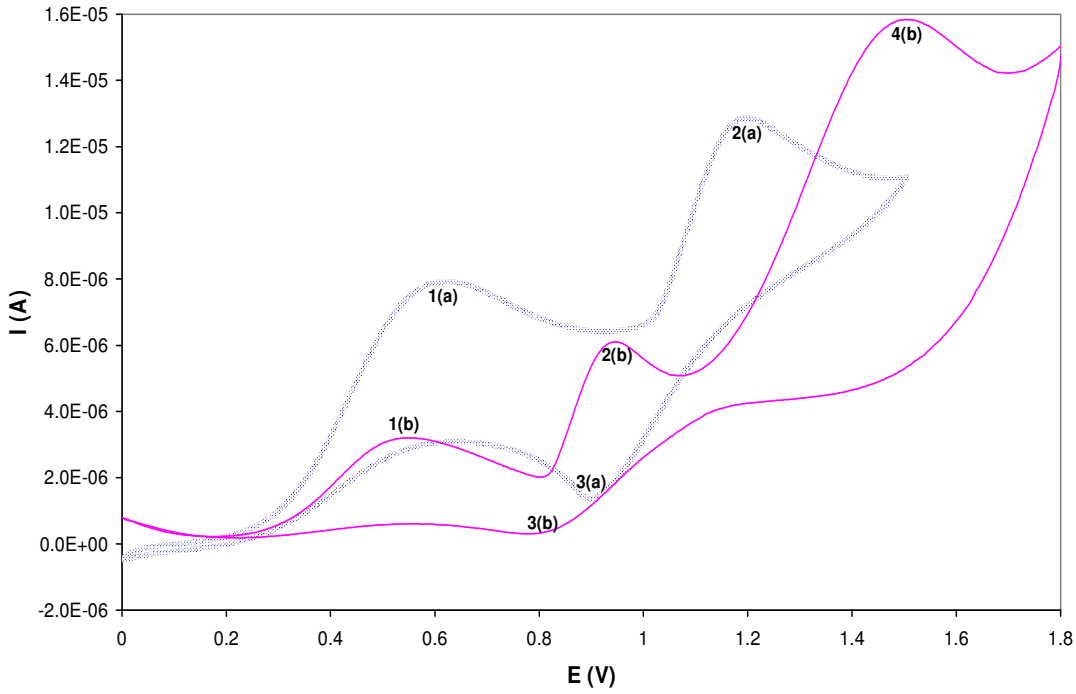

Figure 5.16 CV curves obtained in solutions containing $CoCl_2(PPh_3)_2$ in acetonitrile (....) and in a mixture of acetonitrile and pentanol (—) at a Pt disk WE.

We also investigated the electrochemical behaviour of $CoCl_2(PPh_3)_2$ in acetonitrile solutions at a Pt disk WE (Figure 5.16) and only two oxidation peaks were observed at E_p = 0.6 V and 1.2 V and one reduction peak at E_p = 0.9 V. The oxidation peak 4 previously observed from the voltammogram of $CoCl_2(PPh_3)_2$ in a mixture of acetonitrile and pentanol solution (Figure 5.16, solid-line curve) was not observed in acetonitrile solution. The oxidation peak 2 at E_p = 1.2 V agreed in position to the one obtained in solutions containing $CoCl_2$ in acetonitrile, which suggests that it might also have arisen due to oxidation of only a chloride ligand (Figure 5.17) since cobalt is oxidized already at less positive potentials in this complex, $CoCl_2(PPh_3)_2$. Surprisingly, the oxidation peak 1 obtained in $CoCl_2$ solutions was about a factor of 2 times less than the oxidation peak 2 of $CoCl_2(PPh_3)_2$ (even if concentration of both analytes were equal). This might have arisen due to different amounts of water present in acetonitrile. To verify this we compared the two background current CV curves obtained in acetonitrile before measurement of the curves in Figure 5.18 (Figure 5.18).

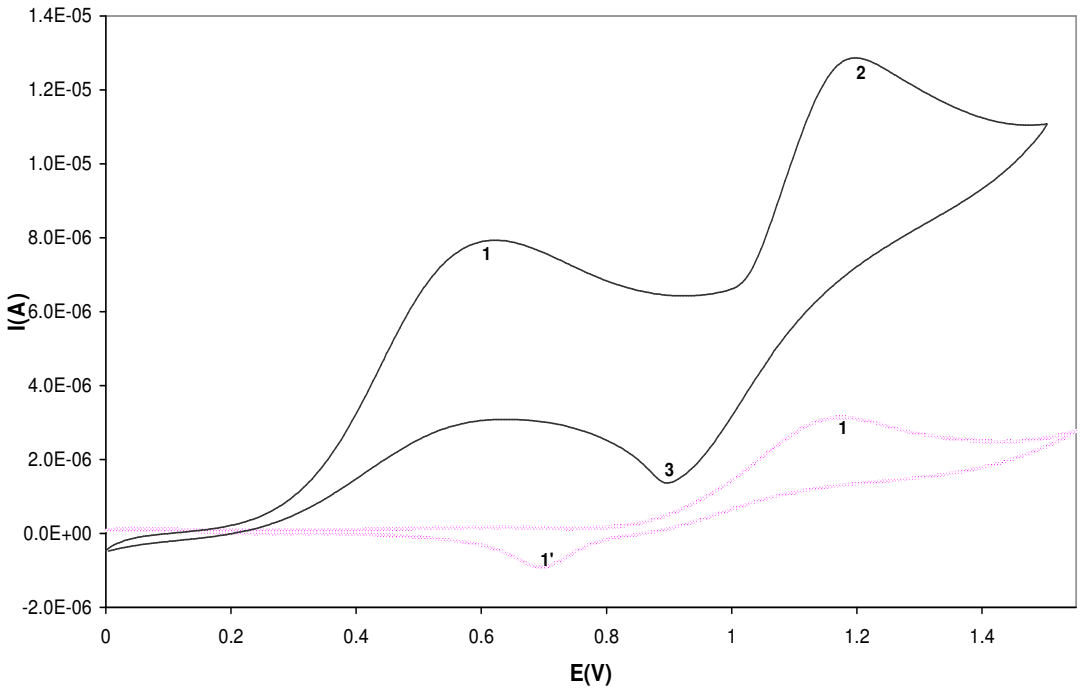

Figure 5.17 Comparison of the CV curves of $CoCl_2(PPh_3)_2$ (—) and $CoCl_2$ (....) obtained in acetonitrile.

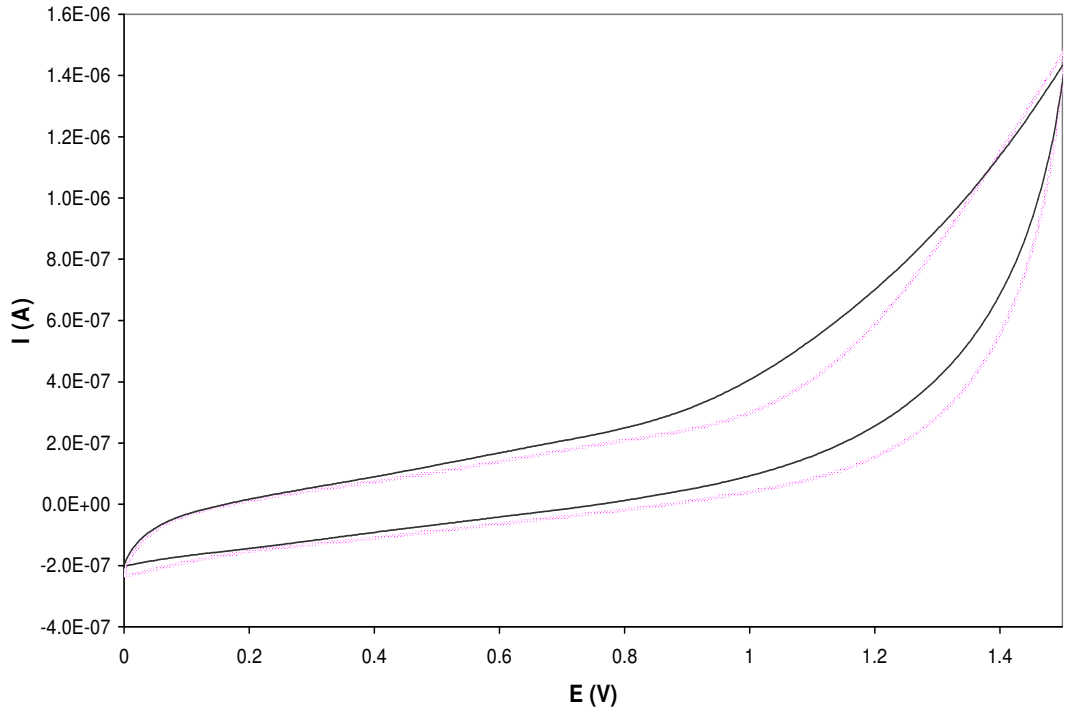

Figure 5.18 Comparison of the background current CV curves recorded in acetonitrile before measurements of the CV curves of $CoCl_2(PPh_3)_2$ (—) and that of $CoCl_2$ (....).

The two background current voltammograms in Figure 5.18 were similar and had the same current and shape. This shows that an increase in peak current for oxidation peak 2 from $CoCl_2(PPh_3)_2$ solutions did not arise because of traces of water present in acetonitrile. We concluded that an increase might have arisen due to just error in concentration measurement. From the above results we concluded that the oxidation peak 2(a) in solutions containing $CoCl_2(PPh_3)_2$, arisen due to oxidation of a chloride ligand.

The oxidation peak at E_p ~ 1.4 V was only observed from the voltammograms of compounds containing chloride in a mixture of acetonitrile and pentanol and it was assigned to a catalytic reaction of chloride with water present in the background solvents. We decided to investigate this further since traces of water were also present in acetonitrile solutions. Figure 5.19 shows comparison of the background current CV curve obtained in acetonitrile (bold solid-line curve) and that obtained in a mixture of acetonitrile and pentanol (solid-line curve). A large increase in current was observed from 1.2 V on the voltammogram recorded in a mixture of acetonitrile and pentanol, whilst no increase in current was observed in solutions containing only acetonitrile (Figure 5.19). These account for a large catalytic oxidation peak current observed in voltammograms of compounds containing chloride in acetonitrile/pentanol solvent mixtures.

Since the oxidation peak at ~ 1.40 V was observed only on CV's of compounds containing chloride in acetonitrile/pentanol solvent mixtures, it was assigned to a catalytic reaction of chloride with traces of water present in the solvent solution mixture (most likely from alcohols). The same behaviour was observed from the voltammograms of LiCl in nitromethane and acetone [68]. In conclusion, the electrode reaction occurring at E_p ~ 0.95 V in $CoCl_2(PPh_3)_2$ was complicated by a catalytic reaction occurring at E_p ~ 1.4 V which caused a diffusion current enhancement. From the above it follows that the mechanistic studies of organometallic compounds containing chloride i.e. $CoCl_2(PPh_3)_2$, should be investigated in acetonitrile solutions in the absence of pentanol and water. But monitoring should be possible in a mixture of acetonitrile and pentanol since one can apply a potential of 0.50 V for studies involving $CoCl_2(PPh_3)_2$ without interference of chloride and water oxidation.

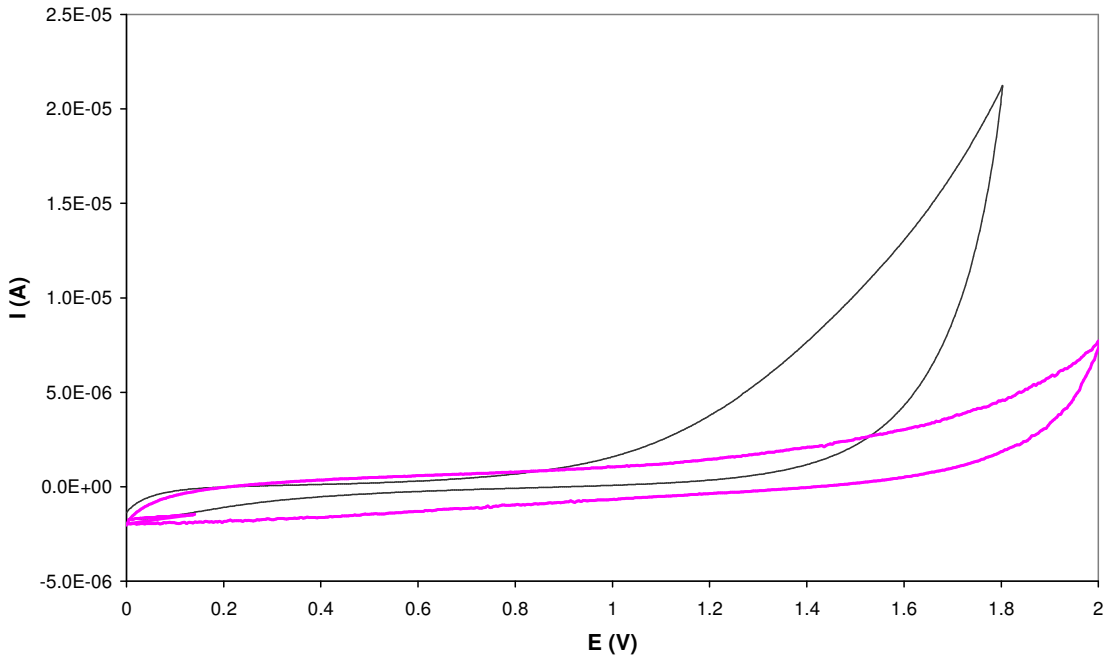

Figure 5.19 Comparison of the background current CV curves recorded in a mixture of acetonitrile and pentanol (1:1) (—) with that recorded in acetonitrile (—).

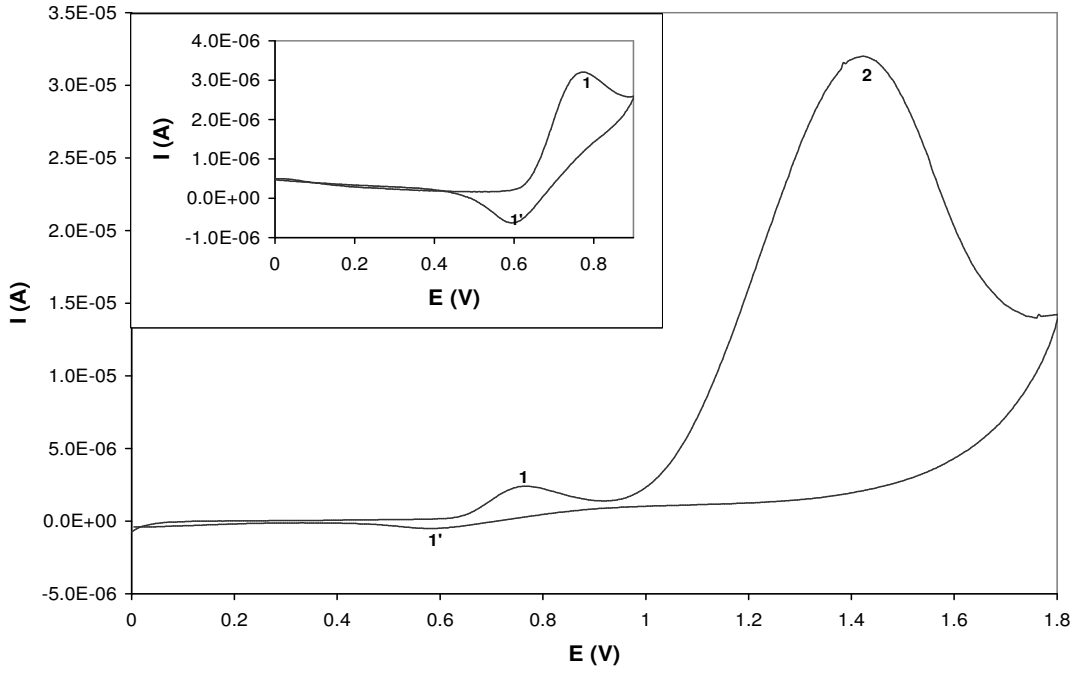

Figure 5.20 CV curves obtained in solutions containing TEACl at a Pt disk WE. CV curve obtained at short potential range up to 1.15 V is shown as an insert.

CV was also recorded in cobalt-free media, using tetraethyl ammonium chloride (TEACl) as a chloride source, to confirm the assignment of the oxidation peak 2 of $CoCl_2(PPh_3)_2$ in a mixture of acetonitrile and pentanol in Figure 5.10.

Voltammograms of TEACl revealed two oxidation peaks 1 and 2 at E_p = 0.75 and 1.40 V and one cathodic peak at E_p = 0.6 V (Figure 5.20). The oxidation peak at E_p ~ 1.40 V agreed exactly in position and shape with the oxidation peak 2 observed in $CoCl_2$ solutions. The oxidation peak 1 at E_p = 0.75 V was assigned to chloride oxidation since chloride was the only electroactive species present in this salt. But from the peak intensity, it appears that the oxidation peak 1 obtained from solutions of $CoCl_2$ was higher than the oxidation peak 1 obtained in TEACl solutions. This proves that the oxidation peaks 1 obtained from CV of $CoCl_2$ arisen due to oxidation of both cobalt and chloride ligand. In conclusion, TEACl cannot be used as a supporting electrolyte because it contained a chloride ion which can be easily oxidized at a Pt WE.

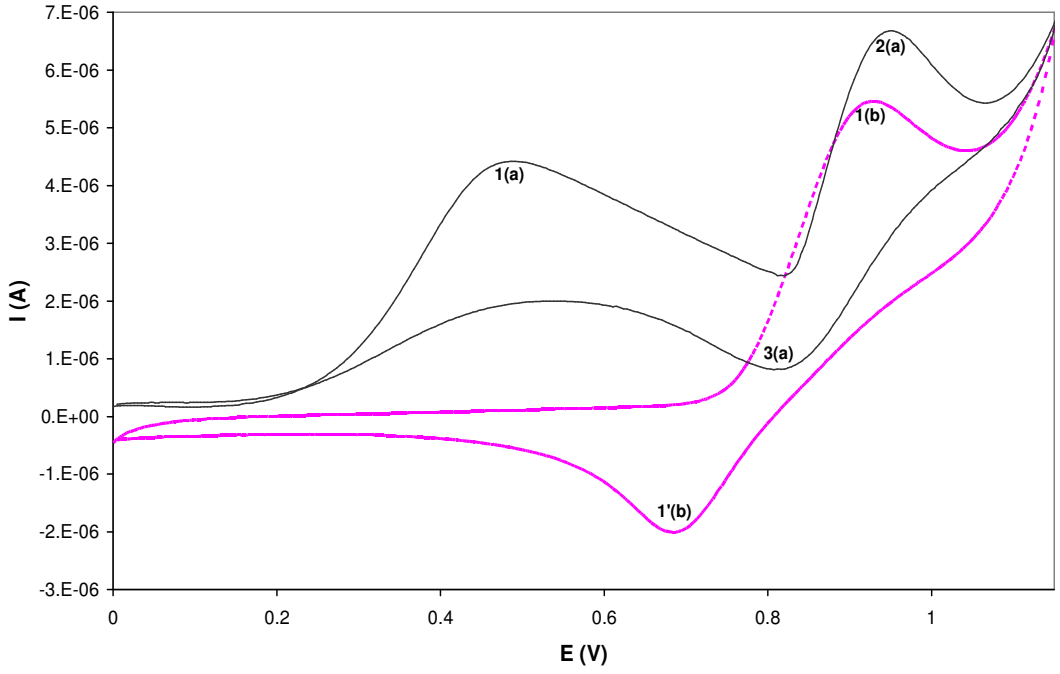

Figure 5.21 Comparison of the CV curve of $CoCl_2(PPh_3)_2$ (—) with that of $CoCl_2$ (—).

To further confirm the assignment of the oxidation peak 2 of $CoCl_2(PPh_3)_2$, we compared the CV curve of $CoCl_2(PPh_3)_2$ with that of $CoCl_2$ and that of PPh_3 obtained in a mixture of acetonitrile and pentanol (1:1). Figure 5.21 shows comparison of the CV curve of $CoCl_2(PPh_3)_2$ with that of $CoCl_2$. The oxidation peak 2(a) of the complex, $CoCl_2(PPh_3)_2$

agreed in position, shape and height with the oxidation peak 1(b) of $CoCl_2$. We suggested that the oxidation peak 2(a) of $CoCl_2(PPh_3)_2$ might have arisen due to oxidation of a chloride ligand from the complex. Comparison of the CV curve of $CoCl_2(PPh_3)_2$ with that of PPh_3 revealed no similarities between the two voltammograms (Figure 5.22).

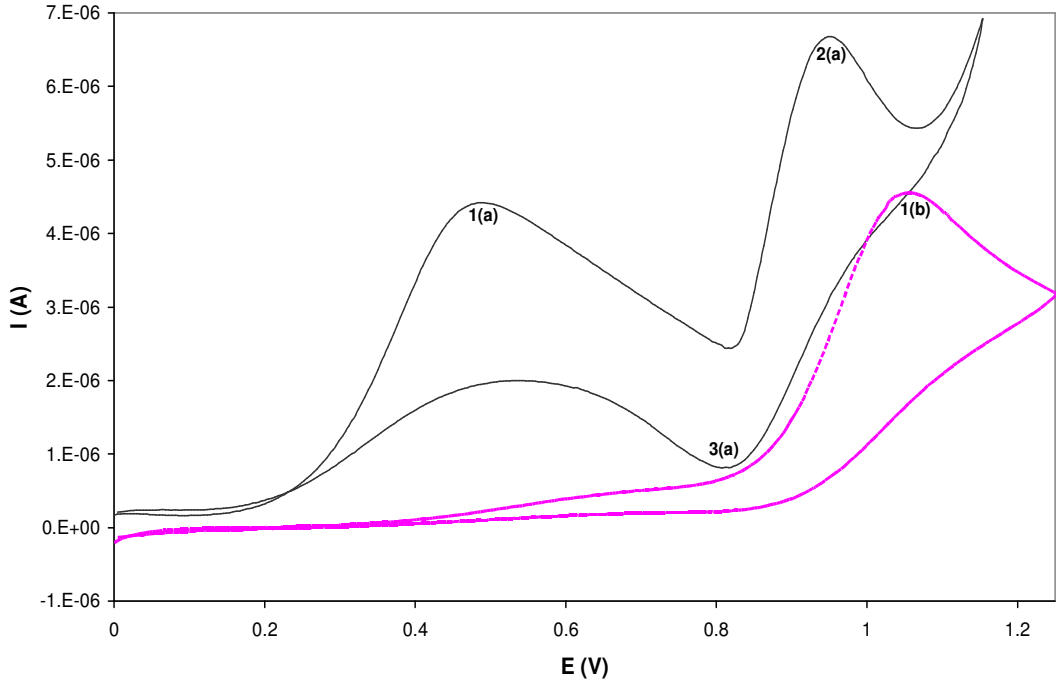

Figure 5.22 Comparison of the CV curves of $CoCl_2(PPh_3)_2$ (—) with that of PPh_3 (—).

The oxidation peak 2(a) of the complex occurred at less positive potentials and had a coupled reduction peak 3(a), whilst the oxidation peak 1(b) of PPh_3 occurred at more positive potential and had no coupled reduction peak. Similar results were also obtained from comparison of the CV curve of $CoCl_2$ with that of PPh_3 (Figure 5.23).

We also compared the oxidation peak 1 of $CoCl_2$ with that of TEACl (Figure 5.24) [Note: the CV curve of $CoCl_2$ and that of TEACl were recorded on the same day using the same solution of background electrolyte, starting with a $CoCl_2$ experiment]. The oxidation peak 1(b) obtained from a TEACl solution was observed at almost the same potential as that of $CoCl_2$ peak 1(a) shown as an insert of Figure 5.24 and the reduction peaks 1'(a and b) were at exactly the same position.

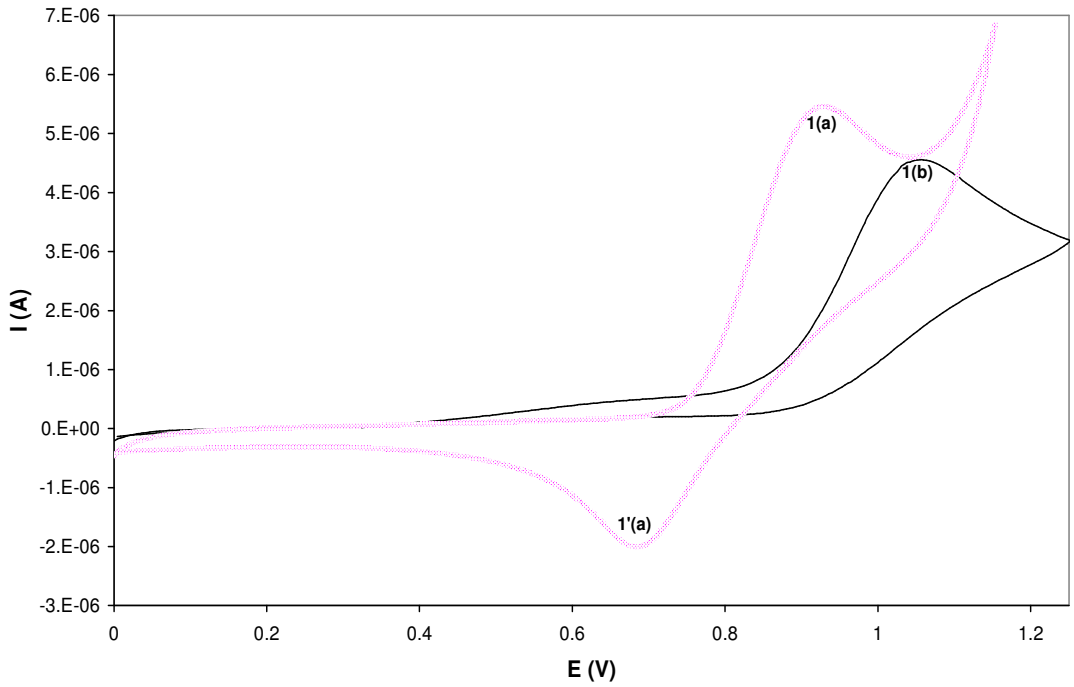

Figure 5.23 Comparison of the CV curve of PPh_3 (—) with that of $CoCl_2$ (....).

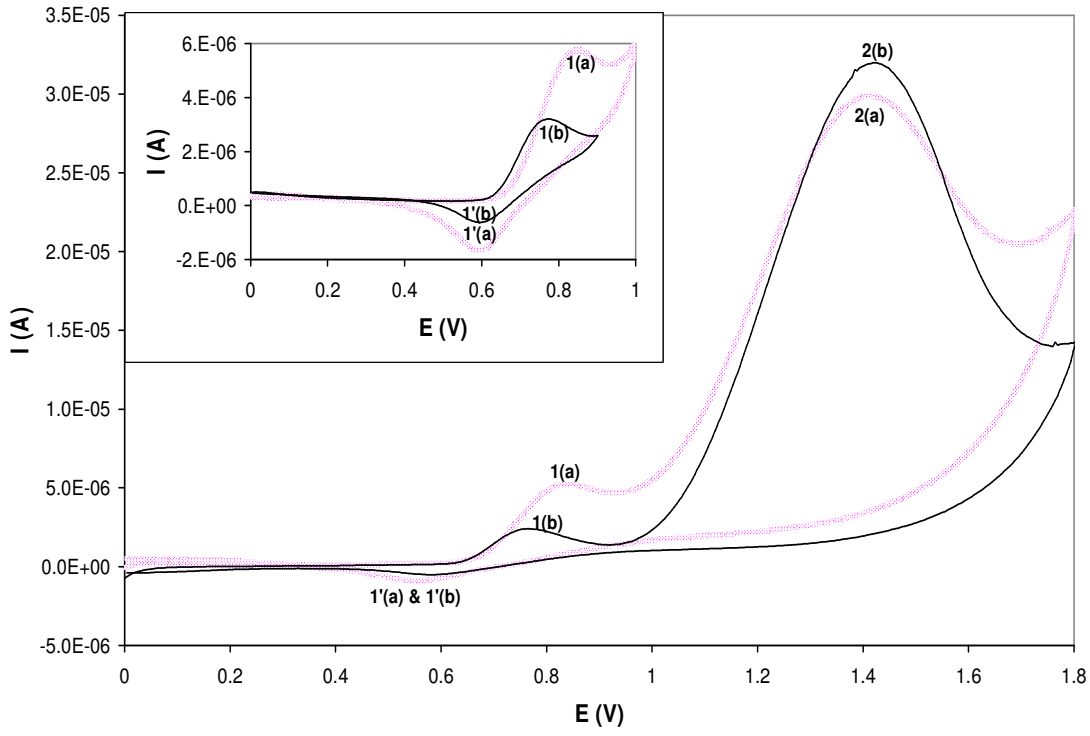

Figure 5.24 Comparison of the CV curves of TEACl (—) with that of $CoCl_2$ (....). CV curves obtained at short potential range up to 1.15 V are shown as an insert.

The peak current of the oxidation peak 1(a) obtained from a $CoCl_2$ solution and its coupled reduction peak 1'(a) are about a factor of two times higher than the peak current obtained for the oxidation peak 1(b) and its coupled reduction peak 1'(b) obtained from a TEACl solution. As it is well known that the peak current depends on the concentration of the oxidized species, an increase in oxidation peak 1(a) of $CoCl_2$ might have arisen due to two chloride ions present in $CoCl_2$ since only one chloride ion was present in TEACl.. Furthermore, the little shift in peak potentials might be related to different solvation energies present in solutions of TEACl and $CoCl_2$ or most likely due to an irreversible nature of the electrochemical reactions.

The oxidation peak 2 in both salts did not show any relation to the concentration of the chloride ion, but seemed to be related to the amount of water present in background solutions (Figure 5.24). The peak current of the oxidation peak 2 increased slightly in TEACl solutions in comparison to that obtained in $CoCl_2$ solutions, due to different amounts of water present in background solutions, as shown by different background current curves of TEACl and $CoCl_2$ in Figure 5.25.

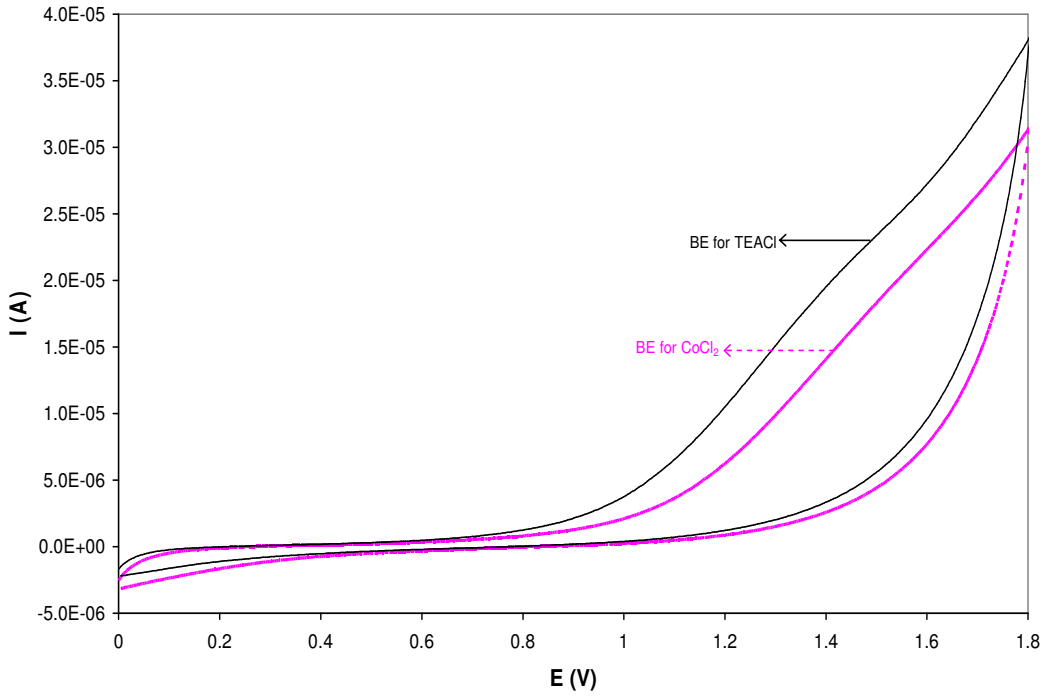

Figure 5.25 Influence of water on the background current CV curves obtained before CV measurements of TEACl and $CoCl_2$ at a Pt disk WE.

In conclusion, the anodic voltammetric studies of $CoCl_2(PPh_3)_2$ revealed three oxidation peaks, the first one involving oxidation of the metal centre, Co^{II} to Co^{III} which was followed by oxidation of chloride ligand from $CoCl_2(PPh_3)_2$ (peak 2) and this was complicated by a catalytic reaction of chloride with water present in the background solvent (peak 3) which caused a diffusion current enhancement.

5.1.3 Electrochemically Monitored Titration of $CoCl(PPh_3)_3$ With Chloride

In this section we focused on titration of the complex $CoCl(PPh_3)_3$ with chloride electrochemically, to investigate the binding ability of the chloride ions to $CoCl(PPh_3)_3$. TEACl was used as a chloride source. We synthesized the complex $CoCl(PPh_3)_3$ and characterised it using elemental analysis and infrared spectroscopy (the results obtained are presented in Experimental Section, Chapter 3).

CV curves of 7.7 x 10^{-4} mol/l $CoCl(PPh_3)_3$ before (solid-line curve) and after (dotted-line curve) addition of an equivalent concentration of TEACl are shown in Figure 5.26. Two oxidation peaks labelled peak 1(a) and 2(a) which had a coupled reduction peak 3(a) were observed from the CV of $CoCl(PPh_3)_3$ (Figure 5.26(a)).

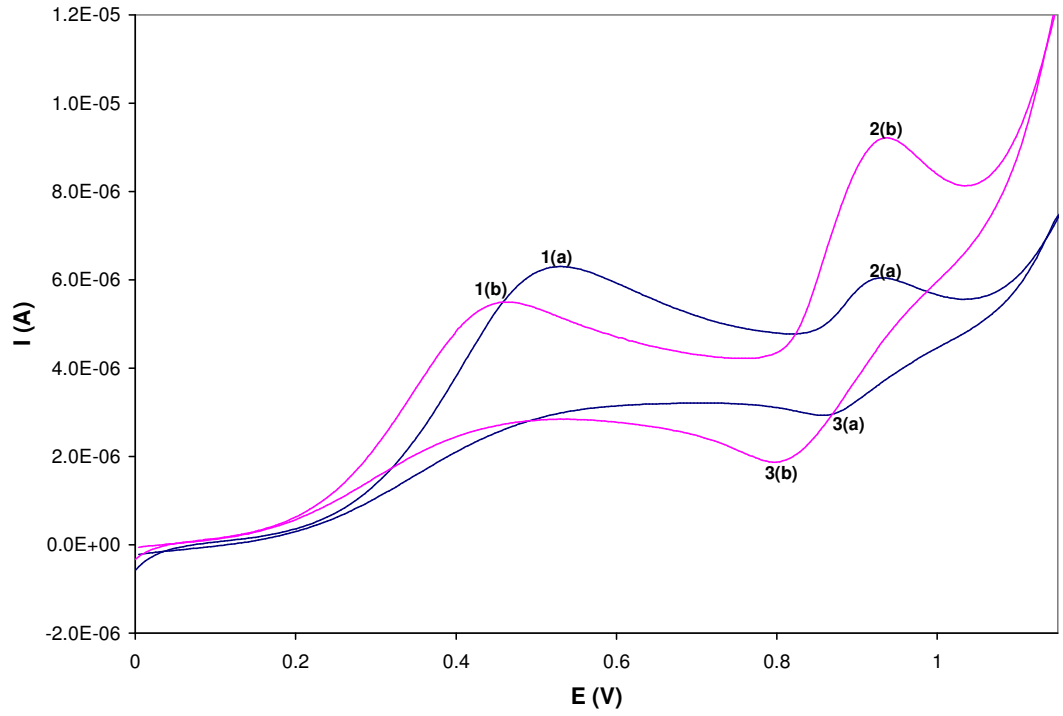

Figure 5.26 Effect of added chloride on the CV curve of $CoCl(PPh_3)_3$. CV curves of $CoCl(PPh_3)_3$ before (—) and after (—) addition of an equivalent concentration of TEACl are presented.

Addition of an equivalent concentration of TEACl to a $CoCl(PPh_3)_3$ solution resulted in a small decrease in the peak current of oxidation peak 1(a) (peak 1(b)) and an increase in current of oxidation peak 2(a) (peak 2(b)) and its coupled reduction peak 3(a) (Peak 3(b)) [Figure 5.26(b)]. An increase in current of oxidation peak 2(a) was assumed to be related to an increase in concentration of added chloride ion to a $CoCl(PPh_3)_3$ complex. Note that peak 1(b) appeared at a less positive potential, whilst peak 2(b) remained at the same potential. An increase in current of peak 2(b) after addition of chloride must indicate formation of another compound (most likely $CoCl_2(PPh_3)_2$).

Comparison of the CV curve of $CoCl_2(PPh_3)_2$ with that of $CoCl(PPh_3)_3$ after addition of an equivalent concentration of TEACl revealed similarities between the oxidation peak 1 and 2; in terms of the peak height, position and shape (Figure 5.27). It appears that electrochemical reactions occurring at peak 2(a) and (b) are the same or are electrochemically reversible whilst electron transfer reactions at peak 1(a) and (b) are irreversible. From this similarity we attributed the oxidation peak 2 of the complexes $CoCl_2(PPh_3)_2$ and $CoCl(PPh_3)_3$ to occur due to oxidation chloride ligand. In conclusion, it appears that chloride is capable of binding to $CoCl(PPh_3)_3$ resulting in replacement of one PPh_3 ligand by a chloride ligand.

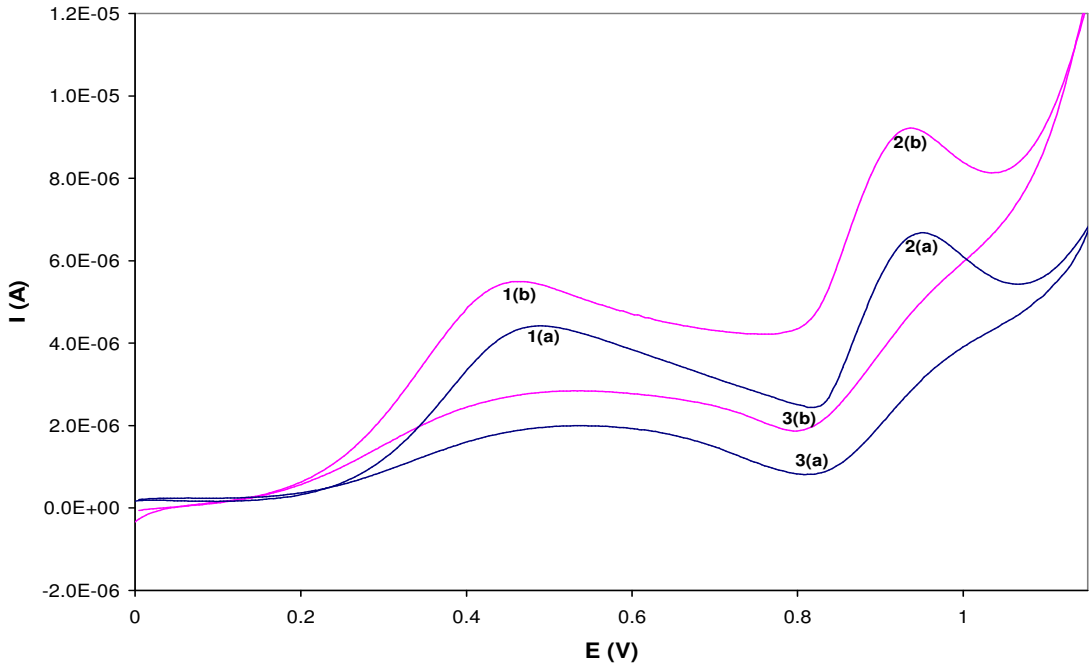

Figure 5.27 Comparison of CV curves of $CoCl_2(PPh_3)_2$ (—) with that of $CoCl(PPh_3)_3$ after addition of an equivalent concentration of TEACl (—).

From the above results, we concluded that addition of chloride (as TEACl) to a solution containing $CoCl(PPh_3)_3$ resulted in addition of a chloride ion to this complex which displaced one PPh_3 molecule from the complex. This was shown by an increase in current of oxidation peak 2(b) (see Figure 5.26(b)) which was previously assigned to chloride ligand oxidation and is evidence of formation of the complex $CoCl_2(PPh_3)_2$ since oxidation peak currents of 2(a) and (b) are equal (see Figure 5.27). Since free PPh_3 was oxidized at E_p = 1.0 V, one would expect its oxidation peak to appear after its replacement by a chloride ligand from $CoCl(PPh_3)_3$ but this was not the case. The explanation to the above statement will be given in the next section (Section 5.1.4) during analysis of CV curves obtained in an experiment involving titration of $CoCl_2(PPh_3)_2$ with PPh_3.

In Figure 5.28 we compared the CV curve of $CoCl(PPh_3)_3$ (b) with that of $CoCl_2(PPh_3)_2$ (a) to further confirm that the oxidation peak 2 arisen due to oxidation of chloride ligand.

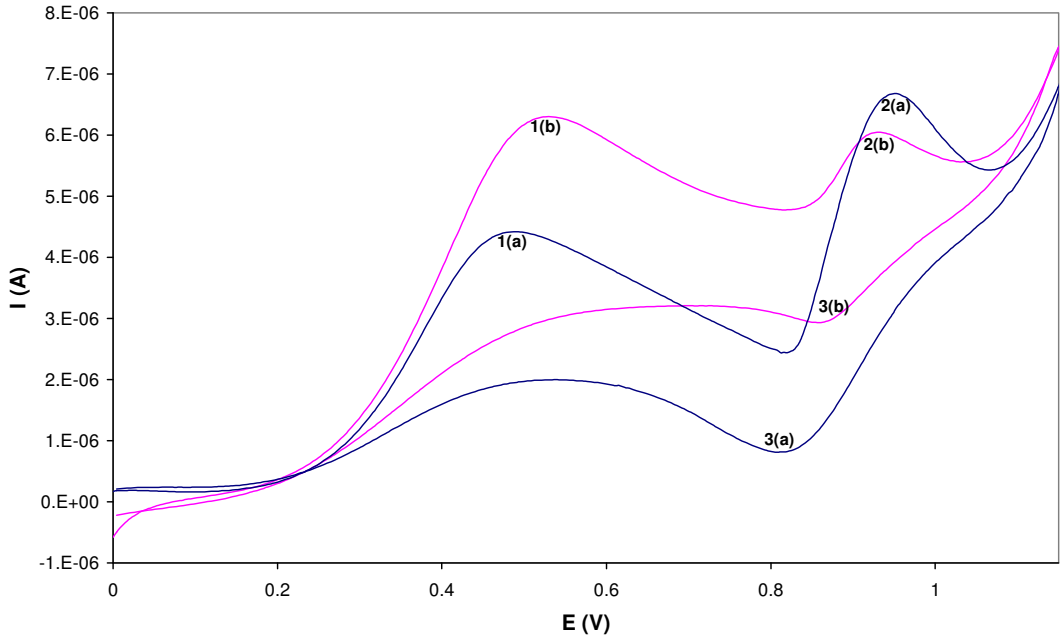

Figure 5.28 Comparison of CV curve of $CoCl_2(PPh_3)_2$ (—) with that of $CoCl(PPh_3)_3$ (—).

It is important to note that when only one chloride ion is attached to a complex molecule i.e. $CoCl(PPh_3)_3$, the current of oxidation peak 2(b) appears lower than for the one obtained from a complex containing two chloride ions i.e. $CoCl_2(PPh_3)_2$ (Figure 5.28). The above result suggests that oxidation peak 2 depends on the concentration of chloride ions attached

to the complex. This further supports the assignment that the oxidation peak 2(a) of $CoCl_2(PPh_3)_2$ arises due to oxidation of chloride ligand. The current of the metal oxidation peak 1(b) of the complex $CoCl(PPh_3)_3$ occurring at E_p = 0.50 V was higher and steeper than that of $CoCl_2(PPh_3)_2$ which we interpreted as involving liberation of two electrons from the complex $CoCl(PPh_3)_3$ [Co^I] to form a Co^{III} complex. We proposed the following overall electrochemical reactions:

Peak 1(b), Figure 5.29: $Co^{I}Cl(PPh_3)_3 \rightarrow [Co^{III}Cl(PPh_3)_3]^+ + 2e^-$ (5.1)

Peak 2(b), Figure 5.28: $Co^{I}Cl(PPh_3)_3 \xrightarrow{TEACl} [Co^{II}Cl_2(PPh_3)_2]^+ + PPh_3 + e^-$ (5.2)

Addition of three (—) and six (**....**) equivalent concentrations of TEACl to a solution containing $CoCl(PPh_3)_3$ resulted in splitting of the oxidation peak 2 into two processes (Figure 5.29). The reduction peaks 3(a) and (b) became broad and shifted to less negative potentials. The metal oxidation peak 1 remained unchanged and shifted only minutely to less negative potentials. The most interesting feature observed from the voltammograms was the appearance of a new oxidation peak 5 at E_p = 0.80 V, which increased in intensity with an increase in concentration of added TEACl.

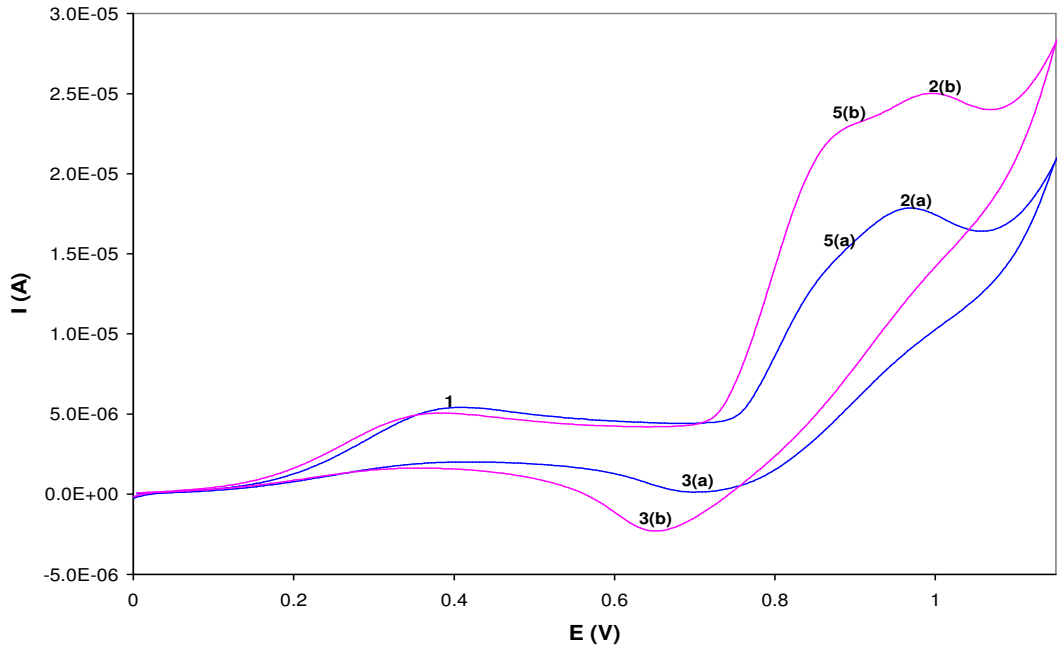

Figure 5.29 CV curves of $CoCl(PPh_3)_3$ after addition of 2.31×10^{-3} mol/l (—) and 4.62×10^{-3} mol/l (—) TEACl.

The appearance of the oxidation peak 5, led us to a conclusion that the broadness and shift to less negative potential of i.e. peak 3(b) was a result of an overlap between this peak and peak 5(b). And from this we concluded that the oxidation peak 5 was due to the oxidation of unbound chloride ion from TEACl present in solution in excess. Also the oxidation peak 5 was at almost the same position as that obtained from a solution containing free TEACl as shown in Figure 5.20.

From the above observation we concluded that the complex $CoCl_2(PPh_3)_2$ is the most stable since addition of excess chloride to $CoCl(PPh_3)_3$ resulted in formation and oxidation of free chloride in solution, thus no further substitution of PPh_3 by chloride could occur.

5.1.4 Monitored Titration of $CoCl_2(PPh_3)_2$ with PPh_3.

5.1.4.1 Cyclic Voltammetry

In this section, the binding ability and the electrocatalytic property of PPh_3 towards the complex $CoCl_2(PPh_3)_2$ is investigated in detail. In the previous section we investigated the binding ability of chloride towards the complex $CoCl(PPh_3)_3$. We found that chloride is capable of binding to $CoCl(PPh_3)_3$ with release of one PPh_3 ligand resulting in formation of $CoCl_2(PPh_3)_2$. CV of $CoCl_2(PPh_3)_2$ before addition of PPh_3 is shown in Figure 5.30.

The oxidation peak 4 was not investigated because an increase in background current was observed at potentials above 1.2 V due to oxygen evolution from traces of water present in the background solvents. As previously assigned, the oxidation peak 1 involved metal oxidation, Co^{II} to Co^{III} whilst oxidation peak 2 involved oxidation of chloride ligand from the complex, $CoCl_2(PPh_3)_2$ (Figure 5.30).

Figure 5.31 shows the CV curve of $CoCl_2(PPh_3)_2$ after addition of 2.5 and 5 equivalent concentration of PPh_3. Addition of 2.5 equivalent concentration of PPh_3 to a $CoCl_2(PPh_3)_2$ solution resulted in an increase in current of oxidation peak 1(a) and a decrease in current of the oxidation peak 2(a) and its coupled reduction peak 3(a) [Figure 5.31(a)]. Addition of 5 equivalent concentration of PPh_3 to a $CoCl_2(PPh_3)_2$ solution resulted in a further increase in peak current of an oxidation peak 1(b) and a further decrease in peak current of an oxidation peak 2(b) [Figure 5.31(b)].

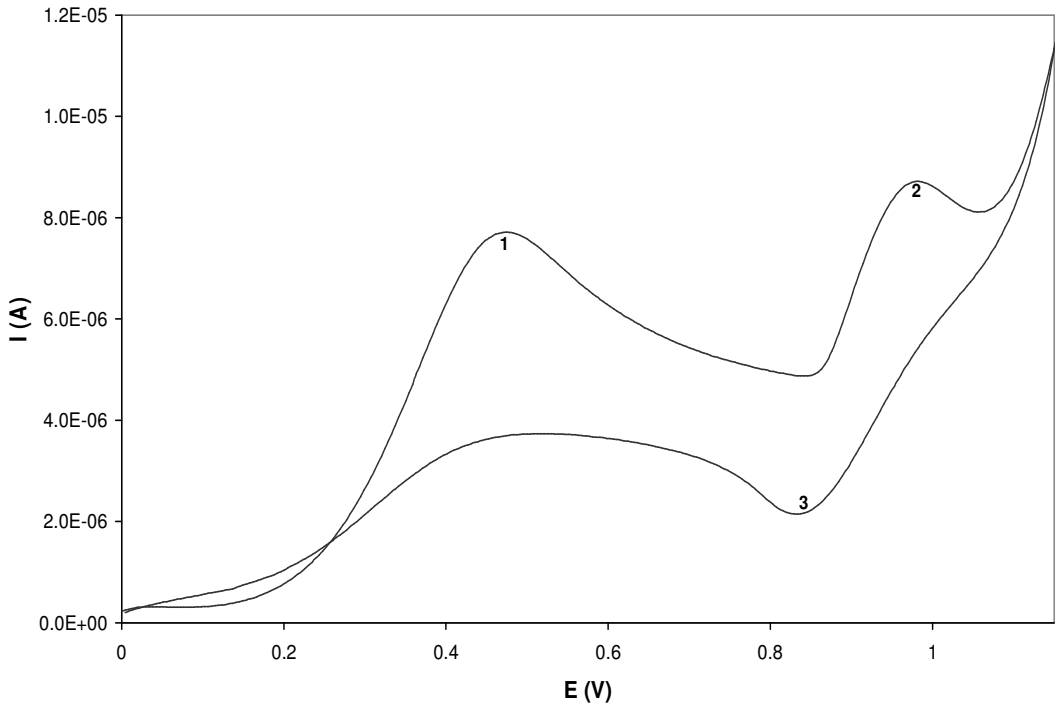

Figure 5.30 CV curves obtained in solutions containing $CoCl_2(PPh_3)_2$ at a Pt disk WE.

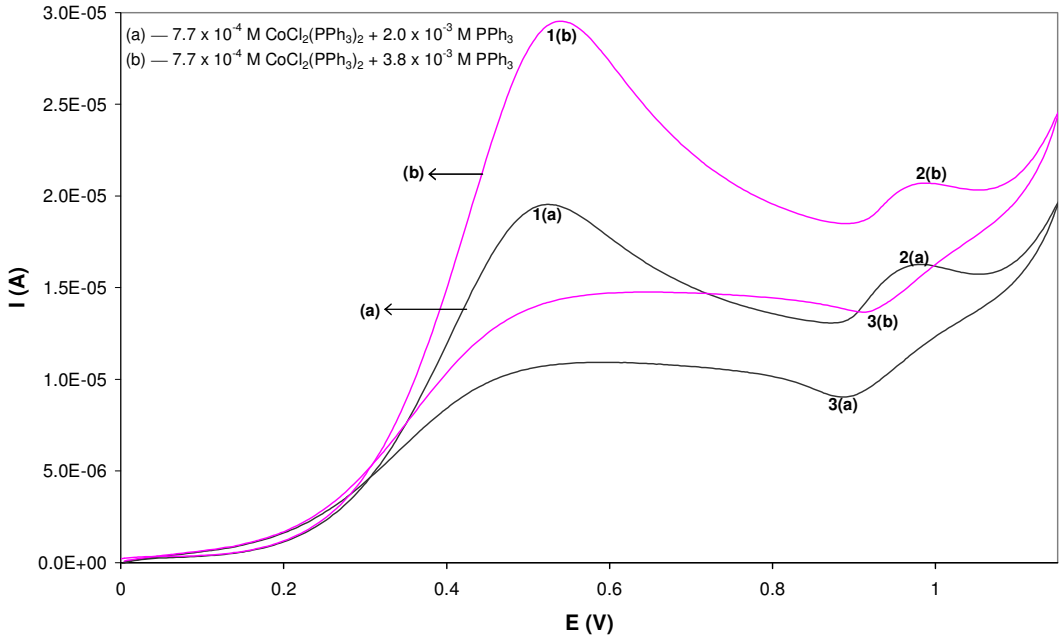

Figure 5.31 CV curves obtained from a solution of $CoCl_2(PPh_3)_2$ after addition of 2.5 (—) and 5 (—) equivalent concentration of PPh_3.

Addition of 15 equivalent concentration of PPh_3 to a $CoCl_2(PPh_3)_2$ solution resulted in an even further increase in current of an oxidation peak 1 and disappearance of an oxidation peak 2 (Figure 5.32).

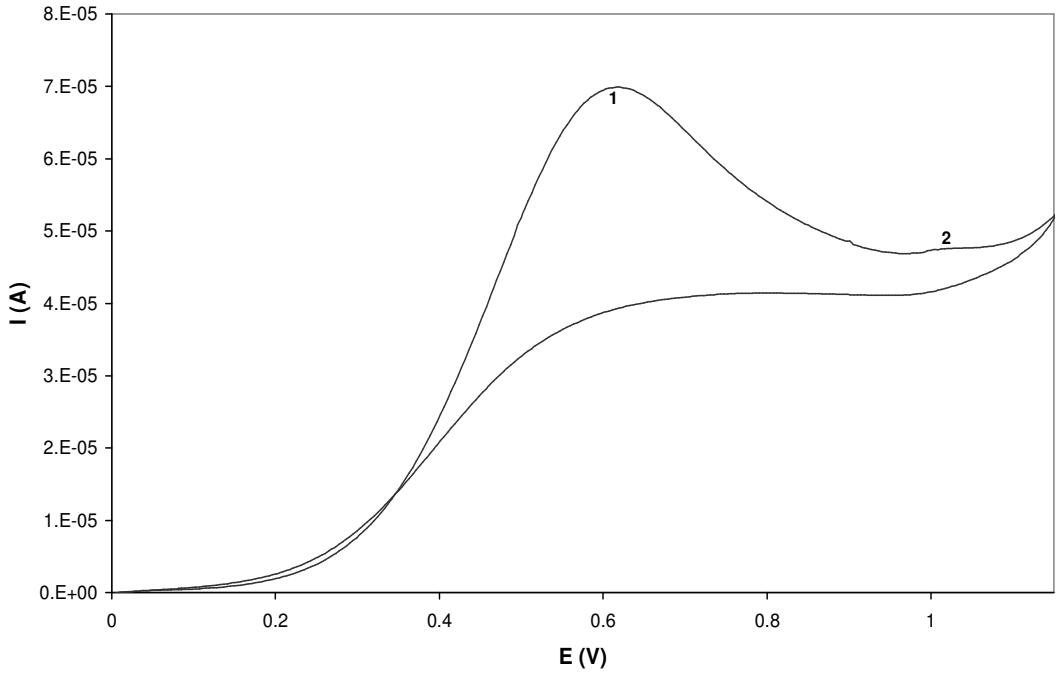

Figure 5.32 CV curve obtained from a solution of $CoCl_2(PPh_3)_2$ after addition of 15 equivalent concentration of PPh_3.

An oxidation peak 2 disappeared either because it is masked by a large oxidation peak 1 or because the species that is oxidized at peak 2 was depleted away from an electrode surface by the added PPh_3. In order to interpret the above results we looked at some literature review on titration of metal complexes with PPh_3.

Switzer and co-workers [72], have studied a CV behaviour of $MeCpMn(CO)_2(CH_3CN)$ in the presence of added PPh_3 in 0.1 M tetraethyl ammonium perchlorate (TEAP) in acetonitrile. They have found that the presence of PPh_3 led to a drastic alteration of the well-behaved, reversible CV of $MeCpMn(CO)_2(CH_3CN)$ which appeared at E_p = 0.22 V. After addition of an equal concentration of PPh_3, another reversible oxidation wave appeared at E_p = 0.55 V, the CV oxidation wave of $MeCpMn(CO)_2(CH_3CN)$ at E_p = 0.22 V became irreversible and decreased in magnitude in proportion to the concentration of PPh_3.

After addition of nine times equivalent concentration of PPh_3 the anodic peak current I_{pa} of $MeCpMn(CO)_2(CH_3CN)$ decreased further in magnitude in proportion to the concentration of PPh_3 and the diffusion current fallen to near zero. This behaviour requires that $MeCpMn(CO)_2(CH_3CN)$ be removed from the vicinity of the electrode by some alternative process that does not require net flow of current. Such a process simultaneously led to the substitution product [P = $MeCpMn(CO)_2(PPh_3)$], which was clearly shown by its reversible CV wave at the higher potential of E_p = 0.55 V. This was confirmed by measuring the CV of the synthesized $MeCpMn(CO)_2(PPh_3)$ and similar results were obtained [72].

The CV behaviour of $CoCl_2(PPh_3)_2$ in the presence of added PPh_3, was explained using the above explanation by Switzer and co-workers [72]. Therefore, we concluded that the disappearance of oxidation peak 2 was a result of depletion of chloride oxidized at this potential away from the electrode surface. This might have resulted in formation of $Co(PPh_3)_4$ in large amounts at the electrode surface, which might explain a large increase in current of oxidation peak 1.

In order to prove that a $Co(PPh_3)_4$ complex is formed, one will have to synthesize this complex using an independent method and record its voltammogram. If the voltammogram can show one irreversible oxidation peak at E_p ~ 0.50 V then we will know for sure that addition of excess PPh_3 results in substitution of all chloride ions from $CoCl_2(PPh_3)_2$ to form $Co(PPh_3)_4$. This behaviour is characteristic of electrocatalysis of ligand exchange.

The CV of $CoCl_2(PPh_3)_2$ after addition of 75 equivalent concentration of PPh_3 is shown in Figure 5.33. Addition of 75 equivalent concentration of PPh_3 to a $CoCl_2(PPh_3)_2$ solution, resulted in an appearance of a new irreversible oxidation peak labelled peak 4 at E_p = 1.0 V (Figure 5.33). The oxidation peak 1 of the complex appeared as a shoulder as it was masked by this new oxidation peak 4 with a very large diffusion current, which appeared when the solution contained large concentration of PPh_3 (Figure 5.33). An irreversible oxidation peak 4 was assigned to oxidation of a free PPh_3, since the CV curve was similar to that of a free PPh_3; and it had no coupled reduction peak. We can conclude that, only when the amount of cobalt from the complex was insufficient to consume all the added PPh_3 was then that the peak for oxidation of free PPh_3 was observed (which happened after addition of ~ 30 equivalent concentration of PPh_3).

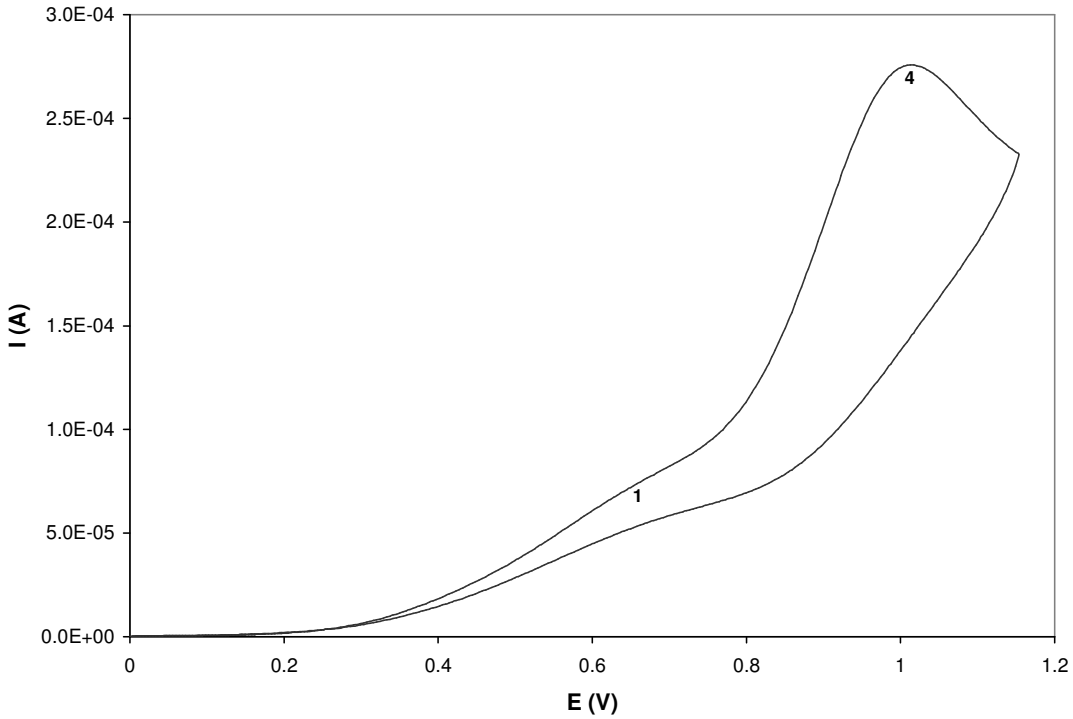

Figure 5.33 CV curve obtained from a solution of $CoCl_2(PPh_3)_2$ after addition of 75 equivalent concentration of PPh_3.

This also explains why we did not observe the oxidation peak of a free PPh_3 in solutions containing $CoCl(PPh_3)_3$ after addition of an equivalent concentration of chloride (Section 5.1.3). Since we concluded that addition of chloride ion to $CoCl(PPh_3)_3$ resulted in replacement of one PPh_3 ligand by a chloride ligand which in turn resulted in formation of a $CoCl_2(PPh_3)_2$ complex.

5.1.4.2 Ultraviolet-Visible Spectroscopy

UV-Visible spectrometry was also used to determine the fate of the bound PPh_3 ligand on the complex $CoCl_2(PPh_3)_2$, by titration of the complex with PPh_3 and comparing the UV-Visible spectrum of a free triphenylphosphine with that of $CoCl_2(PPh_3)_2$.

A UV-Visible spectrum was recorded first from a background solution to check if there is any absorption of the solvent impurities or the supporting electrolyte (Figure 5.34). There was no evidence of absorption of any of the background components from the UV-Vis spectra of the background solution. Nevertheless there is a negative dip in the spectrum of the background solution which might have arisen due to impurities or other substances present in the background solution. The UV-Visible spectrums of PPh_3, $CoCl_2$ and

$CoCl_2(PPh_3)_2$ in a mixture of acetonitrile and pentanol (1:1) containing 0.05 M TBAHFP are presented in Figures 5.35, 5.36 and 5.37.

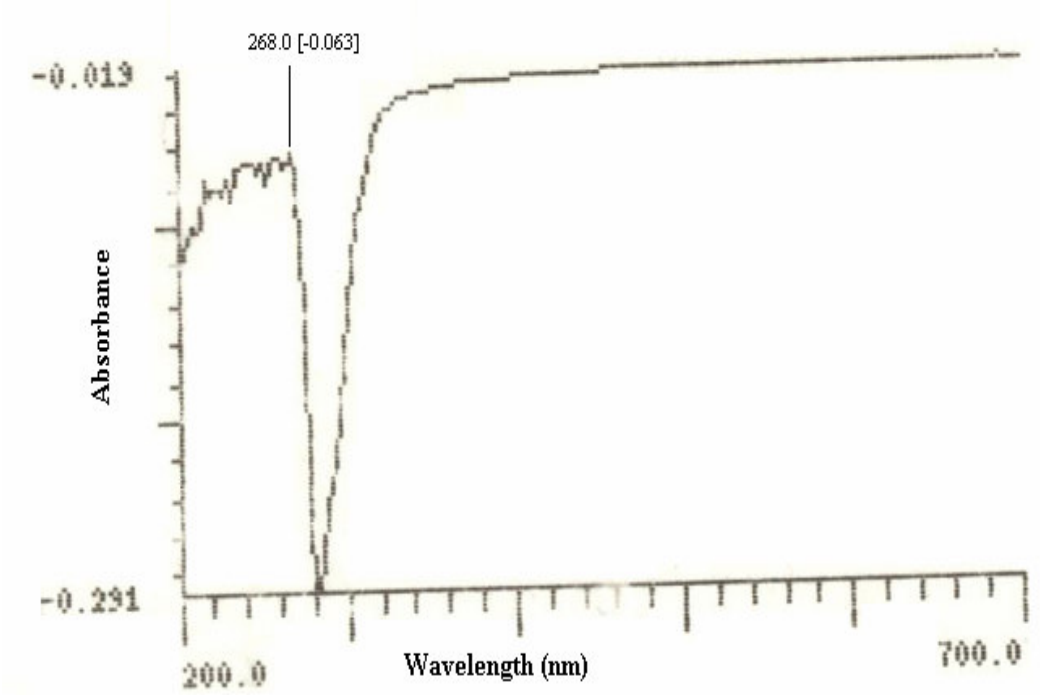

Figure 5.34 UV-Visible spectrum recorded in an acetonitrile background solution containing 0.05 M TBAHFP.

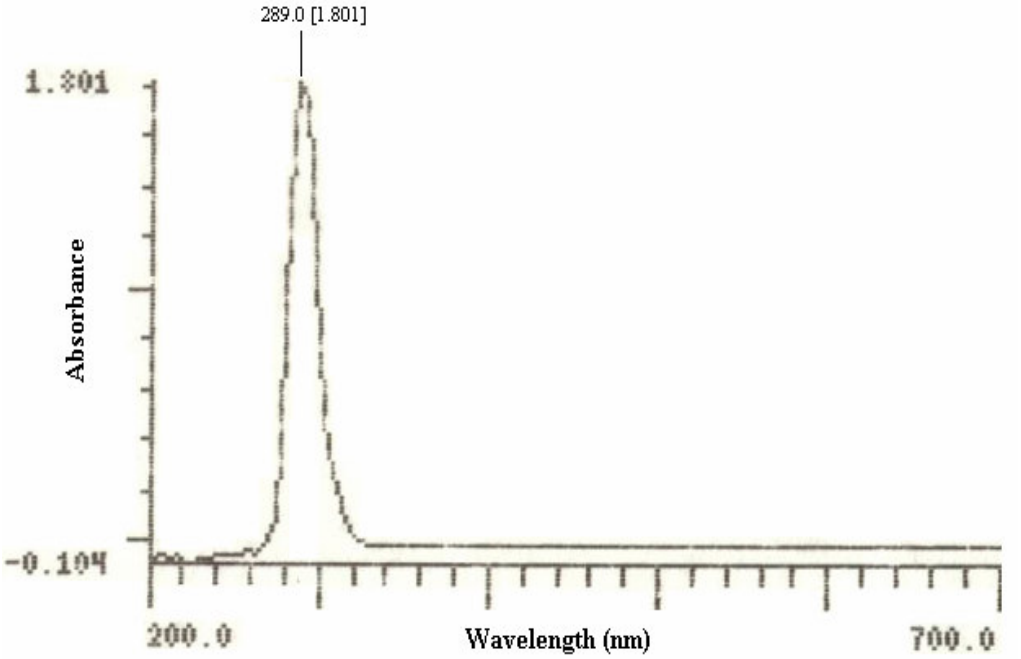

Figure 5.35 UV-Visible spectrum of a 7.7×10^{-4} mol/l PPh_3.

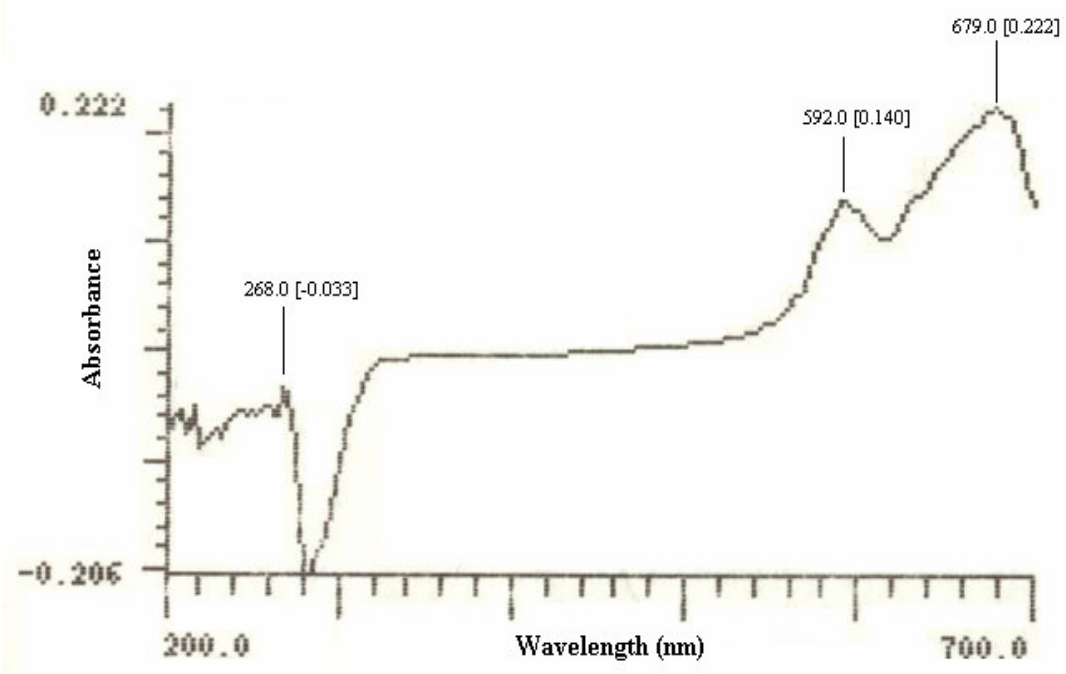

Figure 5.36 UV-Visible spectrum of a 7.7×10^{-4} mol/l $CoCl_2$.

A spectrum of PPh_3 revealed one major intense absorption band at 289 nm; with no bands appearing at higher wavelengths in reasonable agreement with a literature value of 261 nm [73] and 260 nm in acetonitrile, DMF and ethyl alcohol [74] (Figure 5.35). A negative dip observed from the spectrum of the background solution was not observed during measurement of PPh_3 or it was suppressed by a huge peak of PPh_3 absorption at 289 nm. A spectrum of $CoCl_2$ revealed two absorption bands at 592 and 679 nm (Figure 5.36), which are in reasonable agreement with literature values of 600 and 690 nm observed in DMF [75]. A negative dip in spectrum was also observed from the spectrum of $CoCl_2$ and it is at the same position as the one observed from the spectrum of the background solution. The observation of the negative dip might be due to the fact that the absorption peak of $CoCl_2$ are observed at a wavelength far away from were the dip occurs and also because the absorption peaks are very weak. From these results it follows that UV-Visible spectroscopy is very sensitive to PPh_3 since it can be detected easily with a very high absorption signal, but insensitive to cobalt present in $CoCl_2$, as shown by small absorption bands. One can, however, distinguish the UV-Visible spectrum of $CoCl_2$ from that of PPh_3.

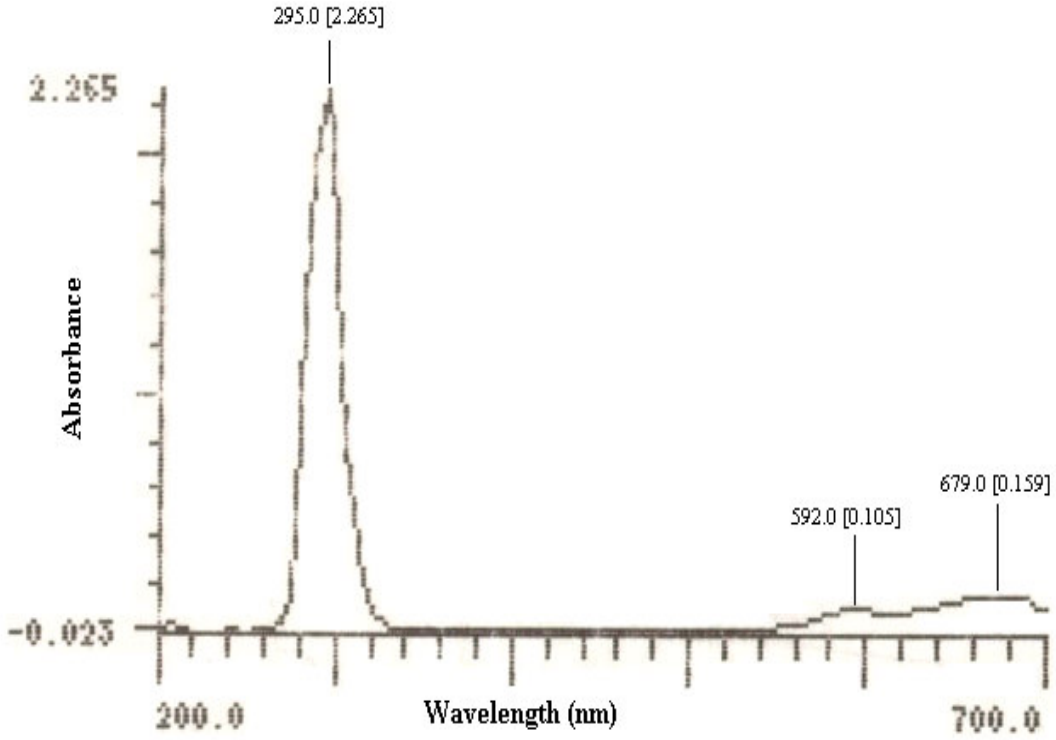

Figure 5.37 UV-Visible spectrum of a 7.7×10^{-4} mol/l $CoCl_2(PPh_3)_2$.

$CoCl_2(PPh_3)_2$ complex on the other hand revealed a major broad absorption band at 295 nm and other two small bands at higher wavelengths of 592 and 679 nm (Figure 5.37). Three absorption bands were found in the literature for a $CoCl_2(PPh_3)_2$ complex in ethyl acetate ($CH_3COC_2H_5$) as 581, 638 and 682 nm and another broad, weak absorption band appeared at ~ 100 to 160 nm [61].

It was mentioned that an absorption band at ~ 100 to 160 nm was so broad that no precise energy values could be ascertained from them, although in truly tetrahedral complexes they provide fairly precise information [61]. Broadening of the UV-Vis spectroscopy of the ligands in $CoCl_2(PPh_3)_2$ (band at 295 nm) indicates a dynamic ligand exchange in both bis- and tris-phosphorus complexes [76]. It is shown from the UV-Visible spectrum of $CoCl_2(PPh_3)_2$ and PPh_3, that one cannot distinguish between the two since they both have a large absorption band at shorter wavelength ~ 290 nm.

In order to assign this band at 297 nm from the UV-Visible spectrum of the complex, we recorded a UV-Visible spectrum of $CoCl_2$ alone in solution and then after addition of 2 equivalent moles of PPh_3 as we have done with cyclic voltammetry.

A UV-Visible spectrum of $CoCl_2$ shown in Figure 5.36, revealed two absorption bands at longer wavelengths of ~ 592 and 679 nm.

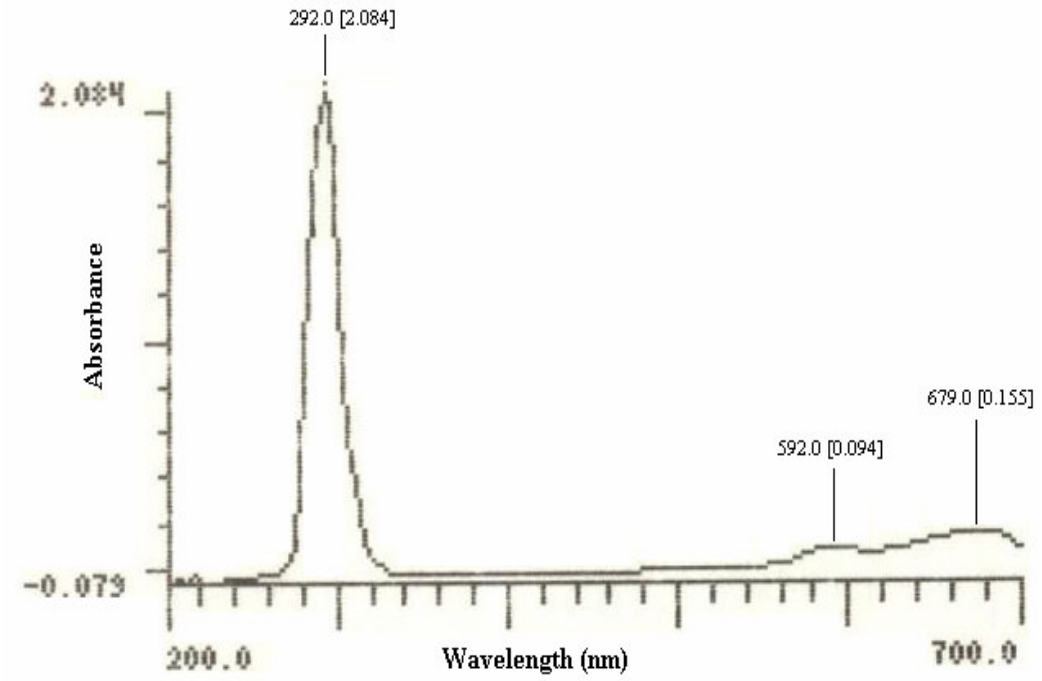

Figure 5.38 UV-Visible spectrum of 7.7×10^{-4} mol/l $CoCl_2$ after addition of 1.54×10^{-3} mol/l (2 equivalent concentration) of PPh_3.

After addition of 2 equivalent moles of PPh_3, another absorption band of large intensity appeared at 292 nm (Figure 5.38). The absorption band at 292 nm agrees in position, shape and height with the one observed from a UV-Visible spectrum of $CoCl_2(PPh_3)_2$. Since this band appeared only after mixing of the two starting materials it was assigned to cobalt absorption from the complex.

Titration of the complex $CoCl_2(PPh_3)_2$ with PPh_3 did not give us any additional information, meaning we did not observe an appearance of a peak for a free PPh_3 even after addition of 75 equivalent moles of PPh_3. This might have arisen due to overlap of the cobalt absorption band from the complex and that of PPh_3 and also no significant change was observed on the absorption bands that appeared at longer wavelengths. The UV-Visible curves for the titration are presented in an Appendix B 2 (Figure B.5 to B.8).

5.1.4.3 ^{31}P Nuclear Magnetic Resonance Spectroscopy

NMR spectroscopy was also used to investigate the effect of added PPh_3 on the NMR spectra of $CoCl_2(PPh_3)_2$. An NMR spectrum of a free triphenylphosphine was recorded first for convenience (Figure 5.41). An NMR spectrum of PPh_3 in $CDCl_3$ shows a main peak at – 4.0465 ppm, in reasonable agreement with a literature value of – 4 ppm recorded in the same solvent $CDCl_3$ [76] and another minor peak appeared at + 31.0421 ppm (Figure 5.39).

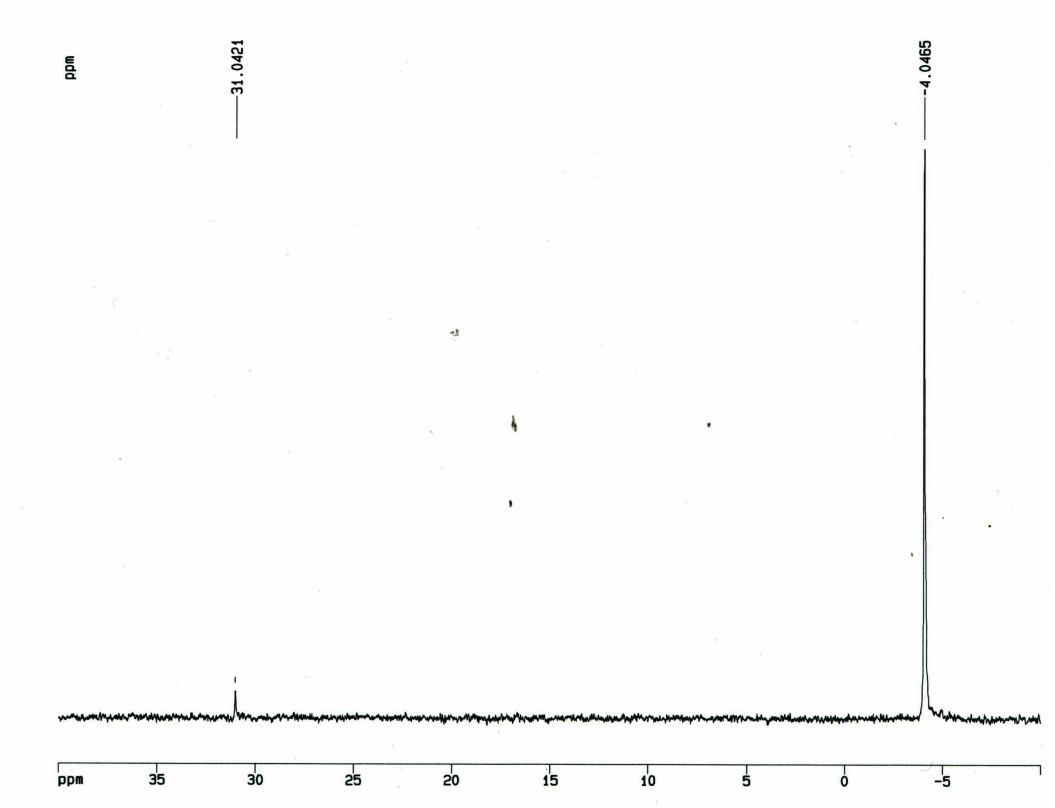

Figure 5.39 ^{31}P NMR signals of triphenylphosphine (PPh_3).

Figure 5.40 shows an NMR spectrum of the complex $CoCl_2(PPh_3)_2$ which revealed a broad peak at – 4.0063 ppm. This peak is at around the same position as that for a free triphenylphosphine. The difference is that the peak shifted downfield and became broad. The broadening of an NMR peak of $CoCl_2(PPh_3)_2$ and the roughness of an NMR baseline arisen due to the presence of paramagnetic ions from cobalt. Furthermore, the peak that appeared up field at + 31.0421 ppm from an NMR spectrum of PPh_3 did not appear from an NMR spectrum of $CoCl_2(PPh_3)_2$. The broadening of the resonance peak of the complex

$CoCl_2(PPh_3)_2$ indicates rapid ligand exchange on the NMR time scale [76]. Most of the phosphorus resonances are also broadened upon complexation [76].

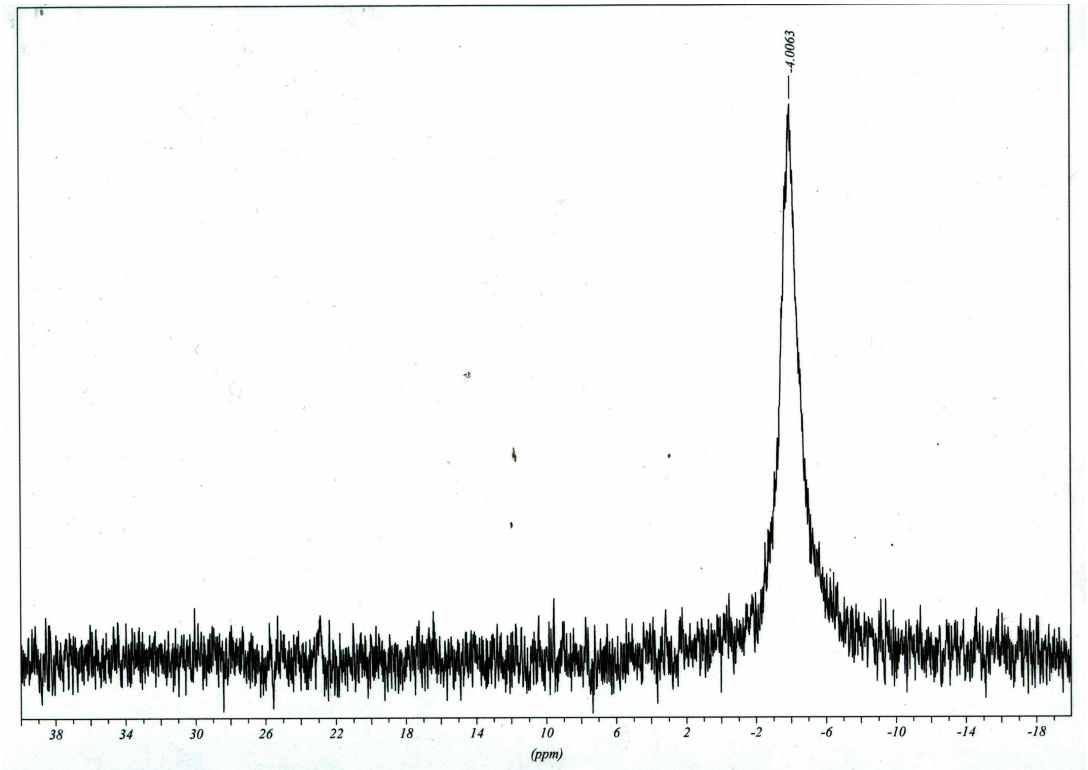

Figure 5.40 ^{31}P NMR signals of $CoCl_2(PPh_3)_2$.

Titration of the complex $CoCl_2(PPh_3)_2$ with PPh_3 resulted in an appearance of a new peak resonance at ~ + 30 ppm, which appeared only after addition of 15 equivalent moles of PPh_3 and increased with an increase in concentration of PPh_3. The peak at ~ – 4 ppm shifted to more negative resonance with an increase in concentration of PPh_3. The shift in peak position for a peak that appears downfield at ~ – 4 ppm to more negative resonance and the appearance of another peak up field at ~ + 30 ppm, indicates the formation of a free PPh_3 in solution. The NMR curves obtained during titration are presented in Appendix B 3 (Figure B.9 to B.12).

5.2 FERROCENE AS AN INTERNAL STANDARD FOR ELECTROCHEMICAL MEASUREMENTS

In this section we will focus on the electrochemical behaviour of cobalt compounds in the presence of added ferrocene as an internal standard. Ferrocene was chosen as it is oxidized reversibly with transfer of one-electron and because like cobalt it is a transition metal

compound. After the electrochemistry attributed to the compound of interest has been identified, ferrocene was added to the working compartment of the cell. The electrochemical experiment (a CV scan) was repeated, and the position of the CV peaks were directly compared to the potential of ferrocene. If ferrocene is used as an internal standard the reversible oxidation peaks of it must be observed at an appropriate position. It is also worth noting that the $Fe^{2+}Cp/Fe^{3+}Cp$ couple may be inappropriate as an internal standard for some systems due to overlapping signals. In these cases other compounds like cobaltocene or any of a variety of aromatic compounds, can be used as internal standards [77].

Employing a redox couple as an internal standard in electrochemical experiments can be compared to the use of internal standards in nuclear magnetic resonance spectroscopy. For example, in proton NMR spectroscopy tetramethylsilane is commonly used to reference chemical shifts of other protons but is sometimes replaced by chloroform or other materials to avoid overlapping signals. As with NMR standards, an ideal electrochemical internal standard should not interact with any species in solution [77]. Also comparing the CV curves of cobalt compounds and those of mixture of cobalt compounds and ferrocene, we should be able to detect from the spectra if we can distinguish the oxidation potentials of different metals present in the same solution. This experiment was performed in a mixture of acetonitrile and pentanol (1:1) containing 0.05 M $TBAPF_6$.

5.2.1 Investigations involving $CoCl_2(PPh_3)_2$, $CoCl_2$ and PPh_3.

In this sub-section we focussed on the analysis of the CV curves of $CoCl_2(PPh_3)_2$, $CoCl_2$ and PPh_3 in the presence of added ferrocene as an internal standard. Figure 5.41 presents a CV of $CoCl_2(PPh_3)_2$ before and after addition of equivalent concentration of ferrocene. CV of ferrocene in the same solvent mixture is also shown for reference. CV of $CoCl_2(PPh_3)_2$ reveals two oxidation peaks labelled 1(a) and 2(a) at E_p = 0.55 V and 1.0 V and one reduction peak labelled 3(a) at E_p = 0.80 V (Figure 5.41). Addition of an equivalent concentration of ferrocene resulted in an appearance of a reversible oxidation peak of ferrocene labelled peak 4(b) at E_p = 0.19 V. Oxidation peak 1(a) of $CoCl_2(PPh_3)_2$ shifted to more positive potentials and became broad (peak 1(b)). The oxidation peak 2(a) and reduction peak 3(a) disappeared. Comparison with the CV curve of ferrocene showed that the current of a reversible oxidation peak 4(c) of ferrocene became 2 times higher after

addition to $CoCl_2(PPh_3)_2$ (peak 4(b)). An increase in a reversible oxidation process of ferrocene and a disappearance of a chloride oxidation peak 2(a) might suggest that ferrocene is oxidizing chloride. The most interesting feature observed from the voltammogram was an appearance of another rather small, ill-defined reduction peak at less negative potentials of ~ – 0.10 V.

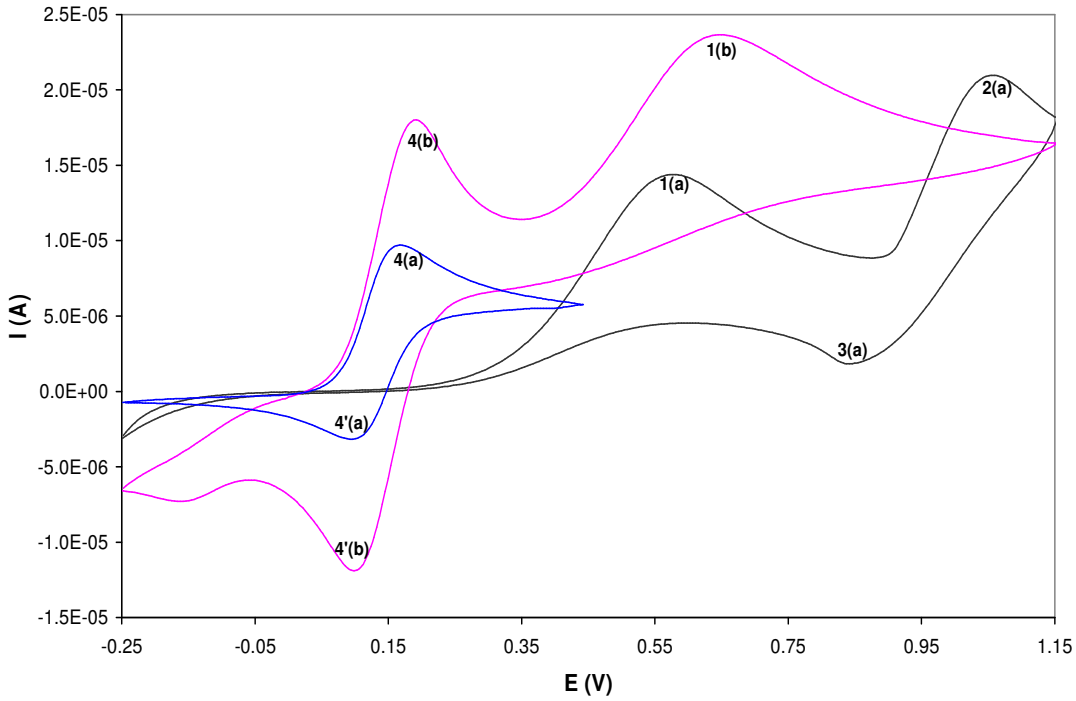

Figure 5.41 CV curve of a 2.0×10^{-3} mol/l $CoCl_2(PPh_3)_2$ before (—) and after (—) addition of an equivalent concentration of ferrocene as an internal standard. CV of a 2.0×10^{-3} mol/l ferrocene (—) is shown for reference.

To further verify the above observations, we analysed the CV curve of $CoCl_2$ before and after addition of an equivalent concentration of ferrocene (Figure 5.42). CV of $CoCl_2$ reveals one oxidation peak labelled 1(a) at E_p = 1.0 V and one reduction peak labelled 1'(a) at E_p = 0.65 V (Figure 5.42). Addition of an equivalent amount of ferrocene resulted in appearance of one broad oxidation peak 2(b) at E_p = 0.35 V and reduction peak 2'(b) at E_p = 0 V. The oxidation peak 1(a) and its coupled reduction peak 1'(a) for the oxidation of $CoCl_2$ disappeared. A new reduction peak was also observed at less negative potentials of ~ – 0.20 V. These results are similar to those observed from the CV of $CoCl_2(PPh_3)_2$ where oxidation peak 2 disappeared and a ferrocene oxidation peak current increased.

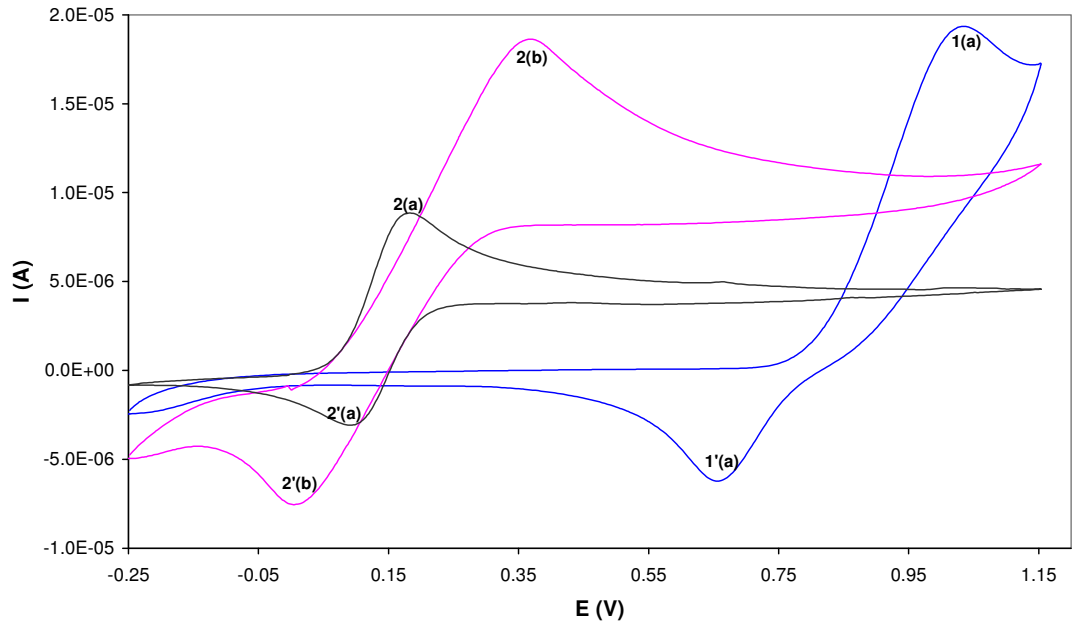

Figure 5.42 CV curve of a 2.0×10^{-3} mol/l $CoCl_2$ before (—) and after (—) addition of an equivalent concentration of ferrocene as an internal standard. CV of a 2.0×10^{-3} mol/l ferrocene (—) is shown for reference.

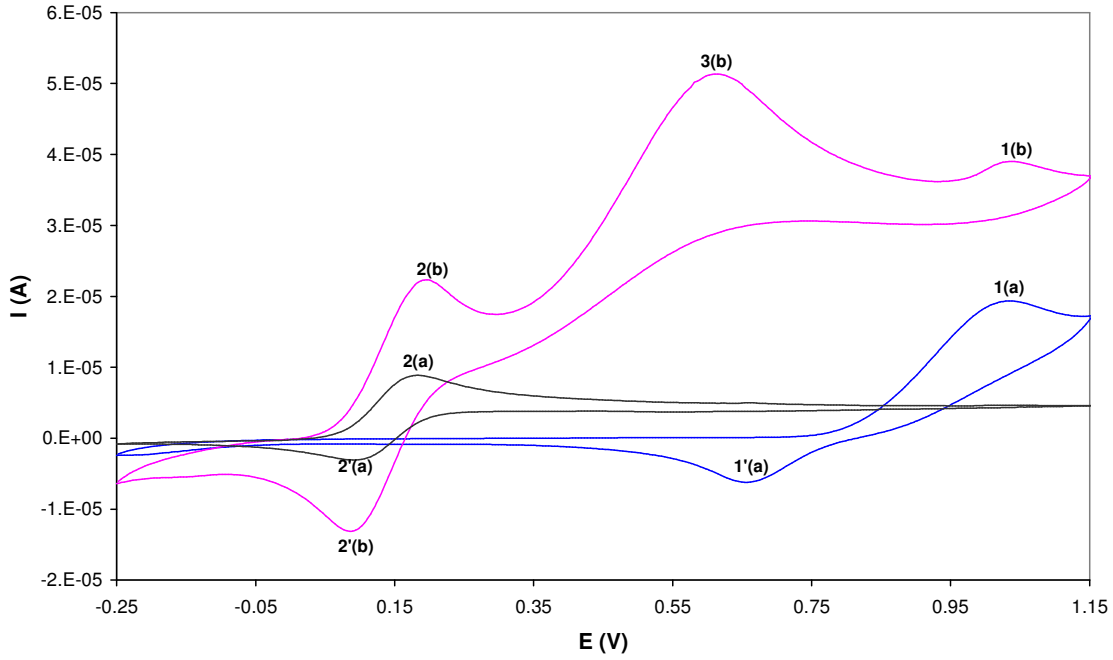

Figure 5.43 CV curve of a 2.0×10^{-3} mol/l $CoCl_2$ before (—) and after (—) addition of an equivalent concentration of ferrocene as an internal standard and 4.0×10^{-3} mol/l PPh_3. CV of a 2.0×10^{-3} mol/l ferrocene (—) is shown for reference.

This result verifies the assignment made above that ferrocene oxidize chloride resulting in formation of another species since the oxidation peak of ferrocene was also not observed. It appears that ferrocene can only oxidize chloride (the species oxidized at peak 2(a) Figure 5.41), but it cannot oxidize Co^{II} (a species oxidized at peak 1(a)) from the CV of $CoCl_2(PPh_3)_2$. To further confirm this two equivalent concentrations of PPh_3 were added to a solution containing both ferrocene and $CoCl_2$ (Figure 5.43).

It can be seen from Figure 5.43 that addition of two equivalent concentrations of PPh_3 resulted in a appearance of another irreversible oxidation peak of cobalt at E_p = 0.6 V due to the formation of a complex $CoCl_2(PPh_3)_2$. The oxidation peak 1(a) of $CoCl_2$ decreased tremendously in height and its reduction peak 1'(a) disappeared. Electrochemically oxidized ferrocene resulted in formation of redox couple $Fe^{2+}Cp_2/Fe^{3+}Cp_2$ that in turn oxidized chloride leading to a tremendous increase in height of the ferrocene peaks. This result supports the above conclusion that ferrocene oxidized chloride but did not oxidize Co^{II} from the complex.

In principle, the reversibility of the ferrocenium couple suggests that the ferrocenium ion can be used only with compounds with negative formal oxidation potentials [78]. Ferrocene has the ability to interact with other compounds and may catalyze electron-transfer reactions normally occurring at more positive potentials [78]. In such cases use of substituted ferrocenes with electron withdrawing substituents is permitted as potential mediators of the electron-transfer-catalyzed oxidation of compounds with $E_{1/2}$ more positive than 0.0 V. The substituted ferrocenium ions themselves need not be isolable, and a catalytic cycle would be sustained if the redox couple is reversible and its members are both inert to side reactions [78]. From this literature studies it appears that ferrocene caused catalyzed electron-transfer reactions of $CoCl_2(PPh_3)_2$ and $CoCl_2$ since these compounds in the absence of ferrocene are oxidized at more positive potentials.

To further confirm the conclusion that there is an interaction between ferrocene and the studied cobalt compounds, we analysed the CV of PPh_3, in the presence of added ferrocene since PPh_3 is also oxidized at more positive potentials. CV curve of PPh_3 before and after addition of an equivalent concentration of ferrocene is presented in Figure 5.44. CV of PPh_3 reveals one irreversible oxidation peak labelled 1(a) at E_p = 1.0 V (Figure 5.44). Addition of an equivalent concentration of ferrocene resulted in an appearance of a reversible oxidation

peak of ferrocene labelled peak 2(b) at E_p = 0.19 V, an irreversible oxidation peak 1(b) of PPh_3 remained at the same position and retained its current intensity. Surprisingly, peak currents of a reversible ferrocene couple increased by a factor of 2 after addition to PPh_3. Also a reduction peak observed at less negative potentials of – 0.10 V and – 0.20 V from the CV of $CoCl_2(PPh_3)_2$ and that of $CoCl_2$ was not observed from the CV of PPh_3 after addition of ferrocene. This suggests that a new reduction peak might be related to the reduction peak of chloride ion at 0.85 V for the complex $CoCl_2(PPh_3)_2$ and at 0.65 V for $CoCl_2$ since it disappeared after addition of ferrocene.

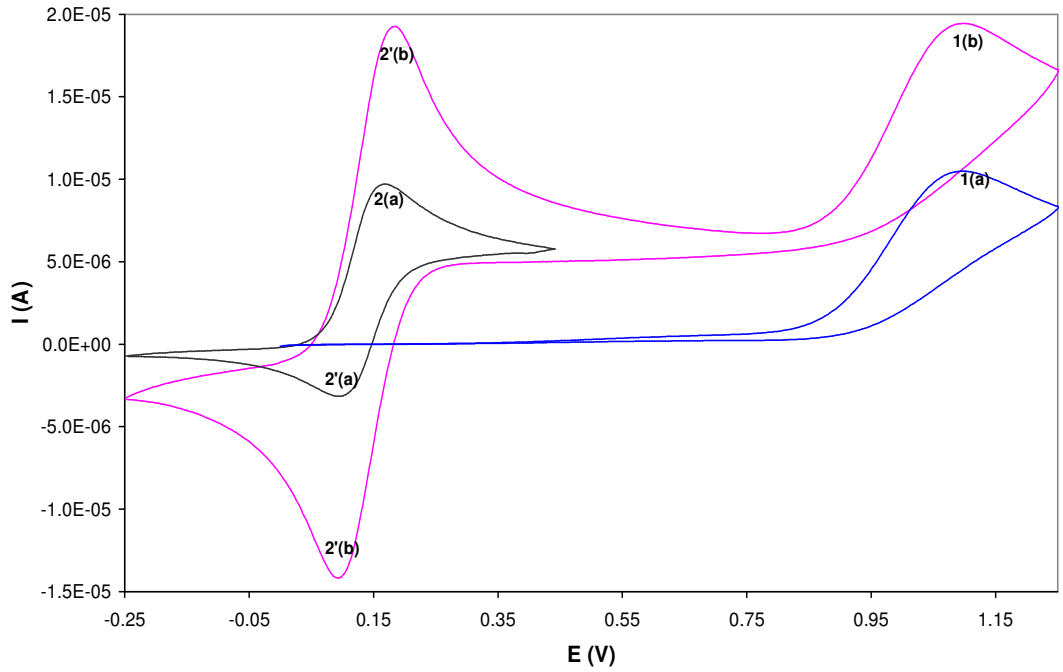

Figure 5.44 CV curve of a 2.0×10^{-3} mol/l PPh_3 before (—) and after (—) addition of an equivalent concentration of ferrocene as an internal standard. CV of a 2.0×10^{-3} mol/l ferrocene (—) is shown for reference.

From the above results we concluded that an increase in peak current of the ferrocene couple arisen due to interaction or catalytic reaction of ferrocene with $CoCl_2(PPh_3)_2$, $CoCl_2$ and PPh_3 since they are all oxidized at more positive potentials. And a disappearance of a chloride oxidation peak 2(a) and 1(a) from the complex $CoCl_2(PPh_3)_2$ and from $CoCl_2$ arisen because they were oxidized by ferrocene. Moreover, a disappearance of a reduction peak 3(a) and 1'(a) from $CoCl_2(PPh_3)_2$ and $CoCl_2$ and an appearance of new reduction peaks at less negative potentials might also be related to oxidation of chloride by ferrocene. This

then led to a shift in oxidation peak potentials to more positive and a shift in reduction peak potentials to less negative.

In order to verify that chloride is oxidized by ferrocene, we recorded the CV curves starting with ferrocene alone in solution and then adding an equivalent concentration of $CoCl_2(PPh_3)_2$ (Figure 5.45).

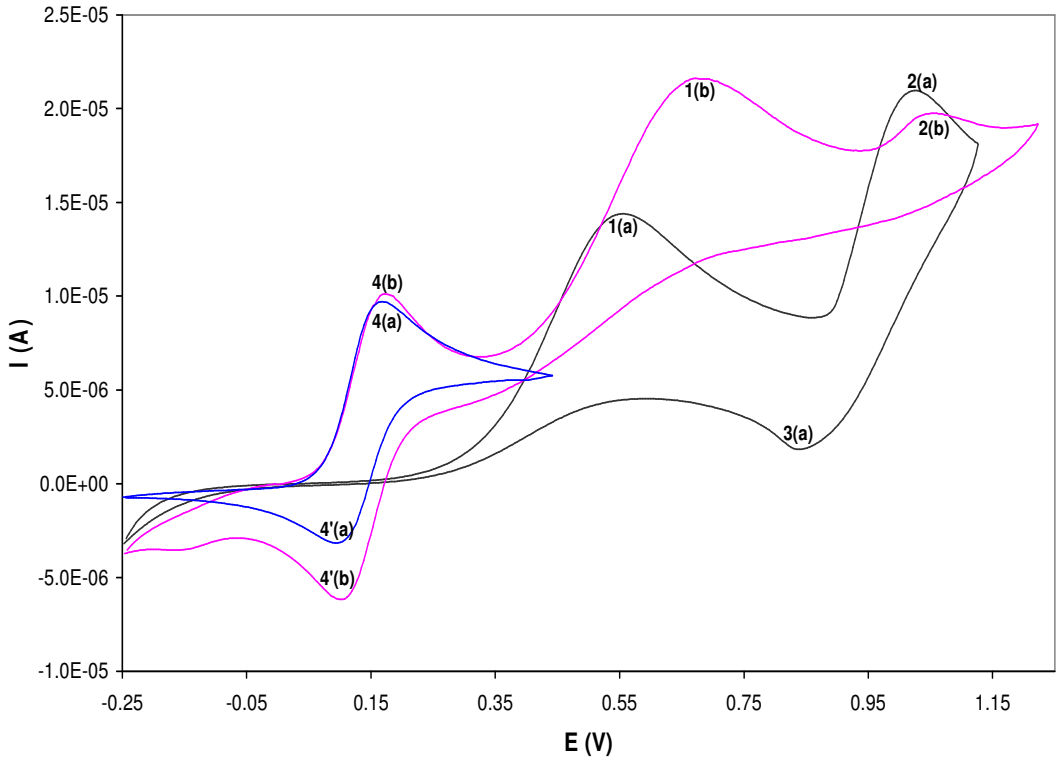

Figure 5.45 CV curve of a 2.0×10^{-3} mol/l ferrocene before (—) and after (—) addition of an equivalent concentration of $CoCl_2(PPh_3)_2$. CV of a 2.0×10^{-3} mol/l $CoCl_2(PPh_3)_2$ (—) is shown for reference.

If we start recording the CV with ferrocene in solution, and then add an equivalent concentration of $CoCl_2(PPh_3)_2$, peak 4(a) for the oxidation of ferrocene remains unchanged but the reduction peak 4'(a) slightly increases in current. Peak 1(a) shifted to more positive potentials as before but retained its shape and height. Peak 2(a) decreased tremendously in current and its coupled reduction peak 3(a) disappeared and a new reduction peak was observed at less positive potentials of ~ – 0.10 V. Before analysis of the above we performed a similar experiment using $CoCl_2$.

The same behaviour was observed from a CV of ferrocene after addition of $CoCl_2$ (Figure 5.46). No significant change was observed from the oxidation peak of ferrocene, whilst peak 1(a) for the chloride oxidation decreased tremendously to almost zero current and its coupled reduction peak 1'(a) disappeared. A new reduction peak was also observed at less negative potentials of ~ – 0.20 V.

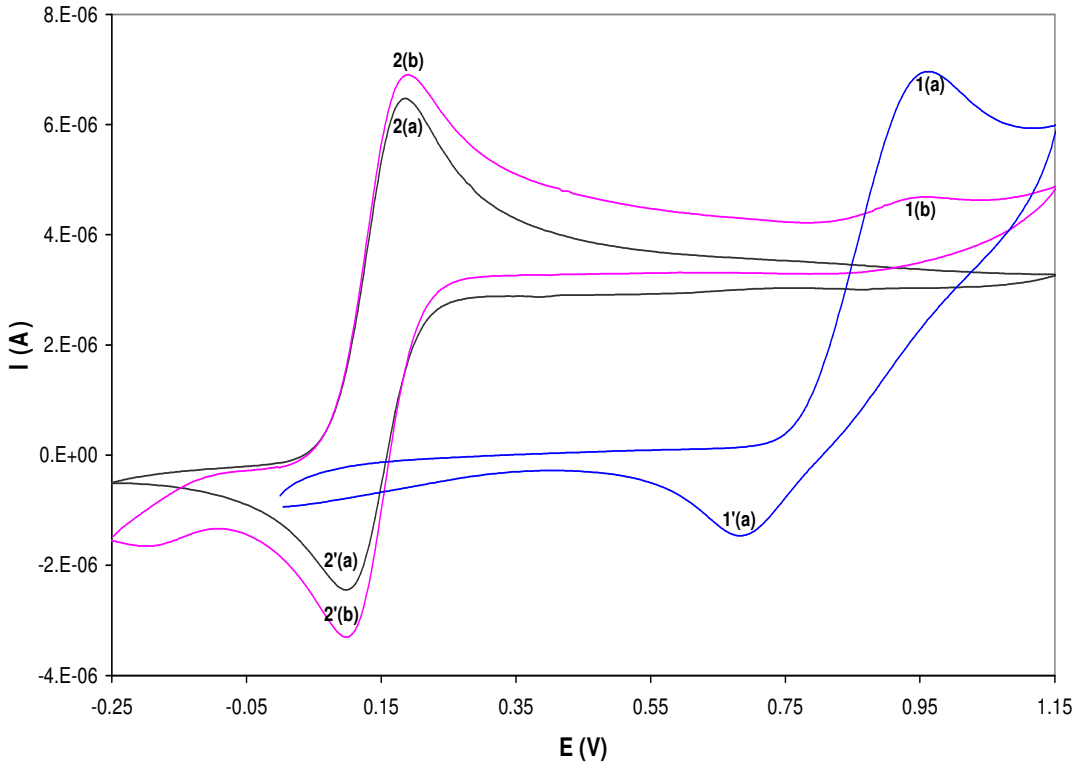

Figure 5.46 CV curve of a 7.7 × 10^{-4} mol/l ferrocene before (—) and after (—) addition of an equivalent concentration of $CoCl_2$. CV of a 7.7 × 10^{-4} mol/l $CoCl_2$ (—) is shown for reference.

Addition of 2 equivalent concentrations of $CoCl_2$ (Figure 5.47) resulted in an increase in peak current of an oxidation peak 1(a). The reduction peak 1'(a) is still absent and a new reduction peak at less negative potentials of ~ – 0.20 V increased in height. From these results we can conclude that ferrocene is capable of oxidizing chloride ion resulting in a shift in the chloride oxidation peak to less positive potentials. In conclusion, we cannot recommend the use of ferrocene as an internal standard for compounds containing chloride so one will have to choose other compounds like substituted ferrocene that can be used as internal standards that are inert to side reactions.

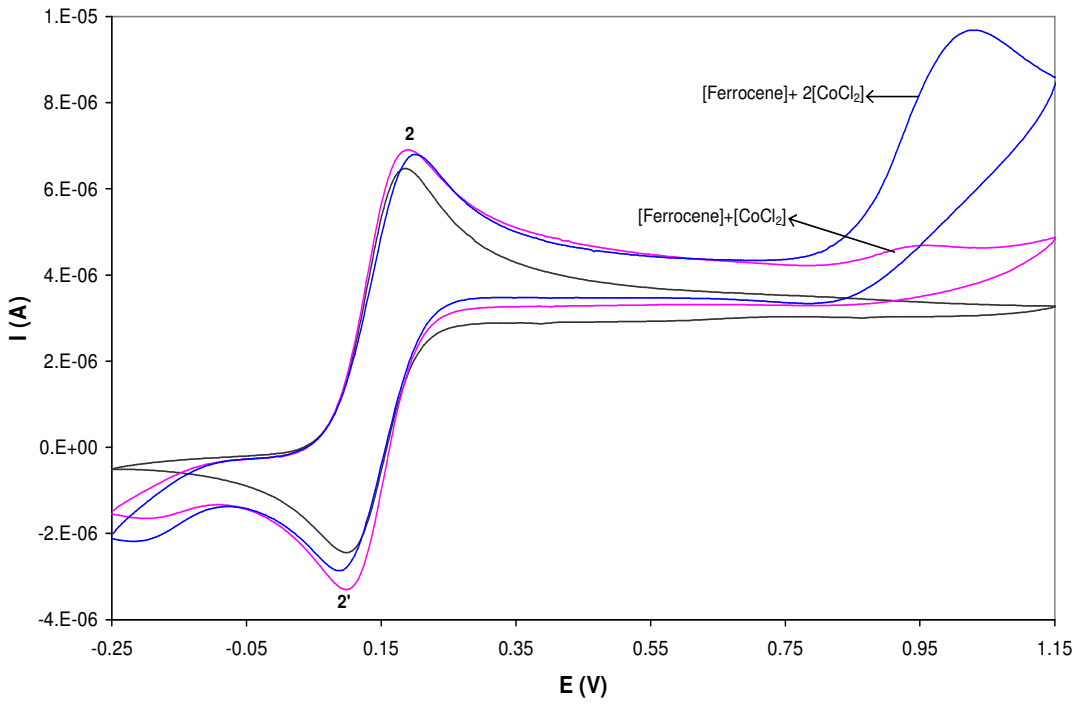

Figure 5.47 CV curve of a 7.7 × 10^{-4} mol/l ferrocene before and after addition of several concentrations of $CoCl_2$.

5.3 DETERMINATION OF PHYSICAL PARAMETERS USING CHRONOAMPEROMETRY

This subsection will focus on determination of the diffusion coefficient (D, in cm^2/s), electrochemical surface area (A, in cm^2) of the working electrode (WE) and number of electrons (n, in mol^{-1}) involved during oxidation of the studied cobalt compounds. Chronoamperometry has proven useful for the measurement of diffusion coefficients of electroactive species. An average value of $it^{1/2}$ over a range of time is determined at an electrode with an area which is accurately known and with a solution of known concentration. The diffusion coefficient can then be calculated from $it^{1/2}$ via the Cottrell equation. Although the electrode area can be physically measured, a common practice is to measure it electrochemically by performing the chronoamperometric experiment on a redox species whose diffusion coefficient is known (because a physically measured A does not take into account other factors like surface area roughness). The value of A is then calculated from $it^{1/2}$. Such an electrochemically measured surface area takes into account

any unusual surface geometry that may be difficult to measure geometrically [2]. The Cottrell equation is given as:

$$i_t = {nFACD^{1/2}}/{\pi^{1/2}t^{1/2}} \quad (5.3)$$

where C is a concentration of the electroactive species (mol/cm^3), F is the Faraday's constant (96485 A.s), i_t is a current at time t (A) and t is the time (s).

Ferrocene was used to measure the electrochemical surface area of the WE, since it is a well-studied reversible redox active species, which involves transfer of one-electron and its diffusion coefficient is known in many non-aqueous solvents. In this section we will first show the data obtained with ferrocene to determine the electrochemical surface area and the diffusion coefficient of ferrocene in a mixture of acetonitrile and pentanol. We will then use the electrochemically determined electrode area to determine the diffusion coefficient and number of electrons involved in the oxidation of the studied cobalt compounds.

Figure 5.48 presents the voltammograms of ferrocene obtained, in acetonitrile and in a mixture of acetonitrile and pentanol. CV was recorded first to determine the applied potentials that can be used in chronoamperometric experiments. A potential of 0.20 V was applied for ferrocene solutions in acetonitrile whilst 0.25 V was applied for ferrocene solutions in a mixture of acetonitrile and pentanol, the corresponding chronoamperometric plots are shown in Figure 5.49. And from these plots a current versus square root of time curve, known as a Cottrell plot, was constructed (Figure 5.50).

The slope was obtained using a linear regression analysis and was used to calculate the electrochemical surface area as follows:

$$i_t = {nFACD^{1/2}}/{\pi^{1/2}t^{1/2}}$$

Therefore, slope for Cottrell plot = $it^{1/2}$

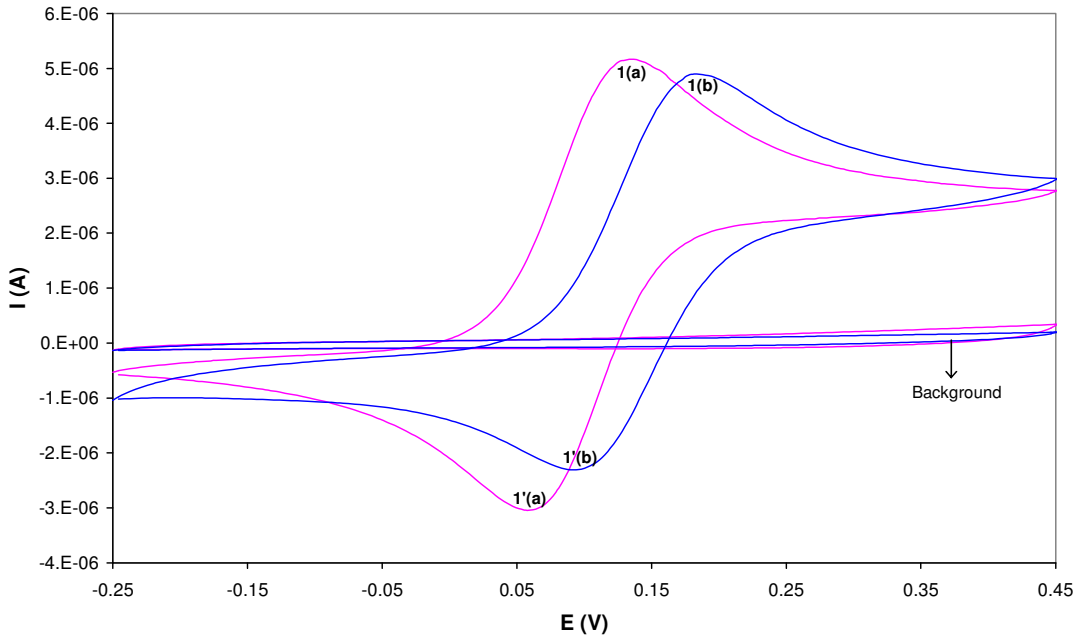

Figure 5.48 CV curves of ferrocene obtained in (—) acetonitrile and in (—) a mixture of acetonitrile and pentanol (1:1).

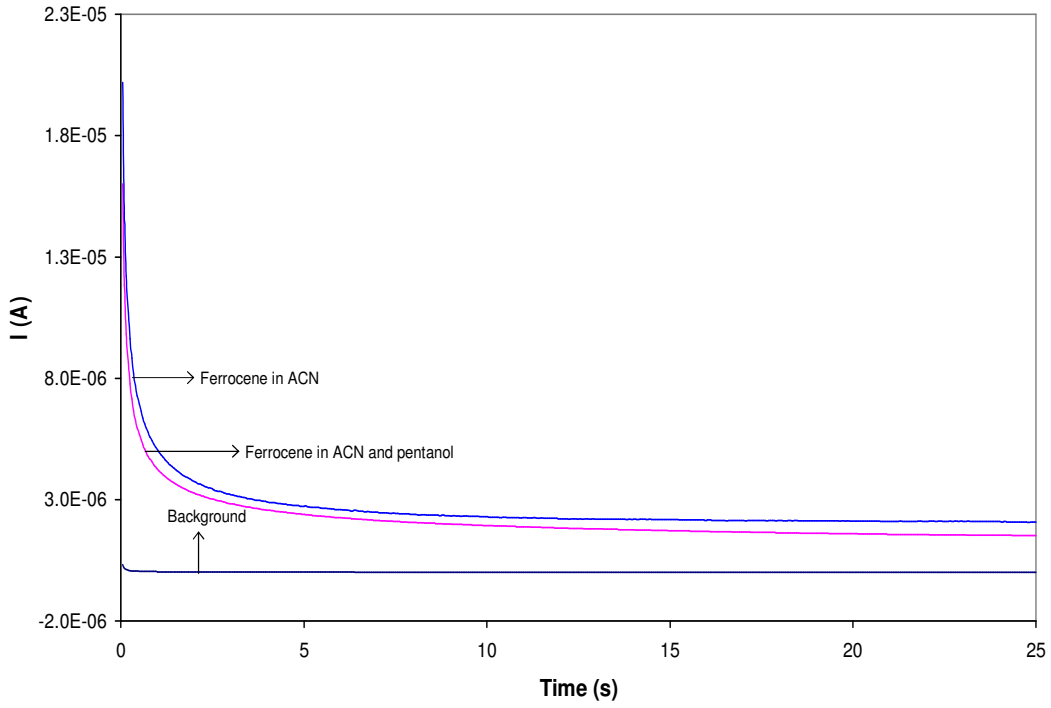

Figure 5.49 Chronoamperometric plots for Ferrocene obtained in acetonitrile ($E_{applied}$ = 0.2 V) and in a mixture of acetonitrile and pentanol ($E_{applied}$ = 0.25 V).

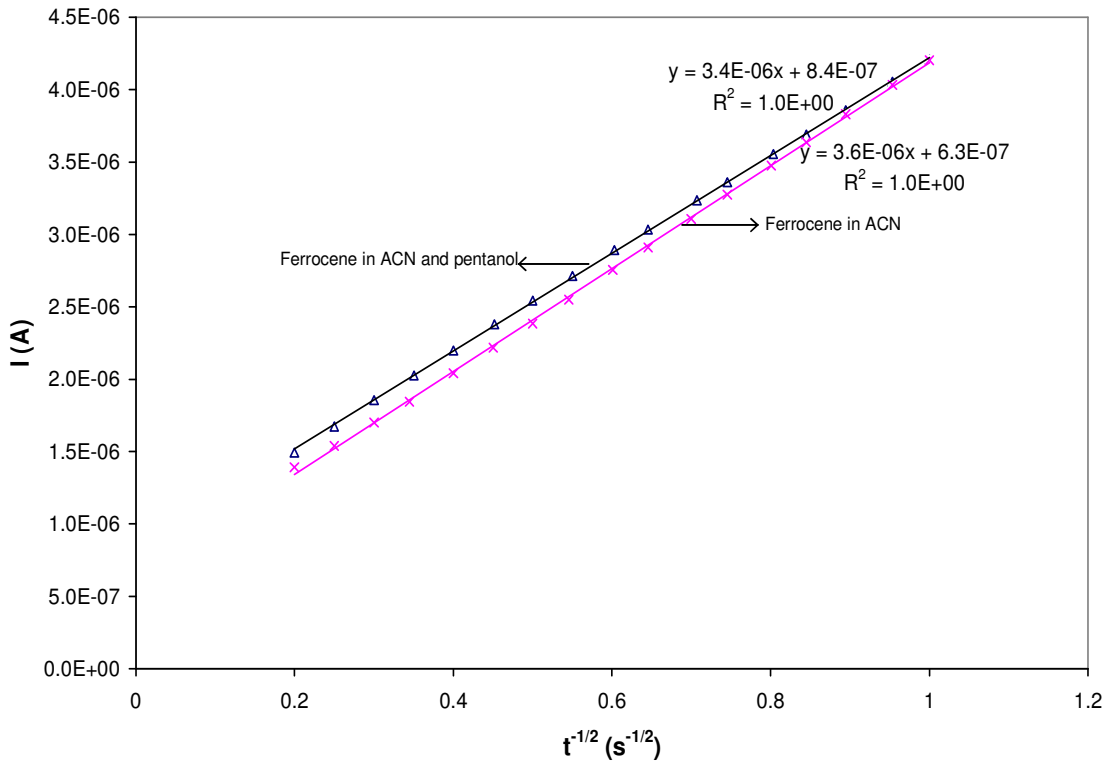

Figure 5.50 Cottrell plots obtained from data in Figure 5.49.

Hence, Slope = $nFAC(D/\pi)^{1/2}$

Area $= it^{1/2} / nFC(D/\pi)^{1/2}$

Slope $= 3.6 \times 10^{-6}$ A.s$^{1/2}$

D $= 2.37 \times 10^{-5}$ cm^2/s [63]

C $= 7.7 \times 10^{-7}$ mol/cm^3

F $= 96485$ A.s

n $= 1$ mol^{-1}

$$A = \left[3.6\times10^{-6}\ As^{1/2} \Big/ (1\ mol^{-1})(96485\ A.s)(7.7\times10^{-7}\ mol/cm^3)\left(\sqrt{2.37\times10^{-5}\ cm^2/s/\pi}\right) \right]$$

$$= 0.0176\ cm^2$$

We used the measured electrochemical surface area of the working electrode to determine the diffusion coefficient of ferrocene in a mixture of acetonitrile and pentanol. A current

versus time curve of ferrocene in a mixture of acetonitrile and pentanol is shown in Figure 5.49 and the corresponding Cottrell plot is shown in Figure 5.50. From the Cottrell plot a slope was found using a linear regression analysis. From the value of slope the diffusion coefficient was calculated as follows:

Slope = 3.4×10^{-6} A.s$^{1/2}$

$A = 0.0176$ cm^2

$C = 7.7 \times 10^{-7}$ mol/cm^3

$F = 96485$ A.s

$n = 1$ mol^{-1}

Slope = $nFAC(D/\pi)^{1/2}$

$$D^{1/2} = \left[3.4\times10^{-6}\ A.s^{1/2} \Big/ \left((1\ mol^{-1})(96485\ A.s)(0.0176\ cm^2)(7.7\times10^{-7}\ mol/cm^3)/\sqrt{\pi}\right)\right]$$

$$D = (4.61\times10^{-3}\ cm.s^{-1/2})^2$$

$$= 2.12\times10^{-5}\ cm^2/s$$

We attempted to determine the number of electrons involved during oxidation of cobalt (peak 1) from a CV of $CoCl_2(PPh_3)_2$. In order to do this a compound was required that had a diffusion coefficient very similar to $CoCl_2(PPh_3)_2$. $CoCl_2$ was chosen as it was found to be one of the products formed during oxidation of $CoCl_2(PPh_3)_2$ and was oxidized at peak 2. Studies involving reduction of cobalt bromides are well documented in the literature and one one-electron reduction peak was found to arise due to reduction of both Co^{II} and a bromide ligand [14]. In order to confirm that indeed oxidation of $CoCl_2$ involved transfer of one electron, we compared the slopes obtained from the Cottrell plots of $CoCl_2$ with that of ferrocene in acetonitrile. First we plotted a Cottrell curve of I vs. $t^{-1/2}$ and obtained the slope which was the best fit value of $it^{1/2}$. From the slope we calculated the value of D of $CoCl_2$ using the Cottrell equation.

A Chronoamperometric plot of $CoCl_2$ obtained applying a potential of 1.3 V is shown in Figure 5.51, with the corresponding CV curve shown as an insert. The corresponding Cottrell plot obtained from data in Figure 5.51 is shown in Figure 5.52.

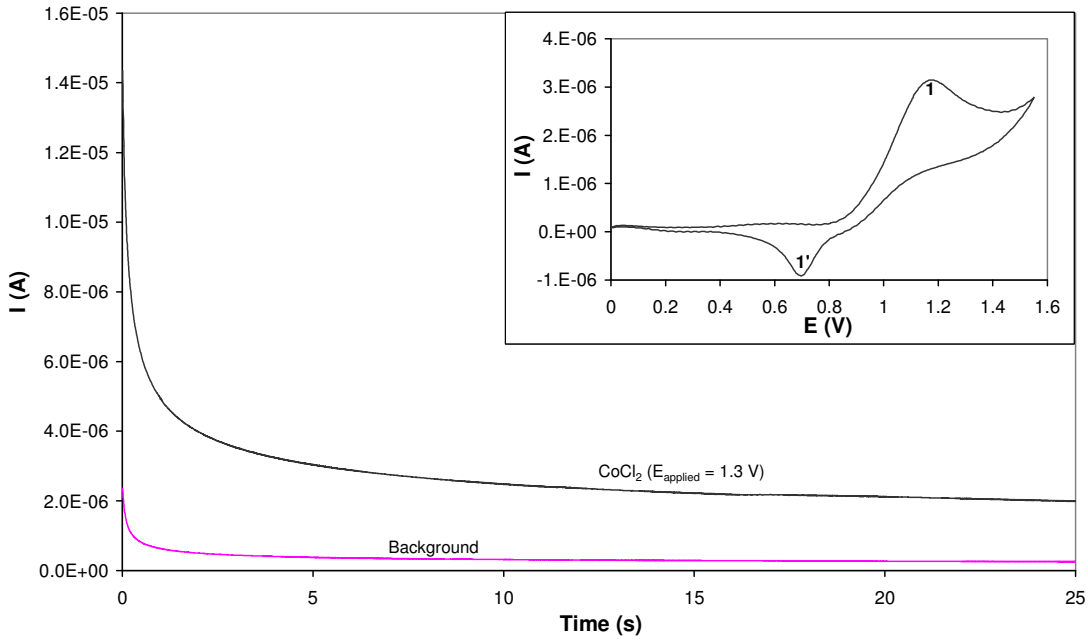

Figure 5.51 Chronoamperometric plot of $CoCl_2$ in acetonitrile. A CV curve of $CoCl_2$ is shown as an insert.

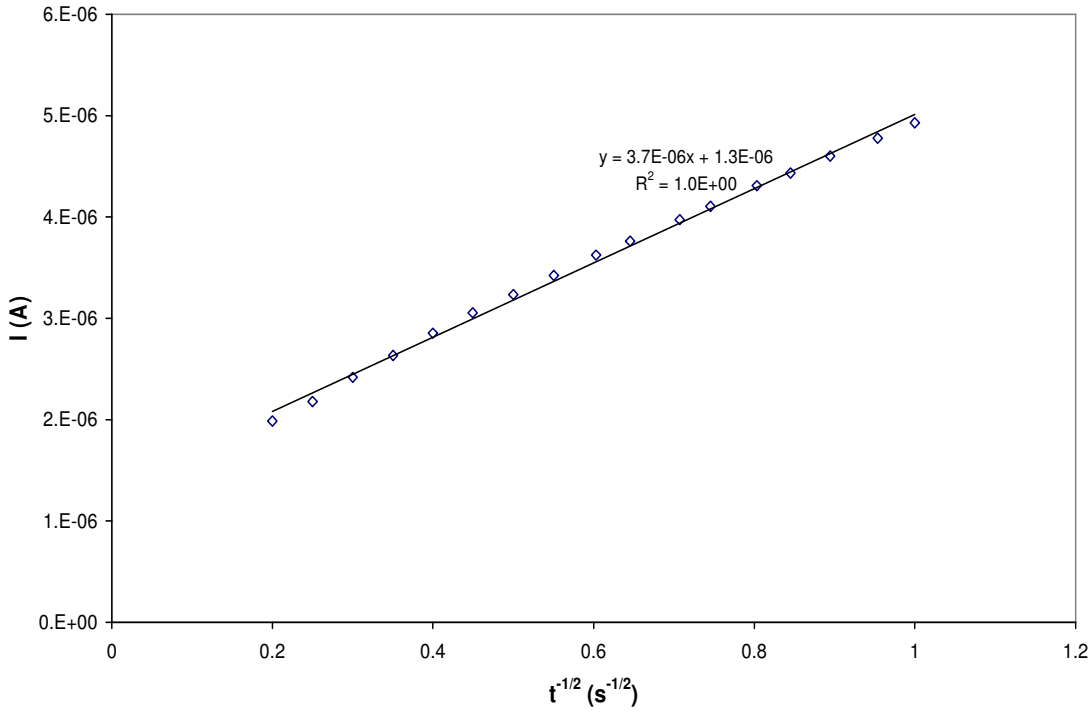

Figure 5.52 Cottrell plot obtained from data in Figure 5.51.

From a value of slope the diffusion coefficient was calculated as follows:

Slope = 3.7×10^{-6} A.s$^{1/2}$

$A = 0.0176$ cm^2

$C = 7.7 \times 10^{-7}$ mol/cm^3

$F = 96485$ A.s

$n = 1$ mol^{-1}

Slope = $nFAC(D/\pi)^{1/2}$

$$D^{1/2} = \left[3.7\times10^{-6}\ A.s^{1/2} \Big/ \left((1\ mol^{-1})(96485\ A.s)(0.0176\ cm^2)(7.7\times10^{-7}\ mol/cm^3)/\sqrt{\pi}\right)\right]$$

$$D = (5.01\times10^{-3}\ cm.s^{-1/2})^2$$

$$= 2.52\times10^{-5}\ cm^2/s$$

After obtaining a diffusion coefficient of $CoCl_2$, we plotted a Cottrell plot $i\pi^{1/2}/FACD^{1/2}$ vs. $t^{-1/2}$ in order to confirm the number of electrons involved during its oxidation (Figure 5.53).

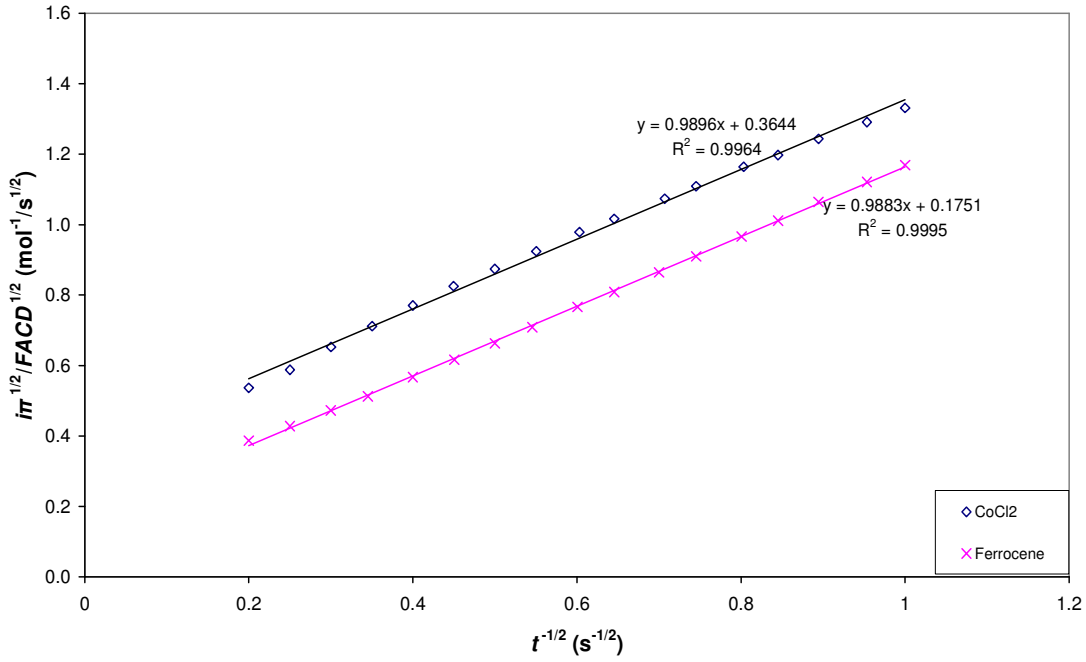

Figure 5.53 Data plotted as $i\pi^{1/2}/FACD^{1/2}$ vs. $t^{-1/2}$ for comparison of slopes obtained from ferrocene and $CoCl_2$ data in acetonitrile, for the determination of number of electrons.

From comparison of the slopes we immediately concluded that one electron was involved during oxidation of $CoCl_2$. The above experiment was repeated for $CoCl_2$ in a mixture of acetonitrile and pentanol. As we have done above we first determined a diffusion coefficient of $CoCl_2$ in a mixture of acetonitrile and pentanol. Figure 5.54 presents a typical current time response of $CoCl_2$ following a potential step from 0.4 to 1.0 V. CV of $CoCl_2$ is also shown as an insert in Figure 5.55. From this data, a Cottrell plot was constructed and the slope was determined using linear regression analysis (Figure 5.55) and was a best fit value of $it^{1/2}$.

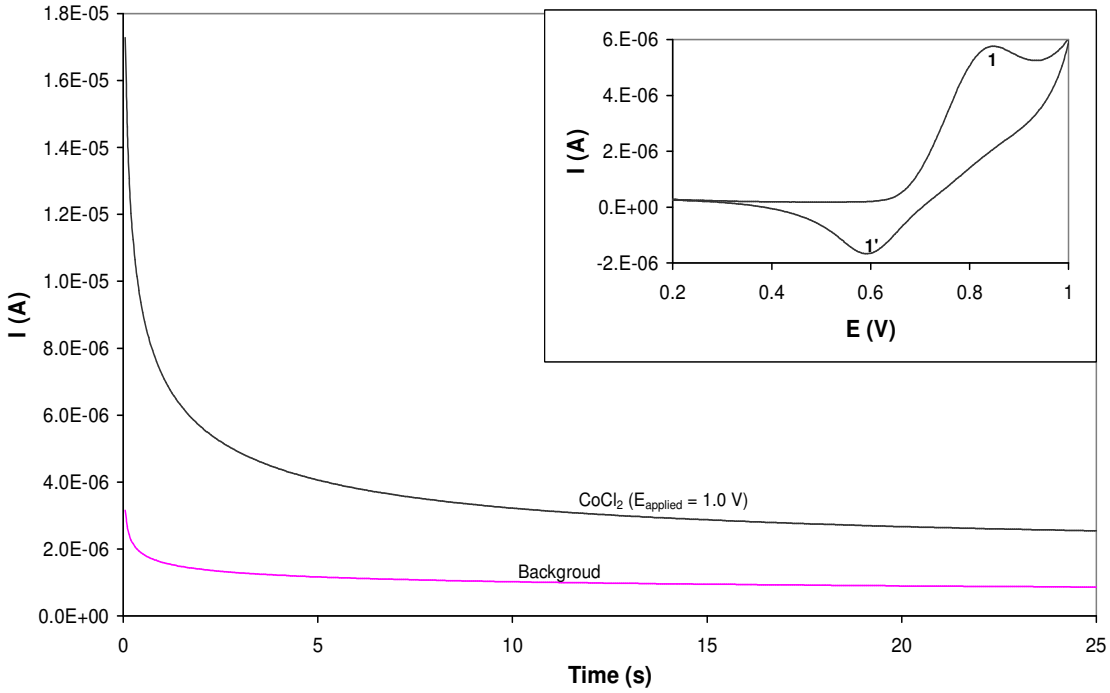

Figure 5.54 Chronoamperometric plot of $CoCl_2$ in a mixture of acetonitrile and pentanol (1:1). A CV curve of $CoCl_2$ is shown as an insert.

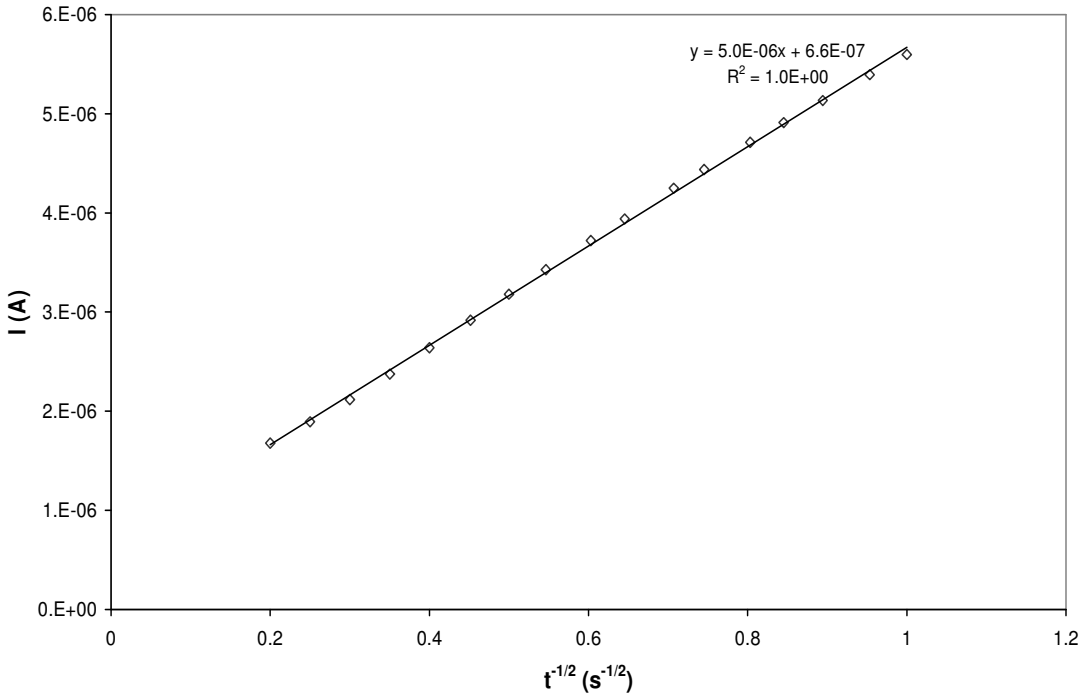

Figure 5.55 Cottrell plot obtained from data in Figure 5.54.

From the value of slope the diffusion coefficient of $CoCl_2$ in a mixture of acetonitrile and pentanol was calculated as follows:

Slope = 5.0×10^{-6} A.s$^{1/2}$

A = 0.0176 cm^2

C = 7.7×10^{-7} mol/cm^3

F = 96485 A.s

n = 1 mol^{-1}

Slope = $nFAC(D/\pi)^{1/2}$

$$D^{1/2} = \left(5.0\times10^{-6}\ A.s^{1/2} \Big/ (1mol^{-1})(96485A.s)(0.0176cm^2)(7.7\times10^{-7}\ mol/cm^3)/\sqrt{\pi} \right)$$

$$= 6.78\times10^{-3}\ cm.s^{-1/2}$$

$$D = (6.78\times10^{-3}\ cm.s^{-1/2})^2$$

$$= 4.59\times10^{-5}\ cm^2/s$$

After obtaining a diffusion coefficient of $CoCl_2$, we plotted a Cottrell plot of $i\pi^{1/2}/FACD^{1/2}$ vs. $t^{-1/2}$ in order to confirm the number of electrons involved during its oxidation (Figure 5.56).

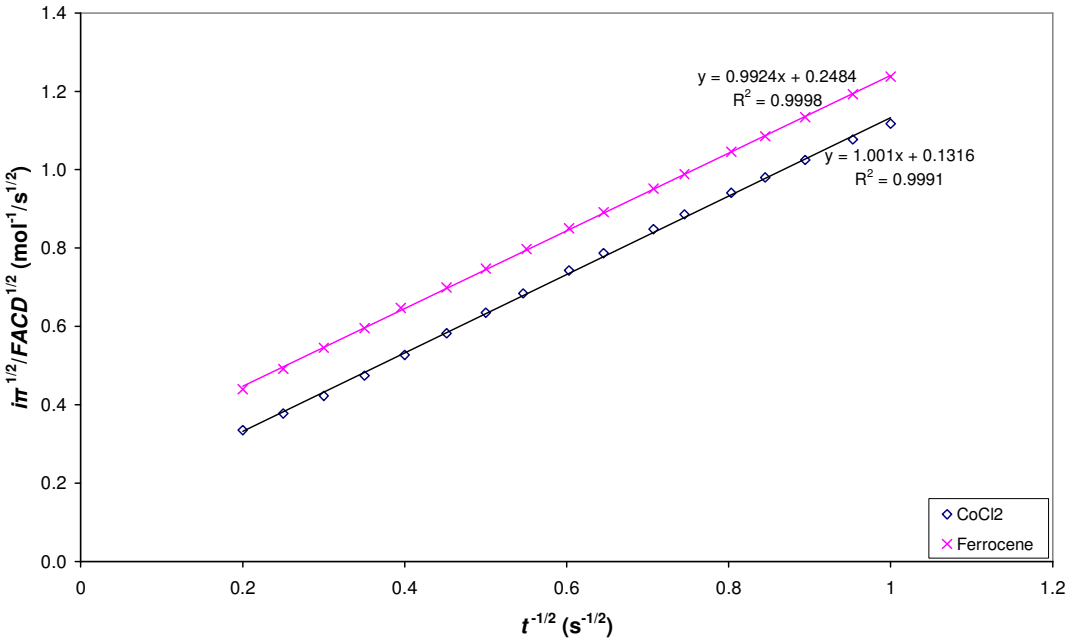

Figure 5.56 Data plotted as $i\pi^{1/2}/FACD^{1/2}$ vs. $t^{-1/2}$ for comparison of slopes obtained from ferrocene and $CoCl_2$ data in a mixture of acetonitrile and pentanol, for the determination of number of electrons.

From comparison of the slopes we immediately concluded that one electron was involved during oxidation of $CoCl_2$. But the slopes obtained from $CoCl_2$ in a mixture of acetonitrile and pentanol deviated a little from one when comparing it with that obtained in acetonitrile. This might have occurred due to involvement of an oxidation peak 2 for the catalytic reaction of chloride with water which complicates the electrode reaction; we applied a potential of 1.0 V and at this potential an increase in current was already observed as the catalytic reaction already starts at this potential. For best results one will have to apply a potential of ~ 0.9 V. The suggested overall electrochemical reaction is as follows:

$$CoCl_2 \leftrightarrow [CoCl]^{2+} + Cl^- + e^- \quad [79] \qquad (5.4)$$

In order to determine the number of electrons involved during oxidation of Co^{II} from $CoCl_2(PPh_3)_2$ we assumed that this complex had the same diffusion coefficient as $CoCl_2$. The number of electrons was determined from comparison of the slopes obtained from the Cottrell plot of $CoCl_2$ with that of $CoCl_2(PPh_3)_2$ in a mixture of acetonitrile and pentanol. A Chronoamperometric plot of $CoCl_2(PPh_3)_2$ is shown in Figure 5.57. In this experiment (refer to Figure 5.57), a potential was stepped abruptly from 0.2 V, where $CoCl_2(PPh_3)_2$ is

electroinactive, to 1.1 V a potential where both $CoCl_2(PPh_3)_2$ and $CoCl_2$ are oxidized concurrently. CV curve of $CoCl_2(PPh_3)_2$ is shown as an insert in Figure 5.57.

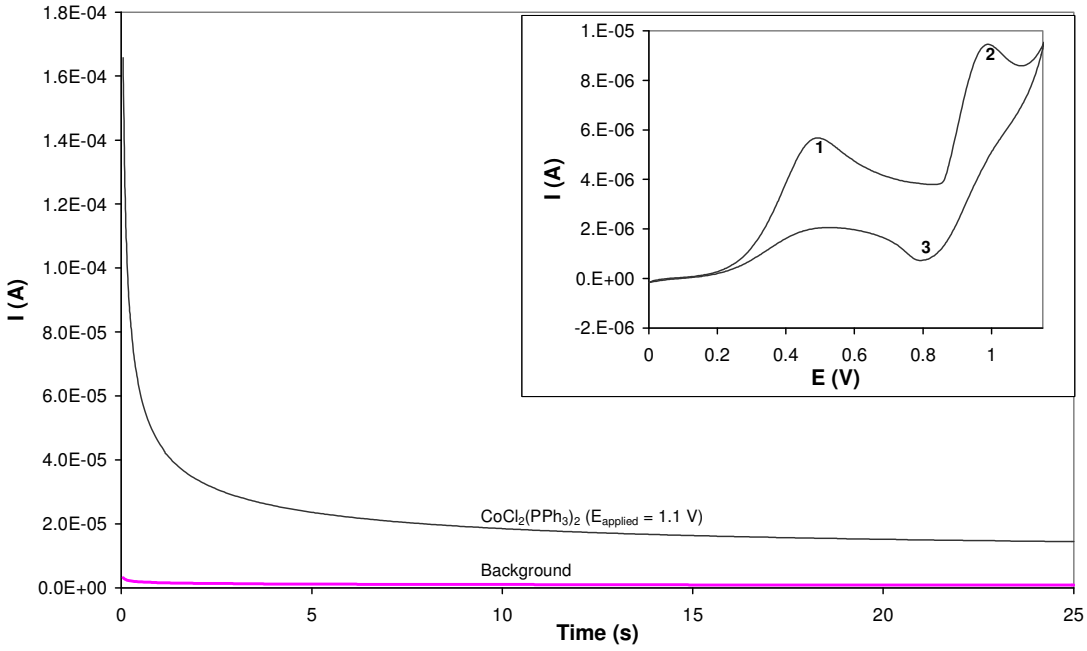

Figure 5.57 Chronoamperometric plot of $CoCl_2(PPh_3)_2$ in a mixture of acetonitrile and pentanol (1:1). A CV curve of $CoCl_2(PPh_3)_2$ is shown as an insert.

A Cottrell plot of $i\pi^{1/2}/FACD^{1/2}$ vs. $t^{-1/2}$ was constructed for the determination of number of electrons involved during oxidation of Co^{II} from $CoCl_2(PPh_3)_2$ (Figure 5.58). From Figure 5.58 we concluded that since a one-electron process from $CoCl_2$ gave a slope of 1.001 mol^{-1}, the corresponding slope of 2.0196 mol^{-1} for the oxidation of $CoCl_2(PPh_3)_2$ must represent an overall two-electron process. When we subtract the one electron that is required to oxidize $CoCl_2$ from this total, we immediately conclude that one electron is required to oxidize Co^{II} to Co^{III} in $CoCl_2(PPh_3)_2$ complex. A little deviation of slopes from one might be due to involvement of some catalytic or chemical reactions of the species oxidized after peak 2 (i.e. a catalytic reaction of chloride with water observed at peak 3 from the CV of the complex, Figure 5.10).

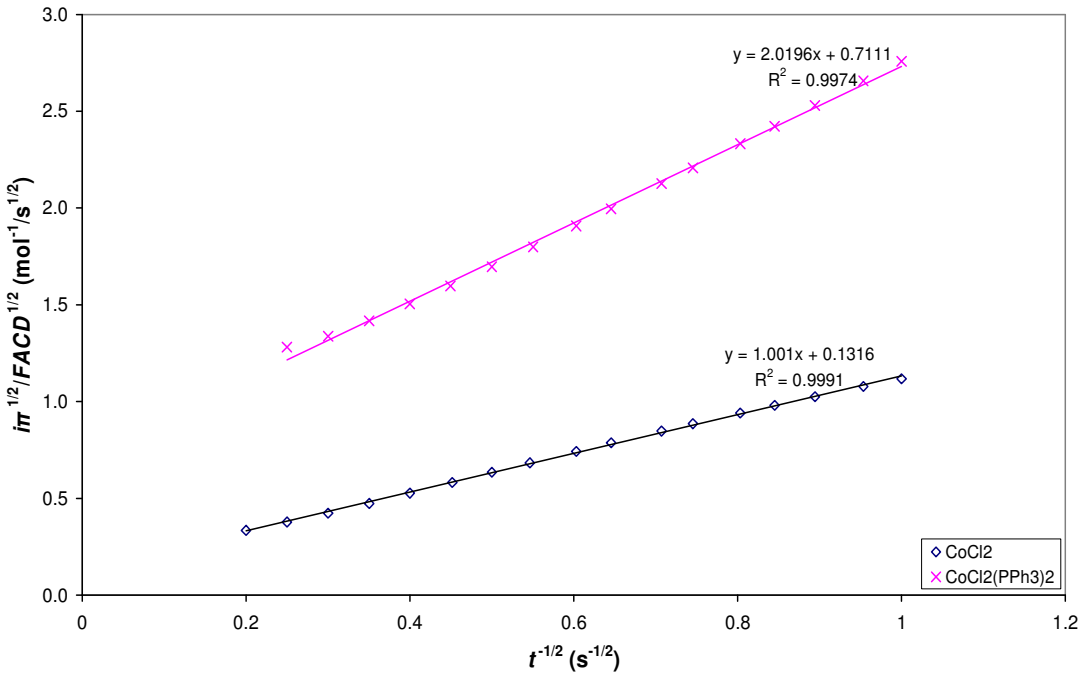

Figure 5.58 Cottrell plot of the data shown in Figure 5.57. The Cottrell plot for $CoCl_2$ is also shown for comparison.

The suggested overall electrochemical reactions are as follows:

Oxidation peak 1: $Co^{II}Cl_2(PPh_3)_2 \rightarrow [Co^{III}Cl_2(PPh_3)_2]^+ + e^-$ [this work] (5.5)

Oxidation peak 2: $CoCl_2 \leftrightarrow [CoCl]^{2+} + Cl^- + e^-$ [79] (5.6)

5.4 QUANTITATIVE ANALYSIS

In this section we will present the voltammograms obtained in solutions containing different concentrations of $CoCl_2(PPh_3)_2$ in a mixture of acetonitrile and pentanol, after IR drop correction (Figure 5.59) and the corresponding calibration plot was also constructed for quantitative analysis (Figure 5.60).

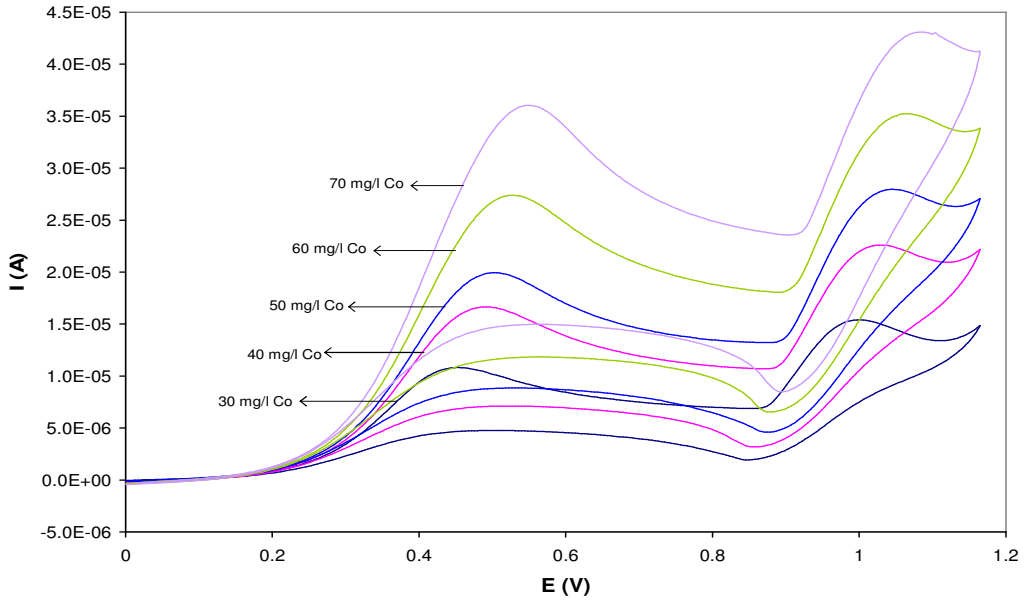

Figure 5.59 CV curves obtained in solutions containing different concentrations of Co from $CoCl_2(PPh_3)_2$.

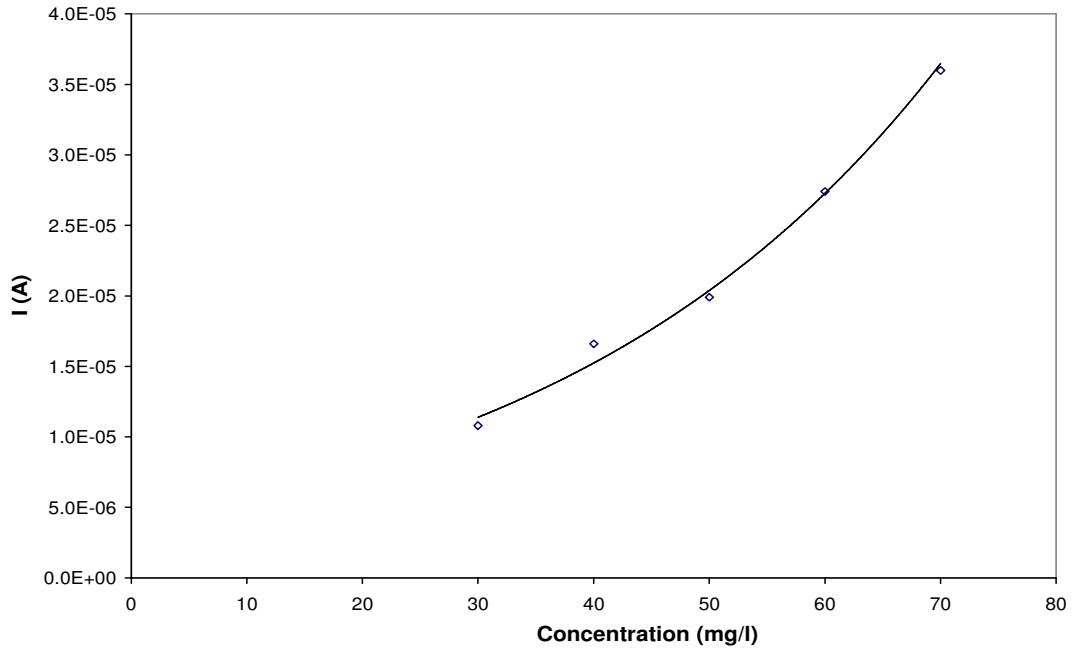

Figure 5.60 Calibration plot obtained using the oxidation peak at ~ 0.5 V shown in Figure 5.59.

The peak height increases with an increase in concentration, giving a non-linear relationship between current and concentration. The non-linearity might be due to the presence of complicated chemical reactions, occurring during oxidation of chloride occurring at E_p ~

0.95 V. For better quantitative analysis, we measured the voltammograms of $CoCl_2(PPh_3)_2$ scanning up to 0.9 V, to exclude the chloride oxidation peak observed at more positive potentials.

Figure 5.61 shows cyclic voltammograms of $CoCl_2(PPh_3)_2$ for the anodic peak obtained at ~ 0.50 V for various concentrations, when scanning to potential of 0.9 V, and the corresponding calibration plot is shown in Figure 5.62. The peak height increases with increase in concentration, giving a linear relationship between current and concentration. This proves that the non-linearity observed in Figure 5.60 was due to the presence of chloride oxidized at more positive potentials which complicated an electrode process occurring at E_p ~ 0.50 V.

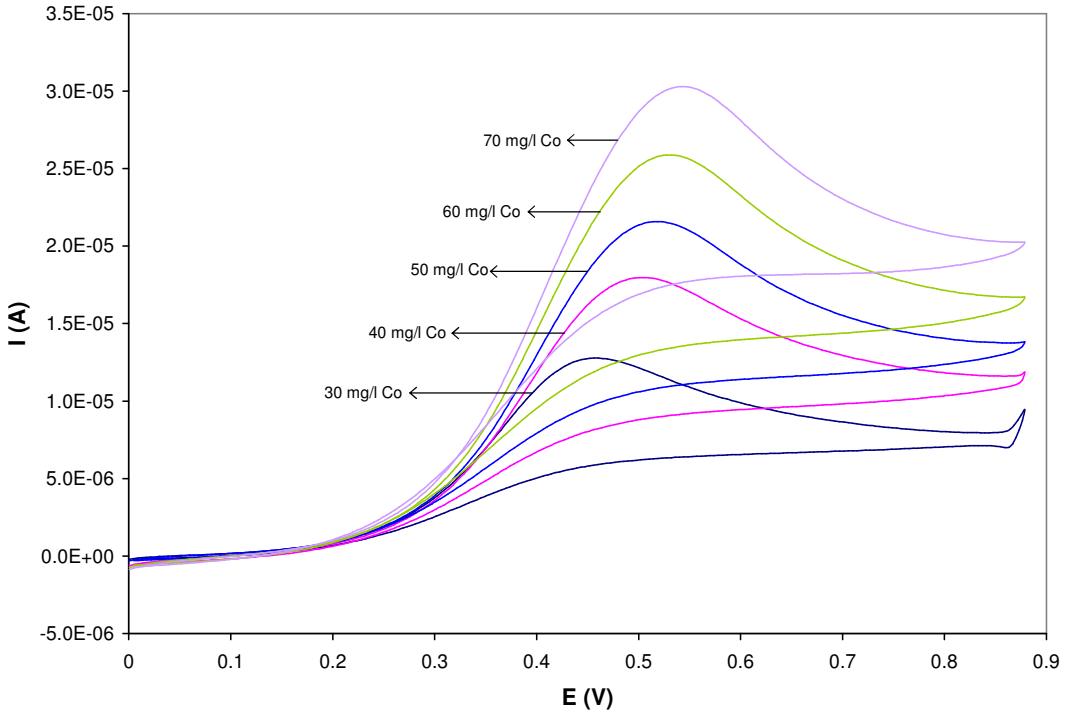

Figure 5.61 CV curves obtained in solutions containing different concentrations of Co from $CoCl_2(PPh_3)_2$ at a short potential range excluding the chloride oxidation peak.

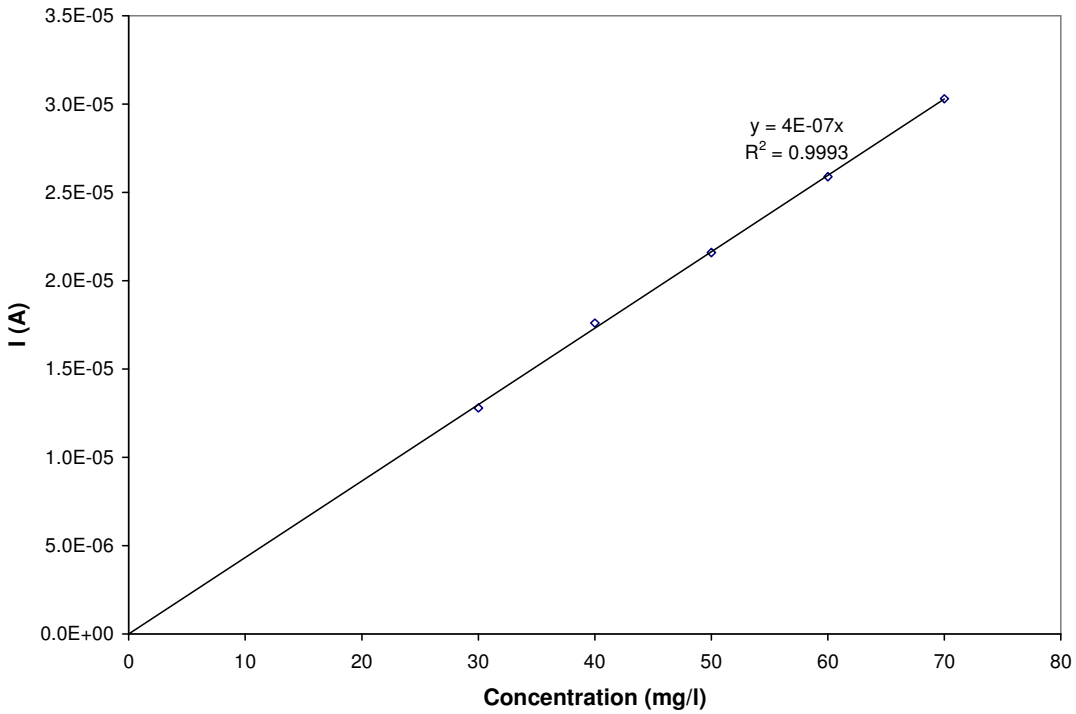

Figure 5.62 Calibration plot of the data shown in Figure 5.61.

In conclusion, chloride modifies the electrode surface resulting in a change in the chemistry of the compound which is evident from an exponential calibration plot observed for the metal oxidation peak when the CV was scanned to a potential after oxidation of chloride.

CHAPTER 6 CONCLUSIONS

In this chapter we will show how the research objectives stated in Chapter 1, were achieved. To facilitate this discussion a summary of the research aims and objectives will be provided prior conclusions of each Chapter or section.

6.1 Design of Flow-Through Cells and Development of Methodology to Correct for IR Voltage Drop Using an Open Cell.

The flow-through cells were successfully designed using different geometries to suit different applications. PEEK material was used for development of these cells since there was no negative influence of solvents used in this study on this material in a long term. Calibration of these flow-through cells using ferrocene was effective. High concentration of background electrolyte solution was recommended for minimizing the resistance. Since IR voltage drop depends on metal charges, it was found that IR cannot be the same for different compounds even if they were measured at the same experimental conditions.

6.2 Testing of the Three Flow-Through Cells.

The designed flow-through cells were tested using ferrocene as an electroactive species by varying the flow rate and scan rate during CV experiments.

- With all the three flow cells it was possible to choose the experimental conditions that favour convection/diffusion-controlled (polarogram-shaped) or diffusion-controlled (peak-shaped) voltammograms.
- With the flow–by electrochemical cell 1, processes were not controlled purely by convection, i.e. at slow scan rates of 50 mV/s and high flow rates of 1.52 ml/min; they were controlled by mixed mode (convection and diffusion). At slow scan rates of 50 mV/s and low flow rates of 0.46 ml/min, processes were controlled only by diffusion and result were very much similar to those obtained in the bulk solution in an open cell. Flow-by cell was by far more versatile as it can be used for fundamental, mechanistic, speciation, quantitative and qualitative studies performed on-line.

- With wall-jet cells all processes were controlled purely by convection at slow scan rates. Processes controlled by mixed-mode (convection and diffusion) were only achieved at high scan rates (~ 200 mV/s and above) and low flow rate (0.46 ml/min). A wall-jet cell was recommended for quantitative analysis as it generated a significantly higher analytical signal.
- On-line mixing proved to be a very convenient method to be used in quantitative analysis as one could prepare solutions of different concentrations on-line. This resulted in a linear relationship between peak current and concentration after IR voltage drop correction. A linear relationship was not achieved before IR voltage drop correction since the anodic peak potential shifted to more positive potentials with increase in analyte concentration. IR voltage drop correction played a major role since it resulted in anodic potentials which are independent of the analyte concentrations. It follows that one should redesign the cells to bring the reference electrode much closer to the working electrode to minimize IR drop and this can be achieved when using flow-by cell.

6.3 Electrochemical Behaviour of $CoCl_2(PPh_3)_2$ in a Mixture of Acetonitrile and Pentanol (1:1)

- Investigation of the influence of a kind of working electrode material used on recorded voltammograms.
  - Pt electrode demonstrated an electrochemical activity at E_p values above 1.2 V in this solvent mixture, which was attributed to oxygen evolution which arisen because there were traces of water present in background solvents leading to formation of PtO at the electrode surface.
  - GC showed no electrochemical activity in this solvent mixture at a studied potential range (from 0 to + 1.8 V). However, the activity of the GC WE could not be maintained for more than a few cycles in solutions containing $CoCl_2(PPh_3)_2$, $CoCl_2$ and TEACl. GC appeared to be an excellent WE to use for electrochemical studies in non-aqueous solutions containing traces of water since it had the largest available potential window in comparison to Pt WE. GC electrode appeared to be an excellent electrode for studying compounds in non-aqueous solutions containing water, as it gave a flat or small background current,

but because of the chloride present in the studied compounds it was difficult (or impossible) to study these compounds using this electrode. Moreover, GC WE can be recommended for monitoring of compounds that do not oxidize it, for example PPh_3.

- Gold electrode gave rise to an irreversible oxidation peak at E_p = 1.20 V in the solvent mixture, so it was immediately ruled out as a possible electrode material.
- Among the three electrodes investigated above, we decided to use Pt since it gave well-defined oxidation peaks of the complex, $CoCl_2(PPh_3)_2$ even in the presence of moisture in the solvents. Moisture could not be eliminated entirely from the system since we a simple distillation procedure was used for distillation of solvents and the curves were recorded in batch solutions open to air and moisture.

- Identification of the electrode processes observed from the voltammograms.
  - Cyclic Voltammetry indicated that the complex $Co^{II}Cl_2(PPh_3)_2$ can be oxidized into three different forms or stages, the first oxidation potential involving a metal oxidation Co^{II} to Co^{III}, and was followed by a chloride ligand oxidation at E_p = 0.95 V which was complicated by a catalytic reaction occurring after the electrode reaction causing a considerable diffusion current enhancement at E_p = 1.40 V.
  - Chloride is capable of binding to $CoCl(PPh_3)_3$ resulting in replacement of one PPh_3 ligand by a chloride ligand forming $CoCl_2(PPh_3)_2$. No further replacement of PPh_3 by chloride could occur which suggested that the complex $CoCl_2(PPh_3)_2$ was the most stable. This was seen from appearance of a new chloride oxidation peak at less positive potentials after addition of excess chloride.
  - CV showed that addition of excess PPh_3 resulted in depletion of chloride ions away from the WE surface leading to formation of an autocatalytic reaction. Addition of 30 equivalent concentration of PPh_3 resulted in appearance of an irreversible oxidation peak of free PPh_3. UV-Vis and ^{31}P NMR spectroscopy did not provide us with any further information since the absorption peaks of $CoCl_2(PPh_3)_2$ and that of PPh_3 were observed at almost the same position.
  - Chronoamperometry showed that one-electron is involved during oxidation of Co^{II} to Co^{III} (oxidation peak 1) and another one-electrons is involved during oxidation of a chloride ligand (peak 2) from the complex $CoCl_2(PPh_3)_2$.

- Ferrocene as a possible internal standard to be used during electrochemical measurements.
  - Use of ferrocene as an internal standard for compounds containing chloride cannot be recommended since ferrocene oxidized chloride ion. One will have to choose other compounds like substituted ferrocene that can be used as internal standards that are inert to side reactions.
- Determine a diffusion coefficient of ferrocene in a mixture of acetonitrile and pentanol (1:1).
  - The value of diffusion coefficient of ferrocene was found to be 2.12×10^{-5} cm^2/s.

REFERENCES

1. D. Astruc. *Electron Transfer and Radical Processes in Transition-Metal Chemistry*. VCH Publishers Inc. New York. (1995) 89.
2. P. T. Kissinger and W. R. Heineman. *Laboratory Techniques in Electroanalytical Chemistry*. Marcel Dekker, Inc. New York. (1984) 9 – 10; 27; 29; 42 – 43; 86 – 87.
3. R. W. Murray and C. N. Raillery. *Electroanalytical Principles*. Interscience. New York. (1963) 2145.
4. A. J. Bard and L. R. Faulkner. *Electrochemical Methods. Fundamentals and Applications*. John Wiley & Sons. 2nd Edition. (2001) 28 – 29; 475.
5. J. Heinze. *Angew. Chem. Int. Ed. Engl*. **32** (1993) 1268 – 1288.
6. A. J. Bard. *Encyclopedia of Electrochemistry of the Elements. Volume III. Co, Ni, P*. Marcel Dekker, Inc. New York. (1975) 153 – 154; 110.
7. H. Taube. *Chem. Rev*. **50** (1952) 69 – 126.
8. A. Wolberg and J. Manassen. *J. Am. Chem. Soc*. **92** (1970) 2982 – 2991.
9. D. K. Lavallee and M. J. Bain. *Inorg. Chem*. **15 (9)** (1976) 2090 – 2093.
10. K. M. Kadish, B. C. Han and A. Endo. *Inorg. Chem*. **30** (1992) 4502 – 4506.
11. F. D'Souza, A. Villard, E. Van Caemelbecke, M. Franzen, T. Boschi, P. Tagliasta and K. M. Kadish. *Inorg. Chem*. **32** (1993) 4042 – 4048.
12. K. M. Kadish, X. Q. Lin and B. C. Han. *Inorg. Chem*. **26** (1987) 4161 – 4167.
13. S. Fukuzumi, K. Miyamoto, T. Suenobu, E. Van Caemelbecke and K. M. Kadish. *J. Am. Chem. Soc*. **120** (1998) 2880 – 2889.
14. O. Buriez, C. Cannes, J-Y. Nédélee, and J. Périchon. *J. Electroanal. Chem*. **495** (2000) 57 – 61.
15. P. Gomes, O. Buriez, E. Labbé, C. Gosmini and J. Périchon. *J. Electroanal. Chem*. **562** (2004) 255 – 260.
16. K. M. Kadish, W. Koh, P. Tagliatesta, D. Sazou, R. Paolesse, S. Licoccia and T. Boschi. *Inorg. Chem*. **31** (1992) 2305 – 2313.
17. V. A. Adamian, F. D'Souza, S. Licoccia, M. L. Di Vona, E. Tassoni, R. Paolesse, T. Boschi and K.M. Kadish. *Inorg. Chem*. **34** (1995) 532 – 540.
18. K. Broadley and N.G. Connelly and W.E. Geiger. *J. Chem. Soc. Dalton Trans*. (1983) 121 – 125.
19. N. G. Connelly and J. D. Payne. *J. Chem. Soc. Dalton Trans*. (1983) 295 – 299.

20. E. Masahiro, L. Masami, M. Hiroaki and K. Takashi. *Inorg. Chimic. Acta*. **357** (2004) 1236 – 1242.
21. P. J Cameron, L. M Peter, S. M. Zakeeruddin, and M. Grätzel. *Coord. Chem. Rev.* **248** (2004) 1447 – 1453.
22. M. Arewgoda, P. H Rieger, B. H Robinson, J Simpson and S. V Visco. *J. Am. Chem. Soc*. **104** (1982) 5633 – 5640.
23. D. Osella, L. Milone, C. Nervi and M. Ravera. *J. Organomet. Chem*. **488** (1995) 1 – 7.
24. *Flow Injection Analysis: An Essay Review and Analytical Methods*. HMSO Books. London. (1990) 7.
25. M. Burguera, J. L. Burguera, D. Rivas, C. Rondón, P. Carrero, O. M. Alarcón, Y. P. de Peña, M. R. Brunetto, M. Gallignani, O. P. Márquez, and J. Márquez. *Talanta*. Article in Press. (2005).
26. E. Maestre, I. Katakis, A. Narváez, and E. Domínguez. *Biosensors and Bioelectronics*. Article in Press. (2005).
27. S. Jaenicke, R. M. Sabarathinam, B. Fleet, and H. Gunasingham. *Talanta*. **45** (1998) 703 – 711.
28. B. Haghighi, N. Maleki, and A. Safavi. *Microchemical Journal*. **57** (1997) 339 – 345.
29. P. Masawat, S. Liawruangrath, Y. Vaneesorn, and B. Liawruangrath. *Talanta*. **58** (2002) 1221 – 1234.
30. P. A Flowers and S-A Callender. *Anal. Chem*. **68**(1) (1996) 199 – 202.
31. A. Economou, A.K Clark and Fielden. *Analyst*. **126**(1) (2001) 109 – 113.
32. A. D. Modestov, J. Gun, I. Savotine and O. Lev. *J. Electroanal. Chem*. **565**(1) (2004) 7 – 19.
33. C. Colombo, C. M. G Van der Berg and A. Daniel. *Anal. Chimic. Acta*. **346** (1997) 101 – 111.
34. J. Janata and J. Růžička. *Anal. Chimic. Acta*. **139** (1982) 105 – 115.
35. J. Janata, N. Thorgersen and J. Růžička. *Anal. Chem*. **55** (1983) 1986 – 1988.
36. D. Astruc. *Chem. Rev*. **88** (1988) 1189 – 1216.
37. S. W. Feldberg and L. Jeftic. *J. Phys. Chem*. **76** (1972) 2439 – 2446.
38. M–H Delville. *Inorg. Chim. Acta*. **291** (1999) 1 – 19.
39. J. W. Hershberger, R. J. Klingler and J. K. Kochi. *J. Am. Chem. Soc*. **105** (1983) 61 – 73.

40. J. W. Hershberger, C. Amatore and J. K. Kochi. *J. Organomet. Chem*. **250** (1983) 345 – 371.
41. J. W. Hershberger and J. K. Kochi. *J. Am. Chem. Soc. Chem. Commun.* (1988) 472.
42. J. W. Hershberger, R. J. Klingler and J. K. Kochi. *J. Am. Chem. Soc*. **104** (1982) 3034 – 3043.
43. Z. Liu and S. L. Gipson. *J. Organomet. Chem*. **553** (1998) 269 – 275.
44. O. N. Efimov and V. V. Strelets. *Coord. Chem. Rev*. **99** (1990) 15 – 53.
45. Y. Rollin, M. Troupel, G. Meyer and J. Perichon. *J. Electroanal. Chem*. **183** (1985) 247 – 260.
46. G. Bontempelli, S. Daniele and M. Fiorani. *J. Electroanal. Chem*. **160** (1984) 249 – 260.
47. G. Zotti and S. Zecchin. *J. Electroanal. Chem*. **175** (1984) 241 – 250.
48. I. Cukrowski. Unpublished Work.
49. J. Heinze. *Angew. Chem. Int. Ed. Engl.* **23** (1984) 831 – 847.
50. P. R. Unwin. *Encyclopedia of Electrochemistry. Instrumentation and Electroanalytical Chemistry*. **3** (2003). Wiley–VCH. Weinheim. 91; 90; 93.
51. C. H. Hamann, A. Hamnett, W. Vielstich. *Electrochemistry*. Wiley-VCH. Weinheim. New York. (1998) 224 – 226; 234 – 23.
52. D. K. Gosser, Jr. *Cyclic Voltammetry Simulation and Analysis of Reaction Mechanisms*. (1993) 75.
53. J. Obirai and T. Nyokong. *Electrochim. Acta*. **50** (2005) 5427 – 5434.
54. B. Karlberg and G. E. Pacey. *Flow Injection Analysis: A Practical Guide.* Elsevier Science Publishers B. V. Oxford. New York. (1989) 1.
55. J. Růžička and E. H. Hansen. *Flow Injection Analysis*. 2nd Edition. **62** (1988) 2.
56. J. M. Calatayud. *Flow Injection Analysis of Pharmaceuticals: Automation in the Laboratory*. Taylor & Francis. London. (1996) 7 – 8.
57. M. Vulcárcel and M. D. Luque de Castro. *Flow–Injection Analysis: Principles and Applications*. Ellis Horwood Limited. England. (1987) 56 – 60.
58. N. Thorgersen; J. Janata and J. Růžička. *Anal. Chem*. **55** (1983) 1986 – 1988.
59. P. Masawat, S. Liawruangrath, Y. Vaneesorn and B. Liawruangrath. *Talanta*. **58** (2002) 1221 – 1234.
60. H-Y Chen and Y-T Long. *Anal. Chimic. Acta*. **382** (1999) 171 – 177.
61. F. A. Cotton, O. D. Faut, D. M. L. Goodgame and R. H. Holm. *J. Am. Chem. Soc*. **83** (1961) 1780 – 1785.

62. S. Kamiya. *Synthesis of Organometallic Compounds. A Practical Guide*. John Wiley and Sons. New York. (1997) 226 – 227.
63. S. A. Jacob, Qi Hong, B. A. Coles, and R. G. Compton. *J. Phys. Chem*. B. **103** (1999) 2963 – 2969.
64. A. M. Bond, K. B. Oldham and G. A. Snook. *Anal. Chem*. **72** (2000) 3492 – 3496.
65. S. H. Hong, C. Kraiya, M. W. Lehmann and D. H. Evans. *Anal. Chem*. **72** (2000) 454 – 458.
66. V. Gold. *Advances in Physical Organic Chemistry*. Academic Press. London. **12** (1976) 2 – 111.
67. I. M. Kolthoff and J. F. Coetzee. *J. Am. Chem. Soc*. **79** (1957) 1852 – 1858.
68. I. V. Nelson and R. T. Iwamoto. *J. Electroanal. Chem*. **7** (1964) 218 – 221.
69. V. Vojinovic, S. Mentus and V. Komnenic. *J. Electroanal. Chem*. **547** (2003) 109 – 113.
70. H. E. Zittel and F. J. Miller. *Anal. Chim. Acta*. **37** (1967) 141 – 150.
71. L. Sereno, V. A. Macagno and M.C. Giordano. *Electrochim. Acta*. **17** (1972) 561 – 575.
72. J. A. Switzer, J. F. Endicott, M. A. Khalifa, F. P. Rotzinger, and K. Kumar. *J. Am. Chem. Soc*., **105** (1983) 61 – 73.
73. R. F. Hudson. *Organic Chemistry. A Series of Monographs.* Academic Press. London. **6** (1965) 24 – 25.
74. K. S. V. Santhanam and Allen J. Bard. *J. Am. Chem. Soc*, **90** (1968), 1118 – 1122.
75. A. Ciana and C. Furlani. *Electrochim. Acta*. **10** (1965) 1149 – 1159.
76. E. Stulz, M. Maue, N. Feeder, S. J. Teat, Yiu-Fai Ng, A. D. Bond, S. L. Darling and J. K. M. Sanders. *Inorg. Chem.*, **41** (2002) 5269 – 5275.
77. R. R. Gagne, C. A. Koval and G. C. Lisensky. *Inorg. Chem*. **19** (1980) 2855 – 2857.
78. N. G. Connelly and W. E. Geiger. *Chem. Rev*. **96** (1996) 877 – 910.
79. W. C. Trogler. *Organometallic Radical Processes*. Elsevier. New York. (1990) 149.

APPENDICES

APPENDIX A: Presented here are the CV curves of a 50 mg/l Ferrocene in acetonitrile before and after IR drop correction obtained at various scan rates.

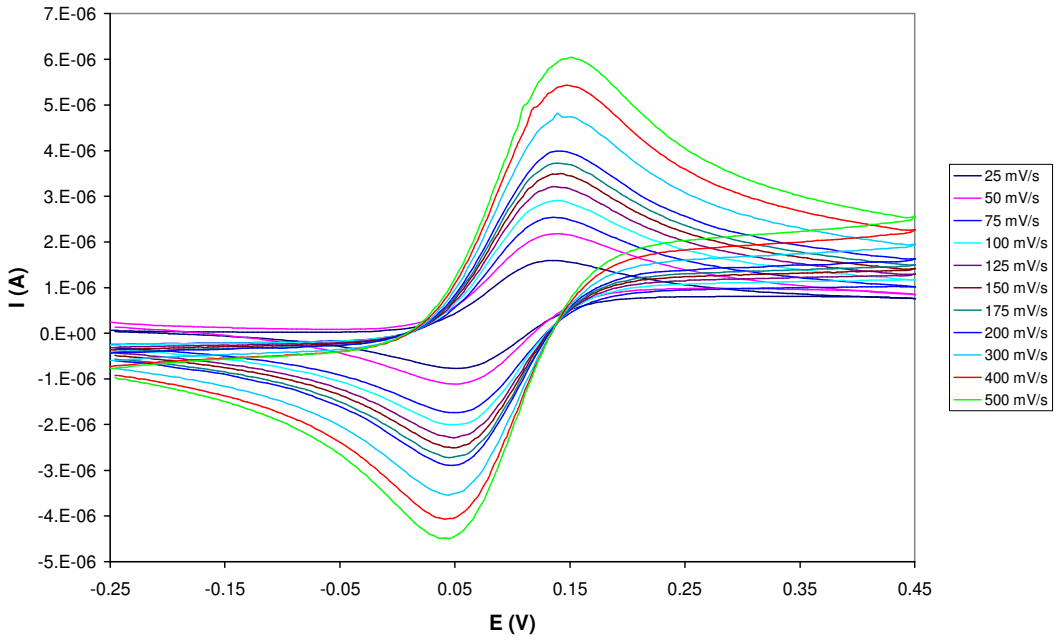

Figure A.1 CV curve of ferrocene in solution containing 0.01 M TBAHFP.

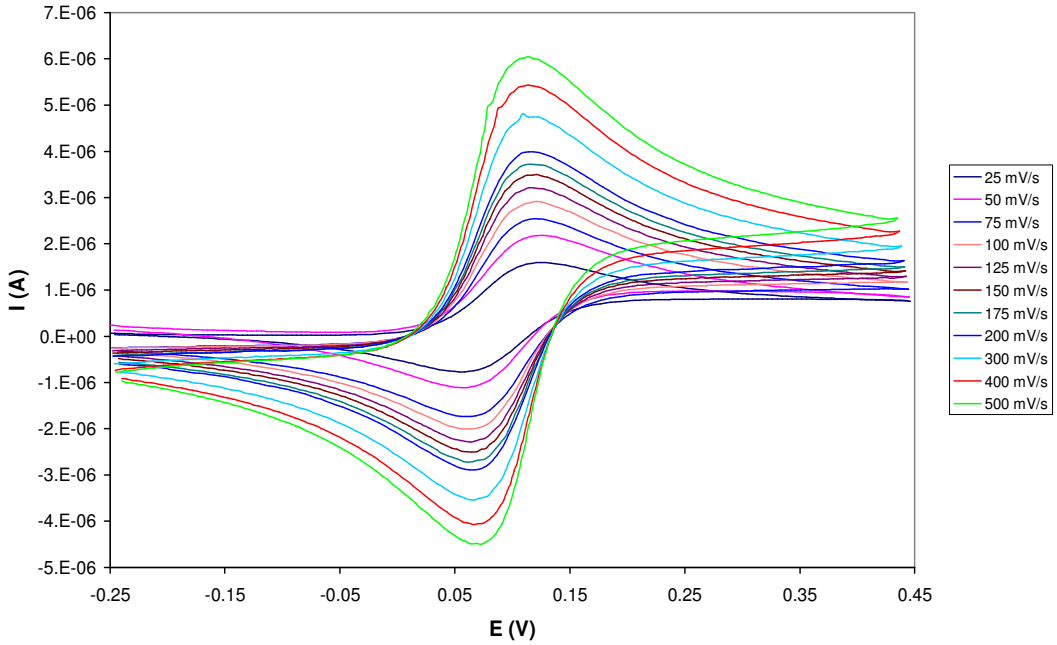

Figure A.2 CV curves of ferrocene from data in Figure A.1 after IR drop correction.

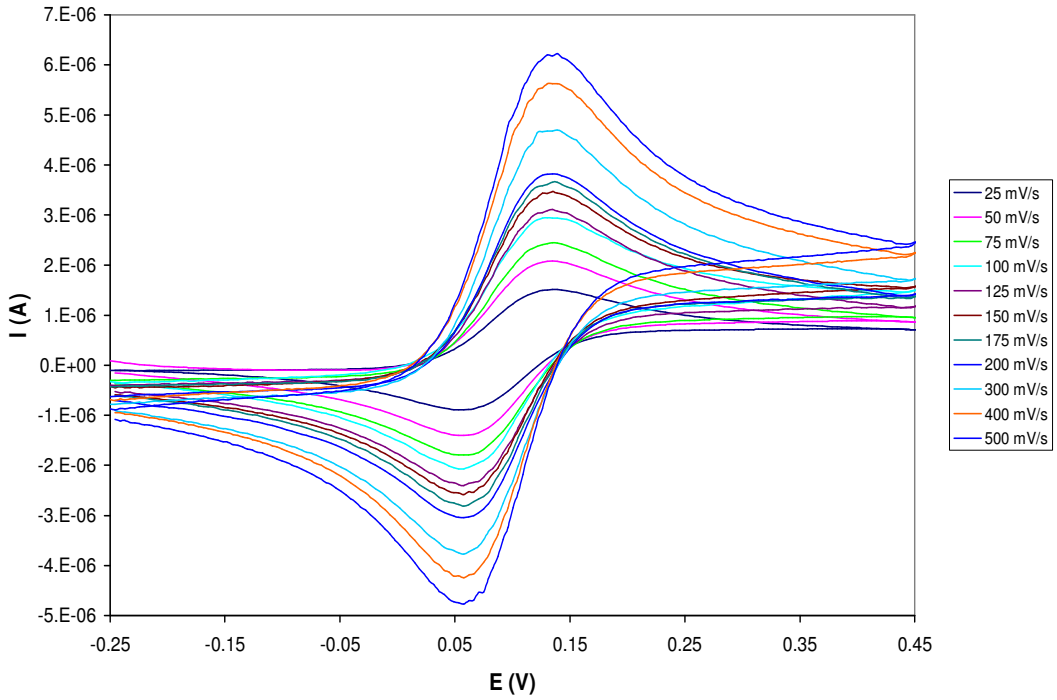

Figure A.3 CV curve of ferrocene in solution containing 0.05 M TBAHFP.

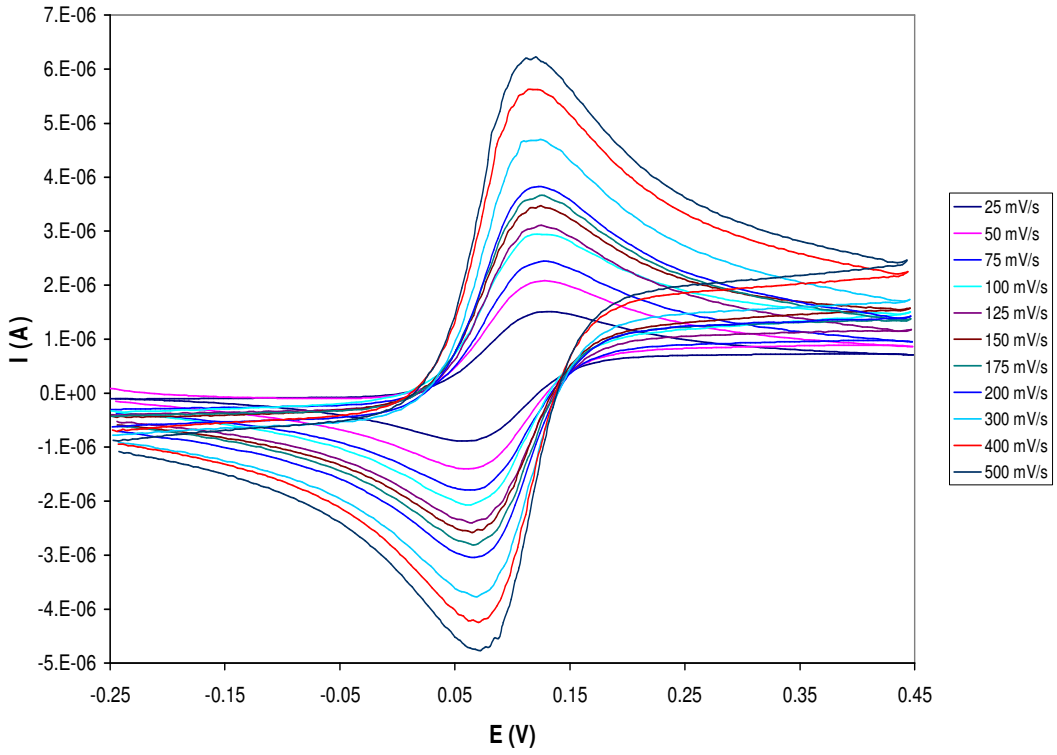

Figure A.4 CV curves of ferrocene from data in Figure A.3 after IR drop correction.

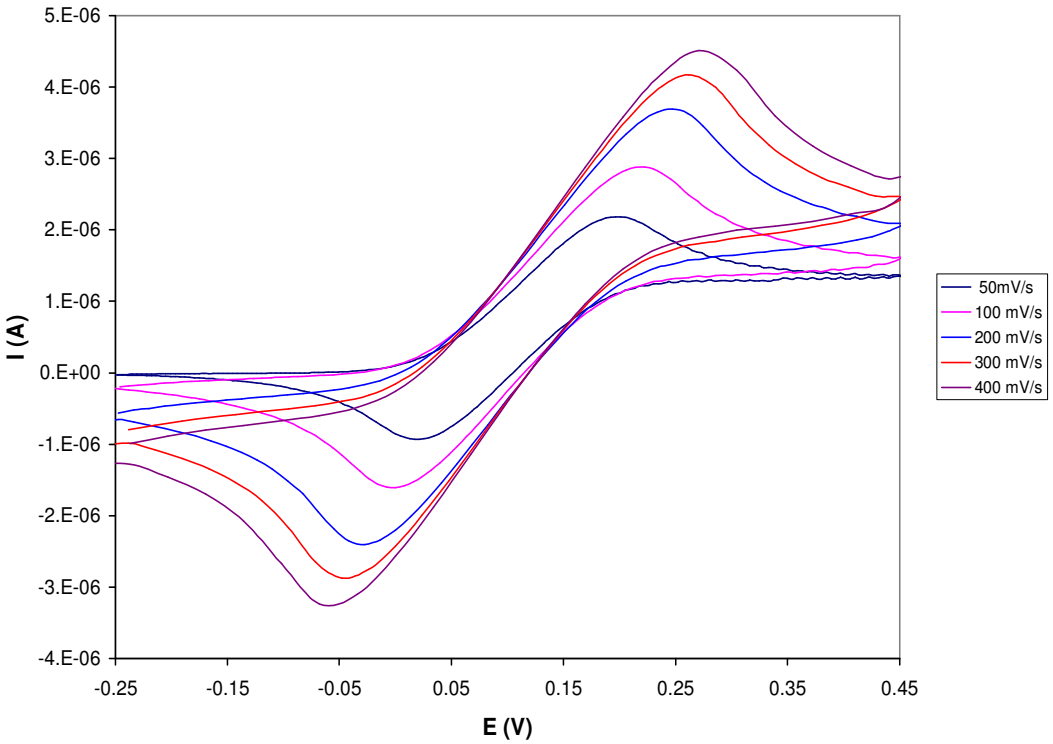

Figure A.5 CV curve of ferrocene in flowing solution containing 0.01 M TBAHFP using a flow-by cell, flow rate = 0.46 ml/min.

APPENDIX B

B 1 Characterization of $CoCl_2(PPh_3)_2$ and $CoCl(PPh_3)_3$

B 1.1 Elemental Analysis

ANALYSIS REPORT: ARC - INSTITUTE FOR SOIL, CLIMATE AND WATER
ONTLEDINGSVERSLAG: LNR - INSTITUUT VIR GROND KLIMAAT EN WATER

ARC • LNR

600 Belvedere Street, Arcadia, Pretoria. P.Bag X79, Pretoria, 0001.
Telephone: (012) 310 2500 Telefax (012) 323 1157

Report Number: F 2005/06-1113

Report on: Analysis of Co complexes from Univ. Pretoria, Electrocemistry Res.(W. Maboya).

Lab No.	F524
Sender No.	1
Formula	$CoCl_2(PPh_3)_2$
C% 1	65.71
C% 2	65.89
H% 1	4.53
H% 2	4.67
C% Mean	65.80
H% Mean	4.60
C% Expect	66.06
H% Expect	4.62

Lab No.	F525
Sender No.	2
Formula	$CoCl(PPh_3)_3$
C% 1	68.02
C% 2	68.31
H% 1	4.63
H% 2	4.86
C% Mean	68.17
H% Mean	4.75
C% Expect	73.59
H% Expect	5.15

B 1.2 Infrared Spectrums

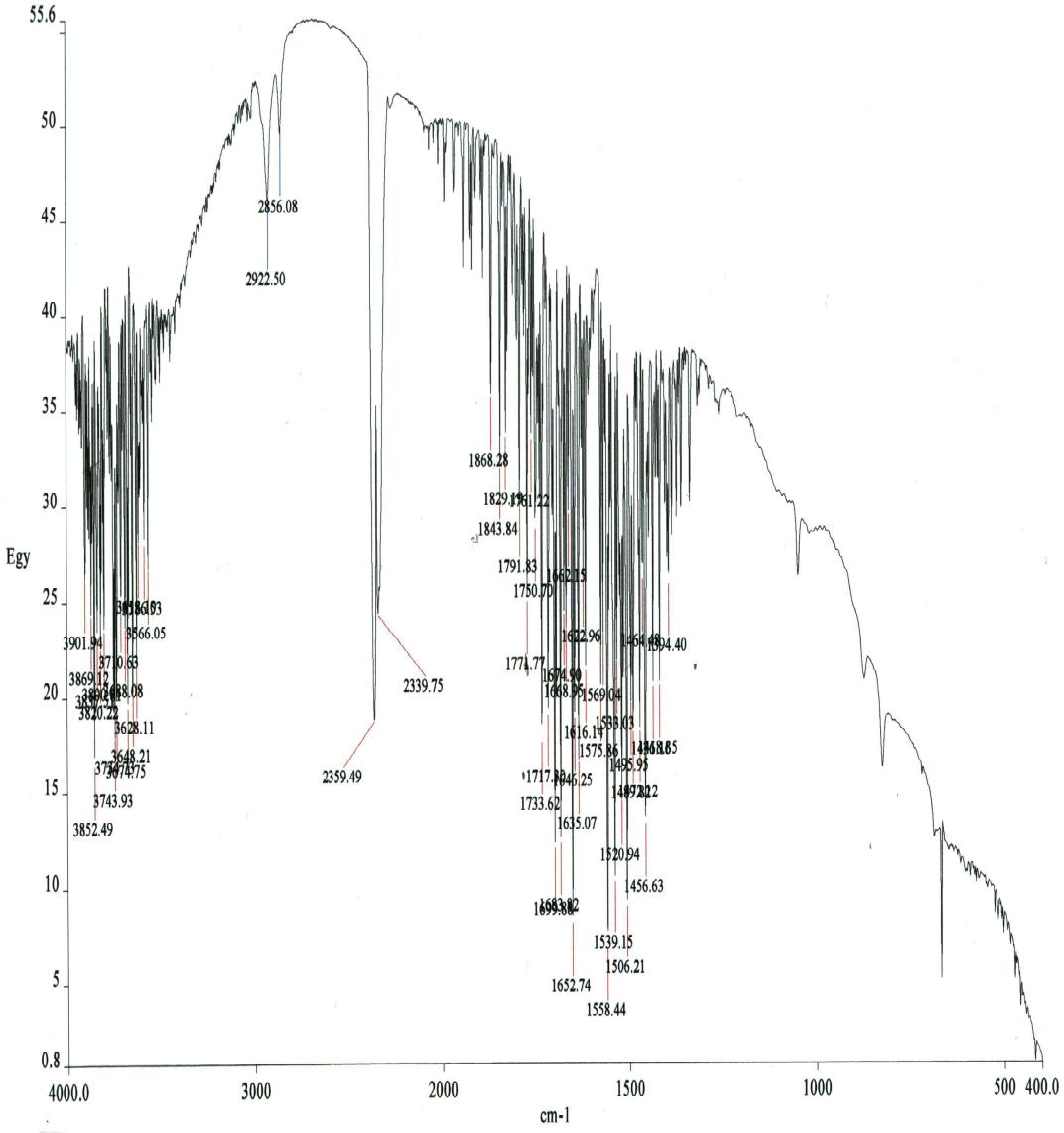

Figure B.1 Infrared spectrum of the background KBr in the wavelength (Δv) range of 4000–400 cm^{-1}.

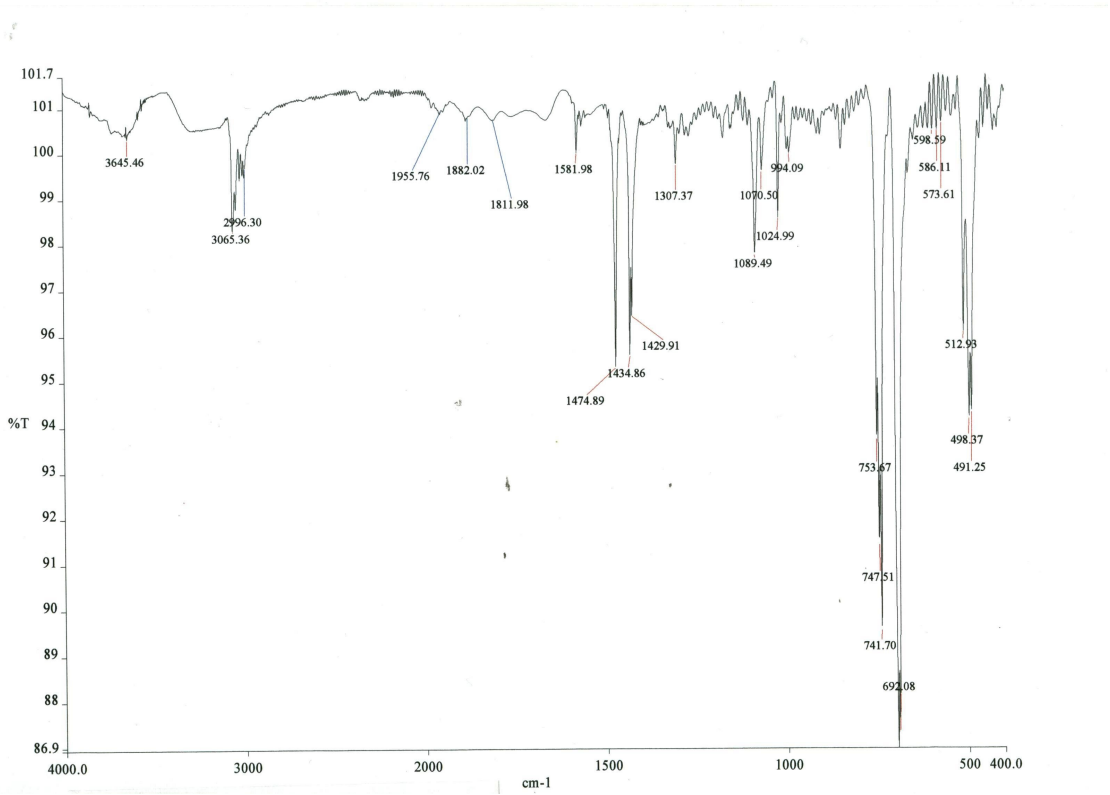

Figure B.2 Infrared spectrum of a free ligand PPh_3 in the wavenumber (Δv) range of 4000–400 cm^{-1}.

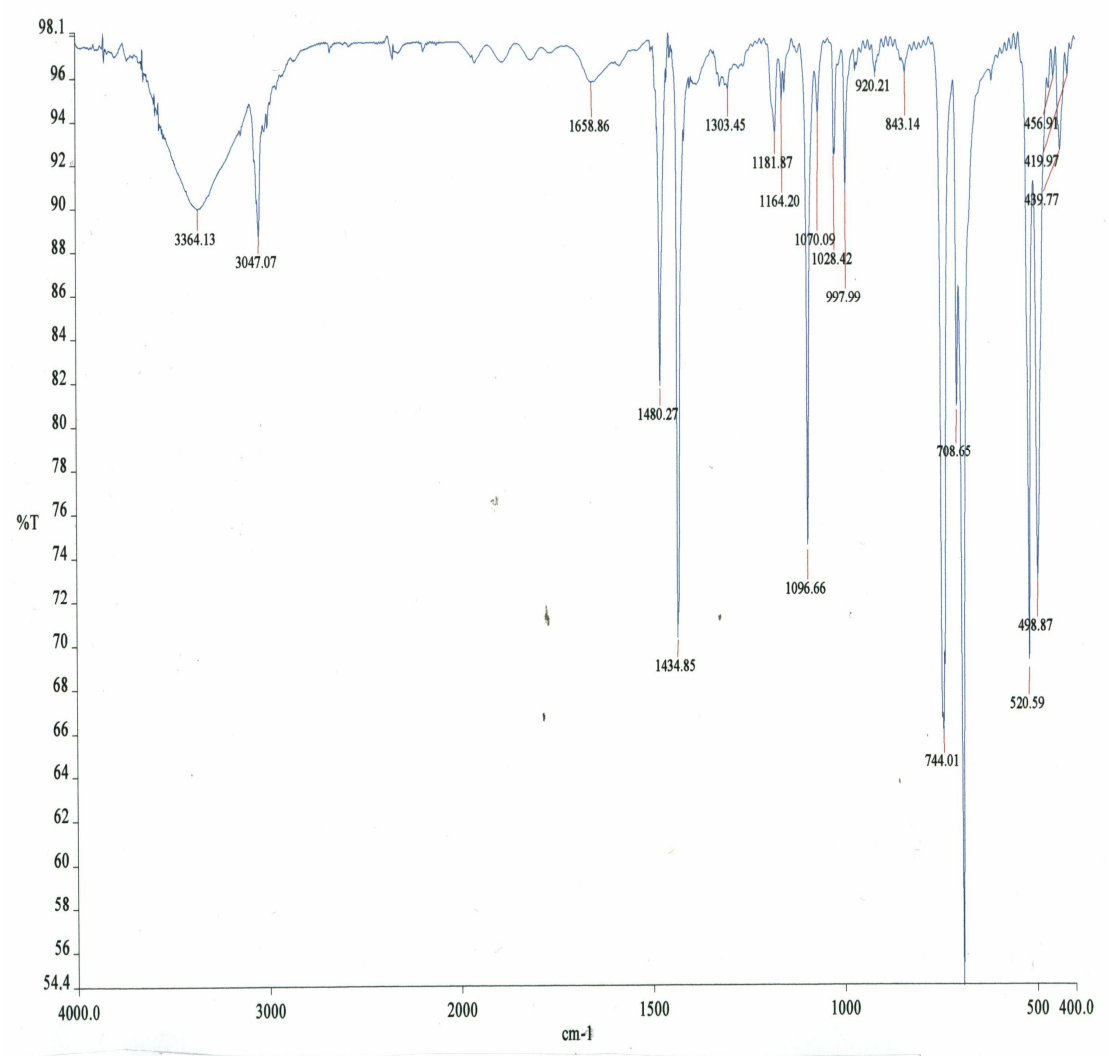

Figure B.3 Infrared spectrum of $CoCl_2(PPh_3)_2$ in the wavenumber (Δv) range of 4000–400 cm^{-1}.

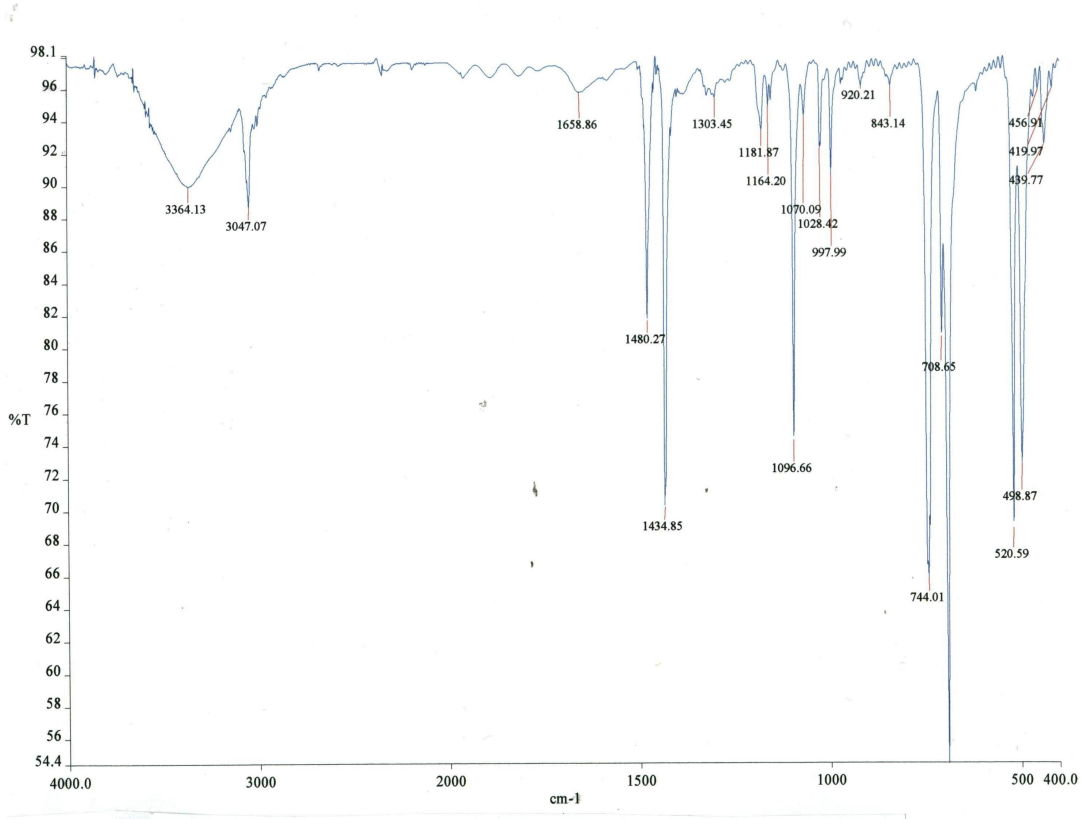

Figure B.4 Infrared spectrum of $CoCl(PPh_3)_3$ in the wavenumber (Δv) range of 4000–400 cm^{-1}.

B 2 Monitored titration of 7.7×10^{-4} mol/l $CoCl_2(PPh_3)_2$ with PPh_3 in a mixture of acetonitrile and pentanol containing 0.05 M $TBAPF_6$ using UV-Vis spectroscopy.

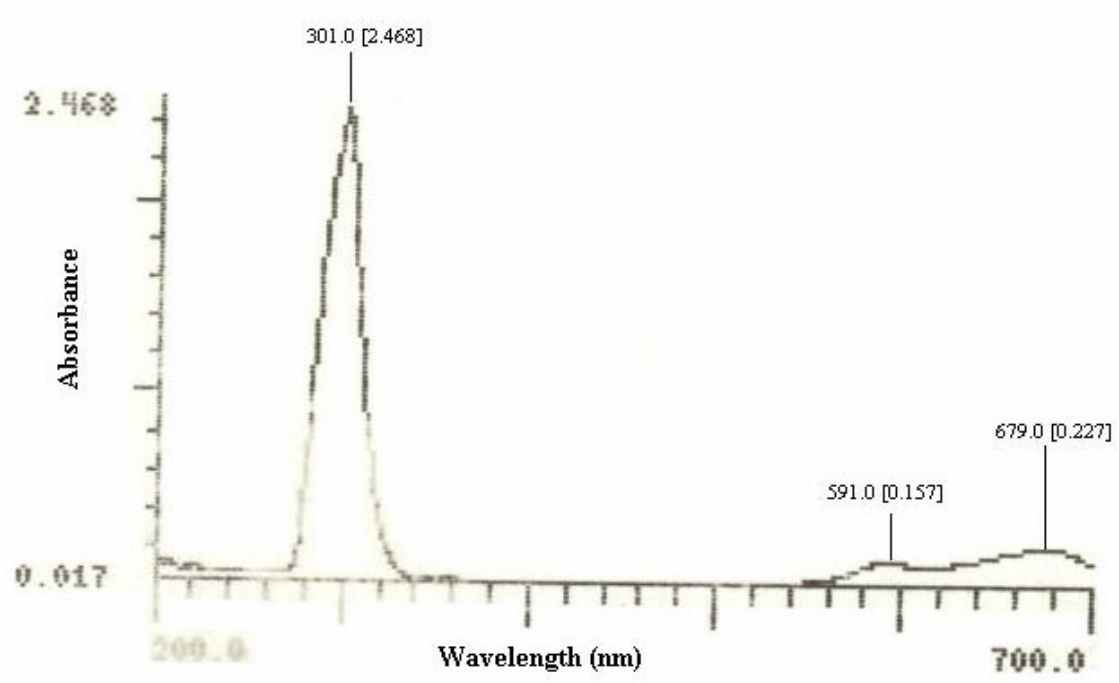

Figure B.5 UV-Visible spectrum of $CoCl_2(PPh_3)_2$ after addition of 2.5 equivalent moles of PPh_3.

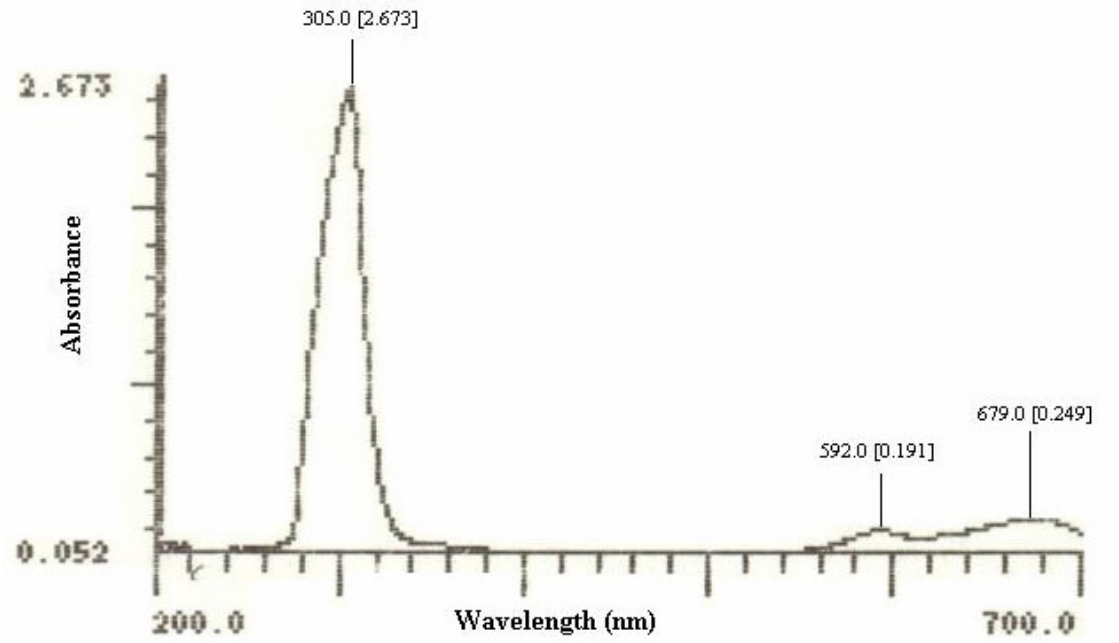

Figure B.6 UV-Visible spectrum of $CoCl_2(PPh_3)_2$ after addition of 5 equivalent moles of PPh_3.

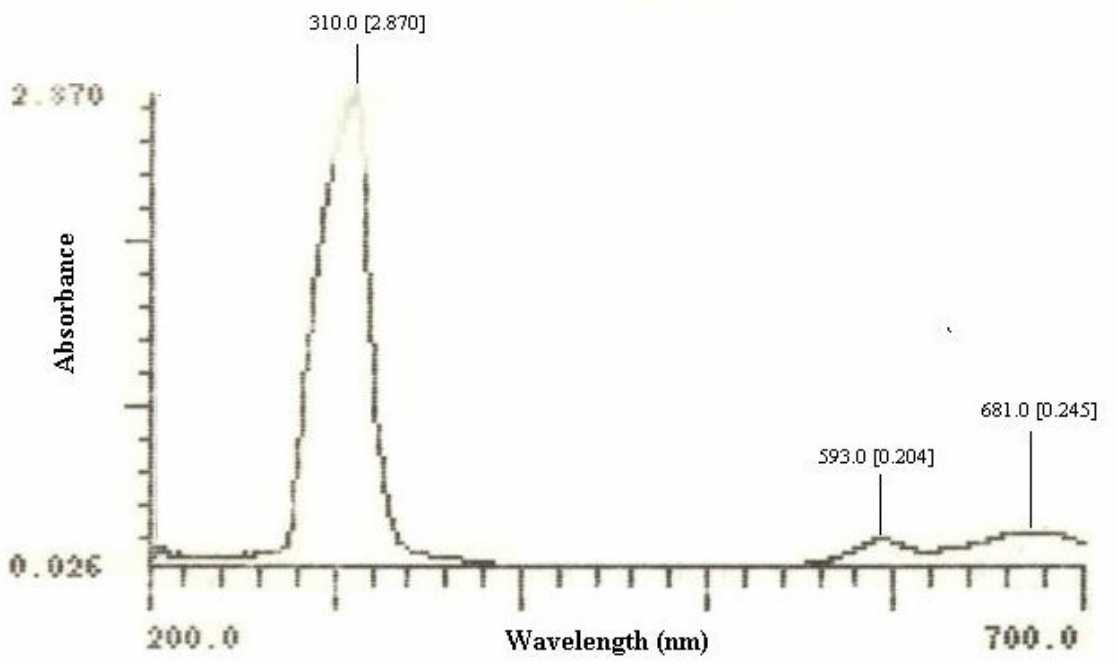

Figure B.7 UV-Visible spectrum of $CoCl_2(PPh_3)_2$ after addition of 15 equivalent moles of PPh_3.

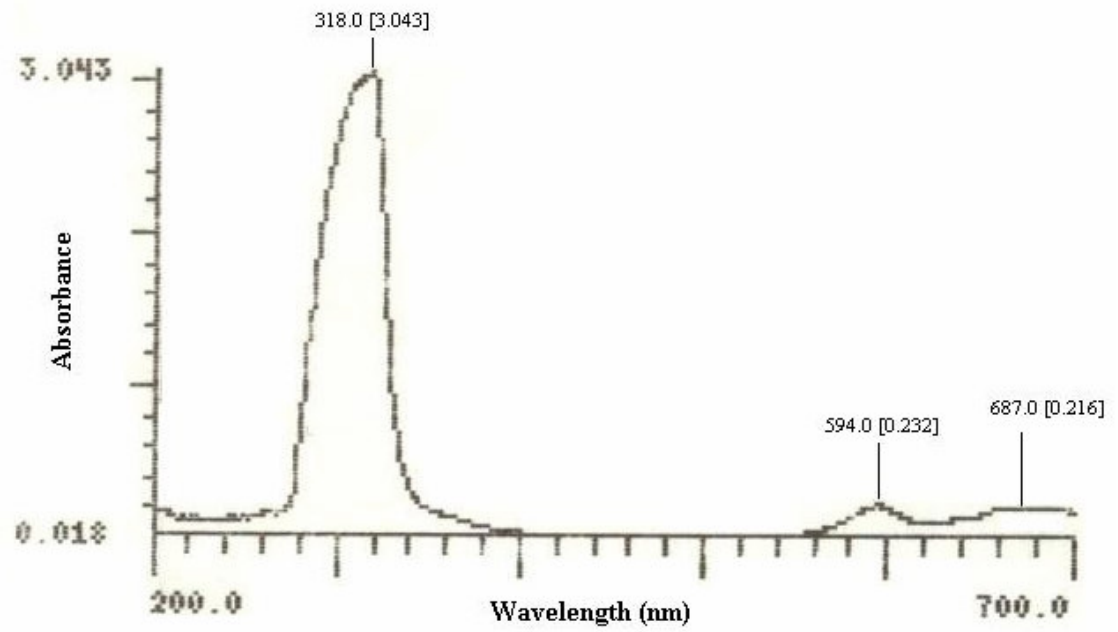

Figure B.8 UV-Visible spectrum of $CoCl_2(PPh_3)_2$ after addition of 75 equivalent moles of PPh_3.

B 3 Monitored Titration of $CoCl_2(PPh_3)_2$ with PPh_3 in deteriorated chloroform ($CDCl_3$) at room temperature.

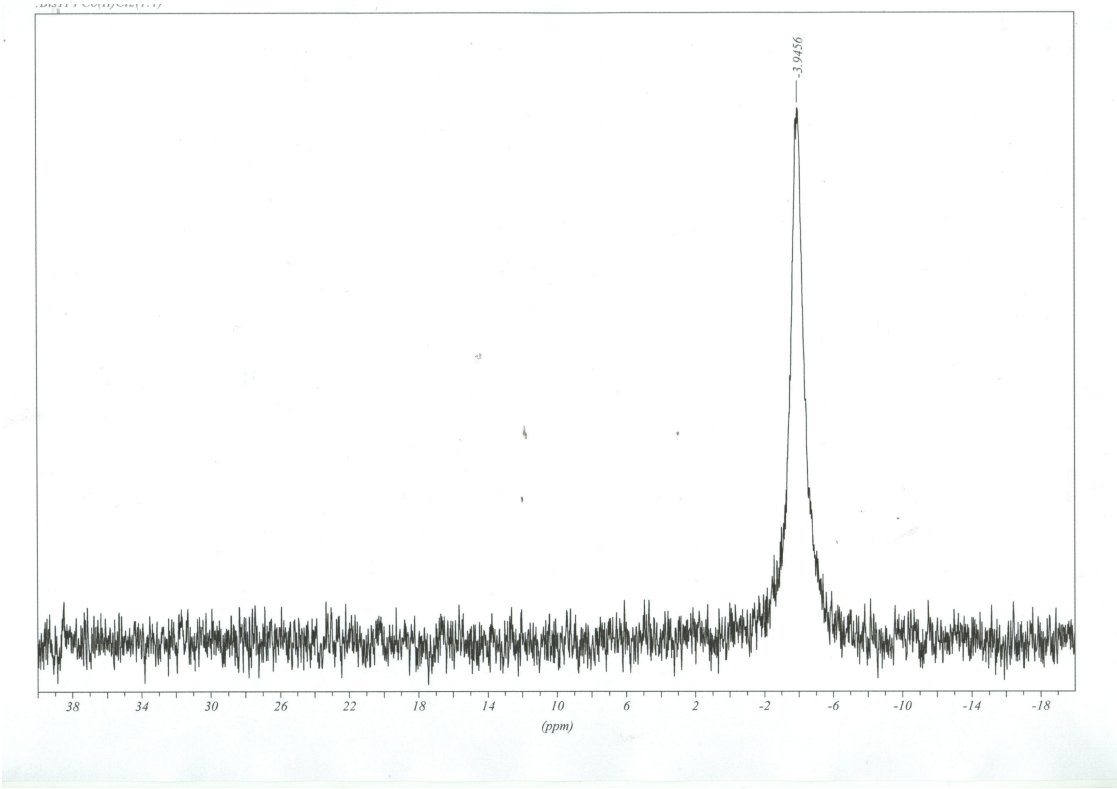

Figure B.9 ^{31}P NMR signals of a mixture of $CoCl_2(PPh_3)_2$ and PPh_3 (1:2.5 mole ratio).

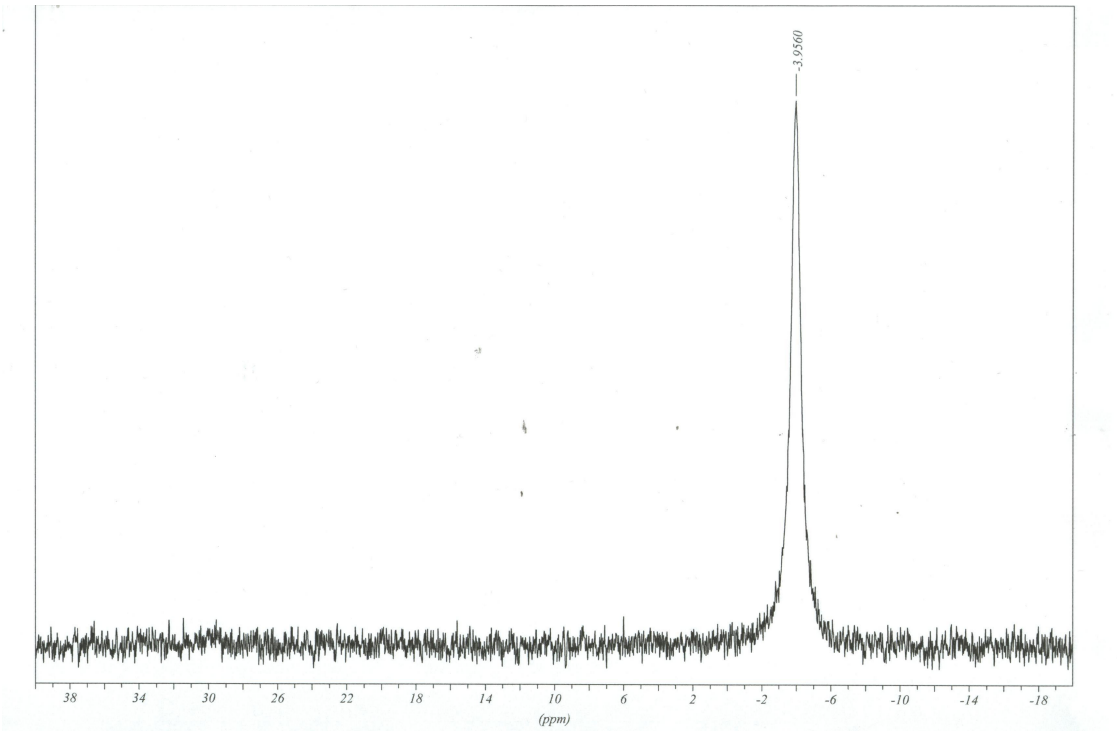

Figure B.10 ^{31}P NMR signals of a mixture of $CoCl_2(PPh_3)_2$ and PPh_3 (1:5 mole ratio).

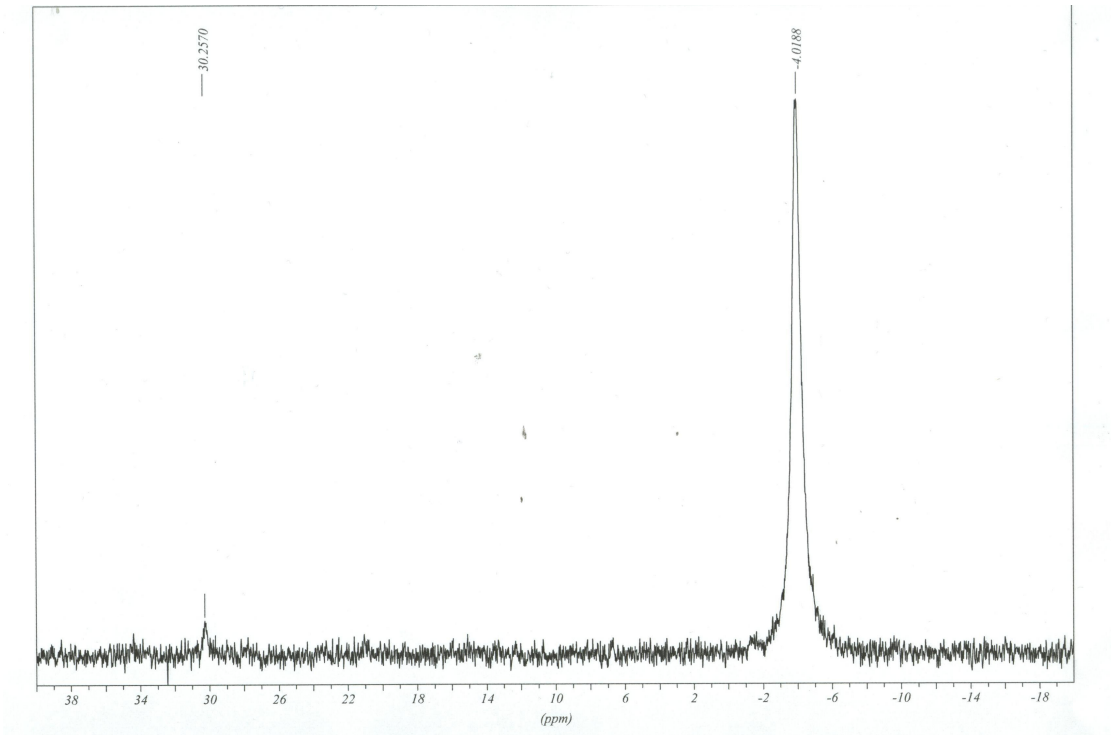

Figure B.11 ^{31}P NMR signals of a mixture of $CoCl_2(PPh_3)_2$ and PPh_3 (1:15 mole ratio).

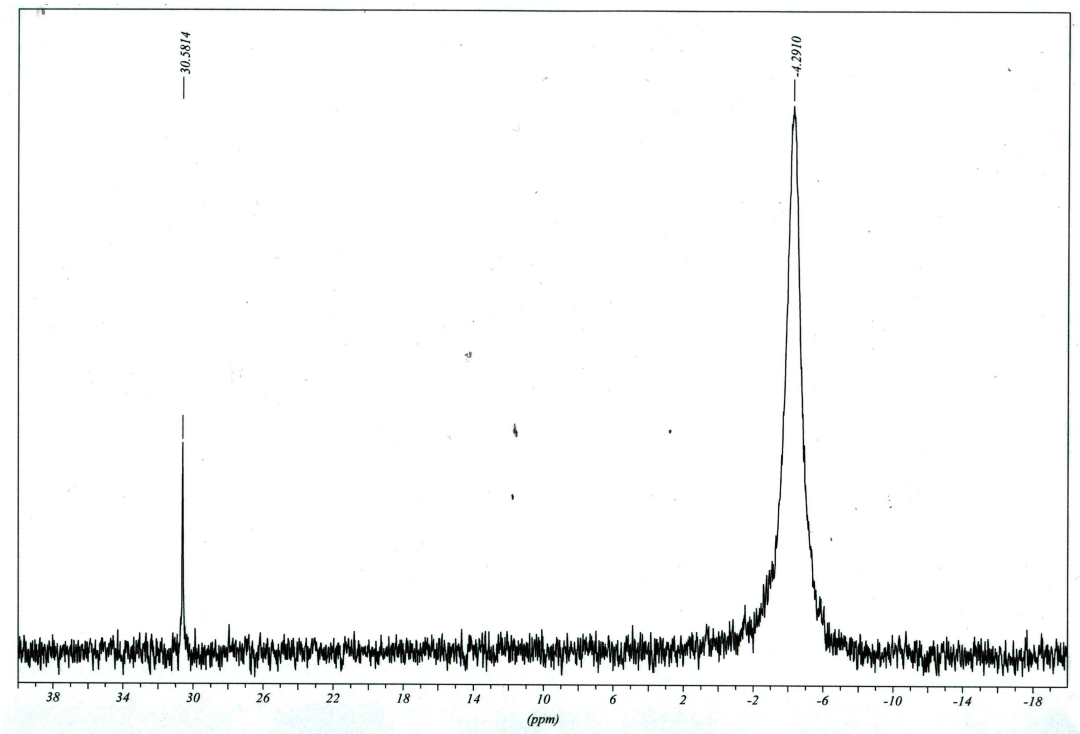

Figure B.12 ^{31}P NMR signals of a mixture of $CoCl_2(PPh_3)_2$ and PPh_3 (1:75 mole ratio).